ENGINEERING NOVEL SURFACES FOR THE LONG-TERM PROPAGATION OF HUMAN PLURIPOTENT STEM CELLS

YAP YAN WEN

(*B.Sc.* (*Hons*), NTU)

A THESIS SUBMITTED

FOR THE DEGREE OF DOCTOR OF PHILOSOPHY

NUS GRADUATE SCHOOL FOR INTEGRATIVE SCIENCES AND ENGINEERING

NATIONAL UNIVERSITY OF SINGAPORE

2012

DECLARATION

I hereby declare that the thesis is my original work and it has been written by me in its entirety. I have duly acknowledged all the sources of information which have been used in the thesis.

This thesis has also not been submitted for any degree in any university previously.

21 December 2012

_____

Yap Yan Wen

ACKNOWLEDGEMENTS

I would first like to thank my thesis supervisors, Professor Simon M. Cool, Professor Victor Nurcombe and Dr. Andre Choo, for their patience, guidance and unwavering encouragement. Professor Simon M. Cool is pivotal to the success of this project. From the first day I joined his laboratory; he showed me the ropes in doing research and constantly challenged me to strive harder. I would like to thank him for being dependable and under his good mentoring, I have learnt and explored tremendously, enabling me to realize my full potential. I am thankful to Professor Victor Nurcombe for being a self-sacrificial advisor, who stood by my side during the radioactivity experiments and spent hours editing my thesis. I am grateful to Dr Andre Choo for always being a kind, patient and inspiring advisor and for imparting meaningful life and research skills.

I am deeply thankful to my thesis advisory committee members, namely, Professor James Goh and Dr. Steve Oh, for the exhilarating discussions and inputs on a regular basis that ensured the progression of my project to its completion. I would like to say special thanks to Professor Shaul Reuveny for agreeing to be my committee chair person despite the last minute notice.

I would like to extend my heartfelt gratitude to all the current and ex-colleagues from the Stem Cells and Tissue Repair group, Institute of Medical Biology, A*STAR, for their help and fun times that we shared. I would like to say special thanks to Drs. Murali Sadasivam, Diah Bramono, Ling Ling, Bina Rai, Wang Chunming, Christian Dombrowski, Janine Harrison, Gajadhar Bhakta and Andrew Ekaputra, for sharing the 'tricks and treats' of graduate studies and for all the stimulating scientific discussions. I am also truly grateful to all research officers, Ms. Wennie Tan, Mr. Clement Foong, Ms Goh Ting Hwee, Ms Lin Tingxuan, Ms Zhuo Ying Jie, and Ms Siti Shahera binte Anwar, for all the help they have given me and for being both colleagues and friends.

I am thankful to my peers Dr. Sampath Jeewantha Wijesinghe, Mr Jonathan Lee, Ms Zophia Lim and Ms Rebekah Margaret Samsonraj for all the insightful discussions and hilarious times that made my time in the laboratory enjoyable. I am glad to have shared tears, anguish and joy during this journey with such great people.

I would also want to thank all my colleagues from the Stem Cells group at Bioprocessing Technology Institute, A*STAR, especially Dr.Vanessa Ding for

teaching me hESC culture and always lending a listening ear. I would like to say special thanks to Dr. Allen Chen for facilitating my cell culture research in the laboratory, Miss Jo'an Ow and Lim Yu Ming for their selfless weekend cell culture media changes and help in all experiments, Miss Sim Lyn Chin for her expertise in capillary electrophoresis, cakes and jokes that we shared and all the other colleagues in the group for their assistance in one way or another.

I am grateful to my collaborators Dr. William Birch and Dr. Li Jian from the Institute of Material Research and Engineering, A*STAR, for their help and contribution to my project. I am thankful to Professor Rob Short, Dr. Jason Whittle and Dr. David Robinson from the Mawson Institute, University of South Australia, for his kindness in hosting and teaching me the plasma polymerization technique in their laboratory, which was a crucial component for my project, and providing me with an invaluable overseas opportunity.

Last but not least, I would like to thank my family for their unwavering support and love. I would like to say special thanks to my father and mother for their selfless support and guidance throughout my entire life and Yin Peng and Kang Wei for being such understanding and fun siblings. I am immensely grateful to my sister who assisted me in making the decision to study science 11 years ago, which was instrumental for my life. I am also thankful to Ms Yap Yuet Meng and Mrs Yip Mei Chan for being such wonderful aunts, who I can always depend on. I am extremely thankful to Mr Fairuz Leong, for his love, patience, and unwavering support throughout the good and difficult times of the last 4 years.

TABLE OF CONTENTS

SUMMARY

Much of the promise that human embryonic stem cells (hESCs) hold for regenerative medicine is dependent on the development of a feeder-free and xenogenic-free culture platform. Matrigel™ and inactivated fibroblasts currently dominate as the field culture substrates; however concerns about contamination and batch inconsistency are its limitations. Defined substrates that can maintain hESC pluripotency are therefore of high interest. Attempts to address these issues have centred on the use of peptide/protein substrates. Of those examined, the adhesive extracellular matrix (ECM) protein vitronectin (VN) has been shown to be particularly effective. However little is known about either the defining parameters or threshold levels of surface-bound VN that are required to maintain hESC pluripotency.

To establish this baseline, a range of VN solution concentrations were examined and the minimum amount of tissue culture-treated polystyrene surface-bound VN able to support long-term propagation of pluripotent cells (> 10 passages) determined. Analyses highlighted a particular VN surface threshold, 250 ng/cm^2, which was able to maintain the growth of pluripotent hESCs.

If the use of its VN for the culture expansion of hESC is ever to replace Matrigel™ or cell feeders as a routine substrate, clearly the coating efficiency needs to be greatly improved. To address this issue, a novel strategy was developed based on the ionic and sequence-based binding of proteins to heparan sulfate (HS), a structural component of the ECM.

Through the use of its affinity to a synthesized peptide containing the heparin-binding domain of VN, an HS variant (HS9^{+ve}) was purified by affinity chromatography from porcine-derived HS. The binding avidity of HS9^{+ve} for VN was

determined using a combination of biochemistry and capillary electrophoresis assays. The data clearly demonstrated the improved specificity of the $HS9^{+ve}$ variant for VN as compared to other ECM proteins. Thus a strategy by using a tuned HS as a bound substratum to capture and present VN was explored next.

To develop a substrate-sandwich consisting of tissue culture-treated polystyrene (TCPS) surface coated with $HS9^{+ve}$ and VN, the TCPS needed to be made positively charged so as to bind the negatively charged HS. This was achieved by plasma polymerization of surface allylamine (AA) polymers. Subsequently, HS binding was confirmed by a combination of radiolabeled HS and dye-based assays. The coating efficiency and threshold surface density of VN able to support the propagation of pluripotent hESC was then re-evaluated with saturating amounts of precoated $HS9^{+ve}$.

When AA surfaces were coated with $HS9^{+ve}$, and then VN, they proved to be equally effective in all the hESC bioassays as compared to the surfaces at the VN threshold density of 250 ng/cm^2. Cells cultured on AA+$HS9^{+ve}$ and 5 μg/ml of VN coating solution retained their pluripotency for > 8 passages, remained karyotypically normal and were able to readily differentiate *in vitro* and *in vivo* when stimulated. Importantly, although the AA+$HS9^{+ve}$+VN5 surface density (150 ng/cm^2) contained ~ 30 % less VN than that passively adsorbed to TCPS (250 ng/cm^2), the hESCs were still easily propagated without adversely affecting their pluripotency. This represents a significant reduction in the VN surface density needed for hESC maintenance and highlights the importance of surface configuration of ECM matrices for cell scale-up.

LIST OF TABLES

LIST OF FIGURES

LIST OF SYMBOLS

^{125}I-VN	^{125} I radioisotope labelled vitronectin
1H-NMR	Proton nuclear magnetic resonance
2-D	2-Dimensional
3-D	3-Dimensional
^{3}H-heparin	Tritiated heparin
^{3}H-HS^{pm}	Tritiated heparan sulfate from porcine intestinal mucosa
AA	Allylamine
AA+GAG	Allylamine surface coated with GAG
AA+heparin	Allylamine surface coated with heparin
AA+HS9^{+ve}+VN2.5	Allylamine surface coated with HS9^{+ve} variant and vitronectin at 2.5 μg/ml
AA+HS9^{+ve}+VN5	Allylamine surface coated with HS9^{+ve} variant and vitronectin at 5 μg/ml
AA+HS9^{-ve}+VN2.5	Allylamine surface coated with HS9^{-ve} variant and vitronectin at 2.5 μg/ml
AA+HS9^{-ve}+VN5	Allylamine surface coated with HS9^{-ve} variant and vitronectin at 2.5 μg/ml
AFM	Atomic force microscopy
AFP	Alpha-feto protein
APMAAm	N-(3-Aminopropyl) methacrylamide hydrochloride
BSA	Bovine serum albumin
C	Carbon
cDNA	Complementary deoxyribonucleic acid
CE	Capillary electrophoresis
Ci	Curie
CM	Conditioned medium
CS	Chondroitin sulfate
Da	Dalton
DACH	Diaminocyclohexane
DAPI	4, 6-diamidino-2-phenylindole
DMEM	Dulbecco's Modified Eagle's Medium
DMEM/F12	Dulbecco's Modified Eagle's Medium/ Ham's F-12

DMSO	Dimethylsulfoxide
DNA	Deoxyribonucleic acid
Dp	Degree of polymerization
DS	Dermatan sulfate
E.C.	Enzyme commission number
EB	Embryoid body
EC	Embryonic carcinomas
ECM	Extracellular matrix
EDC	1-Ethyl-3-[3-dimethylaminopropyl] carbodiimide hydrochloride
EDTA	Ethylenediaminetetraacetic acid
ELISA	Enzyme-linked immunosorbent assay
EM	Electrophoretic mobility
EOF	Electro-osmotic flow
EpCAM	Epithelial cell adhesion molecule
FACS	Fluorescence activated cell sorting
FAK	Focal adhesion kinase
FBS	Fetal bovine serum
FCS	Fetal calf serum
FDA	Food and Drug Administration
FGF-2	Fibroblast growth factor-2
FGFR1	Fibroblast growth factor-2 receptor
FN	Fibronectin
GAG	Glycosaminoglycan
GAPDH	Glyceraldehyde-3-phosphate dehydrogenase
GATA6	GATA binding factor 6
GFAP	Glial fibrillary acidic protein
GlcA	β-L-glucuronic acid
GlcNAc	2-deoxy-2-acetamido-α-D-glucopyranosyl
GlcNS (6S)	2-deoxy-2-sulfamido-α-D-glucopyranosyl-6-O-sulfate
GlcNS	2-deoxy-2-sulfamido-α-D-glucopyranosyl
h	Hour (s)
H&E	Haematoxylin and Eosin
H_2SO_4	Sulphuric acid

HA	Hyaluronic acid
HAND1	Heart- and neural crest derivatives-expressed protein 1
HBD	Heparin-binding domain
hESC	Human embryonic stem cell
HPLC	High-performance liquid chromatography
hPSCs	Human pluripotent stem cells
HRP	Horseradish peroxidase
$HS9^{+ve}$	Heparan sulfate variant with high VN binding affinity
$HS9^{-ve}$	Heparan sulfate variant with low VN binding affinity
HSPA8	Heat shock 70-kDa protein 8 isoform
HSPG	Heparan sulfate proteoglycan
HS^{pm}	Heparan sulfate from porcine intestinal mucosa
ICC	Immunocytochemistry
IdoA	α-L-iduronic acid
IF	Intermediate filament
IGF	Insulin growth factor
IGFBP	Insulin growth factor binding protein
iPS cells	Induced pluripotent stem cells
kDa	Kilodalton
KS	Keratan sulfate
KSR	KnockOut™ serum replacement
kV	Kilovolt
LIF	Laser-induced fluorescence
LN	Laminin
M	Molarity
mAb	Monoclonal antibody
MALDI	Matrix-assisted laser desorption/ionization
MAP2	Microtubule-associated protein 2
MC	Microcarrier
MEF	Mouse embryonic fibroblast
mESC	Mouse embryonic stem cell
mg/ml	milligram per millilitre
min	Minute (s)
ml	Millilitre

MS	Mass spectroscopy
MSH	Muscle segment homeobox 1
N	Nitrogen
N: C	Nitrogen carbon ratio
NA domain	Non-N sulfate domain
NaAc	Sodium acetate
NaCl	Sodium chloride
NaOH	Sodium hydroxide
Neu5Gc	N-glycolylneuraminic acid
NFH	Neurofilament heavy chain
NHS	*N*-hydroxysulfosuccinimide
nm	nanometer
NMR	Nuclear magnetic resonance
NS domain	N-sulfate domain
O	Oxygen
^{o}C	Degree Celsius
OCD	Organ culture dish
OCT-4	Octamer-binding transcription factor 4
p.s.i.	Pound force per square inch
PAGE	Polyacrylamide gel electrophoresis
PAI-1	Plasminogen activator inhibitor-1
PAS	Peptide-acrylates
PAX6	Paired box protein 6
PBS	Phosphate buffered saline
PCR	Polymerase chain reaction
PD	Population doublings
PG	Proteoglycan
PLL	Poly-L-Lysine
PMEDSAH	Poly [2-(methacryloyloxy) ethyldimethyl-(3-sulfopropyl) ammonium hydroxide]
PMVE-alt-MA	poly (methyl vinyl ether-alt-maleic anhydride
PODXL	Podocaylxin-like protein
PSC	Pluripotent stem cells
qRT-PCR	Quantitative real-time polymerase chain reaction

R.S.D.	Relative standard deviation
Ra	Profile roughness parameter
RGD	arginine-glycine-aspartate
RNAi	RNA interference
SAX-HPLC	Strong anion exchange – high performance liquid chromatography
sccm	Standard cubic centimetres per minute
SCID	Severe combined immunodeficiency
SDS	Sodium dodecyl sulfate
Sec	Second (s)
SEM	Standard error of mean
SOX2	Sex determining region Y-box 2
SSEA	Stage specific antigen
TAT	Thrombin anti-thrombin
TBST	Tris-Buffered Saline and Tween 20
TCPS	Tissue culture-treated polystyrene
TGF-1	Transforming growth factor 1
TMB	3,3′,5,5′-Tetramethylbenzidine
UA	Uronic acid
uPA	Urokinase-type plasminogen activator
uPAR	Urokinase-type plasminogen activator receptor
VN	Vitronectin
VN1.25	Surfaces coated with 1.25 μg/ml VN solution
VN2.5	Surfaces coated with 2.5 μg/ml VN solution
VN5	Surfaces coated with 5 μg/ml VN solution
VN-HBD	Vitronectin heparin-binding domain
v/v	Volume per volume
w/v	Weight per volume
XPS	X-ray photospectroscopy
ΔE-MEF	Immortalized mouse embryonic fibroblast

CHAPTER 1 : LITERATURE REVIEW

1.1. Introduction

Human pluripotent stem cells (hPSCs) can be isolated from either the inner cell mass of blastocysts, or induced from somatic cells ("induced pluripotent stem cells," iPSCs). These cells have the dual ability to divide indefinitely, and to differentiate into lineages characteristic of each of the 3 germ layers, endoderm, mesoderm and ectoderm. Hence the clinical potential of pluripotent cells is substantial. The usual methods of culturing these cells typically mandates the use of either inactivated mouse or human fibroblast cells as feeder layers, or a basement membrane extract from mouse cells (Matrigel^{TM}). However, these poorly defined cell culture substrates are not suitable for the culturing of clinical grade hPSCs for therapy. Clearly, better surfaces need to be explored.

In response to this constraint, several surfaces have been developed, including coatings incorporating extracellular matrix (ECM) proteins (laminin, fibronectin, vitronectin, collagen IV), peptides (vitronectin heparin-binding domain peptide, or RGD derivatives) and polymers (Table 1.1). The surface density of the active ingredients of these coatings is again either poorly defined, or not defined at all. Moreover, the method of immobilizing ECM proteins onto culture surfaces involves passive adsorption, a method that is both poorly understood and non-specific.

Of the ECM proteins, vitronectin (VN) is amongst the most promising. It has already been shown that it supports hESC culture by engaging $\alpha V\beta 5$ integrins on their cell surfaces (Rowland *et al.* 2010) and that cell glycosaminoglycans (GAGs) are critical mediators of VN binding via unique heparin-binding peptide domains (Klim *et al.* 2010). Hence the idea of creating a novel surface using a combination of heparan sulfate (HS) and VN, and to understand the surface threshold requirement for the long-term culture of hPSCs has a rational basis.

Thus, this study set out to determine the surface density of VN that can support long-term propagation of pluripotent cells using a natural ECM component, heparan sulfate, as a pre-coating to adsorb functional VN efficiently. This is key, because unless surfaces can be produced that are scalable, cost effective, reliable and reproducible, the possibilities for cultured cells to be of therapeutic value decline markedly.

1.2. Pluripotent stem cells

Precursor cells can be categorized into pluripotent, multipotent or unipotent based on their differentiation potential. Pluripotent cells are defined as being capable of dividing and producing all the differentiated cell types; multipotent cells have the potential to give rise to cells of multiple, but limited number of lineages; and unipotent cells have the capacity to differentiate into only one cell type (Hoffman & Carpenter 2005a).

Human pluripotent stem cells (hPSCs) are not only a promising platform for the study of complex human developmental processes, but a source of undifferentiated cells for drug testing and cell-based therapy (Fig. 1.1).

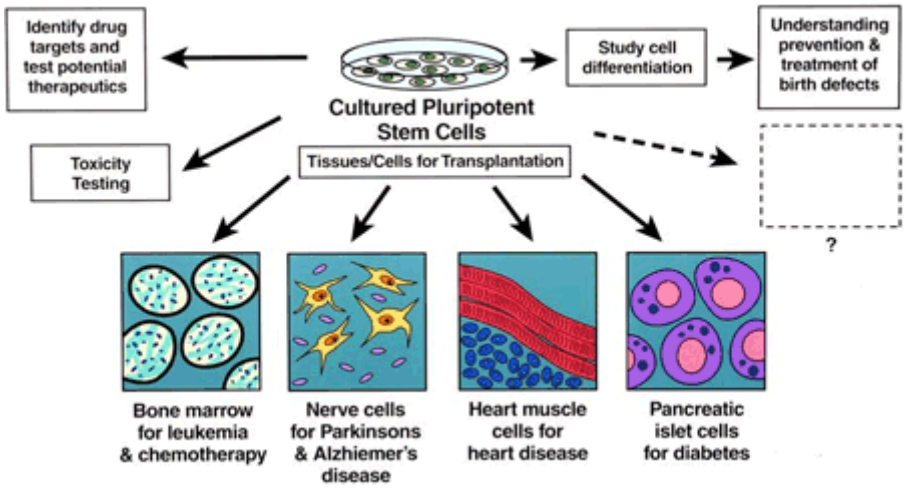

Figure 1.1. Potential clinical applications of hPSCs. (Evans & Kaufman 1981)

1.2.1. Sources of hPSCs

Two groups, Evans and Kaufman, and Martin *et al.* in the early 1980s were the first to isolate mouse embryonic stem cells (mESCs) from the inner cell mass of embryos (Evans & Kaufman 1981, Martin 1981).This breakthrough opened the possibility of using these cells as a source for the derivation of all the cell types of the body (endoderm, mesoderm and ectoderm) (Fig. 1.2). Consequently, human embryonic stem cells (hESCs) were isolated from the inner cell mass (Reubinoff *et al.* 2000, Thomson *et al.* 1998), and resembled mESCs in their ability to both self-renew indefinitely, and differentiate into the three germ layers *in vivo* and *in vitro* (Ben-Hur *et al.* 2004, D'Amour *et al.* 2006, Lavon *et al.* 2004, Mummery *et al.* 2003, Phillips *et al.* 2007, Reubinoff *et al.* 2001, Xu *et al.* 2001a).

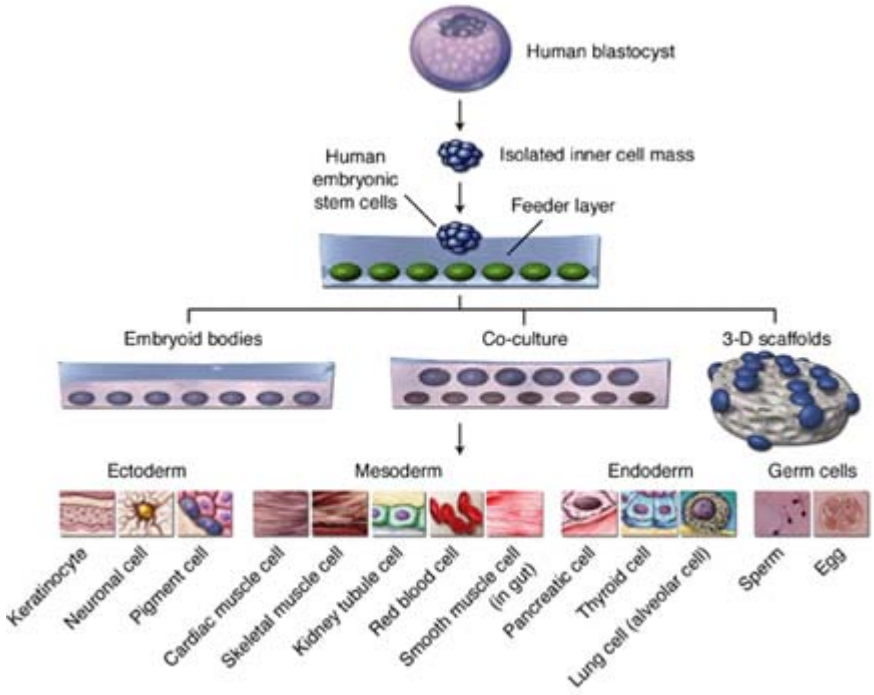

Figure 1.2. Sources and differentiation potential of hESCs (Hyslop *et al.* 2005a).

Although hESCs promise much, many ethical and legal challenges remain. Embryos must be destroyed to obtained hESCs. In 2006, Yamanaka *et al.* overcame this obstacle by demonstrating the ability of mouse fibroblasts to be reprogrammed back to pluripotent states by retrovirally introducing stem cell-associated genes (OCT-4, Sox2, c-myc, and Klf4); these cells were dubbed induced pluripotent stem cells (iPSCs) (Takahashi & Yamanaka 2006). This discovery abrogated the ethical concerns and opened a whole new field for regenerative medicine.

However, several challenges are also associated with these improved techniques; in particular, retroviruses have major safety concerns. In addition, the introduced c-myc is an oncogene which can cause cancer (Marion *et al.* 2009). Overall, reprogramming has low efficiency (0.01-1 %) (Takahashi *et al.* 2007) and the possibility that cells with incomplete reprogramming will form a teratoma are problematical (Zhao *et al.* 2009). Yamanaka *et al.* reported that about 20 % of the

mice they tested developed tumours from iPSCs. In a later study they reported that iPSCs can be generated without c-myc, but the process takes longer and is not efficient (Aoi *et al.* 2008, Takahashi *et al.* 2007). Many other groups have addressed these problems by either using small compounds that mimicked the effects of the transcription factors (Huangfu *et al.* 2008, Shi *et al.* 2008), or using alternate vectors such as plasmids (Zhou & Freed 2009) or micro RNA molecules (Judson *et al.* 2009).

Both human and mouse iPSCs resemble embryonic stem cells in every aspect tested: gene expression, chromatin methylation patterns, doubling time, embryoid body formation, teratoma formation and viable chimera formation (reviewed by (Amabile & Meissner 2009, Kiskinis & Eggan). Although the sources of iPSCs are not as controversial as ESCs, the field is still in its infancy, and many technical issues remain to be addressed. Other methods that do not rely on the integration of transgenes have proven inefficient (0.0001 to 1 %), while those that do rely on the integration of transgenes face the problems of incomplete reprogramming and tumourigenesis. Thus it is still premature to dispense with the advantages of ESCs; hence the focus of this thesis will be on hESCs and the way they react to defined environments.

1.2.2. Characterization of hESCs

The most reliable way of determining the pluripotent state of hESCs is by monitoring the expression of a set of phenotypic markers with fluorescence-activated cell sorting (FACS). These markers can be broadly categorized into cell surface markers and intracellular markers, including transcription factors.

Unique surface markers are used to characterize the state of ESCs, the antigens predominately identified from previous studies of embryonic carcinoma (EC)

cells. At present, amongst the key markers are the stage-specific embryonic antigens SSEA-3 and SSEA-4, Tra-1-60 and Tra-1-80. More recently, the successful generation by several groups of monoclonal antibodies (mAbs) specific to hESCs has added to the list of useful markers. The antigens that have proved most useful are the heat shock 70-kDa protein 8 isoform (HSPA8) (Son *et al.* 2005), podocaylxin-like protein-1(PODXL) (Choo *et al.* 2008) and the epithelial cell adhesion molecule (EpCAM) (Ng *et al.* 2010).

A network of transcription factors, chiefly octamer-binding transcription factor 4 (OCT-4), SRY (sex determining region Y)-box 2 (Sox2), and Nanog have been found to be critical for efficient maintenance of ESC self-renewal (Bowles *et al.* 2000, Chambers *et al.* 2007, Mitsui *et al.* 2003, Parslow *et al.* 1984). The first of these, OCT-4, which binds to the octamer sequence ATGCAAT, is highly expressed in both mouse and human ESCs (Parslow *et al.* 1984). This is the most widely accepted molecular marker of undifferentiated ESCs. Knockdown of OCT-4 in human and mouse ESCs with RNA interference (RNAi) triggers a rapid differentiation into a trophoblast lineage (Hay *et al.* 2004, Matin *et al.* 2004). This transcription factor has been employed by several groups as one of the genes in the reprogramming cocktail that re-specifies somatic cells to iPSCs (Shi *et al.* 2008).

Sox2 is a target gene of OCT-4, a member of the high mobility group (HMG) box DNA-binding protein family (Bowles *et al.* 2000). Together with OCT-4, Sox2 helps to regulate downstream target genes; it also shares an expression pattern similar to OCT-4 in mouse pre-implantation development (Avilion *et al.* 2003). Repression of Sox2 using RNAi in mESCs results in trophectoderm differentiation in a manner that resembles the RNAi knockdown of OCT-4 (Masui *et al.* 2007). In contrast, over-expressing Sox2 in cells triggers the differentiation of mESCs (Kopp *et al.* 2008).

However, the loss of Sox2 does not greatly affect downstream Oct/Sox target genes, making Sox2 dispensable if OCT-4 levels are elevated (Masui *et al.* 2007). Despite this potential redundancy, Sox2 is one of the most widely used of the reprogramming genes.

Nanog was first identified through *in silico* analysis of mESC-specific transcription by two independent groups (Chambers *et al.* 2003, Mitsui *et al.* 2003). It is a homeobox-containing transcription factor thought to play a key role in pluripotency. Over-expression of Nanog in mESCs can maintain cells in an undifferentiated state in the absence of leukaemia inhibitory factor (LIF) (Mitsui *et al.* 2003) and also enables hESCs to grow in the absence of feeder layers (Darr *et al.* 2006). Knockout of Nanog causes both mESCs and hESCs to differentiate into other cell types (Chambers *et al.* 2007, Hyslop *et al.* 2005b, Mitsui *et al.* 2003, Zaehres *et al.* 2005). Notably, Nanog is absent in Yamanaka's cocktail of reprogramming genes, because although it stabilizes cells in an undifferentiated state, it is not central to the maintenance of pluripotency (Chambers *et al.* 2007).

As well as FACS analysis, other assays such as chromosomal stability, chromatin methylation pattern, doubling time, *in vivo* and *in vitro* differentiation potential and chimera formation are also standard methods for the characterization of ESCs. Karyotypic stability is a major concern with the clinical use of these cells. There have been many reports that chromosomal abnormalities, including aneuploidy (trisomy 12 and amplification of 17q) and other translocations may provide a selective advantage to hESCs over the long term. Interestingly, the Nanog gene is located on 12p (Baker *et al.* 2007). A study by The International Stem Cell Initiative analyzed 125 hESC lines from 11 laboratories world-wide and found that cells adapted to

culture tend to acquire changes on chromosomes 1, 12, 17 and 20, with the BCL2L1 gene emerging as a strong candidate for driving culture adaptation (Amps *et al.* 2011).

One of the hallmarks of ESCs is their ability to differentiate *in vitro* as embryoid bodies (EBs) and give rise to all 3 germ lineages, and when injected into SCID mice, they are able to form teratomas containing structures from all 3 lineages (Reubinoff *et al.* 2000, Wobus *et al.* 1984). Thus, before ESCs are cultivated *in vitro*, their pluripotency must be verified both by their ability to form EBs when cultured, and to form multi-germline teratomas *in vivo*.

1.2.3. Defined hESC culture platforms

The clinical possibilities for stem cells rest on the ability to generate them in large numbers. This requirement has prompted the FDA to set out requirements for stem-cell based therapies to ensure that downstream processing does not pose a risk for either contamination or harm (Halme & Kessler 2006).

Human ESCs derived from the inner cell mass of blastocysts have been most often grown in laboratories in co-culture systems with mitotically-inactivated mouse embryonic fibroblast (MEF) cells (Lee *et al.* 2011, Reubinoff *et al.* 2000, Thomson *et al.* 1998). This feeder layer supports the growth of hESCs in the presence of 20 % fetal calf serum (FCS) (Whateley & Knox 1980). Many of the cell lines available in cell banks are derived using this standard method. Although this co-culture platform can support hESCs, it is labour-intensive and imposes significant limitations on subsequent large-scale expansion. As well as this, the presence of FCS and mouse feeders is not suitable for the development of clinical-grade hESCs, due to the xenogenic risks they introduce. Non-human sera (such as FCS) are potential sources of contamination via prions or viruses, or may induce immune reactions to the foreign

proteins (Lim & Bodnar 2002). Thus the removal of FCS as a serum source and MEFs as feeders would represent a major advance. While human feeders have been developed that can successfully replace MEFs (Choo *et al.* 2004, Genbacev *et al.* 2005), these cells may carry-over during hESC removal and thus adversely affect hESC purity. Feeders thus limit experimental interpretation as the data generated may in fact be a combined response from cells and feeder layers to any stimuli or treatment (Moore 2006).

The other problem is that spontaneous differentiation occurs frequently under these conditions. Thus, Amit and co-workers developed the use of KnockOut™ Serum Replacement (KSR) in combination with recombinant basic fibroblast growth factor (FGF-2) as an alternative cocktail to replace serum in media (Amit *et al.* 2000). KSR contains AlbuMAX I, a lipid-rich serum albumin derived from bovine plasma, which is markedly less complex than the protein mix of FCS. Amit *et al.* also introduced the use of enzymatic treatment with Collagenase IA for the subculturing of cells, allowing a method of culturing them at much higher density and lesser differentiation (Amit *et al.* 2000). This marked the beginning of rational, larger scale culturing of hESCs, albeit still requiring the use of feeders as supporting cells.

To produce clinical-grade hESCs for therapeutic application, hESCs will need to be cultured in a feeder-free platform (Halme & Kessler 2006). Some feeder-free platforms have been developed. Xu *et al.* demonstrated the use of Matrigel™; a gelatinous basement membrane extract derived from mouse Engelbreth-Holm-Swarm tumour cells, as an alternative substrate (Xu *et al.* 2001a). Xu and co-workers successfully cultured hESCs on Matrigel™ together with conditioned media (CM) from MEFs supplemented them daily with FGF-2 and used collagenase to passage

cells. This form of passaging has since become a common technique in many laboratories.

Despite these advances, the use of Matrigel™ is plagued by batch-to-batch variability, and the possibility of transferring the highly immunogenic non-human sialic moiety, N-glycolylneuraminic acid (Neu5Gc), to the hESCs (Nasonkin & Koliatsos 2006). Matrigel™ is also known to contain a diverse and variable number of factors that include laminin-111, entactin, HS proteoglycans (HSPGs) as well as several growth factors (Xu *et al.* 2001a). This variability is problematical. As well as this, the CM from MEFs can also contain contaminants, particularly xenogenic antigens, which could possibly be transferred to the hESCs. It has been recently been shown that as many as 136 unique proteins can be identified in the CM from MEFs, including proteins that trigger cell growth and differentiation (Lim & Bodnar 2002). Indeed these results have yielded several more candidates for testing in attempts to construct a fully defined culture platform.

Several defined media to replace the CM, including XVIVO-10 (Lonza) (Li *et al.* 2005), DMEM/F12 (Invitrogen) (Li *et al.* 2005), IMDM/F12 (Invitrogen) (Vallier *et al.* 2005), hESF9 (CSTI) (Furue *et al.* 2008), StemPro (Invitrogen) (Wang *et al.* 2007) and mTeSR™1 (Stem cell technologies) have also been developed (Ludwig *et al.* 2006a). A comparative study by 5 separate laboratories assessed the different cell culture media for their ability to support 10 different hESC lines over 10 passages. Of the eight culture systems, only the two commercial media, mTeSR™1 and STEMPRO, supported maintenance of the majority of the cell lines over 10 passages (Akopian *et al.* 2010). Hence, mTeSR™1 will be used to culture hESCs in attempts to maintain cells in a more pluripotent state in this thesis.

A further development was described by Ludwig and colleagues, who reported that a combination of human collagen IV, fibronectin (FN), laminin (LN) and vitronectin (VN) was able to support hESCs over several passages when combined with a xeno-free culture medium (TeSR1) (Ludwig *et al.* 2006b). However this relies on four different human matrix proteins as a substrate, adding significantly to the cost of scale-up. Moreover, the cells were found to be karyotypically abnormal (Ludwig *et al.* 2006b), which may explain their ready adaptation to these conditions. In other approaches, hESCs have been shown to propagate on separate matrices of FN, LN, LN-511, E-cadherin and VN (Amit & Itskovitz-Eldor 2006, Braam *et al.* 2008, Miyazaki *et al.* 2008, Rodin *et al.* 2010). Such findings suggest that a defined, scalable substrate to propagate hESCs may be a possibility. Also, the iPSC line IMR90 has recently been successfully propagated on plasma-purified VN (Rowland *et al.* 2010). Manton *et al.* have demonstrated that a chimeric VN: insulin-like growth factor 1 (IGF-1) complex, when added into serum-free media, could maintain pluripotent hESCs. However in their study, hESCs were cultured on a substrate of murine Laminin, which does not meet the requirements for a xeno-free culture platform (Manton *et al.* 2010). The experiments in fact suggested that VN, of the several ECM proteins being investigated, may be most useful for the propagation of pluripotent stem cells.

Although these surfaces are able to support hESC propagation, the method of immobilizing ECM proteins is problematical; in almost all cases it is by passive physical adsorption, which gives no control over the amounts or activity of the proteins once on the surface.

Defined model surfaces, in the form of immobilized peptide arrays, have been used previously as substrates for hESC adhesion and expansion (Derda *et al.* 2007,

Liu *et al.* 2011, Orner *et al.* 2004). While dilution is used to tune the peptide surface density, the actual amounts of peptide that attach to the substrate are almost never quantified or even measured. Furthermore, the analysis of hESC pluripotency is limited to detecting endogenous alkaline phosphatase and OCT-4 expression, without any examination of karyotypic stability or the differentiation potential of the expanded hESCs. In a study by Kolhar *et al.*, cyclic RGD peptide sequences immobilized using the Michael addition reaction were shown to be capable of promoting hESC attachment and propagation (Kolhar *et al.* 2008). Using this platform, hESCs could be cultured for > 10 passages, without adversely affecting karyotype or differentiation potential. Although indirect estimates of final peptide surface density (10-30 fmol/cm^2) were obtained from fluorescence measurements and enzyme-linked immunosorbant assay (ELISA), no direct quantification of the peptide surface density or other surface characterization was carried out.

Other than recombinant, truncated or whole ECM protein as a possible substrate, studies by Villa-Diaz *et al.*, Irwin *et al.*, Brafman *et al.*, Melkoumian *et al.* and Klim *et al.* have all demonstrated the ability of synthetic polymers poly[2-(methacryloyloxy)ethyl dimethyl-(3-sulfopropyl)ammonium hydroxide] (PMEDSAH), N-(3-Aminopropyl)methacrylamide hydrochloride (APMAAm), poly(methyl vinyl ether-alt-maleic anhydride (PMVE-alt-MA), peptide-acrylates (BSA-PAS, VN-PAS), and alkanethiol-conjugated peptides (VN-HBD) to support hESCs over the long-term in culture (Table 1.1) (Brafman *et al.* 2010, Irwin *et al.* 2011, Klim *et al.* 2010, Melkoumian *et al.* 2010, Villa-Diaz *et al.* 2010). Although these defined surfaces are promising, these methods are still in their infancy, and they are yet to be proven as robust or as stimulatory as Matrigel^{TM} or other protein-based methods. The common theme for both peptide-acrylates and the peptide conjugates is

the requirement for VN, either whole or in part, to be immobilized onto the cell culture surface, in some cases via biotinylation to streptavidin-coated surfaces. It is clear that the means of immobilizing VN to retain its native conformation is of crucial importance hence better immobilizing strategy is needed.

Hakala *et al.* compared the use of Matrigel™ with different feeder-free hESC culture substrates including various biomaterials, human ECM proteins, human and animal sera matrices. In this study, Matrigel™ was superior in terms of the maximum passage number attained, as well as hESC morphology and the pluripotent markers expressed (Hakala *et al.* 2009). Therefore, Matrigel™ is used as a positive surface for the culture of hESC in this thesis. These results thus set the background for this study to combine engineering and biology to generate better-defined, VN-based surfaces.

Table 1.1 Defined substrates developed for long-term growth of hESCs in a feeder-free microenvironment.

	Method of preparation
Biological components	
Recombinant E-cadherin	Absorption by surface (Nagaoka *et al.* 2010)
Recombinant laminin-511	Absorption by surface (Rodin *et al.* 2010)
Recombinant vitronectin	Absorption by surface (Braam *et al.* 2008)
RGD and vitronectin heparin-binding peptide	Biotinylated peptides bound to streptavidin-coated surface (Klim *et al.* 2010)
RGD domains of bone-sialoprotein and vitronectin	Peptides bound to acrylate-coated surface (Melkoumian *et al.* 2010)
Synthetic components	
PMEDSAH	Polymer synthesis by surface-initiated graft polymerization (Villa-Diaz *et al.* 2010)
APPMAAm	Polymer synthesis by photoinitiated radical addition polymerization (Irwin *et al.* 2011)
PMVE-alt-MA	Polymer synthesis by free radical polymerization (Brafman *et al.* 2010)

The overall progress towards a fully defined culture system only addresses a variant of the multi-faceted set of problems surrounding the translation of hESCs into the clinic. Another challenging problem is to be able to achieve sufficient cell numbers for stem cell transplantation. Only limited numbers of cells can be cultured on 2-dimensional (2-D) TCPS in a cost-effective manner, and thus other scalable methods need to be explored. The problem can be overcome by growing cells in controlled bioreactors at industrial scales. Oh *et al.* have demonstrated the successful, robust, serial culturing and passaging of hESCs on microcarriers (MC) in such a way that retains their pluripotency. MCs allow cells to grow in much higher numbers in bioreactors as compared to 2-D cell culture (Oh *et al.* 2009). Recently Heydarkhan-Hagvall *et al.* created a 3-dimensional (3-D) microenvironment by electrospinning gelatin type B and PCL together (Heydarkhan-Hagvall *et al.* 2012). These scaffolds were used to culture mESCs after their adsorption with collagen IV, FN, LN, VN, Matrigel^{TM} or gelatin. He observed that cell numbers were higher in scaffolds coated with LN or VN as compared to the other factors. His results are consistent with the many previous studies that demonstrated VN can serve as a very promising substrate for the 2-D and 3-D culture of hESCs (Braam *et al.* 2008, Li *et al.* 2010, Rowland *et al.* 2010, Yap *et al.* 2011).

1.3. Extracellular Matrix proteins

During embryonic development, the ECM plays a critical role in directing the proliferation, differentiation and migration of cells, particularly at the blastocyst, and later stages. In tissue culture, cells avidly interact and respond to specific ECM cues to attach, proliferate and differentiate (Evseenko *et al.* 2009, Hakala *et al.* 2009, Kato

et al. 1995). Thus, the ECM remains an indispensible component for any culture surface development.

The central importance of ECM was first established by Gospodarowicz and colleagues, when they published in their seminal study "The permissive effect of the ECM on cell proliferation *in vitro*" (Gospodarowicz *et al.* 1980). He reported the superior proliferation with a coincident, increased growth factor sensitivity of bovine granulosa and adrenal cortex cells cultured on detergent-exposed ECM, produced by corneal endothelial cells, compared to tissue culture plastic. He also discovered that cells cultured on this decellularized matrix proliferated without exogenous FGF-2, the key mitogen for cells cultured on plastic. Further research revealed that bovine bone cells normally synthesize FGF-2 and store it in their ECM (Globus *et al.* 1989). A further comparison using hepatocarcinoma cells cultured on either the decellularized matrix or the plastic revealed differences in their morphology, doubling time and migratory activity, confirming the superiority of ECM for cell culture (Gospodarowicz *et al.* 1978, Vlodavsky *et al.* 1980). Grunert et al. also showed that the decellularized matrix of osteoblastic cells contained glycosaminoglycans that regulated bone-morphogenetic protein 2 (BMP-2) activities (Grunert *et al.* 2007).

ECM consists of proteoglycans, non-proteoglycan polysaccharides, fibres and ECM proteins (Aumailley & Gayraud 1998). It sequesters a wide range of growth factors within the saccharide compartment, so serving as the external protein reservoir for cells (Folkman *et al.* 1988, Taipale & Keskioja 1997).

1.3.1. Vitronectin

Vitronectin (VN) is a 459 amino acid, multifunctional, 75 kDa (Schvartz *et al.* 1999a) glycoprotein that is found in abundance in the ECM and serum (Hayman *et al.*

1983). Carbohydrates account for about 30 % of VN's total mass (Schvartz *et al.* 1999a). It was first discovered as a "serum spreading" factor that could adhere to glass (Hayman *et al.* 1983, Stanley 1986). Its amino acid sequence was deduced from a human liver complementary DNA (cDNA) library (Solem *et al.* 1991), and human VN shares about 80% homology with mouse and rabbit forms (Preissner *et al.* 1997).

VN is involved in various functions, and interacts with glycosaminoglycans (GAGs) to assist in the processes of cell adhesion and cell spreading (Francois *et al.* 1999). It also binds to plasminogen, plasminogen activator inhibitor-1 (PAI-1), thrombin-antithrombin (TAT) complexes, several collagens and the urokinase-type plasminogen activator (uPAR) (Francois *et al.* 1999, Morris *et al.* 1994, Schvartz *et al.* 1999b) that participates in the blood clotting cascade. It also inhibits the membrane-rupturing effects of the cytolytic complement pathway by binding to serine protease inhibitors, so promoting cell survival (Declerck *et al.* 1988, Milis *et al.* 1993, Schvartz *et al.* 1999a).

This ECM protein is primarily synthesized in the liver, and secreted into the circulation together with a 19 amino acid signal peptide which is cleaved during processing (Schvartz *et al.* 1999b). VN is heterogenic, presenting in two structurally and functionally distinct forms: the monomeric form, found in the circulation in significant concentrations (0.4 mg/ml) (Schvartz *et al.* 1999b) and then deposited extra-vascularly into many tissues and ECM. This ECM association triggers the second heparin-binding multimeric form (Francois *et al.* 1999, Gibson & Peterson 2001, Izumi 1989, Podor *et al.* 2002, Seiffert & Schleef 1996).

VN is made up of 5 domains: the N-terminal somatomedin B domain (residues 1-39) which was originally thought to be mitogenic, and contains binding sites for PAI-1 and uPAR; the connecting region, containing an arginine-glycine-aspartic acid

(RGD) sequence (residues 45-47), which mediates the attachment of hESCs via αVβ5 integrin (Braam *et al.* 2008); the 'linker' region (residues 45 - 130) which contains both a TAT complex and collagen binding sites within a highly unstructured domain (Xu *et al.* 2001b); a central domain with hemopexin homology (residues 131-286) that has been proposed to contain a secondary heparin-binding site (Liang *et al.* 1997); and finally a C-terminal domain which also has hemopexin homology (residues 269-459), and contains sites for plasminogen binding and the primary binding site for heparin (Fig. 1.3). It was also found that heparin-binding domain (HBD) of insulin-like growth factor binding protein 3 and 5 (IGFBP-3 and IGFBP-5) enhance IGF-1 binding to VN (Firth *et al.* 1998, Grulich-Henn *et al.* 2002).

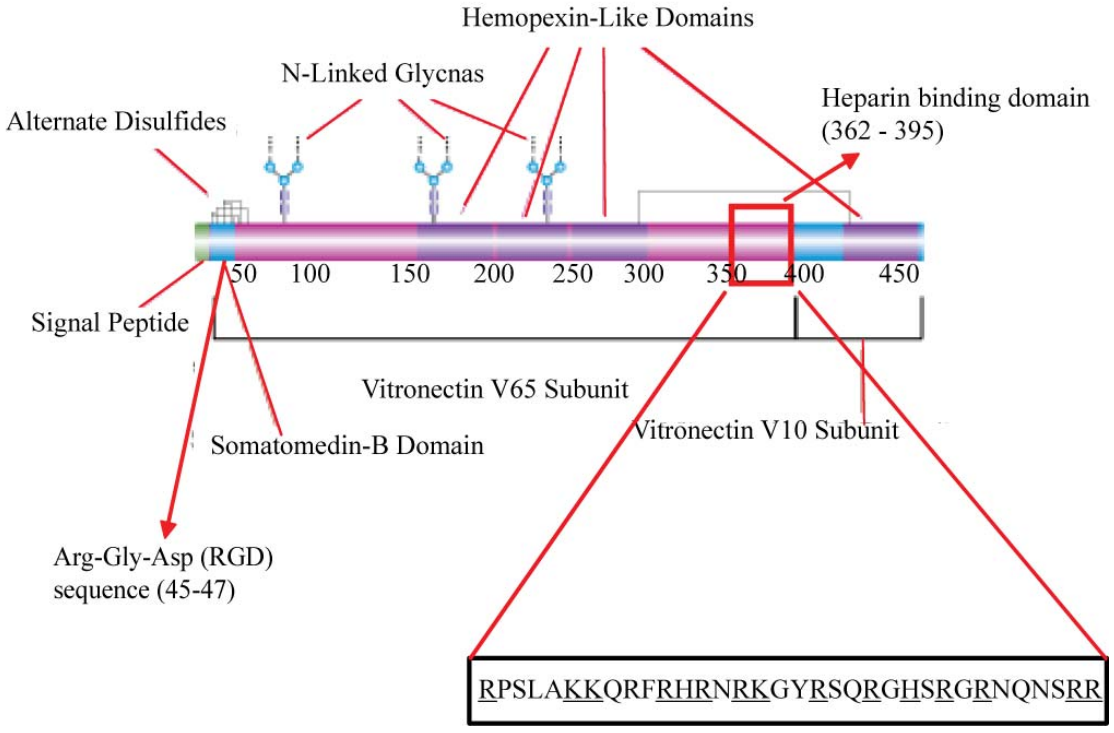

Figure 1.3. Structure of vitronectin, encompassing N-terminal Somatomedin B, hemopexin and heparin-binding domains (Schvartz *et al.* 1999b). The underlined residues are the basic amino acids involved in the electrostatic binding to negatively-charged heparin.

The RGD sequences in VN interact with the integrins on cell surfaces, which in turn triggers a cascade of cellular events (Jones & Walker 1999) such as allowing cells to migrate through ECM to new locations (Germer *et al.* 1998, Zanetti *et al.* 1994). Association of VN with integrins enhances both the survival of glioma cells under insult from drug-induced apoptosis (Uhm *et al.* 1999), and protects microvasular endothelial cells from apoptosis via αVβ3 and αVβ5 integrins (Isik *et al.* 1998). Such data suggests that the αV integrin subunit is important for VN-induced anti-apoptotic response. The integrin receptor activation also led to clustering and formation of focal adhesion contacts on the cell membrane which link extracellular signalling to the cell cytoplasm. Optimal cell response to growth factors is also known to depend on prior integrin-mediated cell attachment to the ECM (Eliceiri 2001, Giancotti & Ruoslahti 1999) . It is clear that integrin engagement is important for the optimization of growth-factor induced biological processes, as there is a great deal of cross-talk between the two systems.

Suzuki *et al.* used the cyanogen bromide technique to chemically sequence VN, and revealed a highly basic region near the C-terminus. This region incorporates the heparin-binding domain (HBD) and occurs at residues 362-395; (RPSLAKKQRFRHRNRKGYR SQRGHSRGRNQNSRR, Figure 1.3) (Suzuki *et al.* 1984). The basic amino acids arginine, lysine and histidine in the VN-HBD play key roles in this interaction, and engage the precisely spaced, negatively charged sulfate and carboxylate groups within GAGs (Cardin & Weintraub 1989). The binding of VN to heparin also induces structural changes to the molecule, whereby cryptic sites are revealed, exposing extra loci for other ligands (Morris *et al.* 1994, Seiffert & Smith 1997). The "true" position of the HBD in VN has been much debated over the years (Fig. 1.4). Studies by several authors have shown that the HBD is buried in the native

molecule, stabilized by a cluster of negative charges. This cryptic binding site becomes exposed when VN undergoes heating or chemical denaturation (Hayashi *et al.* 1985, Izumi 1989, Preissner & Mullerberghaus 1987). However, other studies support another model, wherein the HBD is actually exposed in the native and denatured VN protein, not hidden, so allowing the binding of GAGs without denaturation and exposure of any cryptic binding site (Gibson *et al.* 1999, Xu *et al.* 2001b, Zhuang *et al.* 1997). These models are summarized in Figure 1.4.

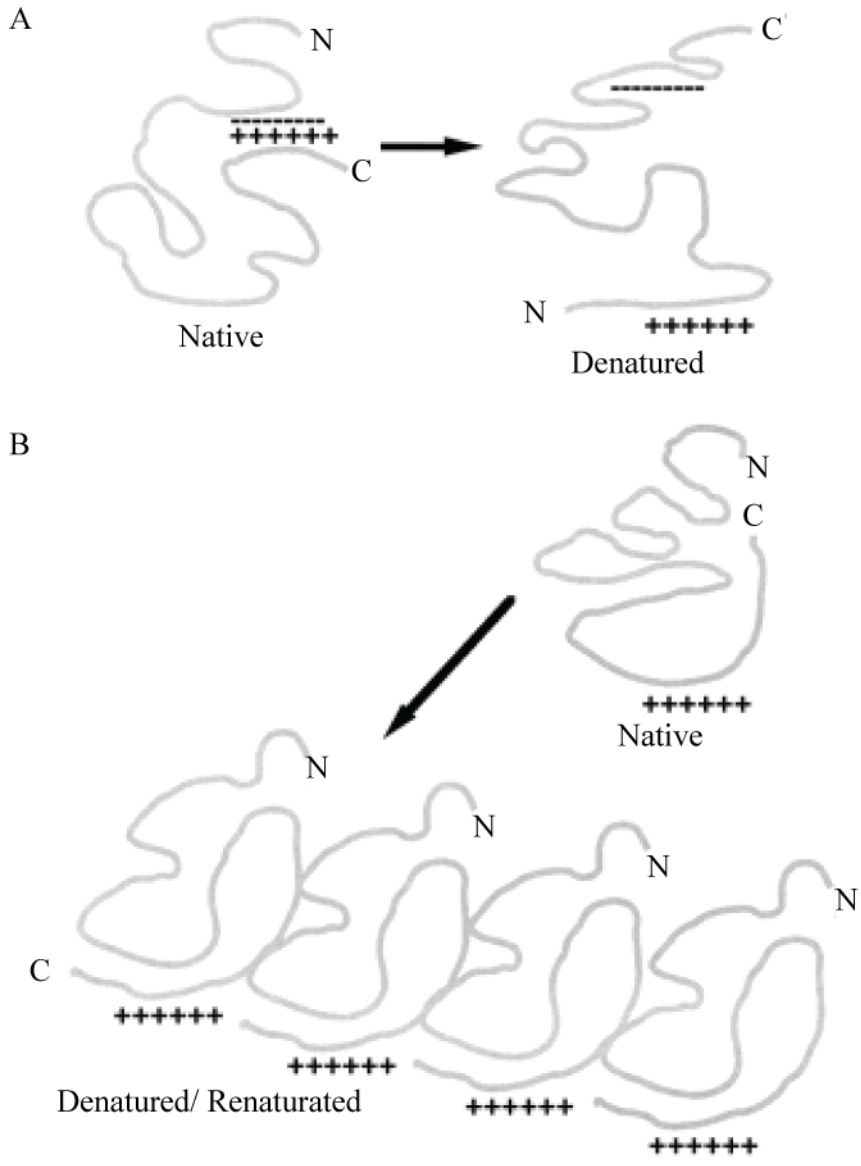

Figure 1.4. The two proposed models for the HBD in VN. (A) HBD basic residues are buried in native VN, and are stabilized by the acidic residues at the N-terminal. The HBD domain gets exposed by heat or chemical denaturation. (B) The HBD is

exposed on the surface of native VN, and denaturation is accompanied by the self-association of VN into its multivalent form (Zhuang *et al.* 1997).

These contradicting positions will only be resolved with the 3-D structural resolution of VN. However, attempts to crystallize the whole protein have been unsuccessful, due to its large size and extensive glycosylation. Moreover, the protein is too large for high-resolution structural determination by nuclear magnetic resonance. Lynn and colleagues used computational analysis to predict the 3-D form for the complete protein (Lynn *et al.* 2005). They surmised that VN is a bi-lobed cylinder, with the N-terminal within the upper smaller lobe, a hemopexin-like domain (containing the HBD) filling the lower lobe, and the flexible linker domain between them. They found that all domains were both presented and accessible on the surface of the molecule, which supported the latter model of the VN-HBD. It is best envisaged with a radius of 30.3 $\pm$ 0.6 Å and a length of 110 Å (Fig. 1.5) (Lynn *et al.* 2005). Xu *et al.* also employed computational analysis to predict a 3-D structure for VN, and then used docking experiments to provide clues for the binding of heparin to it (Fig. 1.6) (Xu *et al.* 2001b). This computed structure predicts that the central and C-terminal domains form a groove wherein the HBD lies. Together these results tend to support the model that the VN in solution is open-faced with little interaction between the acidic and basic residues.

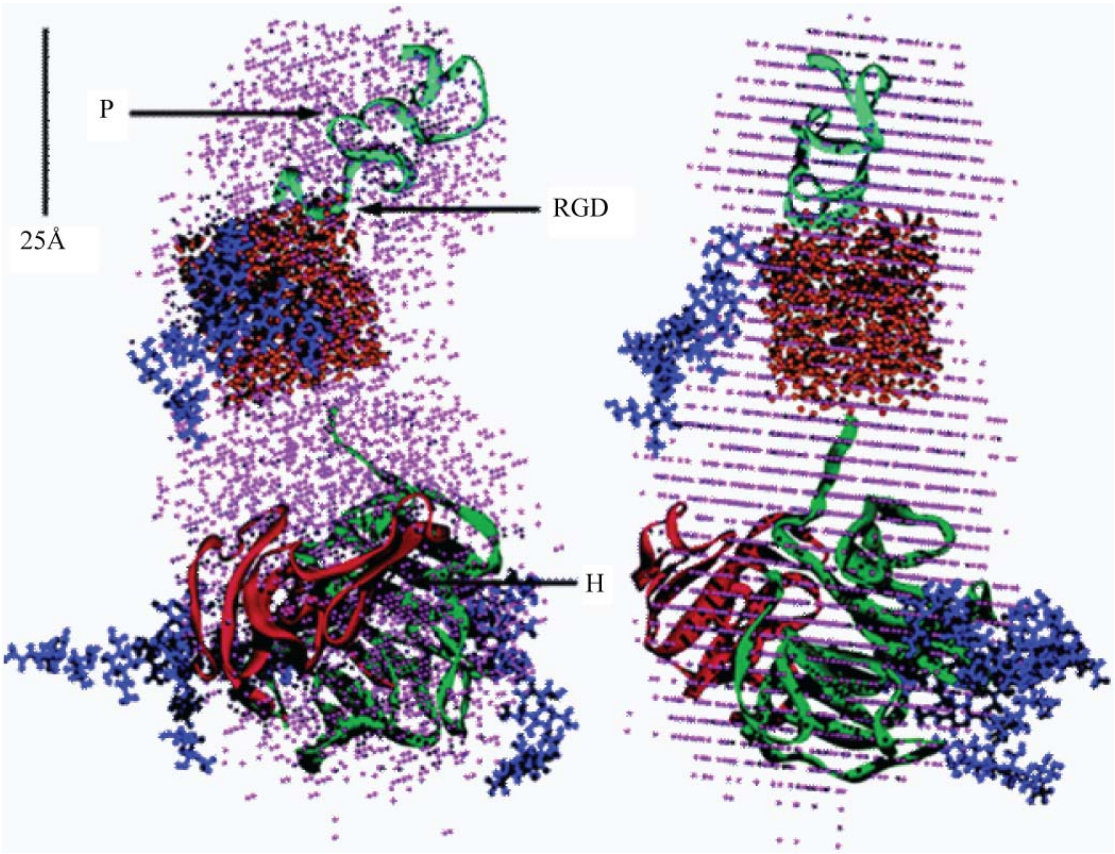

Figure 1.5. Two orthogonal views of the proposed 3-D VN model produced by CONTRAST docked into the GA_STRUCT software. The somatomedin B domain is coloured cyan, the linker region amber, the central domain green, the heparin-binding domain red, and the carbohydrates blue. The consensus envelope is coloured violet. Binding sites for ligands are indicated with arrows and labels: P for PAI-1, RGD for integrins, and H for heparin (Lynn *et al.* 2005).

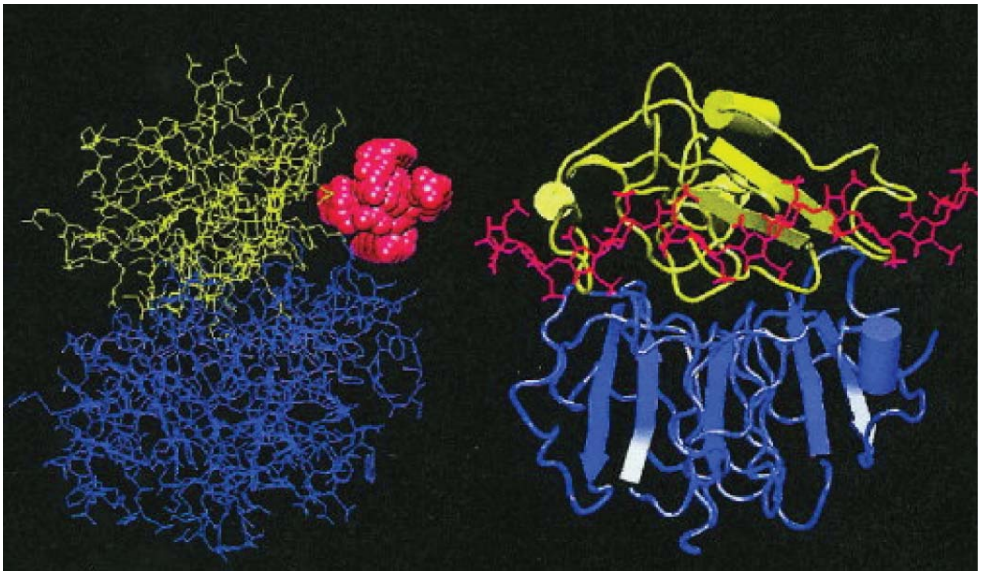

Figure 1.6. Two different views of computed docking conformation between heparin and VN. Heparin is in red; the combined structure of the central and C-terminal are in blue and yellow respectively (Xu *et al.* 2001b). It predicts a groove between central and C-terminal domains for the binding of heparin.

In a landmark paper, Braam *et al.* reported the successful culture of hESCs, for at least 10 passages, on surfaces precoated with 5 μg/ml of recombinant VN (Braam *et al.* 2008). They also identified αVβ5 integrin as the VN receptor. A study by Isik *et al.* showed that αV integrin receptors are important for VN-induced anti-apoptotic survival responses (Isik *et al.* 1998). Rowland *et al.* and Prowse *et al.* both reported using a 10 μg/ml coating of plasma-purified VN for the culture of iPSCs and a 17.5 μg/ml coating of recombinant VN for hESC culture respectively (Prowse *et al.* 2010, Rowland *et al.* 2010). However, neither of these reports determined the threshold amount of VN necessary for the long-term propagation of hESCs, indicating a need to quantify VN substrates (Oh & Choo 2008, Skottman *et al.* 2006, Unger *et al.* 2008). The combination of the ability of VN to support hESC culture, and the presence of an HBD makes VN particularly amenable to further manipulation.

1.3.2. Other ECM proteins

The laminins are a family of glycoproteins with a M_r of ~10^6 that are an integral part of the ECM, particularly the basement membrane. Each of the isoforms contain an α-chain, a β-chain, and a γ-chain, with five, four, and three genetic variants respectively (Timpl *et al.* 1979). Xu *et al.* observed that hESCs are able to avidly attach and proliferate on LN (Xu *et al.* 2001a) and Rodin and colleagues demonstrated that the recombinant LN-511 variant can be used to successfully culture hESCs over many passages (Rodin *et al.* 2010).

Fibronectins (FNs) are a class of structural glycoproteins, with a molecular weight of ~440 kDa, that are found in loose, mesenchymal ECM and exist as protein homodimers linked by disulfide bonds (Hynes 1985). They consist of repeating homologous units of 40, 60 and 90 amino acids. FN binds to cells primarily via the α5β1 integrin and also participates in cell growth, migration and differentiation (Ruoslahti 1988). FN, together with fibrin, plays a critical role in wound healing, contributing to the formation of the blood clots that stop bleeding (Ruoslahti 1988). A key feature of FN-FN assembly is the conformational change from a compact soluble form into the extended, activated dimer via heparin binding (Bushuev *et al.* 1985, Khan *et al.* 1990).

Collagens are the most abundant structural fibres of the ECM, and account for > 90 % bone matrix protein content (Kern *et al.* 2001). They have either a homo- or heterotrimeric α chain structure containing collagenous and noncollagenous domains. The α chain differs in its primary sequence (the Gly-X-Y motifs) and alternative splicing adds to the diversity of this molecule. The collagenous portion of the three α chains forms a coiled-coil structure which constitutes the basic building block. The most abundant form in basement membrane is collagen IV, with its 6 genetically

different α chains. Ludwig *et al.* demonstrated the culturing of hESCs underlayed by a combination of human collagen IV, FN, LN and VN. However, the resulting abnormal karyotype in these cells implied that this complex substrate is not sufficient for such cells (Ludwig *et al.* 2006a).

A comparison of the HBDs in VN, LN and FN is illuminating. The HBDs in LN and FN are juxtaposed to RGD sequences (Aumailley & Gayraud 1998, Timpl & Brown 1994). However, the HBD and RGD motif in VN are at either ends of the protein. This suggests that the act of heparin binding to VN does not directly affect integrin binding. Thus the novel strategy of immobilizing VN via its HBD to GAG-substrates in this thesis deserves a thorough examination of its potential.

1.3.3. Protein immobilization strategies

There are many strategies for immobilizing proteins onto surfaces. These include the non-covalent adsorption of proteins by hydrophobic or electrostatic interactions; classical chemoligation; bioorthogonal site-specific chemoligation; non-covalent biologically-mediated immobilization; covalent immobilization via enzymatically-active fusion proteins; enzyme-catalyzed labelling and immobilization; and non-enzymatic biologically mediated covalent immobilization (Wong *et al.* 2009). However, these methods have their limitations, including reduced or altered protein activity after fixation, low selectivity and/or low immobilization yields. In particular, Marson *et al.* has shown that immobilization of proteins onto surfaces can lead to loss-of-function via steric hindrance or conformational perturbation (Marson *et al.* 2005).

There is thus a need for a process to immobilize sufficient amounts of functional VN on surfaces without deleterious chemical modification. As VN contains

HBD, exploiting this inherent property to immobilized VN onto a heparan glycosaminoglycans substrate is possible.

1.4. Glycosaminoglycans (GAGs)

Together with DNA and protein, carbohydrates are the third class of informational biopolymers that play key roles over a broad range of biological activities (Bertozzi & Kiessling 2001). Carbohydrates can exist as simple sugars (glucose, fructose and galactose) or as glycans, complex conjugates of many simple sugars. In the development and function of complex organisms, glycans play particularly important roles in cell-cell and cell-matrix interactions. Understanding the function and structure of complex sugar molecules with the new analytical techniques that have become available has opened a new frontier, dubbed 'glycobiology', over the past two decades (Rademacher *et al.* 1988). As the informational content of carbohydrates is vastly greater than DNA per unit of structural backbone, a whole new field of "glycomics" has also arisen (Rademacher *et al.* 1988).

1.4.1. Basic features and function of GAGs

Glycosaminoglycans are complex, linear, highly charged carbohydrates that interact with a wide range of proteins (Casu & Lindahl 2001, Jackson *et al.* 1991). These molecules are found on all animal cell surfaces, usually attached to core proteins, and throughout the ECM. They are known to both bind and regulate the function of chemokines, growth factors, morphogens, enzymes and adhesion molecules (Conrad 1998, Jackson *et al.* 1991). GAGs *in vivo* are always surrounded by a shell of water molecules, which causes them to fill space, hydrate tissue and provide resistance to pressure (Champe & Harvey 1994).

1.4.2. Proteoglycans

With the exception of hyaluronic acid, most GAGs are found covalently linked to a core protein to yield a proteoglycan (PG). The protein-sugar linkage involves a specific trisaccharide, composed of two galactose (Gal) residues and a xylose (xyl) residue. It binds to a core protein through an *O*-glycosidic bond (GAG-GalGalXyl-*O*-CH_2-protein) on those serine residues that are followed by a glycine (Gandhi & Mancera 2008, Jackson *et al.* 1991). All animal cells produce PGs and either secrete them into the ECM, insert them into plasma membrane, or store them in secretory granules. The complexity of PGs is high due to many factors such as differential expression of genes encoding the core proteins and differential exon usage, as well as variations in the length and type of GAG attached (Varki 1999). Of particular interest are the heparan sulfate proteoglycans (HSPGs).

HSPGs include aggrecan, perlecan, the syndecans and the glypicans, all classified by virtue of their core protein. Aggrecan, the major PG secreted into cartilage, aggregates into hydrating super-complexes; the syndecans, which are made up of four types of transmembrane core capable of carrying both HS and CS; and the glycosylphosphatidylinositol-attached glypicans (Gandhi & Mancera 2008). PGs have long been known to have affinity for growth factors, cell adhesion molecules and enzymes (Conrad 1998). A particularly well established function of HSPGs is the mediation of FGF-2 dimer formation (Schlessinger 2000).

1.4.3. HSPG in stem cells culture

Studies by Levenstein *et al.* demonstrated that the major components secreted by MEFs that support hESC growth are the HSPGs (Levenstein *et al.* 2008). These HSPGs are able to stabilize and extend the half-life of FGF-2 and are required by hESCs to remain pluripotent. Another study by Abraham *et al.* also identified the importance of HSPGs in feeder layers (Abraham *et al.* 2010), and demonstrated that they were able to maintain hESC lines on a combination of mouse sarcoma HSPG and combinations of ECM proteins. Two other studies by Sasaki *et al.* and Furue *et al.* demonstrated the importance of HS and heparin in promoting hESC self-renewal and growth (Furue *et al.* 2008, Sasaki *et al.* 2008). Chillakuri *et al.* also reported that the heparin-binding domain of VN is required for its oligomerization, which reinforces VN activity during cell adhesion and spreading (Chillakuri *et al.* 2010). Together, these studies provide support for the need to further explore how HS and VN interactions can be manipulated.

Other than hESCs, HS has also been shown to be a critical factor for the proliferation and differentiation of other stem cells such as mouse embryonic stem cells, mesenchymal stem cells, hematopoietic stem cells and neuronal stem cells (Brickman *et al.* 1995, Hagihara *et al.* 2000, Holley *et al.* 2011, Manton *et al.* 2007). Holley *et al.* have shown that soluble heparin and HS can influence the differentiation potential of mESCs (Holley *et al.* 2011). Bramono *et al.* recently showed that human bone marrow stroma-derived HS helps in the expansion of hematopoietic stem cells (Bramono *et al.* 2011). Taken together, these studies act as motivators to explore how HS and VN are able to interact.

1.4.4. Classification of GAGs

Carbohydrate chains on HSPGs are often digested by endogenous heparinase to become soluble GAGs *in vivo*. GAGs are long, unbranched polysaccharides of varying length consisting of characteristic repeating disaccharide units with a wide range of molecular weight (10-100 kDa) (Gandhi & Mancera 2008). The repeating units are made up of uronic acid (D-glucuronic acid or its epimer L-iduronic acid) and an amino sugar (D-galactosamine or D-glucosamine). There are two main types of GAGs: non-sulfated and sulfated (Fig. 1.7). Non-sulfated GAGs include hyaluronic acid (HA), which is synthesized without a core protein and is digested by enzymes at the cell surface directly into the extracellular space. Hyaluronan is the major component in the synovial fluid lubricant within body joints (Itano 2008, Laurent *et al.* 1996). As HA is both non-sulfated and unable to bind VN, this molecule is not able to address the problem of efficient immobilization of VN to culture surfaces, and will thus be dismissed from further consideration.

In contrast, sulfated GAGs include chondroitin sulfate (CSs), dermatan sulfate (DS), keratin sulfate (KS), heparin and heparan sulfate (HS). These sulfated GAGs are secreted covalently attached to a core protein on the cell surface to yield the various species of PG described above. This is summarized in Figure 1.7.

The CSs are chains of the alternating sugars N-acetylgalactosamine and glucuronic acid. They have a molecular weight of 5-50 kDa, and are the most abundant GAGs in the mature vertebrate body. They are found particularly in cartilage, tendon, ligament and aorta (Varki 1999). DS is most common GAG in skin, blood vessels and heart valves, with a molecular weight of 15-40 kDa (Trowbridge & Gallo 2002, Varki 1999). KS is the most heterogeneous GAG, and can be found in

cartilage and cornea. It has a molecular weight of 4-19 kDa and may be fucosylated (Funderburgh 2000, Varki 1999).

Of all the many forms of HS, heparin has the highest negative charge of any biological molecule known, and is synthesized and stored exclusively in connective tissue mast cells. In contrast, HS contains higher levels of acetylated glucosamine, and is thus less sulfated than heparin. It is expressed on all mammalian cell surfaces and ECM (Lindahl & Kjellen 1991, Varki 1999). Therefore HS was the GAG of choice in this thesis for the capture of VN.

Glycosaminoglycans	Disaccharide units	Features
Hyaluronic acid	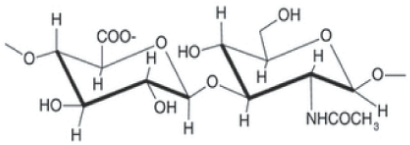 D-GlcA - β(1→4) - D - GlcNAc-α(1→4)	Molecular weight 4 - 8000 kDa Non-sulfated, non-covalently attached to proteins in the ECM, also found in bacteria Usually found in synovial fluid, vitreous humour, ECM of loose connective tissue Excellent lubricators and shock absorbers
Chondroitin sulfate	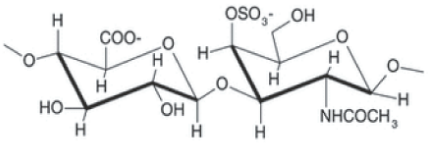 D-GlcA - β(1→3) - D - GalNAc4S-β(1→4)	Molecular weight 5 - 50 kDa Most abundant GAG in the body Found in cartilage, tendon , ligament, aorta Bind to proteins to form proteoglycan aggregates
Dermatan sulfate	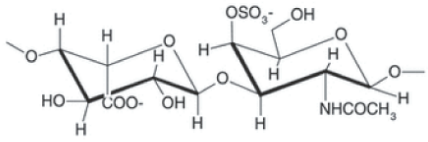 L-IdoA - α(1→3) - D - GalNAc4S-β(1→4)	Molecular weight 15 - 40 kDa Found in skin, blood vessels, heart valves
Keratan sulfate I and II	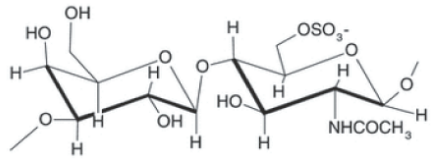 D-Gal- β(1→4) - D - GalNAc6S-β(1→3)	Molecular weight 4 - 19 kDa Most heterogenous GAG KS I found in cormea KS II found in cartilage aggregated with CS
Heparin	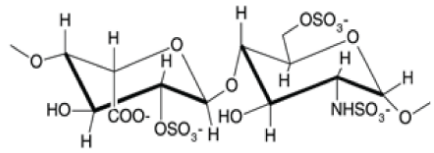 L-IdoA2S- α(1→4) - D - GlcNS6S-α(1→4)	Molecular weight 10 - 12 kDa Intracellular component of mast cells
Heparan sulfate	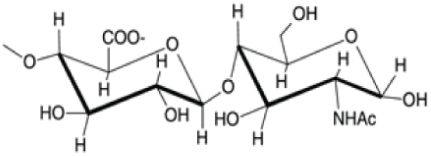 D-GlcA- β(1→4) - D - GlcNAc-α(1→4)	Molecular weight 10 - 70 kDa Extracelluar component found in basement membrane Ubiquitous component of cell surfaces

Figure 1.7. Structures and properties of various glycosaminoglycans. Adapted from Gandhi *et al.* (Gandhi & Mancera 2008).

1.4.5. Sulfated GAGs: heparin/heparan sulfate

Heparin, a hypersulfated variant of the HS family, has been studied extensively because of its well known function in anti-coagulation (Capila & Linhardt 2002). Heparin was first discovered in 1916 in liver extracts; it was discovered through its ability to prolong the process of blood clotting. It went into widespread clinical use as an anti-coagulant in 1935, after its production become industrialized (Best 1959). It has gone on to become one of the most important ever products of medical science (Serruys *et al.* 1998). It provides a reason why other heparin-like sugars may have therapeutic utility (Bramono *et al.* 2012). HS, on the other hand, has a more recent history. It was first identified as an impurity in heparin production, but has since been found to be critically involved in a variety of biological processes (Linker *et al.* 1958).

Heparin and heparan sulfate (HS) consist of repeating uronic acid-(1→4)-D-glucosamine disaccharide subunits. Unlike other GAGs, the highly variable pattern of substitutions on their subunits gives rise to different, highly complex N-sulfation, O-sulfation and N-acetylation sequences (Fig. 1.8).

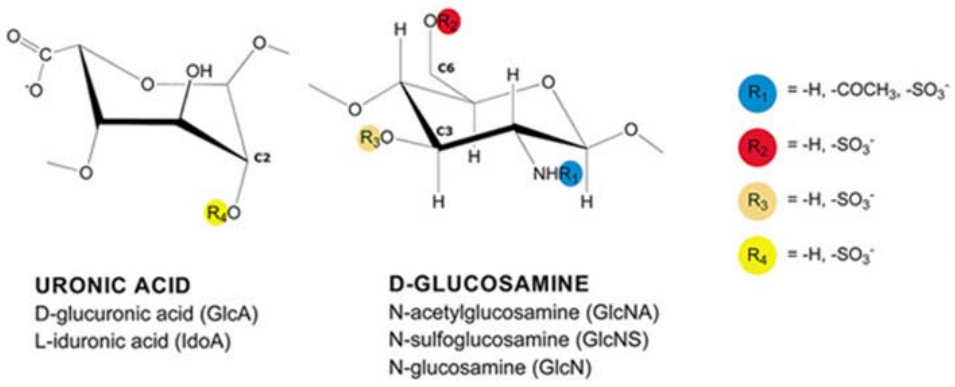

Figure 1.8. Diagram of the various N-, O- and N- substitutions on a monosaccharide subunit of heparin and HS (Ori *et al.* 2008).

The most abundant disaccharide in heparin is the trisulfated IdoA(2S)-(1→ 4)-GlcNS(6S) unit, which gives rise to the extraordinarily high charge density of these chains (an average 2.5 sulfate groups per disaccharide) (Linhardt *et al.* 1992). One corollary of this density is heparin's propensity to promiscuously bind a vast range of proteins. In contrast, the most common disaccharide in HS is the unsulfated GlcA-(1→4)-GlcNAc, which in turn is organized in such a way as to give rise to segregated blocks of unsulfated N-acetyl (NA) residues and "domains" of highly sulfated, heparin-like IdoA-(1→4)-GlcNS disaccharides. It thus has an average of less than 1 sulfate per disaccharide (Lane 1989). This classic domain structure was first proposed by Gallagher and colleagues (Lyon *et al.* 2000). The N-acetyl (NA) and heparin-like N-sulfated (NS) domains are separated by NA/NS transition domains (Fig. 1.9). Thus, the functionally significant, protein-binding sequences of HS are encompassed in the highly sulfated NS domains spaced out by the intervening unsulfated NA domains such that at least one, and up to 6 distinct protein-binding sites may reside on one chain. Thus HS is a key way of integrating combinations of extracellular signalling on cell surfaces to drive specific patterns of gene expression. The problem of using heparin (which displays low selectivity for proteins) as a model for tissue-relevant HS, (which displays much higher selectivity) becomes apparent.

This diversity of HS structure in turn gives rise to a wide range of biological function. In rare cases, the R1 position of the D-glucosamine subunit is neither sulfated nor acetylated, which affords the possibility of utilizing naked primary amine groups for immobilization reactions (Fig. 1.8). Table 1.2 summarizes the differences between HS and heparin.

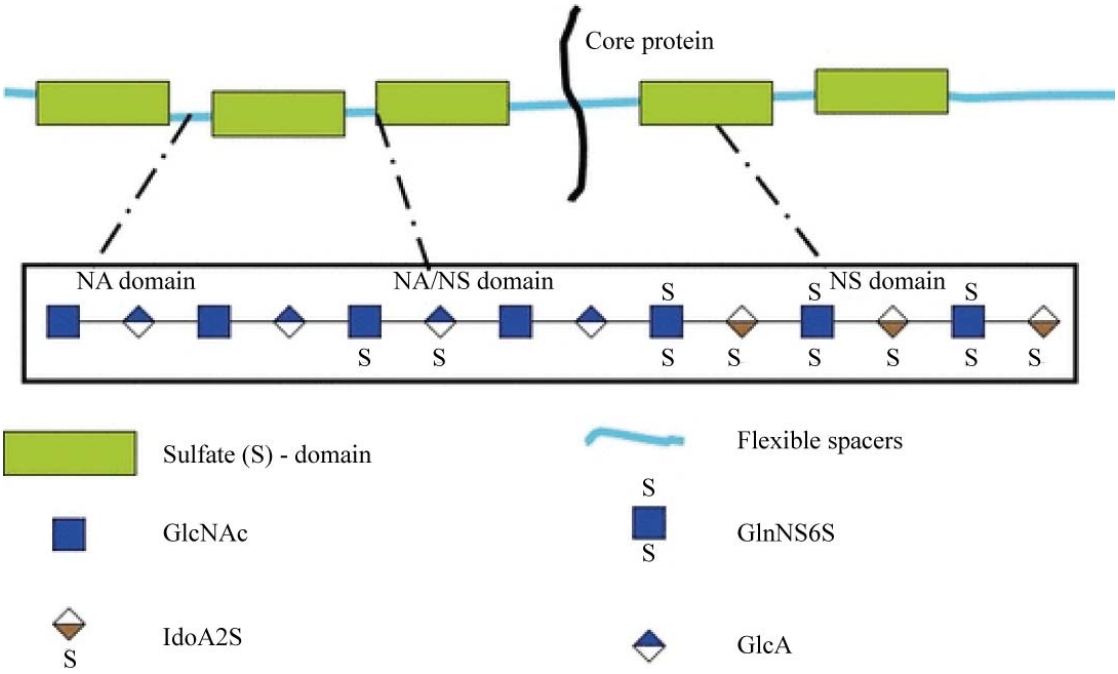

Figure 1.9. Diagram of the sulfated (NS) and non-sulfated (NA) domains in heparan sulfate chains (Gandhi & Mancera 2008).

Table 1.2. Differences between heparin and heparan sulfate (adapted from Gandhi *et al.*) (Gandhi & Mancera 2008).

Characteristics	Heparan sulfate	Heparin
Size	10-70 kDa	7-20 kDa
N-sulfation	40-60%	≥80%
Binding to antithrombin	0-0.3 %	~30%
Site of synthesis	Virtually all cells	Mast cells

The binding of proteins to heparin or HS is primarily electrostatic, involving interactions between functional cationic groups of the protein and the abundant anionic sites on heparin or HS. The other interactions, such as the van der Waals forces, hydrogen bonding and the hydrophobic interactions with the carbohydrate backbone, are comparatively minor in extent (Caldwell *et al.* 1996). The numbers of proteins with heparin-binding propensities number at least several hundred (Table

1.3). Such proteins usually possess a variation on the Cardin-Weintraub consensus sequence XBBBXXBX (where B is lysine, arginine or histidine and X is a hydropathic residue). The proposed sequence arose from an analysis of the structures of 21 heparin-binding proteins (Cardin & Weintraub 1989). There has been an increasing realization over the last 20 years that the specific sequences in the NS and NA/NS domains have been selected for their ability to interact with targeted proteins, which results in regulation of that protein's activity (Lindahl *et al.* 1998, Salmivirta *et al.* 1996, Turnbull *et al.* 2001). What is most notable from examination of such heparin-binding sequences is that each sequence is different (Table 1.3), implying that there is a different, specific sugar domain for each protein. On the other hand, the non-selective binding of proteins to heparin is almost certainly due just to the sheer charge density of the sulfate groups (Salmivirta *et al.* 1996).

Table 1.3. A small subset of the heparin-binding proteins that contain variations on the Cardin–Weintraub consensus sequence XBBBXXBX (Cardin & Weintraub 1989).

Proteins	XBBBXXBX
Annexin II	KIRSEFKKKYGKSLYY
Vitronectin	QRFRHRNRKGYRSQRG
ApoB	KFIIPSPKRPVKLLSG
FGF-2	GHFKDPKRLYCKNGGF
NCAM	DGGSPIRHYLIKYKAK
Protein C inhibitor	GLSEKTLRKWLKMFKK
AT-III	KLNCRLYRKANKSSKL
ApoE	SHLRKLRKRLLRDADD
Fibrin	GHRPLDKKREEAPSLR
FGFR-1	AAPVAHLKKEMK
B-thromboglobulin	PDAPRIKKIVQKKLAG
Insulin-like growth factor-binding protein-3	DKKGFYKKKQCRPSKG

Historically, the most stereotypical heparin-binding protein has been FGF-2. Work on this interaction has progressed to a stage where X-ray crystal structures of a 2:2:2 dimeric ternary complexes of FGF-2, fibroblast growth factor receptor-1 (FGFR1) and a heparin decasaccharide has been resolved (Schlessinger 2000, Turnbull *et al.* 1992). A more physiological model was proposed by Pellegrini *et al.,* who reported a crystal structure with the stoichiometric ratio 2:2:1 of FGFR2:FGF1:heparin decasaccharide underlying the conformational activation of the receptor by the sugar (Pellegrini *et al.* 2000). The crystal structures revealed the precise binding surfaces of FGF-2 for heparin and confirmed a role for heparans in FGF-2-FGFR1 interactions.

The processes of cell attachment, spreading and motility involve HS in the ECM collaborating with cell-surface receptor integrins (Fig. 1.10). In analogy to FGF-2, the large multidomain ECM proteins such as FN, LN and VN all have HBDs, which have allowed for the isolation of ECM-targeted HS isoforms in our laboratory. FN binds to HS chains on the cell surface, so enabling an appropriate integrin to induce cell spreading and focal adhesion formation (Couchman *et al.* 2001). The balance between adhesion and motility in cell depends on the integration of signals mediated through binding to PGs and integrin-based adhesion mechanisms.

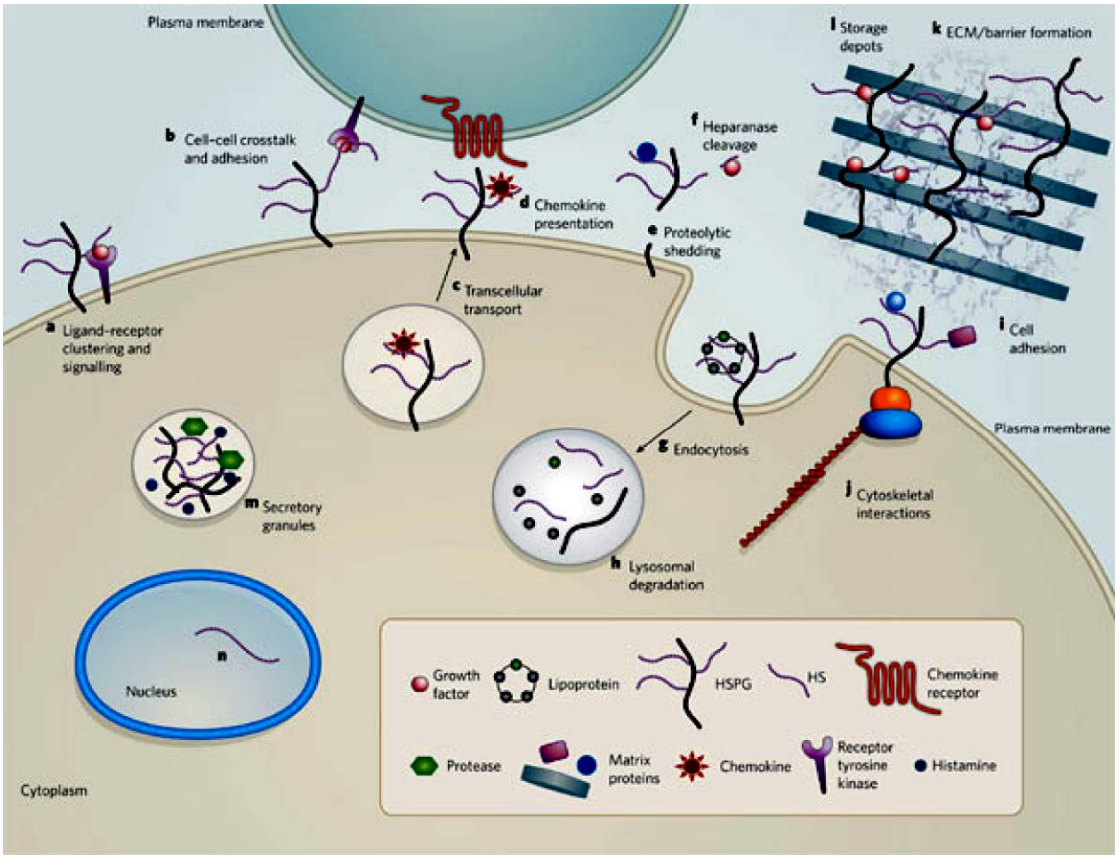

Figure 1.10. Role of HS in cell physiology (Bishop *et al.* 2007).

1.4.6. Structural characterization of heparin/ HS

The development of rapid and reliable methods for the sequencing and synthesis of oligonucleotides and peptides have made the study of protein and DNA structure and function routine. However, the lacks of analogous techniques for the study of complex carbohydrates have made their study exceptionally difficult. Moreover, most oligosaccharides are branched structures and usually present as a heterogeneous population; this further complicates their elucidation. Therefore, glycobiology faces more fundamental challenges than do protein or DNA research.

A complete structural analysis of heparin/HS would involve identification and quantification of the uronic acid (1→4) glucosamine disaccharide building blocks, determination of their sequence within their functional domains, and characterization of the 3-D conformations of the polysaccharide chain, especially after protein

docking. The importance of this is underlined by the first functional HS sequence ever deduced, the pentasaccharide sequence in heparin that is responsible for its anti-thrombolytic activity (Lindahl *et al.* 1979).

The disaccharide composition of HSs can be elucidated through a series of enzymatic cleavages of the glycosidic bond (Desai *et al.* 1993b, Shriver *et al.* 2000, Venkataraman *et al.* 1999) or by deaminative hydrolysis by nitrous acid (Bienkowski & Conrad 1985, Shively & Conrad 1976). The *Flavobacterium heparinium* enzymes heparinase I, II and III have been shown to cleave glucosamine-(1→4) uronic acid glycosidic bonds of differing structure. Heparinase I (Enzyme commission number (E.C. 4.2.2.7)) has high selectivity for IdoA (2S) glycosidic bonds, where the glucosamine can be either GlcNS, GlcNS (6S) or GlcNS (3,6S), and a secondary specificity for GlcA (2S) in highly sulfated regions (Desai *et al.* 1993b, Venkataraman *et al.* 1999). Heparinase II (no E.C. number) will cleave glycosidic bonds containing both 2-O-sulfated and 2-OH uronic acids; hence these two enzymes cut within sulfated domains (Venkataraman *et al.* 1999). Heparinase III (E.C. 4.2.2.8) has high selectivity for 2-OH GlcA-containing glycosidic linkages (Desai *et al.* 1993b, Shriver *et al.* 2000), and thus cleaves between highly sulfated domains to liberate functional domain units. The digestion sites for the heparinases are summarized in Figure 1.11. When all 3 heparinases are used in combination, they can degrade heparin or HS to > 90% completion (Karamanos *et al.* 1997, Vynios *et al.* 2002) (Fig. 1.12). Digestion products can be separated chromatographically by size and degree of sulfation, and a crude compositional analysis performed. However, HS sequence analysis or 3-D structure determination both remain extremely problematical (Skidmore *et al.* 2009, Turnbull *et al.* 1999). Compositional analysis can provide important information about the relative amounts of the disaccharides present in HS. The disaccharides can

be analyzed by strong anionic exchange high performance liquid chromatography (SAX-HPLC) (Skidmore *et al.* 2009), polyacrylamide gel electrophoresis (PAGE) (Hampson & Gallagher 1984) or capillary electrophoresis (CE) (Lamari *et al.* 2001) by comparing their retention rates to those of known disaccharides standards.

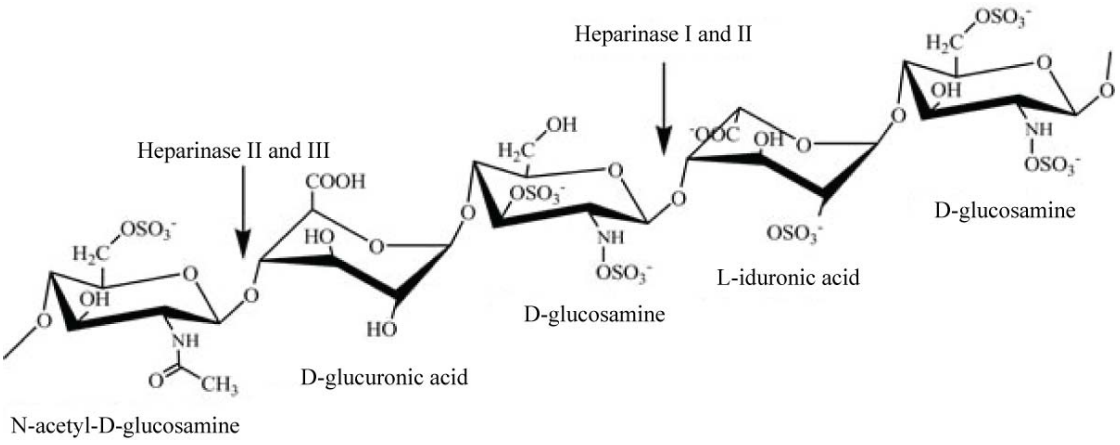

Figure 1.11. Heparinase I, II and III digestion sites on heparin and HS (Malavaki *et al.* 2011).

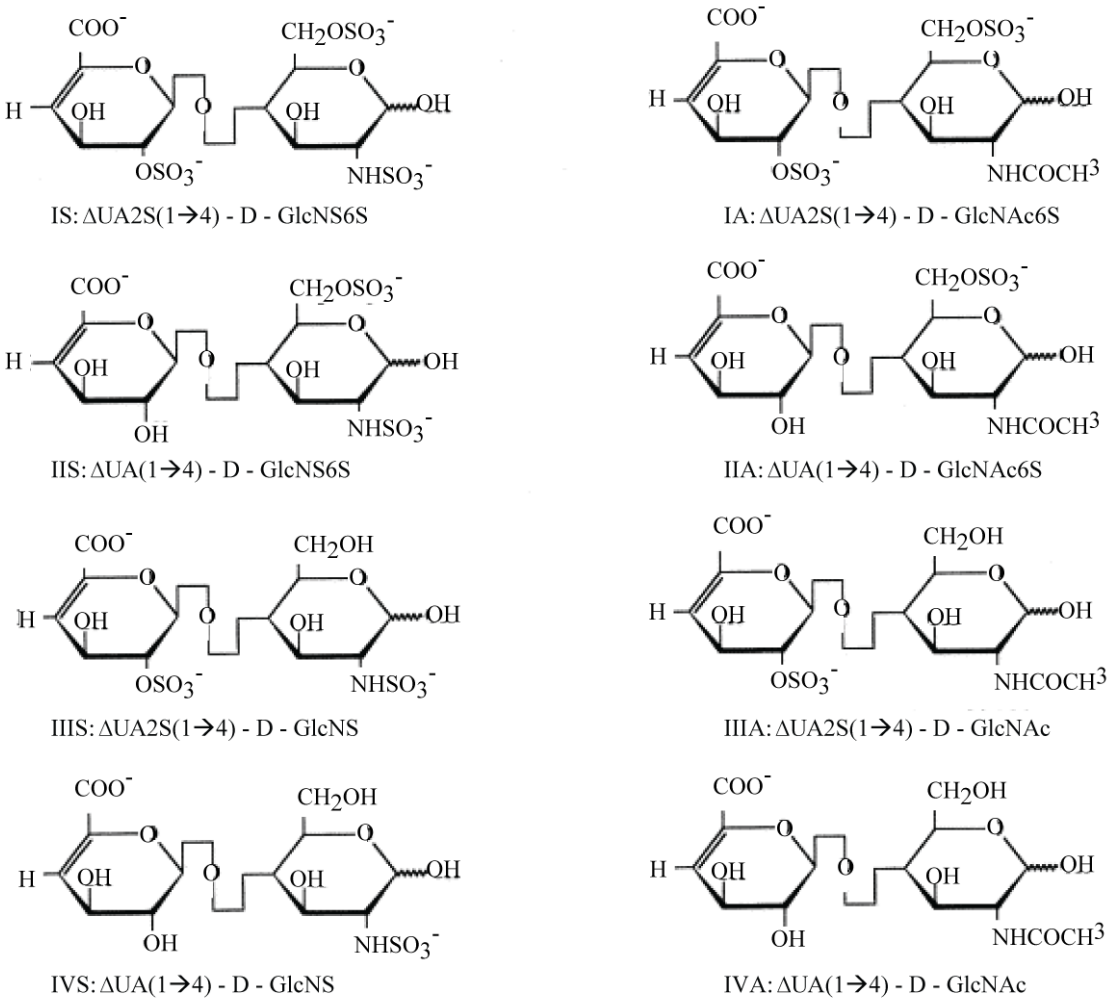

Figure 1.12. The 8 disaccharides generated after digestion of heparin with heparinase I, II and III (Ruiz-Calero *et al.* 1998).

The most convenient mode for disaccharide analysis is CE, which is not only the most sensitive technique but which uses only very small amounts of sample as compared to HPLC and PAGE (Lamari *et al.* 2001). In CE, disaccharides are separated by a voltage through an uncoated fused-silica capillary with reverse polarity and low pH (3.5). When voltage is applied, the walls of the capillary became negatively charged, which causes an electro-osmotic flow (EOF) of the buffer species towards the anode because of the reverse polarity separation. The EOF thus moves all analytes to the anode and the separation of the solutes is by the vector sum of EOF

and electrophoretic mobility (EM), which is proportional to the charge density of the molecule. Disaccharides are negatively charged, so the EM is towards the anode. As these two driving force counteract each other, migration depends on the net difference between the two forces and can be detected at 232 nm. Karamanos *et al.* first described the separation of heparinase-digested disaccharides by 20 kV reverse polarity CE. He was able to distinguish 12 different disaccharides species (Karamanos *et al.* 1996). Ruiz-Calero *et al.* subsequently also demonstrated the separation and quantification of 8 heparin disaccharide species using a formic acid buffer, 15 kV reverse polarity at pH 3 (Ruiz-Calero *et al.* 1998). Militosopoulou *et al.* also described a 30 kV reverse polarity separation of 12 heparinase-digested heparin and HS species in phosphate buffer, pH 3.5 (Militsopoulou *et al.* 2002). An example of just such a CE electropherogram is depicted in Figure 1.13. The latter authors also detected specific fragments of HS disaccharides that bind to FGF2 by incubating the digested species with FGF2 and re-electrophoresing of the mixture. Even higher sensitivities can be obtained by derivatization of digested disaccharides with a-aminoacridone (AMAC) and combining it with laser-induced fluorescence (LIF) detection (Militsopoulou *et al.* 2002).

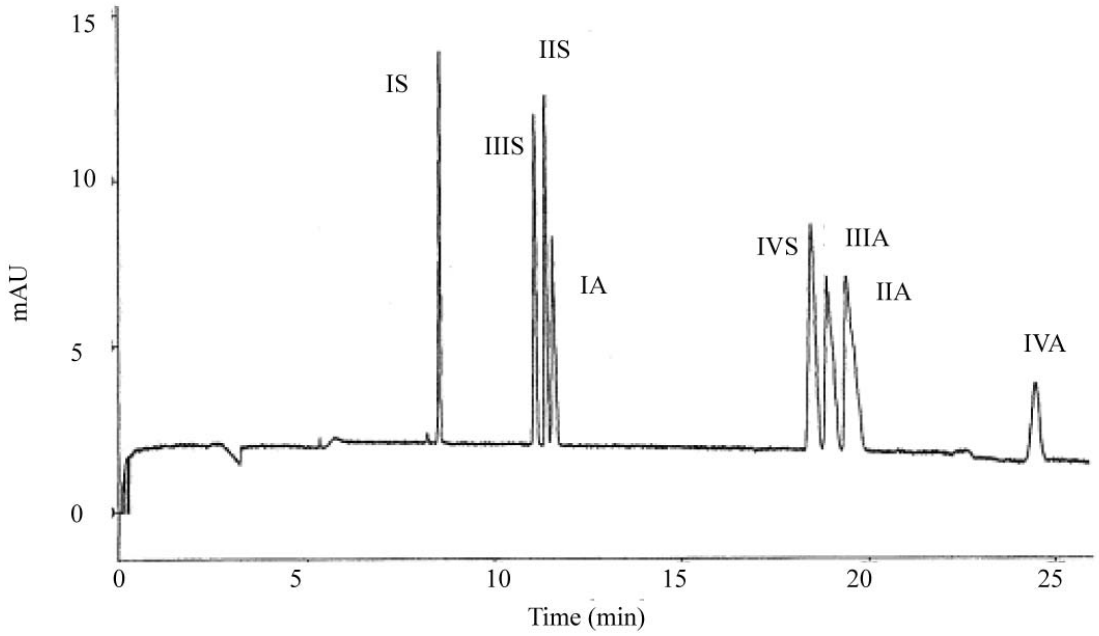

Figure 1.13. An example of CE electropherogram isolated with 60 mM formic acid buffer, reverse polarity of 15 kV at pH 3 (Ruiz-Calero *et al.* 1998). Each peak represents the individual disaccharide units shown in Figure 1.12.

Mass spectrometry (MS) is another method that can provide enormous amounts of information about HS structures. Studies have involved fast-atom bombardment, electrospray ionization, liquid secondary desorption/ ionization MS or matrix-assisted laser desorption ionization (MALDI) MS to determine the mass of sulfated oligosaccharides (Chai *et al.* 1995, Chai *et al.* 1998, Desaire & Leary 2000, Khoo *et al.* 1993, Mallis *et al.* 1989, Rhomberg *et al.* 1998). Chemically discrete oligosaccharides that were produced from the depolymerization of heparin with nitrous oxide or heparinase I and III, followed by two-step separation by size and charge, have also had their masses determined by 2-D ^{1}H-nuclear magnetic resonance (^{1}H-NMR). A major limitation of ^{1}H-NMR is however the large amount of sample required (~0.1 μmol).

As CE is the most sensitive and straight-forward method to determine the composition of HS, this study will employ it to elucidate the composition of each sulfated disaccharide present in heparinase-digested HS samples.

1.5 Methods of immobilizing GAGs

Owning to its avidity for proteins, various heparin-immobilized matrices and surfaces have been developed for both scientific and medical applications (Cox *et al.* 1992, Lincoff *et al.* 1997). For example, polymer-coated stents are being used as controlled release systems for heparin with or without therapeutic proteins, in order to treat the plaques that characterize cardiovascular disease (Serruys *et al.* 1996).

Two broad methods of immobilization of HS, covalent and electrostatic, to couple free GAGs chains to plastic, will now be considered.

1.5.1. Covalent Schiff base chemistry

Heparin oligosaccharides can be produced and readily tethered to amine-coated surfaces with nitrous acid (de Paz *et al.* 2006). The nitrous acid serves to cleave the heparin chain at N-unsubstituted or N-sulfated glucosamine residues, giving rise to a 2,5-anhydromannose unit that contains a reactive aldehyde group at position 1. This aldehyde group is more reactive than the aldehyde group on the reducing end of the sugar, thus allowing Schiff base formation with the amine surface. This method requires an amine-modified surfaces rather than normal tissue culture-treated polystyrene (TCPS) surfaces. The more complicated and specialist processing needed for this precluded this method from our study.

1.5.2. Covalent NHS chemistry

In 2001, Seeberger and colleagues pioneered chemical methods for the automated synthesis of complex carbohydrates directly onto surfaces, in a manner analogous to the printing of DNA and peptide arrays (Plante *et al.* 2001). He utilized 1-ethyl-3-[3-dimethylaminopropyl] carbodiimide hydrochloride (EDC) chemistry to tether the disaccharide unit through an amine added at the reducing end of the synthetic sugar. From this, synthesis is carried out by changing conditions to allow the lengthening of the chains in a step-wise manner by adding extra disaccharide units to produce heparin fragments of a desired length. Such fragments can be used for the study of specific protein interactions with such synthetic HS. It was shown by de Paz *et al.* that protection of the sulfates on chains by azide is important during synthesis and binding of heparin fragments, as the sulfates are critical to FGF-2 binding (de Paz *et al.* 2001).

The process involves mixing small amounts of *N*-hydroxysuccinimide (NHS) with carboxylic acid on the modified surface in a water-free solvent, typically 2-(N-morpholino) ethanesulfonic acid (MES) buffer. EDC is then added to form an unstable active intermediate. EDC is a zero-length cross-linking agent used to couple carboxyl groups to primary amines. This crosslinker has been used in a number of diverse applications, such as forming amide bonds in peptide synthesis, attaching haptens to carrier proteins to form immunogens, and creating amine-reactive NHS-esters of biomolecules (Gao *et al.* 2003, Kimura *et al.* 1991, Mera *et al.* 2008). It reacts with carboxyl to form an amine-reactive O-acylisourea intermediate, and, if this intermediate does not encounter an amine, will hydrolyze and regenerate the carboxyl group (Fig. 1.14). Such a technique may prove attractive for fundamental studies, but over the long-term, the cost and the many steps involved, including the sequential

protection and deprotection of functional groups, render the technique just too inefficient and complicated for large-scale cell culture.

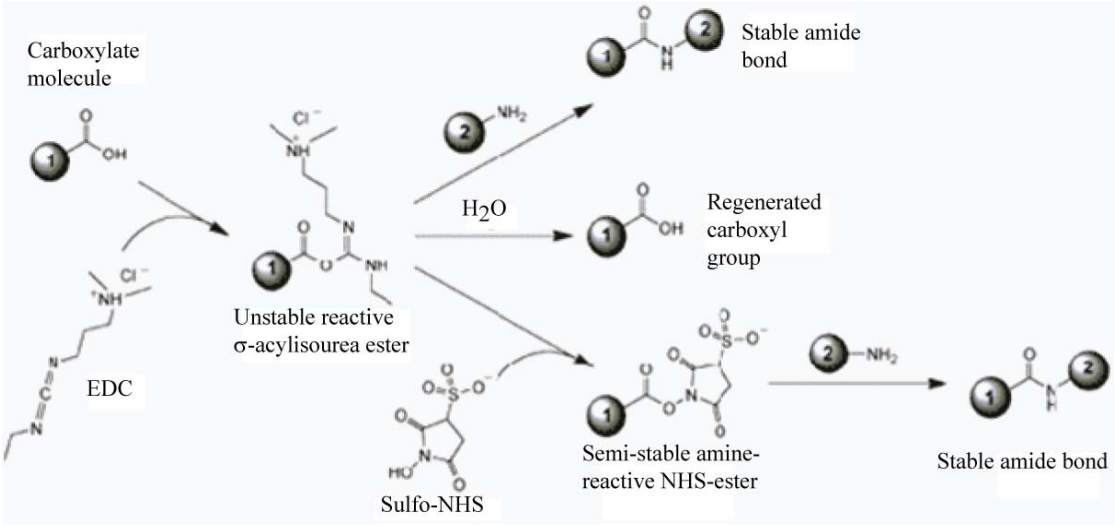

Figure 1.14. EDC reaction scheme (Zhao *et al.* 2010).

In this study, the immobilization of HS onto TCPS was explored using EDC chemistry as a first strategy, primarily because of the domain structure of HS. HS contains ~ 30% primary amines on the glucuronic acid, many of which are available to form covalent amide linkages between the amine and carboxyl group on TCPS.

1.5.3. Coupling of GAGs with BSA

Several groups have reported the covalent coupling of heparin, HS or CS with BSA to facilitate the immobilization of heparin onto surfaces (Feng *et al.* 2004, Hasan *et al.* 1999, Higai *et al.* 2011, Najjam *et al.* 1997, Nishioka *et al.* 2007). It facilitates the immobilization of heparin by utilizing its reducing end and covalently binding it to an acceptor protein via sodium cyanoborohydride. The heparin-BSA complex is then coated onto ELISA plate wells overnight. However, the BSA, being large and globular, is prone to interfering with the steric freedom of the sugar (Rees *et al.* 2004).

1.5.4. Biotinylated GAGs

Another approach for the immobilization of GAGs is their biotinylation and coupling to streptavidin-coated surfaces (Foxall *et al.* 1995, Hasan *et al.* 1999, Najjam *et al.* 1997, Parker *et al.* 2009, Roy *et al.* 2011). A few groups have used this method, either by attaching the biotin to the GAG's carboxylate (Boucas *et al.* 2008, Parkar & Day 1997, Yang *et al.* 1995) or amino groups (Harris *et al.* 2008, Mahoney *et al.* 2005, Nadesalingam *et al.* 2003). However, the efficiency of biotinylation is variable and cannot be controlled; this can have negative effects on GAG function. A study by Roy *et al.* has shown that modifying the sequences of heparin, particularly the N-domains, can have a major impact on its biological activities (Roy *et al.* 2011). Saito *et al.* demonstrated that DS has higher protein-binding activity when biotin is attached to the free amino group instead of the uronic acid (Saito & Munakata 2005). However, other studies have shown that labelling hyaluronan is more effective if the carboxylate group was used, notwithstanding that this reaction is known to alter the activity of heparin (Yang *et al.* 1995). The contradictions kicked up by such studies highlight the fact that any method for immobilizing GAG via biotinylation needs to be carefully optimized, and is GAG-specific.

1.5.5. Passive adsorption to TCPS

Both proteins and GAGs are polyelectrolytes that contain functional groups that can fully dissociate in solution. Heparin has an average of 2.5 sulfates (SO_3-) per disaccharide unit. In a solution containing uncharged entities, the chain will adopt a random conformation. However, in heparin, the combination of the high negative charge and restriction of the rotation of glycosidic bonds in each disaccharide repeats acts to cause repulsion, thus keeping the structure in an open right-handed twist

conformation when in water (Ferro *et al.* 1990, Mikhailov *et al.* 1997). If high salt is added, it acts to screen the negative charge and lessen the effect of repulsion, allowing a more coiled structure. In physiological solutions, GAGs do not bind to plastic surfaces, as shown by both Mahoney *et al.* and Robinson *et al.*, thus restricting its application to passive adsorption onto TCPS (Mahoney *et al.* 2004, Robinson *et al.* 2008).

1.5.6. Plasma polymer films

Plasma-based approaches have gained popularity for the creation of surfaces designed to be in contact with biological environments; such surfaces are known as bio-interfaces. This method inserts chemically reactive groups onto non-reactive substrates. Plasma methods can be classified into 3 broad categories: plasma treatment, plasma etching and plasma polymerization. Plasma treatment utilizes gases such as argon, nitrogen, oxygen or methane in order to insert or substitute chemical functionalities onto substrates or to create radicals for crosslinking or surface grafting. Plasma etching is the bombardment of surfaces with high speed positive charge, so creating charged species on the surface of the material. Plasma polymerization involves the fragmentation of the precursor and deposition of organic monomers, so creating a coated polymer film on surfaces that do not contain regular repeats such as conventional polymers (Ward & Short 1993, Ward & Short 1995). It is done under reduced pressure, and highly functionalized surfaces can be produced (Beck *et al.* 2001, Rinsch *et al.* 1996). This study will utilize plasma polymerization of amine-containing groups onto TCPS surfaces to create a net positive charge surface (Chatelier *et al.* 1997) for the immobilization of negatively charged HS.

Amine polymers are easy to fabricate, and a good coating can be obtained over a broad range of plasma parameters. Amine-containing surfaces can be prepared via either ammonia plasma treatment or plasma polymerization of allylamine (AA) monomers. Ammonia plasma treatment has the drawback of the short-lived nature of the treatment on some polymer substrates, such that the treated substrate reverts back to its original state (Chatelier *et al.* 1995a, Chatelier *et al.* 1995b, Xie *et al.* 1992). Therefore, plasma polymerization with AA monomers is the method utilized in this study. Although it is also possible to create amine groups on TCPS using nitrogen plasma treatment, its efficiency and selectivity is low (Meyer-Plath *et al.* 2003). Barry *et al.* have shown that plasma polymerization of scaffold matrices can encourage cells to migrate into the pores and increase the population density of cells throughout the scaffold (Barry *et al.* 2005). This demonstrated that plasma polymerization is cell culture-compatible.

Many different aminated monomers have been used to create positively-charged surfaces, including allylamine (Gancarz *et al.* 2003, Mahoney *et al.* 2004, Robinson *et al.* 2012, Swaraj *et al.* 2005), diaminocyclohexane (DACH) (Lassen & Malmsten 1997), heptylamine (Gengenbach *et al.* 1994, Kingshott *et al.* 2002) and ethylenediamine (Gengenbach *et al.* 1996). This study will focus on allylamine polymerization, because the density of amine groups created by each methods is such that DACH > allylamine > heptylamine (Kingshott *et al.* 2002, Muller & Oehr 1999). Even though DACH yields higher amine group density, measurements done with surface fluorescence spectroscopy neither correlate with the percentage of nitrogen measured by XPS nor the content of primary amino groups with apparent fluorescence.

Allylamine ($C=C-C-NH_2$) has a double bond that encourages higher deposition rates through a combination of plasma polymerization and conventional radical addition polymerization. The density of amine groups on substrates can be controlled using octa-1,7-diene (France *et al.* 1998).

There are many studies that show bioactive molecules can be successfully immobilized onto plasma-treated amine groups, including DNA (Zhang *et al.* 2005, Zhang *et al.* 2003), Protein A (Sano *et al.* 1993), hyaluronic acid (Mason *et al.* 2000), heparin (Steffen *et al.* 2000) and enzymes (Gancarz *et al.* 2003, Muguruma *et al.* 2000) using EDC chemistry. However, there are drawbacks to using EDC to covalently link carboxyl and amine groups onto surfaces. The EDC can activate carboxyl groups in such a way that they bind to amine groups on the same molecule, or molecules other than the amine groups on the designated surface. This leads to the aggregation of molecules, and adsorption to surfaces and thus biological function being compromised. Thus using EDC to link HS onto amine surfaces is a risky option. For this reason, we will employ here non-covalent methods for immobilizing HS onto amine surfaces.

A recent study by Robinson *et al.* demonstrated that AA could be coated onto the internal surfaces of microplates using plasma polymerization (Fig. 1.15) (Robinson *et al.* 2012). This surface is able to bind GAGs electrostatically without affecting biological function. This was shown when the GAGs retained the ability to bind osteoprotogerin and the tissue inhibitor of metalloproteinases-3. Other studies also confirmed this finding using ELISA (Mahoney *et al.* 2004, Marson *et al.* 2005).

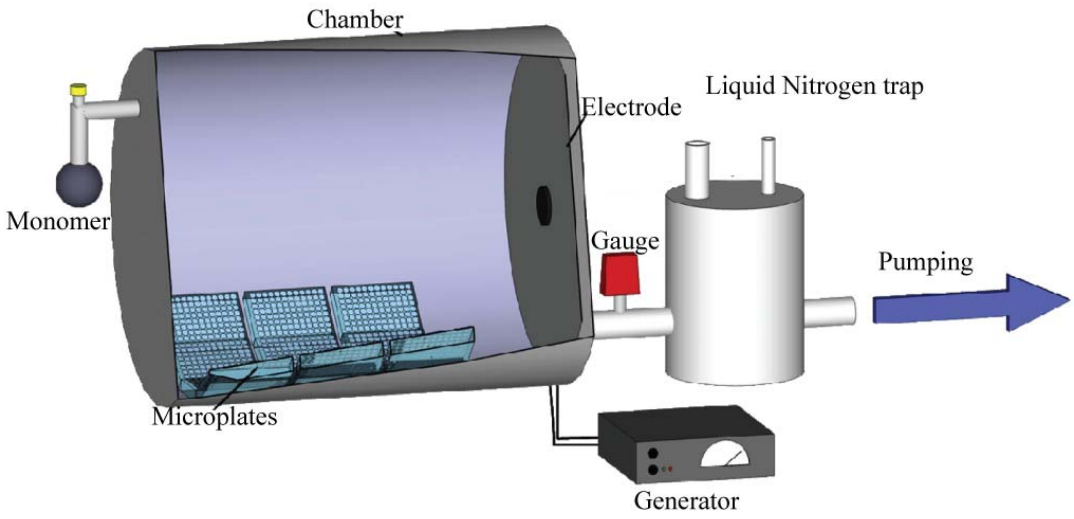

Figure 1.15. A schematic of the plasma reactor. The plates are placed inside the chamber and the generator creates an electromagnetic field that ionizes the allylamine to create plasma. The activated molecules are polymerized onto the plate surface. The gauge serves to isolate the chamber during the reaction and the liquid nitrogen trap acts as waste collection (Robinson *et al.* 2012).

1.6. Surface characterization

For the reliable interpretation of such complicated interactions as the bio-interfacial junctions between adsorbed protein and applied cells, detailed surface analyses of biomaterials is necessary (Castner & Ratner 2002). Therefore, a combination of surface chemical analysis methods and X-ray photoelectron spectroscopy (XPS) will be used in this study to analyze the nitrogen: carbon (N:C) ratio after generating the allylamine polymer coating on TCPS, together with measurements of VN surface density. XPS is a unique and valuable tool for such surface analysis and able to measure the elemental composition of materials at 1 - 10 nm distances from the surface (Delgass *et al.* 1970). Robinson *et al.* used XPS to quantify the amount of carbon, nitrogen and oxygen on AA polymerized surfaces (Robinson *et al.* 2012).

Atomic force microscopy (AFM) will also be used to test the physical roughness of the VN-coated surfaces. AFM is a high resolution (nm) microscope that consists of a cantilever with a sharp tip that scans the material surfaces (Meyer 1992). The forces between the tip and sample lead to the deflection of the cantilever according to Hooke's law and is measured with a suitable detector.

1.7. Thesis outline

1.7.1. Motivation

There is a strong correlation between the global economic burden of critical illness to society and the potential for stem cells to alleviate such problems (Fig. 1.16) (Boston 2001). This is driving stem cell therapy sales exponentially, despite their limited effectiveness (Summit 2007). The potential for hESC therapy to contribute to this growing market are substantial.

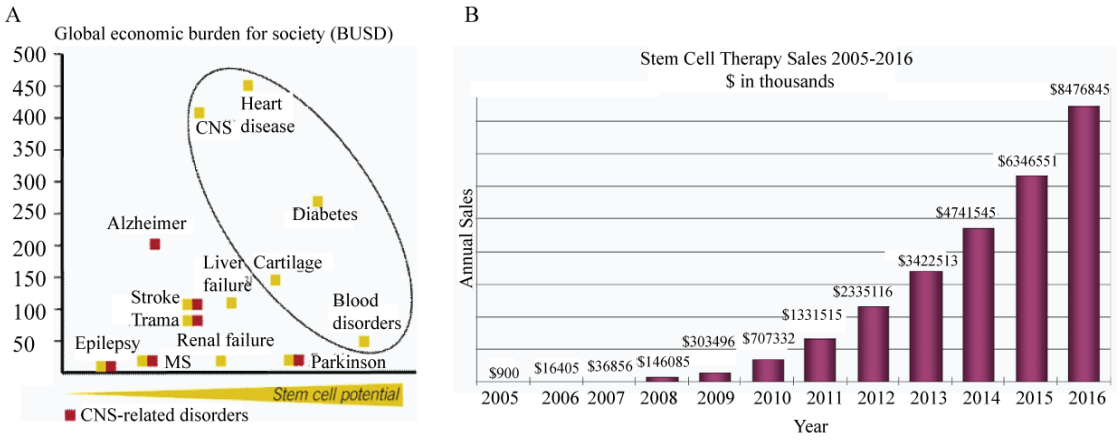

Figure 1.16. Stem cells market research analysis (Adapted from Boston Consulting Group and Stem cell summit, 2007 http://www.stemcellsummit.com/2007/stem-cell-fact-sheet.pdf)

Human PSCs have been posited as being central to such therapeutic strategies if their provision can be made reliable (Goldring *et al.* 2011). The directed differentiation of hESCs down the cardiomyocyte, hepatocyte or insulin-producing

cell lineages carries much promise for regenerative medicine. For example, in 2009 and 2010, the U.S. Food and Administration (FDA) approved two clinical trials for the treatment of grade A thoracic spinal cord injury (NCT01217008 and NCT01344993) (Alper 2009) as well as for macular dystrophy and dry-aged related macular degeneration (NCT01345006 and NCT01344993) (Schwartz *et al.* 2012) that employed cells derived from human embryonic stem cells. Although it is an exciting time for stem cell research, the problem remains that it is still very difficult to continuously preserve these cells in their pristine state prior to differentiation, a property that is essential to ensure subsequent directed differentiation to meet future clinical demands.

However several challenges remain. The first and most important is to remove the reliance of inactivated mouse or human feeder cell layers to culture hESCs. The second is to eliminate the use of Matrigel^{TM}, which is a poorly defined product from murine sarcoma basement membrane. Thirdly, we need to dispense with bovine serum albumin (BSA) and fetal calf serum (FCS) from cell culture media. Lastly, we need to be able to propagate the cells in a naïve state in large numbers.

Cell culture media formulation has made rapid progress, and a number of chemically-defined media such as XVIVO-10, hESF9, mTeSR^{TM}1 and STEMPRO are now available. (Furue *et al.* 2008, Li *et al.* 2005, Ludwig *et al.* 2006b, Wang *et al.* 2007) However, in the area of defined cell culture surfaces, there is still much work to be done. Although many research groups have proposed ways of culturing hESC, including laminin (LN) (Rodin *et al.* 2010, Xu *et al.* 2001a), vitronectin (VN) (Braam *et al.* 2008), fibronectin (FN) (Amit *et al.* 2003), E-cadherin (Nagaoka *et al.* 2010), peptides (Klim *et al.* 2010, Melkoumian *et al.* 2010) or PMEDSAH polymers (Villa-Diaz *et al.* 2010), none of these studies calculated the actual surface density of the

applied compounds, nor their economic cost benefits for commercial scale hESC propagation.

The most widely used method to immobilized ECM protein for cell culture is by passive adsorption onto culture surfaces. This method had been shown by Marson *et al.* to lead to steric hindrance or conformational perturbation, resulting in the loss-of-function to the protein (Marson *et al.* 2005). Therefore, utilizing this method to present sufficient VN for hESC culture is not efficient. Instead of modifying the protein, which might lead to deleterious effects, modifying the surface for efficient VN immobilization is a more rational approach. Therefore, this thesis is aimed at exploring the various strategies that allow the capture of sufficient unmodified VN for hESC culture in a cheap, scalable and efficient manner.

1.7.2. Specific Aims

In order to provide a scalable surface for the expansion of pluripotent hESC, the major aim of this thesis is to engineer an effective substrate capable of binding unmodified VN without compromising its biological utility. The hypothesis of this thesis is to increase the surface density of functional VN by using a HS fraction tuned to VN binding. In doing so, considerations of features including cost, simplicity, safety and efficacy will contribute to key characteristics for the development of this substrate. The specific aims of this thesis are to:

1. Establish the optimal VN coating density needed for the expansion of pluripotent hESC.
2. Develop a substrate capable of binding unmodified VN based on its affinity for heparan glycosaminoglycans.
3. Determined the ability of heparan-bound substrates to capture VN and to promote the expansion of pluripotent hESC.

1.7.3. Thesis Organization

This thesis is comprised of five chapters:

Chapter 1 presents a review of literature focusing on four main areas: (1) the culture and characterization of pluripotent hESCs, (2) VN, (3) GAGs and (4) methods for immobilizing GAGs. It will also describe the background, motivation, and objectives of this research.

Chapter 2 presents the initial study of the propagation of hESC lines (HES-3, H1) on TCPS coated with VN solution. This coating was analyzed using a combination of X-ray photoemission spectroscopy (XPS), atomic force microscopy

(AFM), quantification of the VN surface density with Bradford protein assay and ^{125}I-VN binding assays.

Chapter 3 documents the work on the isolation and characterization of VN-binding HS species using VN-HBD peptide affinity chromatography. Various characterization assays, including ELISA, dot blot, heparin-Sepharose competition, isotope labelled-VN binding and capillary electrophoresis (CE) are employed. It also describes the various methods of immobilizing HS variants onto TCPS. The three immobilization methods used were amide bond formation between the carboxyl groups of TCPS and the rare primary amine groups within HS; the electrostatic interaction between PLL and the negative charge of HS; and the electrostatic interaction between the positive charge on allylamine and the negative charge inherent to HS.

Chapter 4 describes the application of allylamine surface coated with HS and VN for the long-term culture of hESCs and the concomitant effects on VN surface density.

Chapter 5 concludes with a summary of the findings of this study and recommendations for future research.

CHAPTER 2 : CHARACTERIZATION OF VN SUBSTRATES

2.1. Introduction

Human embryonic stem cells retain the ability to differentiate into all three germ layers and thus hold the promise of applications for tissue repair and drug development (Thomson *et al.* 1998). Early methods for culturing hESCs relied on co-culture with inactivated mouse embryonic fibroblasts (Thomson *et al.* 1998). This method however is not suitable for the development of clinical-grade hESCs, partly due to the xenogenic risk it introduces.

Other than cell-based feeder layers, Matrigel™, a gelatinous basement membrane extract secreted by mouse Engelbreth-Holm-Swarm (EHS) tumour cells, is now routinely used as the substrate together with conditioned media (CM) from MEFs. Hakala *et al.* compared the use of Matrigel™ with different feeder-free hESC culture substrates (biomaterials, human ECM proteins, human and animal sera matrices) and reported that Matrigel™ was superior in terms of the maximum passage number attained, as well as hESC morphology and pluripotent marker expression adopted (Hakala *et al.* 2009). Despite these advances in feeder-free systems, the use of Matrigel™ is limited by batch-to-batch variability, complex protein mixtures and the possibility of transferring non-human sialic acid, Neu5Gc, to the hESCs (Nasonkin & Koliatsos 2006). These discouraging results have led to the search for other defined systems suitable for the culturing of hESCs.

Defined model surfaces, in the form of immobilized peptide arrays have been used as substrates for hESC adhesion and expansion (Derda *et al.* 2007, Orner *et al.* 2004). However, the peptide densities in these studies were never quantified or otherwise measured. Furthermore, the analysis of hESC pluripotency was limited to detection of endogenous alkaline phosphatase and OCT-4 expression, without any examination of karyotypic stability or differentiation potential of the expanded

hESCs. In a study by Kolhar *et al.*, immobilized cyclic RGD peptide sequences were shown to promote hESC attachment and propagation at an estimated peptide surface density of 10 - 30 fmol/cm^2 (Kolhar *et al.* 2008). The density was calculated from such variable methods as fluorescence measurements and ELISA; unfortunately, no direct quantification of the peptide surface density or other surface characterization was attempted.

A further development of a defined hESC-culture platform was described by Ludwig *et al.*, who reported that a combination of human collagen IV, FN, and LN was able to support several passages of hESCs when combined with a xeno-free culture medium (TeSR1) (Ludwig *et al.* 2006b). However, those cells were found to be karyotypically abnormal, which may explain their adaptation to this platform. In other approaches, hESCs have been shown to propagate on separate matrices of FN, LN and VN (Amit & Itskovitz-Eldor 2006, Braam *et al.* 2008, Miyazaki *et al.* 2008), highlighting that a defined, scalable substrate on which to propagate hESCs may be a possibility. Also, induced pluripotent stem cells (IMR90) have been successfully propagated on plasma-purified VN (Rowland *et al.* 2010), suggesting that VN, of the various ECM proteins being investigated, may be universally applicable for the propagation of pluripotent stem cells.

Vitronectin is an abundant ECM glycoprotein that promotes cell adhesion and spreading (Schvartz *et al.* 1999b). Braam *et al.* and Rowland *et al.* reported the successful culture of hESCs and iPSC on 5 μg/ml of recombinant VN and 10 μg/ml of plasma-purified VN respectively (Braam *et al.* 2008, Rowland *et al.* 2010). Braam *et al.* also identified αVβ5 integrin as the VN receptor (Braam *et al.* 2008). Although studies by them employed VN as a substrate for the culture of hESCs, neither report determined the actual surface density of VN capable of supporting long-term cell

culture. As such, there is a need to better characterize and quantify VN substrates for hESC expansion so as to provide a defined platform for the scale-up of stem cell cultures (Oh & Choo 2008, Skottman *et al.* 2006, Unger *et al.* 2008).

Thus, this chapter will present a more detailed examination of a reproducible and verifiable VN surface and the effect on adhesion, proliferation and long-term maintenance of hESCs compared to Matrigel™. Two culture media, mTeSR™1 and a control MEF conditioned media (CM) were assessed on their ability to support hESC culture. By utilizing Ponceau S staining, the Bradford protein assay and ^{125}I-VN radiolabelling, threshold VN density was determined. A range of direct physical measurement methods, including X-ray photoemission spectroscopy (XPS) to analyze the atomic composition of the surface, and the physical roughness of the surface determined by atomic force microscopy (AFM), were also employed. Lastly the relative uniformity of VN coating was assessed by colloidal gold staining (Stochaj *et al.* 2006).

2.2. Materials and Methods

2.2.1. Culturing of ΔE-MEFs and generation of CM

In order to culture hESCs on Matrigel™ (Beckon Dickinson)-coated surfaces, conditioned media (CM) were generated from inactivated-mouse embryonic fibroblast (MEF) cells. MEF cells were first isolated from the foetuses of 139X1/SvJ mice at day 13.5 post coitum and then immortalized using the E6/E7 retrovirus as described by Choo *et al.* (Choo *et al.* 2006). Immortalized feeders (ΔE-MEF) were cultured in MEF media (90 % Dulbecco's Modified Eagle's medium (DMEM) high glucose, 10 % fetal bovine serum (FBS), 2mM L-glutamine, 25 units/ml penicillin and 25 μg/ml streptomycin). At 90% confluence, ΔE-MEFs were incubated with 10 μg/ml of mitomycin-C (Sigma Aldrich) for 150 min at 37 ^{o}C, after which cells were washed once with DMEM (Invitrogen), three times with PBS (Invitrogen), dissociated into single cells with trypsin-EDTA (Invitrogen) and counted with a haemocytometer. The mitomycin-C treated cells were seeded back into flasks at 4 x 10^5 cells/cm^2 and used for the subsequent preparation of CM (85 % Knock-Out Dulbecco's Modified Eagle's medium (KO-DMEM), 15 % Knock-Out serum replacer supplemented with 1 mM L-glutamine, 1 % nonessential amino acids, 0.1 mM 2-mercaptoethanol, 25 Units/ml penicillin, 25 μg/ml streptomycin and 10 ng/ml FGF-2).

CM was prepared by overnight conditioning over ΔE-MEFs, before collection and use for hESC culture. CM was then sterilized (0.22 μm filtration) and 10 ng/ml of FGF-2 (Invitrogen) added fresh immediately before use.

2.2.2. Preparation of recombinant FGF-2

Fresh recombinant FGF-2 (Invitrogen) was prepared in FGF buffer (10 mM Tris, 0.1 % BSA and stored at -20 ^{o}C) at 10 ng/ml. FGF-2 was added into CM, and media was refreshed daily.

2.2.3. Coating of TCPS with VN, Matrigel^{TM}.

Routine culturing of hESC on TCPS coated with VN or Matrigel^{TM} was performed. Stock plasma-purified VN solution (1 mg/ml) (Millipore) was diluted with PBS to a working solution of 5 μg/ml. From the working solution, 300 μl was added into organ culture dishes (OCD) (Beckon Dickinson) and incubated overnight (18 h) at 4 ºC. The coated plates were then rinsed once with PBS and immediately used for cell seeding.

As a positive control, OCDs were coated with 1:30 Knock-out DMEM (KO-DMEM) diluted Matrigel^{TM} (Beckon Dickinson). Diluted Matrigel^{TM} (1 ml) was added onto the dishes and incubated overnight at 4 ^{o}C. Surfaces were then washed and cells seeded.

2.2.4. Maintenance of hESCs

The human embryonic stem cell lines, HES-3 (46, XX, Female) from ES Cell International and H1 (46, XY, Male) from WiCell Research Institute were routinely cultured on TCPS plates with a VN substrate coating solution of 5 μg/ml (VN5) at 37 ^{o}C in 5 % CO_2 (as described previously). Either CM or mTeSR^{TM}1 (Stem Cell Technologies) were refreshed daily to maintain the cells in a pluripotent state. CM was used as a positive control as previously described by our laboratory (Choo *et al.* 2006).

Confluent cell cultures were passaged at day 7 according to Choo *et al.* (Choo *et al.* 2008). Different passaging techniques were used for cells cultured on Matrigel™ and VN surfaces. Cells grown on Matrigel™ were enzymatically treated with collagenase IV (200 U/ml) (Invitrogen) for 5 min at 37 ^{o}C, washed with PBS and the differentiated cells removed by manual pipetting. Cultures were then separated into small pieces with a pipette and split into new Matrigel™-coated plates at 1:4 ratio.

For cells that were cultured on VN surfaces, mechanical passaging was employed. Differentiated cells were similarly removed by pipette, and the undifferentiated cells scraped into small clumps and seeded onto freshly VN-coated surfaces at a 1:10 passage ratio. Cryopreservation was performed at - 80 ^{o}C in 90 % KO serum replacer (Invitrogen) and 10 % DMSO (Sigma Aldrich).

2.2.5. Cell counting

To determine the number of viable cells for plating, cells were counted with a NucleoCounter NC-100 (Chemometec, Copenhagen, Denmark). The cells were enzymatically lifted from the surface with TrypLE™ express enzymatic dissociation buffer (Invitrogen) and sample (100 µl) used for cell counting. Cells were first lysed with Nucleocounter reagent A (100 µl), that perforates the cell membrane at low pH, and then 100 µl of Nucleocounter reagent B to neutralize the pH of the mixture and allow efficient staining by propidium iodine as per the manufacturer's recommendations. The solution was then mixed and loaded into the NucleoCassette for counting to achieve total cell number. For dead cell number, 100 µl of reagent B was added into another cell sample (100 µl) and counted. To determine viable cell number, the dead cell number was substratcted from the total cell number. Cell

numbers in the sample were then enumerated based on the manufacturer's recommendations:

x cell numbers * 3 * volume of sample = Actual cell numbers in the total volume

2.2.6. Crystal violet adhesion assay

To determine the efficiency of cell adhesion to the various experimental surfaces, the crystal violet adhesion assay was utilized. Crystal violet is a dye that stains DNA so that quantitative information about the relative density of cells can be determined. Surfaces were prepared with VN coating (100 µl) at various concentrations (0, 2.5, 5, 10, 15, and 20 µg/ml) onto 96-well flat bottom TCPS plates (NUNC) as previously described. Wells were then blocked with 200 µl of 2 % BSA (Invitrogen) for 1 h at room temperature. Cells were dissociated with 200 µl TrypLE^{TM} express and counted with the Nucleocounter NC-100 to determine total viable cell numbers (as described in section 2.2.5). Single cells at 3 x 10^5 densities were then seeded into each well with mTeSR^{TM}1. The plates were incubated at 37 ^{o}C, 5 % CO_2 for 45 min to allow attachment. Uncoated wells incubated without cells were used as blanks.

Non-adherent cells were removed with 200 µl Iscove's Modified Dulbecco's Medium (IMDM) (Invitrogen) supplemented with 0.35 % BSA and then once with PBS. Attached cells were fixed in 100 % ethanol (Merck) and stained with 0.4 % crystal violet (Sigma Aldrich) solution in methanol for 5 min. Wells were washed three times with 200 µl MilliQ water (Millipore) to remove the unbound dye, followed by the addition of 1 % sodium dodecyl sulphate (SDS) (Sigma Aldrich) (40 µl) to solubilise the bound dye. The plates were left on an orbital shaker until a

uniform colour was observed in each well and cell adhesion determined at 570 nm. Data were normalized to the uncoated wells.

2.2.7. *In vitro* differentiation assay (EB) and PCR analysis

To assess the quality of the pluripotent cells, spontaneous differentiation of hESCs into the three germ layers using embryoid bodies (EBs) was conducted. Confluent hESCs grown on different substrates were removed with a cell scraper to form random-sized EBs. These cells were grown in suspension for 7 days and re-plated on 0.1 % gelatinized plates for further 14 days, with a media change every 2 days. Total ribonucleic acid (RNA) was extracted from EBs after differentiation using an RNA extraction kit (Qiagen). Quality and amount of RNA was quantified with a ND-1000 Spectrophotometer (Nanodrop Technologies, USA). The RNA was reverse transcribed with oligo dT primers (Invitrogen) and superscript II reverse transcriptase (Invitrogen) into complementary deoxyribonucleic acid (cDNA). Polymerase chain reaction (PCR) was carried out using cDNA with primers specific to the 3 germ layers. The endodermal lineage is detected with Alpha-feto protein (AFP); the mesodermal lineage with Msh homeobox 1 (MSH) and heart- and neural crest derivatives-expressed protein 1 (HAND1); and the ectoderm lineage with neurofilament heavy chain (NFH). Octamer-binding transcription factor 4 (OCT-4) served as the undifferentiated marker and Glyceraldehyde-3-phosphate dehydrogenase (GAPDH) was used as the internal control (Table A1). All primers were synthesized by Sigma Aldrich. In parallel, RNA from undifferentiated hESCs was extracted for comparison to differentiated cells. The amplified products were visualized in ethidium bromide-stained 1 % agarose gels.

2.2.8. *In vivo* differentiation assay (Teratoma analysis)

To confirm the pluripotentiality of hESCs cultured on the various substrates, intramuscular injections of cells were given to severe combined immunodeficiency (SCID) mice and the formation of tumours determined 10 weeks post injection (Choo *et al.* 2008). Cells cultured in various conditions for > 5 passages were dissociated by trypsin-EDTA digestion and an intramuscular injection (hamstring muscle) of 5 x 10^6 cells in 50 µl of sterile PBS was given to 4-week-old female SCID mice with a sterile 22G needle. After 10 weeks, mice were sacrificed, the tumours dissected, fixed in 10 % formalin, embedded in paraffin, then sectioned and stained with haematoxylin and eosin (H&E). The presence of the germ layers (ectoderm, mesoderm and endoderm) in the tumours was assessed by immunohistochemistry, using primary antibodies: polyclonal rabbit anti-cytokeratin (1:250), desmin Clone 33 (1:100) and rabbit anti-glial fibrillary acidic protein (GFAP) (1:250) with matching undiluted secondary antibodies: EnVision+ horse-radish peroxidase (HRP) anti-rabbit and EnVision+HRP anti-mouse. All antibodies were from DAKO. Sections were incubated with chromogen DAB and counter-stained with haematoxylin. Images were then taken under a light microscope (Olympus BX51).

2.2.9. Karyotypic stability

The chromosomal stability of hESCs cultured on VN for > 5 passages was analyzed by the Cytogenetic Laboratories at the Department of Obstetrics and Gynaecology, Kandang Kerbau Women's and Children's Hospital, Singapore. Karyotyping analysis was performed using BrdU/colcemid and 20 cells analyzed for each determination. Cells with more than 2 abnormal chromosomes were considered karyotypically unstable.

2.2.10. Flow cytometry analysis (FACS)

To monitor the pluripotency during serial passaging of hESC on VN-coated surfaces, the cell surface marker, Tra1-60, and intracellular marker, OCT-4, were measured weekly by flow cytometry. Cells were first dissociated with 0.25 % trypsin-EDTA at 37 ^{o}C / 5 % CO_2 for 5 min, washed once with 1 % BSA, and fixed and permeabilised with the Fix and Perm kit (Invitrogen). Reagent A from the kit (100 µl) was added to a washed cell pellet for 15 min, washed with 1 % BSA and spun down at 10,000 rpm for 30 sec. Then a 15 min permeabilization step was performed on the cells with reagent B (100 µl) from the kit. During this step, OCT-4 (1:20) or Tra1-60 (1:50) mouse monoclonal antibodies were incubated together. Cells were then washed with 1 % BSA, spun down and incubated in the dark (15 min) with FITC-conjugated goat anti-mouse antibody at 1:500 dilutions in 1 % BSA. Finally, cells were washed and resuspended in 1 % BSA for measurement on a FACS Calibur (Becton-Dickinson). Data was analyzed using FlowJo software and cell gating (% expression) was done at the intersection between the isotype control and the marker expression (Yap *et al.* 2011).

2.2.11. Ponceau S staining

Quantification of the amount of VN on the surfaces was made with Ponceau S staining assay. The dye binds to proteins and is easily desorbed with NaOH. The kinetics of VN on TCPS surfaces was also determined. This provided information on the rate of adsorption and desorption of VN.

VN-coated OCDs (0 to 20 µg/ml) were washed twice with MilliQ water and dried under nitrogen. Ponceau S staining solution (0.1 %) (Sigma Aldrich) at 500 µl was added and incubated overnight to allow maximal binding of the stains to the

protein (Yap *et al.* 2011). The wells were then washed with water and air-dried, whereupon 400 µl of 0.1 M NaOH (Sigma Aldrich) was added for 20 min with agitation to release bound Ponceau S stain from the surface. Desorbed stain (200 µl) was neutralized with 10 µl of 50 % acetic acid (Merck) and measured at 515 nm on an Infinite® 200 Multimode Microplate Reader (Tecan, Switzerland). Data were then compared to a standard curve using VN at 0 to 10 µg/ml concentration and final concentration of stain desorbed from the VN-coated TCPS was expressed in molarity.

2.2.12. Adsorption and desorption kinetics

Understanding the kinetics of VN on TCPS is useful for the calculation of the rate of adsorption and desorption. The adsorption and desorption kinetics were similarly obtained from the coated OCDs using the Ponceau S staining assay (described previously). To quantitate the adsorption kinetics, OCDs were incubated with VN solution at 5 µg/ml concentration (VN5) for varying times (0 to 32 h) and stained with Ponceau S. For VN desorption, OCDs were incubated with VN5 overnight, washed, and air-dried. PBS (1 ml) was added into the wells and incubated at 37 ºC. At different time points (0 to 48 h), the wells were stained with Ponceau S and rate of desorption determined.

2.2.13. Bradford assay

A Bradford assay was performed to further quantify the amount of VN on surfaces. Final surface density was calculated by determining the amount of VN depleted from the depositing solution (Bradford 1976, Zor & Seliger 1996).

The OCDs were incubated overnight with different VN solutions, 100 µl from each OCD combined, and 1.2 ml of Bradford dye (Sigma Aldrich) added into a 1.5 ml glass vial. To avoid inaccurate quantification, glass vials were used to prevent the absorption of VN onto the surface and all measurements done within 10 min. The solution was mixed for 5 min and 200 µl sampled, and read in a microplate reader at both 590 nm and 450 nm. This was then normalized by subtracting the average A590 / A450 value for PBS (Zor & Seliger 1996). The reading was compared to a standard curve (A590 / A450 against different VN concentrations) to obtain the VN concentration. The difference between this concentration and the depositing concentration is the amount of VN adsorbed. The surface density (ng/cm^2) was calculated by using the surface area of an OCD as 3.5 cm^2, which includes the base and a rim extending 1.5 mm above it.

2.2.14. ^{125}I-VN quantification

Surface densities of VN were also assessed by a highly sensitive radiolabelling study. VN was labelled with the ^{125}I isotope (Perkin Elmer) coupling (on tyrosine residues via lactoperoxidase reaction) using Thermo Scientific Pierce Iodination Beads as per the manufacturer's recommendations. Prior to labelling, 2 iodination beads were washed with PBS and dried on filter paper. Beads were added to 100 µl PBS solution containing 0.5 mCi of ^{125}I isotope for 5 min; subsequently 50 µg of VN was added into the reaction and incubated for another 10 min. The reaction was terminated by separating the solution from the beads with a pipette. The remaining free ^{125}I in the solution was removed with PD Minitrap G-10 desalting columns (GE Healthcare). The ^{125}I-VN was diluted with unlabelled VN (1:9 ratio) for each concentration (0 to 20 µg/ml) and added into spatially removed white-walled

transparent bottom TCPS 96-well plates (Corning) to allow overnight binding of VN at 4 ^{o}C. Following that, wells were washed 3 times with 200 µl of PBS, 200 µl of Ultima Gold scintillation cocktail (Perkin Elmer) added and the plates read in a MicroBeta liquid scintillation counter (Perkin Elmer) for 1 min. Surface density (ng/cm^2) was calculated by comparing to reference concentrations of ^{125}I-VN.

2.2.15. XPS measurements

To measure the surface elemental composition, a quantitative spectroscopic technique, X-ray photospectrometry (XPS) was employed. XPS spectra were obtained by irradiating the material with a beam of X-rays and simultaneously measuring the kinetic energy and number of electrons that escape from the top 1 to 10 nm of the material (Fally *et al.* 1995). The surface chemical composition of each VN coated-TCPS was determined using a Theta Probe X-ray photoelectron spectrometer (Thermo Fisher Scientific), equipped with an aluminium anode (15 kV, 100 W) and a quartz monochromator. The monochromator was set to a 50 º take-off angle (measured from the normal to the plane of the sample surface), yielding a probe depth of ~ 5 nm. Detailed scans of the nitrogen (N1s), oxygen (O1s), and carbon (C1s) peaks were performed on each sample, taking data from a 400 µm^2 spot and using pass energy of 40 eV. Detailed scans were repeated as follows: 20 x for C1s, 15 x for O1s, and 20 x for N1s. A wide scan (binding energy from 0 to 1300 eV) was then performed with pass energy of 200 eV. Peaks were fitted with a mixed Lorentz-Gaussian function. Deconvolution of the C1s signal revealed 5 peaks: aromatic C (284.8 - 284.9 eV), C-C (285 eV), C-NH_2 (285.5 – 286.0 eV), C-O (287.6 – 288.4 eV), and C=O (287.6 – 288.4 eV). Results were analyzed with CasaXPS software.

2.2.16. AFM measurements

Atomic force microscopy (AFM) profilometry was employed because of its high resolution to study the topographical features of different VN-coated TCPS. Air-dried VN-coated and uncoated TCPS were measured using a Bioscope I microscope equipped with a NanoScope IIIa controller and a low noise scanner (Digital Instruments, Veeco Metrology Group, USA). PointProbe® Plus noncontact high resonance frequency (PPP-NCH) silicon cantilevers (Nanosensors, Switzerland) were used in intermittent-contact (also known as tapping) mode to obtain high-resolution images of the samples. Scan rates varied from 0.75 to 1 Hz and free amplitude (A_0) setpoint values were ~ 1.6 V. Images of the TCPS surface morphology and the VN-coated surfaces were taken at 85 - 90 % of the free amplitude. Roughness analysis was performed with Nanoscope software version v5.12rb. Briefly, two-dimensional AFM height maps were used to determine the arithmetic roughness (R_a) of the uncoated and VN-coated TCPS surfaces. The arithmetic roughness describes the absolute value of the surface height, measured relative to a two-dimensional plane, set at the average sample height. R_a was calculated from either the entire (4 μm x 4 μm) image, or several smaller areas (2 μm x 2 μm) within the image. Phase data records the variations in the cantilever oscillation, reflecting changes in surface rigidity and viscoelasticity. This was used to improve the contrast between adsorbed VN aggregates and the TCPS substrate.

2.2.17. Colloidal gold staining

To assess the uniformity of VN adsorption onto TCPS, Colloidal Gold Total Protein Stain (Biorad) was employed. Colloidal Gold stain rapidly detects and stains proteins. VN coated-TCPS were washed and air-dried and then incubated with undiluted Colloidal Gold stain (500 μl) overnight in room temperature. Surfaces were then rinsed with water, air-dried, and photomicrographs taken.

2.2.18. Statistical analysis

All data values are reported as the mean $\pm$ standard error taken from three individual experiments with triplicate runs each. Where appropriate, one-way ANOVA was performed to compare differences across the groups, and $P < 0.05$ was considered as significant. Student's t-test (2-tailed) was done to determine the differences between two sample groups. Graphs were plotted and data transformed using Sigma plot software.

2.3. Results

2.3.1. Stable expansion and analysis of hESCs cultured on VN5

In order to assess the suitability of VN as a substrate for hESCs, HES-3 and H1 cells were cultured for > 10 passages on TCPS coated with a 5 μg/ml VN solution (VN5) in either control CM or experimental mTeSR^{TM}1 media. Both media were used to compare the cell responses to the various substrates. Photomicrographs of cells cultured at passage 15 revealed that both cells retained an undifferentiated morphology characterized by both the formation of compact colonies with distinct boundaries and a high nucleus to cytoplasmic ratio (Fig. 2.1). Weekly flow cytometry analysis was performed to measure the expression of the pluripotent marker, Tra1-60. The expression level during 12 weeks of passaging revealed that both cell lines had > 90 % positive expression (Table 2.1). Cells continued to express high levels of Tra1-60 over 30 passages. Representative FACS analysis on the various substrates is shown in Figure 2.2.

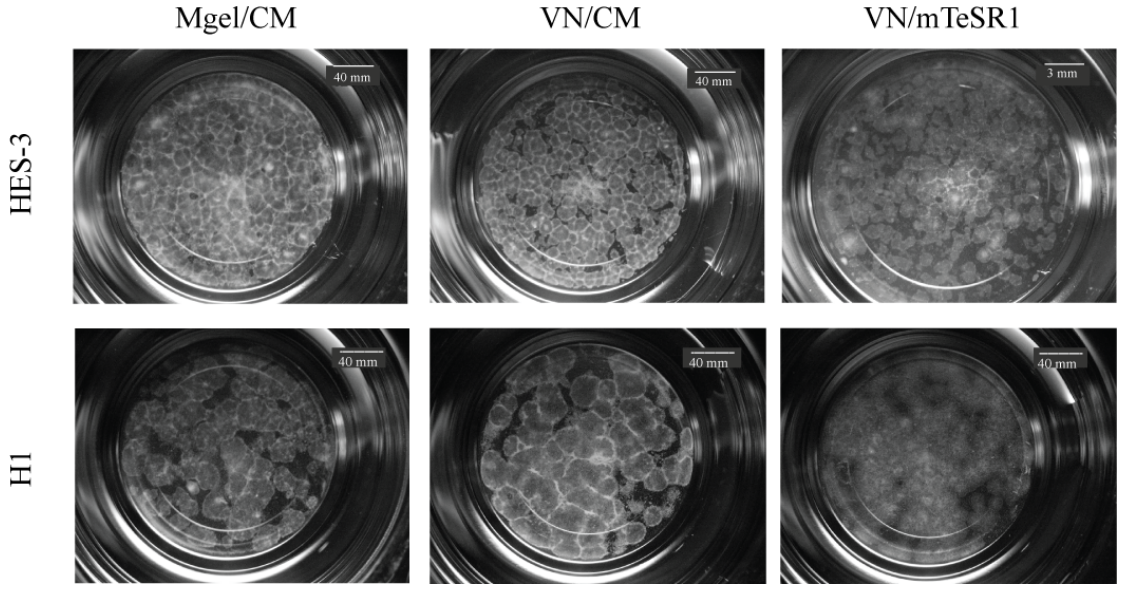

Figure 2.1. Representative images of HES-3 and H1 cells. Cells retained the typical stem cells morphology of compact colonies with distinct boundaries (Yap *et al.* 2011).

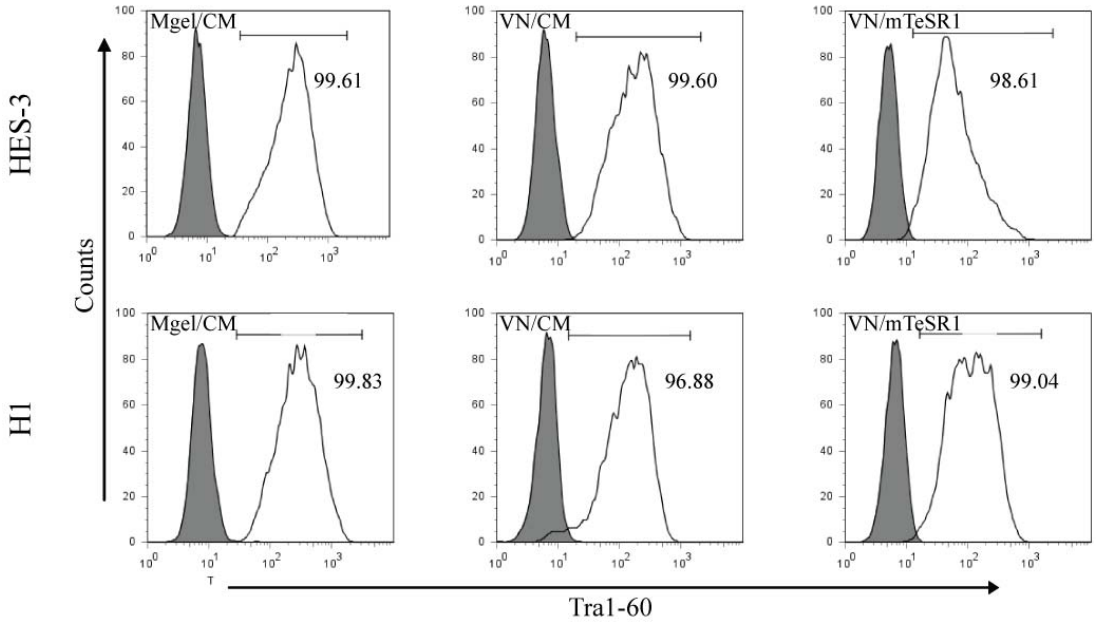

Figure 2.2. FACS analysis of the pluripotent surface marker Tra1-60. HES-3 and H1 were > 90% positive for Tra1-60 suggesting the cells adapted well to VN5. (Yap *et al.* 2011).

Table 2.1. Tra1-60 expression in HES-3 and H1 cells over 12 passages in varying conditions (Yap *et al.* 2011).

	HES-3			H1		
Passage	Matrigel/ CM	VN/ CM	VN/ mTeSR1	Matrigel/ CM	VN/ CM	VN/ mTeSR1
P 2	91.0	96.0	97.0	96.8	99.8	98.3
P 4	98.9	93.0	98.0	99.8	97.4	97.0
P 6	94.2	98.0	95.2	98.0	98.0	98.6
P 8	95.0	99.2	98.6	97.0	96.0	98.0
P 10	96.0	97.6	97.0	98.0	96.0	96.0
P 12	94.0	98.3	99.0	96.0	97.0	98.0

To further determine the suitability of VN as a substrate for hESC expansion, an analysis of karyotype was performed on HES-3 (46, XX) at passage 9 and H1 (46, XY) at passage 5. Data showed that the cells possessed a normal diploid karyotype (Fig. 2.3). This was again repeated at passage 30; with cells maintaining a normal karyotype. As both HES-3 and H1 cells are equally viable and remain pluripotent when serially passaged on VN5, only HES-3 cells were used for subsequent experiments.

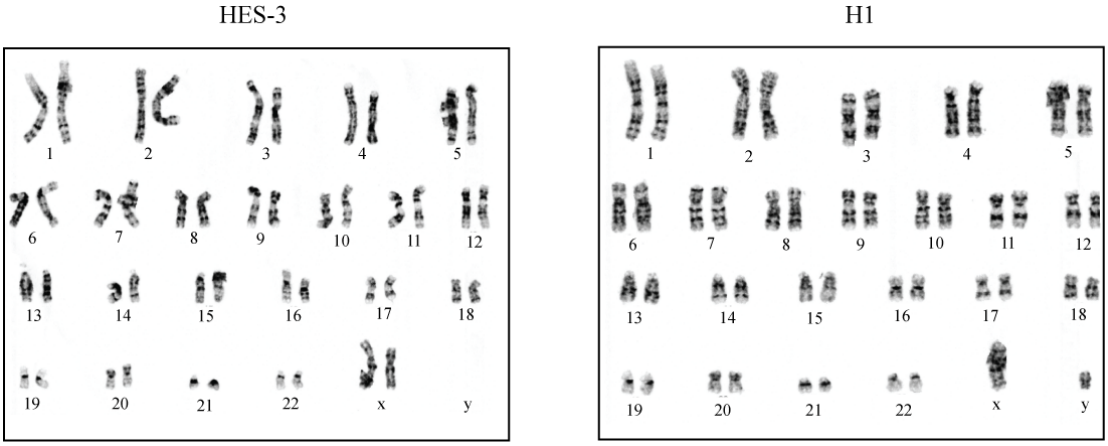

Figure 2.3. Genomic stability of HES-3 and H1 cells on VN5. No chromosomal abnormality for HES-3 and H1 cells was observed at passage 9 and 5 respectively. They retained a normal diploid karyotype, 46, XY and 46, XX. Similar results were also obtained at passage 30 (Yap *et al.* 2011).

A robust, tri-germ layer differentiation potential is a hallmark of pluripotent hESCs. Following propagation on VN5 for 25 passages, HES-3 cells were induced to differentiate *in vitro* through EB formation, and the presence of ectoderm, mesoderm and endoderm probed by PCR. After 21 days of differentiation, HES-3 cells expressed the mRNA transcripts for AFP (endoderm), MSX1 (mesoderm) and NFH (ectoderm) that are normally absent in undifferentiated cells (Fig. 2.4). As expected, the

expression of the pluripotent markers Nanog and OCT-4 were suppressed when the cells were induced to differentiate (Fig. 2.4).

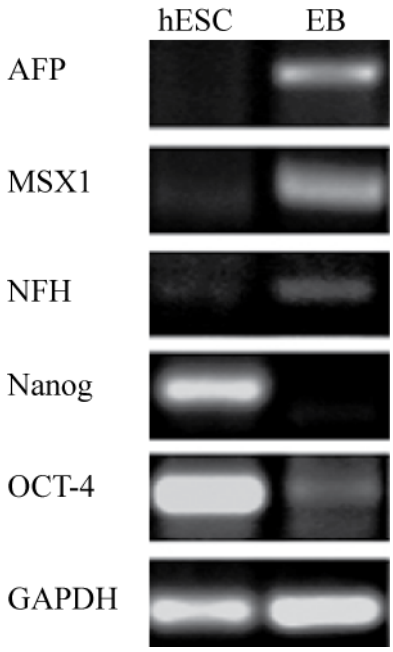

Figure 2.4. mRNA transcript expression from the *in vitro* differentiation of HES-3 cells through EB at passage 25. The expression of AFP (endoderm), MSX1 (mesoderm) and NFH (ectoderm) genes from the three germ layers were absent in the undifferentiated cells. OCT-4 marker diminished after 21 days of differentiation and GAPDH was used as a internal control (Yap *et al.* 2011).

As a final test of pluripotency, the tumorgenicity of HES-3 was investigated *in vivo*. Cells at passage 18 were injected into SCID mice. Teratomas were present and contained structures from all 3 germ layers, as determined by H&E and immunohistochemical staining (Fig. 2.5). Clear evidence of ectoderm (neuroepithelium and pigmented epithelium), mesoderm (bone and cartilage) and endoderm (gut epithelium) was visible. Similarly, the presence of GFAP-positive intermediate filaments (ectoderm), desmin-positive muscle (mesoderm) and cytokeratin-positive epithelium (endoderm) was confirmed by immunohistochemistry.

Collectively, this data suggests that VN5 surfaces are able to support the long-term propagation of pluripotent hESCs in an undifferentiated state.

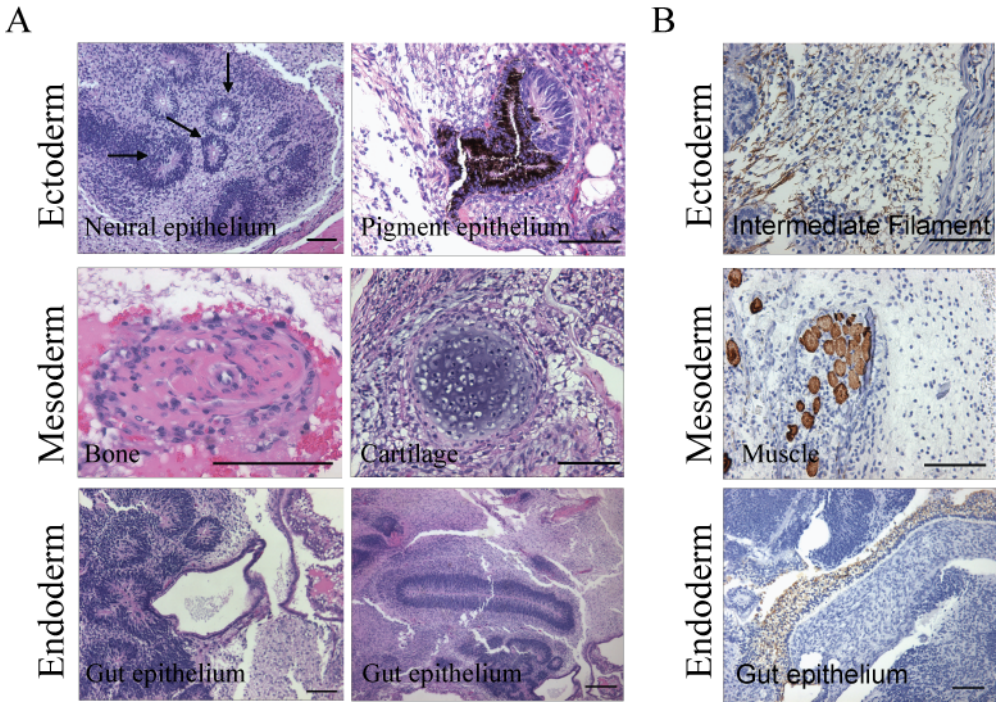

Figure 2.5. Histological sections of teratomas from HES-3 cells (passage 18). A) Tissues representing the three germ layers were analyzed after H&E staining. Neuroepithelium and pigmented epithelium represented ectoderm lineage; bone and cartilage represented mesoderm lineage and gut epithelium represented endoderm lineage. B) Teratomas were also stained with antibodies for GFAP (ectoderm), desmin (mesoderm) and cytokeratin (endoderm). Scale bar = 100 μm (Yap *et al.* 2011).

2.3.2. Threshold concentration of VN that is required for the attachment and propagation of cells

Having established a robust VN5 working condition for hESC culture, we next sought to assess the variation in bio-responses arising from systematic changes in the VN surface density. Cell attachment was compared across a range of VN densities after either 45 min or 1 day in culture (Fig. 2.6A). Cell attachment increased in a VN density-dependent manner, with the greatest number of attached cells occurring at the

highest VN density. Surfaces with higher cell attachment reached confluence earlier but hESC do not exhibit contact-inhibition thus will continue to grow and stack onto each other. If they remain pluripotent with low cell death, cultures can be passage together. Notably, in CM the cell density plateaus at VN2.5, with ~ 2- to 4- fold more cells attached in the presence of mTeSR^{TM}1 as compared to CM. Since no difference in cell adhesion at VN5 and VN10, therefore higher VN concentrations were not explored. No differences in cell number were also observed for either media treatments after 1 day (Fig. 2.6B). There was however a similar VN density-effect between 45 min and 1 day, with ~ 3-fold more attached cells detected in VN2.5 as compared to VN1.25.

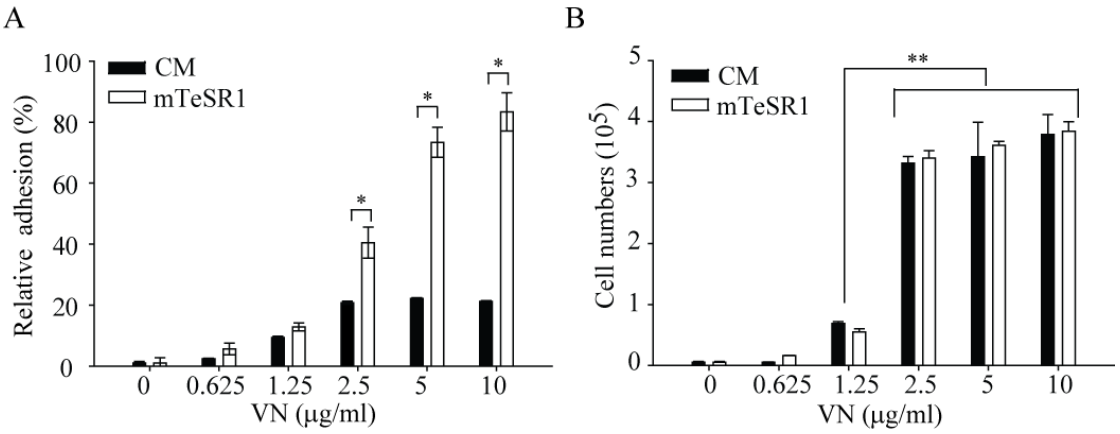

Figure 2.6. Short-term adhesion assay on different VN coatings. A) Crystal violet adhesion assay after 45 min in CM or mTeSR^{TM}1 media. As VN concentration increase so did the number of HES-3 cells attached in mTeSR^{TM}1 media than in CM. B) HES-3 were seeded and a count was performed at day 1. The number of cells attached to < VN1.25 was insignificant as compared to the rest of the conditions. Cell numbers plateau at VN2.5, regardless of the media used. * = $P < 0.05$ ** = $P < 0.001$ (Yap *et al.* 2011).

To fully assess hESC proliferation, changes in cell number after 1 week in culture were calculated on the various VN substrates. When cultured for 7 days, ≥ VN2.5 was required for maximum proliferation, notwithstanding significant growth

differences were also observed between the CM and mTeSR^{TM}1 media, with mTeSR^{TM}1 significantly outperforming CM (~ 30 %) (Fig. 2.7A). A VN2.5 substrate capable of supporting hESC attachment and expansion was also evident from photomicrographs taken after 1 week in culture (Fig. 2.7B). Cells cultured on > VN2.5 had the typical "mosaic/cobblestone" appearance of confluent hESCs, as compared to cells cultured VN1.25 that were sparsely attached and failed to grow.

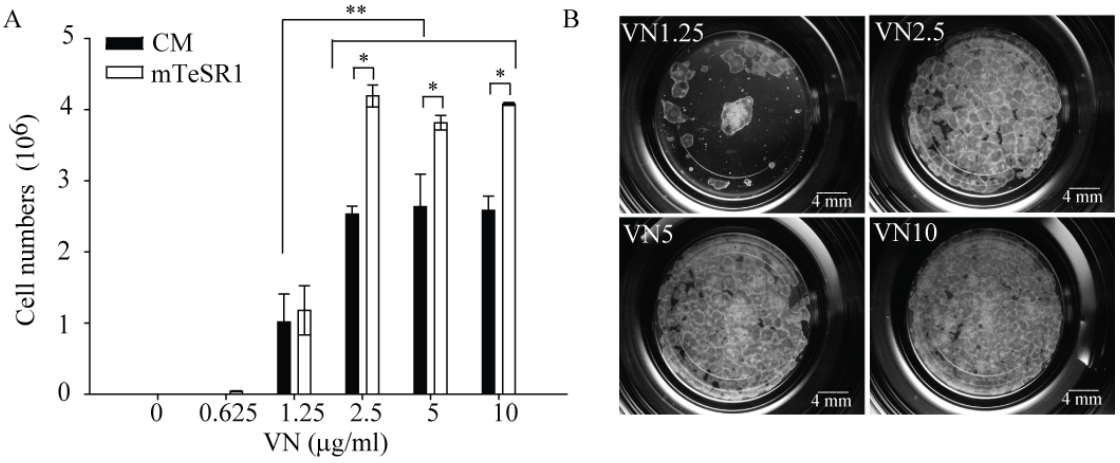

Figure 2.7. Cell counts and micrographs of HES-3 after 1 week in culture at various VN concentrations. A) Cell numbers were similar in VN2.5, VN5 and VN10 but on VN1.25, numbers were significantly lower than the rest. Significant differences were observed in cells cultured on CM and mTeSR^{TM}1 media. * = $P < 0.05$ ** = $P < 0.001$. Data are expressed as mean $\pm$ standard deviation (n = 3). B) Representative day 7 images of HES-3; VN1.25 did not support robust cell expansion as well as the other concentrations, and cultures did not reach confluence by day 7 (Yap *et al.* 2011).

In order to more fully evaluate the threshold VN surface density suitable for the long-term maintenance of pluripotent hESCs, HES-3 cells were cultured for > 5 passages in mTeSR^{TM}1 media. Pluripotency was then assessed by FACS, EB differentiation and teratoma formation. Initially, cells cultured on VN1.25, VN2.5 and VN5 underwent a period of adaptation that was reflected by a decreased

expression of pluripotent markers at passage 1 (Table 2.2). Following subsequent passaging, cultures at passages 2 - 6 were > 90 % positive for Tra1-60 and OCT-4 (Fig. 2.8 and Table 2.2). These levels were similar to those observed for cells maintained on control Matrigel™ surfaces.

Table 2.2. Expression of the pluripotent markers Tra1-60 and OCT-4 in HES-3 over 6 passages. (Yap *et al.* 2011).

	Tra1-60			OCT-4		
VN (μg/ml)	1.25	2.5	5	1.25	2.5	5
P 1	85.0	83.2	89.3	90.0	76.6	89.0
P 2	95.0	95.7	93.4	96.0	91.6	86.2
P 3	94.7	99.6	99.7	90.0	92.9	95.7
P 4	96.0	98.0	99.3	93.0	92.0	96.0
P 5	99.4	99.5	99.8	96.4	96.0	93.1
P 6	99.4	99.6	97.3	91.2	95.1	89.0

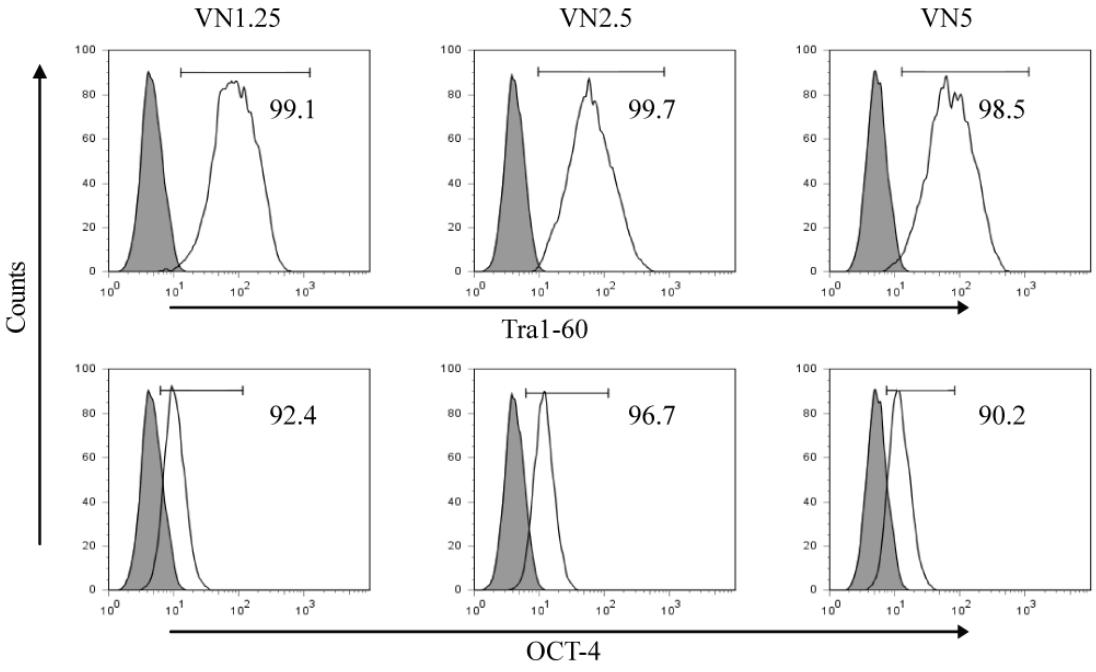

Figure 2.8. Representative expression of Tra1-60 and OCT-4 as determined by FACS at passage 5. HES-3 cells were grown on VN1.25, VN2.5 and VN5 with mTeSR™1. Cells expressed > 90 % positive for these markers (Yap *et al.* 2011).

Next the genomic stability of hESC culture on VN1.25 and VN2.5 was assessed. As with VN5 coatings, HES-3 cultured on VN1.25 and VN2.5 maintained a normal karyotype over 5 passages (Fig. 2.9). Differentiation was then assessed by RT-PCR for germline markers after EB formation. Cells cultured on VN1.25 failed to expand sufficiently for differentiation assays to be conducted, and so were not analyzed further. However, cells readily expanded on VN2.5, with differentiation assays showing the presence of mRNA transcripts for AFP (endoderm), Hand1 (mesoderm) and NFH (ectoderm) and the absence of Nanog and OCT-4 (Fig. 2.10). Importantly, despite their *in vitro* differentiation potential, cells cultured on VN2.5 failed to form teratomas when transplanted into SCID mice. As previously shown, cells cultured on VN5 maintained all the hESC characteristics of growth, differentiation and teratoma formation. Therefore, the VN threshold solution concentration needed to maintain hESC pluripotent during long-term expansion is 5 μg/ml (Table 2.3).

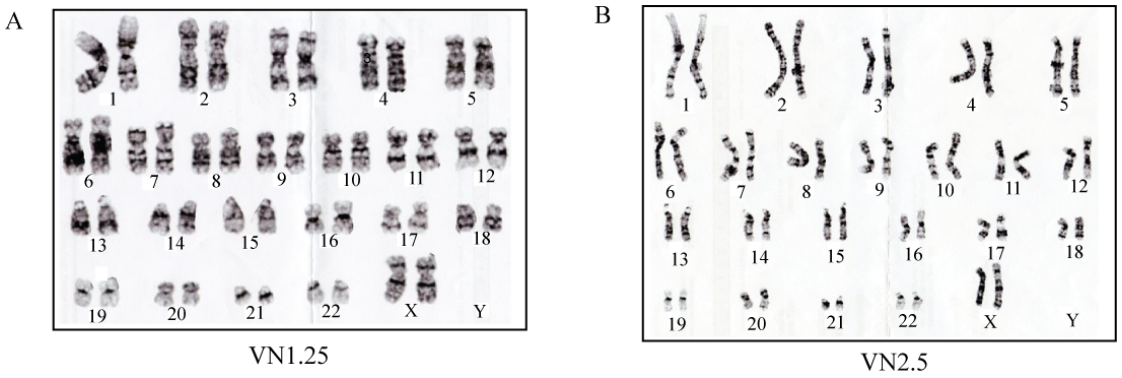

Figure 2.9. Genomic stability of HES-3 cultured on VN1.25 and VN2.5 after 5 passages. Karyotype analysis of HES-3 cells cultured mTeSR^{TM}1. No chromosomal abnormalities were observed in either condition (Yap *et al.* 2011).

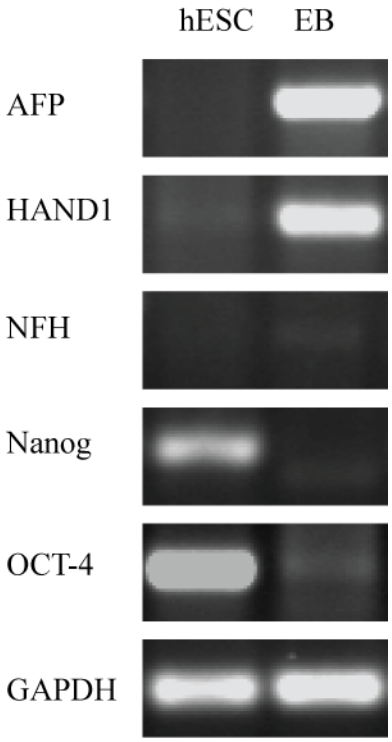

Figure 2.10. HES-3 (passage 5) *in vitro* differentiation assay (EB) when cultured on VN2.5. HES-3 was able to differentiate into the 3 germ layers. Expression of mRNA transcript for AFP (endoderm), Hand1 (mesoderm) and NFH (ectoderm) were present and the pluripotent markers Nanog and OCT-4 absent. GAPDH served as internal control (Yap *et al.* 2011).

Table 2.3. Summary of the different pluripotency criteria for hESCs on VN1.25, VN2.5 and VN5 substrates.

	VN1.25	VN2.5	VN5
Morphology	Yes	Yes	Yes
Pluripotent marker espression (FACS)	Yes	Yes	Yes
Genome stability (Karyotype)	Yes	Yes	Yes
In vitro differentiation (EB)	No	Yes	Yes
In vivo differentiation (Teratoma)	No	No	Yes

2.3.3. VN surface density determination

To determine the amount of surface-bound VN, Bradford protein assays and Ponceau S staining were performed so that the depletion of VN from the original solution concentration could be calculated. Results from both the Bradford protein assay (Fig. 2.11A) and Ponceau S staining (Fig. 2.11B) show matching trends for the adsorbed VN surface density: a steady increase in surface-adsorbed VN with increasing solution concentration that reaches a plateau for VN solution concentrations > 10 μg/ml. These measurements estimated the surface density deposited from VN5 at 250 ng/cm^2, increasing to a maximum of 500 ng/cm^2 for deposition from ≥ VN10. Previous analysis of the cell response indicated that hESCs did not attach, and long-term proliferation was not supported when < VN5 (Table 2.3). Therefore the minimum surface density was set at 250 ng/cm^2.

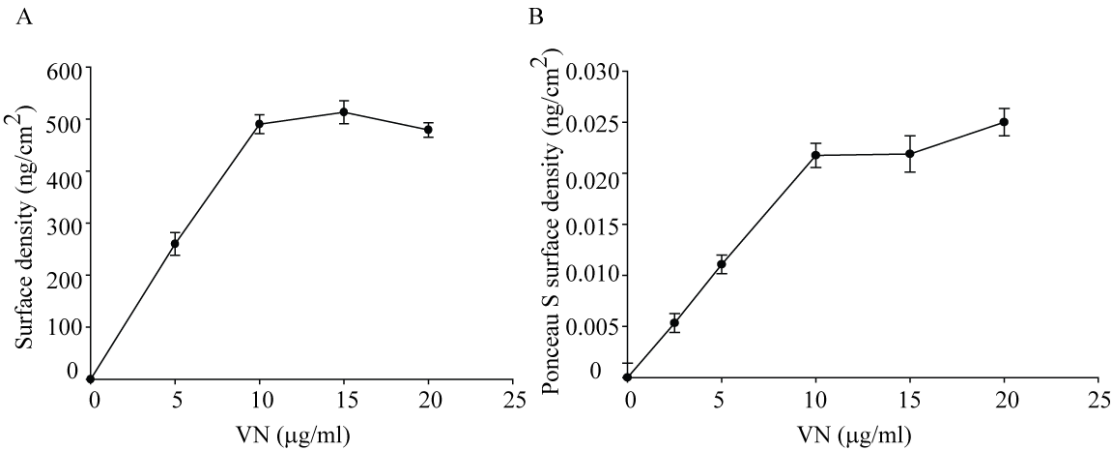

Figure 2.11. Quantification of VN adsorbed to TCPS. A) VN density deduced from VN depletion in the depositing solution as measured by Bradford assay. B) Surface density of VN adsorbed to TCPS stained by Ponceau S dye. Both Bradford assay and Ponceau S staining showed that density plateaus at VN10 (Yap *et al.* 2011).

This threshold surface density was thus estimated at 250 ng/cm^2 by assuming a linear dependence between adsorbed VN with solution concentration, as predicted by the Langmuir adsorption isotherm, and as corroborated by the Ponceau S staining and the Bradford protein assay. However, this assumption might not be strictly accurate; thus a more sensitive method for accurately determining the VN surface density by radiolabelling was performed. VN was iodinated with the ^{125}I-isotope on tyrosine residues via the lactoperoxidase reaction to generate I^{125}-VN, and this then used to coat TCPS overnight. Results showed the same adsorption trends on TCPS as with the Bradford and Ponceau S assays (Fig. 2.12). VN again adsorbed in a dose-dependent manner and saturated at VN10, thus confirming that the VN5 coating adsorbs 250 ng/cm^2 of VN.

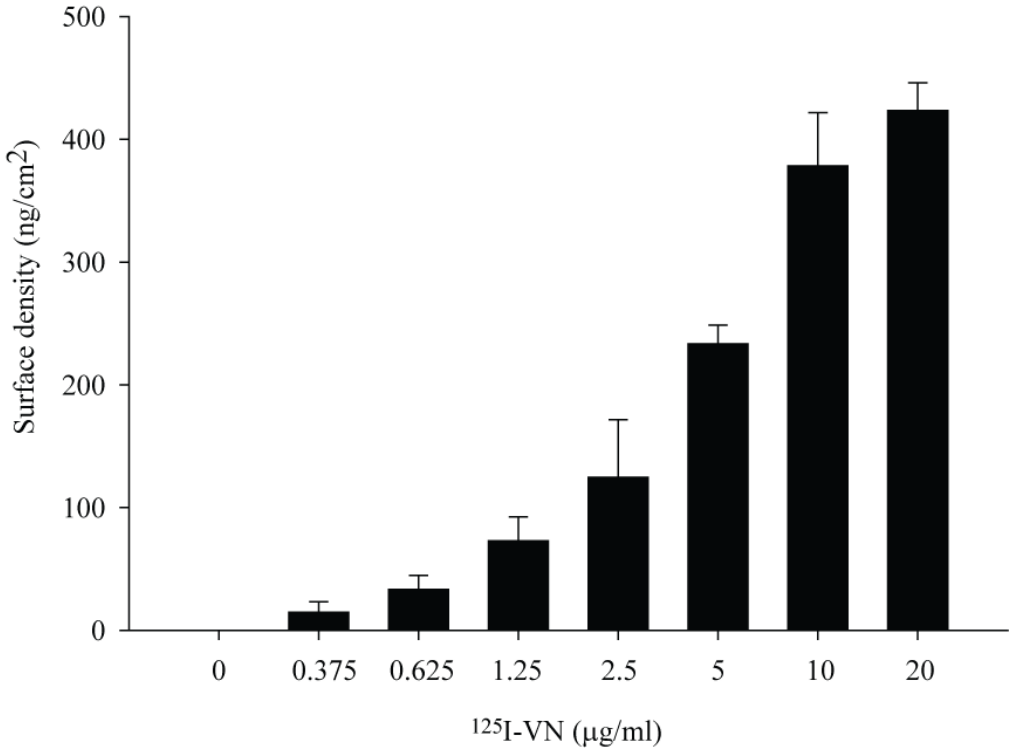

Figure 2.12. ^{125}I-VN binding assay to TCPS. TCPS was coated with increasing concentrations of ^{125}I-VN overnight. Radioactive counts were measured after washing with PBS the next day. Results confirmed that 5 μg/ml of ^{125}I-VN solution adsorbed 250 ng/cm^2 onto the culture surface.

2.3.4. Surface characterization

XPS was used to quantitate the surface chemical composition of VN-coated TCPS, with the data revealing the presence of nitrogen, C-NH2, C-O, and C=O bonds (Fig. 2.13). The increasing signal from N and O atoms (from peptide bonds) with increasing depositing solution concentration confirmed a monotonic increase in VN surface density. This reached saturation at > VN10; thus this finding followed the same trend as observed with Bradford assay, Ponceau S surface staining and I^{125}-VN quantification (Figs. 2.11 and 2.12). This independently confirms the dependence of surface-adsorbed VN on depositing solution concentration.

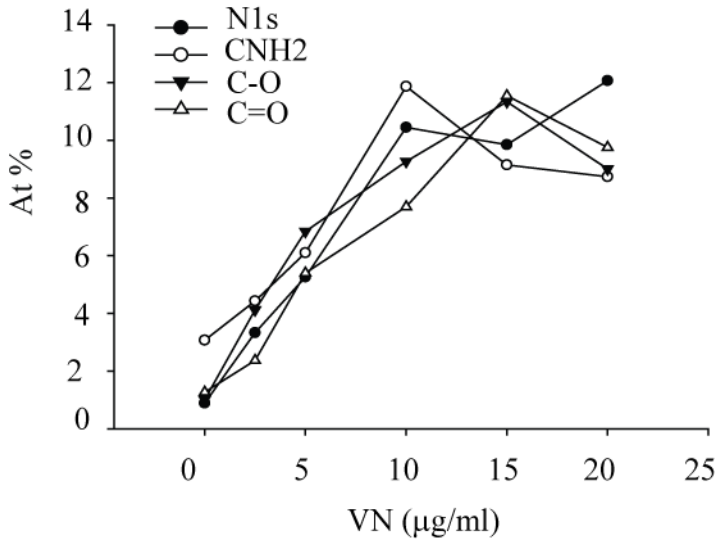

Figure 2.13. XPS quantification of surface composition for VN-coated TCPS. Surface chemical bonds increase linearly and saturates at 10 μg/ml, confirming the presence of VN on the surface by the presence of nitrogen (Yap *et al.* 2011).

To directly observe VN aggregation on TCPS surfaces, AFM analysis was performed. AFM height images reveal the surface profilometry of the cell culture substrate and can be used to directly observe VN aggregates. Uncoated TCPS showed an intrinsic, structured surface roughness, consisting of random line features that were

presumably introduced during the TCPS manufacturing process. The substrate features were observed across all samples, from uncoated, to TCPS coated with 0, 2.5, 5, 10 and 20 μg/ml VN (Figs. 2.14 A to F). TCPS morphology remained unchanged after exposure to the PBS, implying that the features associated with VN aggregates, as observed on the coated TCPS, were not merely an artefact (Fig. 2.14B). The surface roughness (Ra) of the uncoated TCPS substrates was found to range from 2.7 to 3.2 nm. Deposited VN aggregates, in the form of spot-like features, were visible on TCPS coated with VN solution concentrations from 2.5 to 10 μg/ml (Figs. 2.14 C to E). AFM phase images offered enhanced contrast, as seen on TCPS coated with the VN2.5 solution (Fig. 2.14H). A higher magnification of the nominated area in Figure 2.14 H is shown in Figure 2.14 I. The absence of spot-like features, associated with VN aggregates, on the AFM phase image of uncoated TCPS (Fig. 2.14G) confirmed that these arise from the adsorbed VN. The adsorbed VN aggregates did not significantly increase the R_a value for coated samples beyond the range quoted above. Finally, the AFM profilometry of TCPS coated with VN20 showed a loss in resolution; the physical origins of this remain unexplained. Although AFM has previously been used to study VN adsorption on smooth mica surfaces (Zhang *et al.* 2004), the present study will seek to examine VN when adsorbed to TCPS, a surface demonstrated to be successful for the long-term propagation of hESCs.

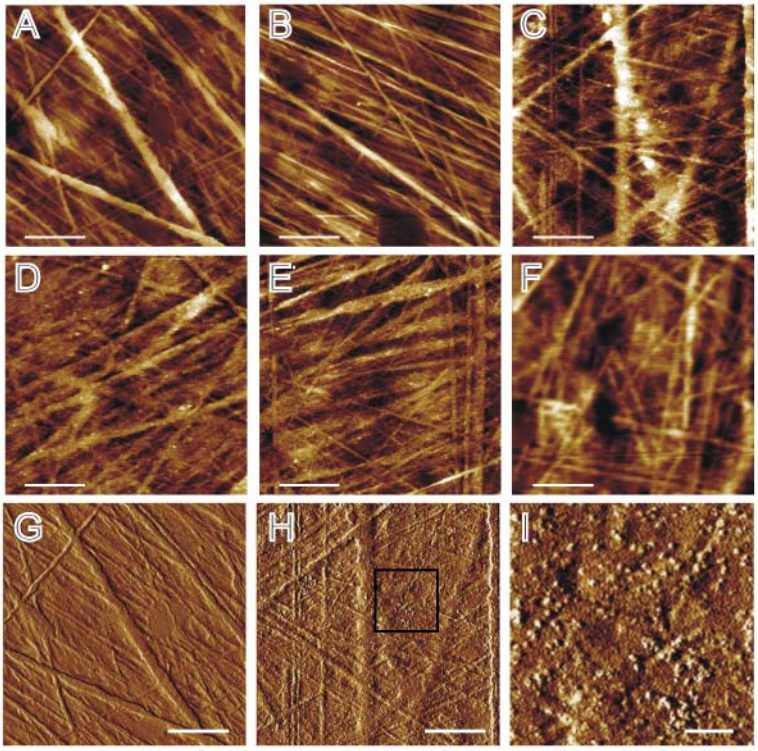

Figure 2.14. AFM height profilometry images. A) Uncoated TCPS, TCPS coated with (B) 0, (C) 2.5, (D) 5, (E) 10, and (F) 20 µg/ml VN solutions. (G to I) are phase images from the same samples (A) uncoated TCPS and (C) 2.5 µg/ml. Image (I) shows a magnified view of the marked area on image H. The height range is 0 – 25 nm, the phase range is 0 – 15 º. The scale bar is 1 µm on all images except image (I), where it is 200 nm (Yap *et al.* 2011).

To observe the coating uniformity, total protein on the surfaces can be stained by colloidal gold. The staining, although not quantitative, may be used to discern the uniformity of the VN coated on the surface. The staining confirmed that the amount of adsorbed VN increased with VN concentration (Figs. 2.15 A to F). The uncoated surface (Fig. 2.15A) demonstrated the absence of colloidal gold staining on TCPS. As the depositing VN solution concentration was increased, the samples shown in Figure 2.15 B did not show any staining, while in Figure 2.15 C, which depicts the coating of VN5, there is barely any discernible stain. Coating from the 10, 15, and 20 µg/ml solutions (Figs. 2.15 D to F), respectively, reveals discernible, increasing

colloidal gold staining, whose uniformity indicates that the VN adsorbed to the surface of TCPS is distributed homogeneously.

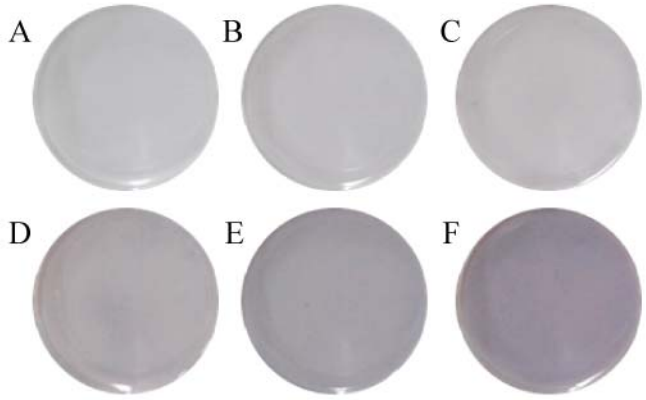

Figure 2.15. Colloidal gold staining of TCPS. VN concentrations of (K) 0, (L) 2.5, (M) 5, (N) 10, (O) 15, and (P) 20 µg/ml were used to coat TCPS. The diameter of each disk is 15 mm (Yap *et al.* 2011).

2.3.5. Adsorption and desorption kinetics of VN on TCPS

Adsorption and desorption kinetics (Fig. 2.16) were modelled assuming exponential time dependence. Modelling the data with an exponential as the square root of time, as proposed by several authors, did not improve the fit (Douglas *et al.* 1993, Sukhishvili & Granick 1998, Sukhishvili & Granick 1999). The associated fitting parameters (Table 2.4) indicated an adsorption time constant of approximately 1 h, and a desorption time constant of approximately 4 h. The desorption time constant may not be accurately represented under actual cell culture conditions, where it was influenced by competing adsorption from other proteins. The y_0 parameter physically represents the VN protein that remains bound to TCPS following a desorption time of 2 days. Figure 2.16 B showed that only about 25 % of the adsorbed VN was desorbed from the TCPS substrate after a 48 h exposure to PBS. The 75 % of

VN adsorbed to TCPS after 2 days may, in small part, have arisen from VN re-adsorbed from the PBS solution. However it can in large part are attributed to VN remaining durably bound to the TCPS substrate.

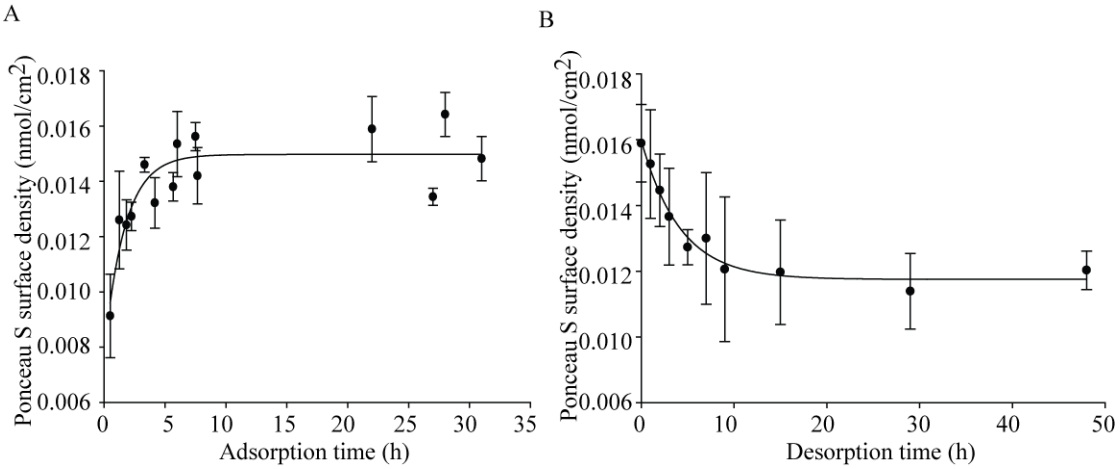

Figure 2.16. Ponceau S staining to give VN adsorption and desorption kinetics onto TCPS. (A) Adsorption kinetics from VN5. (B) Desorption kinetics from TCPS, previously coated with a 5 µg/ml solution. N = 3 ± SEM (Yap *et al.* 2011).

Table 2.4. Equations and fitting parameters for adsorption and desorption kinetics. "x" represents the ordinate and "y" the abscissa, with fitting parameters for adsorption and desorption kinetics of VN on TCPS (data and fitted curves shown in Fig. 2.16). For adsorption, A reflects the maximum surface density of VN and T is the time constant. For desorption, A reflects the initial surface density of VN, T is the time constant, and y_0 reflects staining of non-desorbed VN (Yap *et al.* 2011).

Data	Equation	A	y_0	T
Adsorption	$y = A(1-\exp(-x/T))$	0.0146 ± 0.0003		1.2 ± 0.2
Desorption	$y = A*\exp(-x/T) + y_0$	0.0042 ± 0.0003	0.0118 ± 0.0002	4.2 ± 0.7

2.4. Discussion

The search for defined surfaces for pluripotent hESC culture has led to the development of several defined surfaces, including immobilized peptide arrays and cyclic RGD peptide (Derda *et al.* 2007, Kolhar *et al.* 2008, Liu *et al.* 2011, Orner *et al.* 2004) . Even though these surfaces demonstrated the ability to maintain hESCs, their peptide density was neither directly quantified nor characterized. Moreover, the analysis of pluripotency was limited to endogenous alkaline phosphatase and OCT-4 expression. Other than peptide surfaces, Braam *et al.* and Rowland *et al.* demonstrated the ability of VN to support hESC propagation but they lack details concerning the characterization and quantification of VN on the culture surfaces. Here, I varied the concentration of VN in solution and determined the amount that adsorbed to TCPS with a view to developing a quantifiable platform on which to expand pluripotent hESC over multiple passages, and in a stable manner. TCPS was chosen because it is the most widely used surface for culturing cells, and also has demonstrated to be capable of the long-term propagation of hESCs.

This study showed that a threshold VN surface density of at least 250 ng/cm^2 (VN5) is required for the long-term expansion (> 30 passages) of pluripotent hESCs in a serum-free defined medium (mTeSR^{TM}1). Cells cultured at this VN threshold had sustained positive expression of Tra1-60 and OCT-4 (> 90 %), had a normal diploid karyotype and they maintained a compact morphology. Importantly, the cells retained the potential to differentiate to the 3 germ layers through EBs and readily formed teratomas when transplanted into the muscle pouch of SCID mice. At VN surface densities < 250 ng/cm^2 cell attachment and proliferation were compromised and the cells failed to differentiate in EBs and were unable to develop teratomas *in vivo*.

The absence of *in vivo* teratoma from the transplanted cells when cultured on VN2.5 showed that the cells cultured are not pluripotent, even though all *in vitro* studies confirm otherwise. Thus, *in vivo* teratoma formation is a necessary criterion to confirm the pluripotent state of cells. Without teratoma formation, this study would have erroneously suggested a threshold density of ~ 120 ng/cm^2 from a depositing solution of 2.5 μg/ml, an underestimate of the actual threshold.

It was also observed that hESCs cultured in mTeSR^{TM}1 media achieved higher cell numbers after 1 week as compared to cells grown in CM. This observation is supported by Chin *et al.*, who reported that defined media such as mTeSR^{TM}1 reduce the doubling time of hESCs to approximately 21 h, as compared to cells cultured in CM, that require 28 h (Chin *et al.* 2010).

From the characterization studies we can conclude that the long-term, stable propagation of hESCs is possible with VN5, and that this defined surface is a viable alternative to Matrigel^{TM}. The threshold surface density is estimated at 250 ng/cm^2 of protein by assuming a linear dependence of adsorbed VN with solution concentration, as predicted by the Langmuir adsorption isotherm and corroborated by Ponceau S staining, Bradford protein assay and ^{125}I-VN measurements. Thus, VN is an effective substrate for promoting cell adhesion and expansion of pluripotent stem cells at surface densities well below its saturation, which is estimated at 500 ng/cm^2 as measured by Bradford assay (Fig. 2.11a)

AFM image resolution was limited by the radius of the AFM probe tip, which is nominally 20 nm. This prevented the detection of individual VN molecules, which may be approximated by a cylinder of radius 3 nm and length 11 nm (Lynn *et al.* 2005). Larger VN aggregates appeared as point-like asperities on the randomized line-feature background of the TCPS substrate. Only the height of VN aggregates was

assessed, as dimensions in the plane of the surface are convoluted with the tip diameter. Their size is comparable to that reported by Zhang *et al.* for VN molecules adsorbing onto smooth mica surfaces (Zhang *et al.* 2004). Lynn *et al.* described the formation of VN aggregates in solution and Izumi *et al.* reported the presence of VN aggregates with a Stokes radius of 6.5 nm in human plasma (Izumi 1989, Lynn *et al.* 2005). Thus, the observed VN aggregates may either have been adsorbed from solution, or may be formed as VN adsorbs to TCPS. Higher VN solution concentrations may lead to its adsorption in a different configuration, perhaps giving rise to the observed decrease in resolution when imaging TCPS coated with VN20.

It must also be noted that mTeSR^{TM}1 is not a completely defined media, as the BSA and VN used is from pooled human plasma and not recombinant sources. However, one would not expect this to significantly alter the viable VN platform described here. A further examination of the triggering thresholds could be performed in a completely chemical defined xeno-free medium such as X-VIVO10 from Lonza, TeSR^{TM}-E8^{TM} from Stem Cell Technologies, HEScGRO from Millipore or Nutristem hESC SF from Biological Industries. Although the use of recombinant proteins are clearly advantageous, such proteins are usually cloned and expressed in bacterial or animal cells, which are often sources of foreign antigen such as the highly immunogenic non-human forms of sialic acid (Neu5Gc). Furthermore, animal cells may possess inappropriate glycosylation patterns on their susceptible proteins, rendering them ineffective in the presence of highly glycosylated VN. Serum-derived proteins, despite being subject to lot-to-lot variability and the possibility of contamination from plasma, usually retain all their biological activity. Serum-derived proteins are useful in the studies of most applications. Future biotechnological innovation may provide the means to overcome these drawbacks in the future.

2.5. Summary

This chapter established a robust set of parameters for the coating of surfaces with VN for the long-term propagation of pluripotent hESCs, and summarizes the subsequent surface characteristics of VN-coated TCPS.

Based on the experimental evidence, the following key findings were derived:

(1) Vitronectin coatings are an alternative to Matrigel™ in culturing hESCs. It is a defined ECM protein, in contrast to the poorly characterized Matrigel™. It thus reduces the risk of cell contamination. Cells remain pluripotent in the presence of a defined media (mTeSR™1) without the use of CM.

(2) The minimum threshold concentration of VN required for the successful long-term culture of hESCs is 5 μg/ml, which corresponds to 250 ng/cm^2 as measured with Bradford assay and radioactivity.

(3) *In vivo* differentiation as assessed by teratoma formation is critical for the establishment of the suitability of a substrate. I would strongly recommend doing a teratoma assay to confirm the continuing pluripotency of any cultured hESCs.

Understanding the minimum VN surface density raises the issue of its efficiency and cost-effectiveness within the context of large-scale industrial manufacturing processes for generating clinical-grade stem cells more reliably (Oh & Choo 2008, Skottman *et al.* 2006, Unger *et al.* 2008). The reliable production of large quantities of stem cells may well benefit from optimized VN substrates. Optimized VN substrates can be engineered by extrapolating the relationship between cell surface HS and VN surface. The next chapter will therefore address the means of

isolating and charactering a binding species of HS with tuned affinity for VN by biochemical means.

CHAPTER 3 : ISOLATION, CHARACTERIZATION AND IMMOBILIZATION OF HS9 VARIANT

3.1 Introduction

To better define hESC culture surfaces, and improve the cost-effectiveness of VN coating, a novel strategy is clearly called for. Glycosaminoglycans are complex, linear, highly charged carbohydrates that interact with a wide range of proteins to regulate their function and are usually synthesized attached to core protein. GAGs are classified into nonsulfated (HA) and sulfated (CS, DS, KS, heparin and HS) GAGs.

Among the GAGs, the heparan sulfate (HS) family is of particular interest because of its ability to interact with targeted proteins based on specific sequences within its domains. The family (heparin and HS) consist of repeating uronic acid-(1→4)-D-glucosamine disaccharide subunits with variable pattern of N-, and O-sulfation. For example, the anti-coagulant activity of heparin requires 3O-sulfation in glucosamine residue with a unique pentasaccharide arrangement (Lindahl *et al.* 1979). A unique sulfation pattern is also apparent for ECM proteins; an avid heparin-binding variant for FN is particularly highly charged, with 7 to 8 N-sulfated disaccharides being required, and with a larger domain than normal (> 14 residues) (Falcone & Salisbury 1988, Mahalingam *et al.* 2007). However, HS differs from the sulfated heparin by having highly sulfated NS domains separated by the unsulfated NA domains, which provide a different unique arrangement for binding selective proteins especially without the side effects of heparin(Gandhi & Mancera 2008).

Thus, elucidating the disaccharide composition of HS is essential to understanding its sulfation pattern, and eventually for the future generation of synthetic variants. The disaccharide composition of HS can be elucidated through a series of enzymatic cleavages (Desai *et al.* 1993b, Shriver *et al.* 2000, Venkataraman *et al.* 1999) using *Flavobacterium heparinium* enzymes heparinase I, II and III to cleave the glycosidic bonds. More than 90 % depolymerization of heparin or HS is

possible when all 3 heparinase are used in combination (Karamanos *et al.* 1997, Vynios *et al.* 2002). The disaccharides can be analyzed by PAGE (Hampson & Gallagher 1984), SAX-HPLC (Skidmore *et al.* 2009), or highly sensitive CE (Lamari *et al.* 2001) by comparing to known disaccharides standards. Several authors have described the separation of heparinase-digested disaccharides samples using CE at reverse polarities of – 20 kV (Karamanos *et al.* 1996), – 15 kV (Ruiz-Calero *et al.* 1998) or – 30kV (Militsopoulou *et al.* 2002) at acidic pH.

Numerous studies have also shown that HS is generally important for the maintenance and proliferation of stem cells (Bramono *et al.* 2011, Helledie *et al.* 2012, Klim *et al.* 2010, Levenstein *et al.* 2008, Nurcombe & Cool 2007). Uygun *et al.* demonstrated that GAG-derivatized surfaces are able to promote 5-fold increase in mesenchymal stem cell growth compared to TCPS surfaces (Uygun *et al.* 2009). Therefore, to improve the effective VN density on TCPS, it may be possible to manipulate HS in such a way as to present VN more effectively. Immobilization strategies include coupling GAGs with BSA to allow adsorption onto surfaces (Feng *et al.* 2004, Nishioka *et al.* 2007); EDC chemistry to covalently immobilized disaccharide units (Plante *et al.* 2001); biotinylation of GAGs and coupling to streptavidin-coated surfaces (Foxall *et al.* 1995, Hasan *et al.* 1999, Parkar & Day 1997) and positively charged plasma polymer films (Mahoney *et al.* 2004, Marson *et al.* 2005). As detailed previously, to analyze the elemental composition on plasma-polymerized surfaces techniques such as XPS could be employed (Robinson *et al.* 2012).

This chapter describes the search for an HS variant with high VN-binding ability that can improve VN surface density for cell culture. The approach we adopted followed a path our Glycotherapeutics group (IMB, A*STAR) has pioneered over

several years. This chapter sets out to purify a novel VN-binding HS species from a raw HS starting material by affinity chromatography using the VN-HBD peptide as the capture ligand. A full range of biochemical assays to confirm the binding ability of this purified HS from the non-binding and starting material were employed. The length, sulfation pattern and composition requirements of HS were then analyzed by ELISA and CE. Three different strategies were then explored to immobilize the purified HS variants onto TCPS. A method that utilized allylamine was shown to offer distinct advantages over the other methods tested.

3.2. Materials and Methods

3.2.1. Preparation of VN-HBD peptide surfaces

After establishing the VN5 platform in earlier studies, this chapter seeks to assess the importance of cell surface HS for the binding of hESC to VN-HBD substrates. An N-terminal biotinylated VN-HBD peptide (Biotin-PRPSLAKKQRFRHRNRRKGYRSQRGHSRGRNQNSRR) was synthesized by China Peptides Co. Ltd, Shanghai, China. This peptide, which lacks an RGD motif, was immobilized onto streptavidin-coated surfaces to assess the attachment efficiencies of the heparinase-treated hESCs and is described further on. The streptavidin (Genescipt) was first reconstituted in PBS to 1 mg/ml stock and subsequently prepared as a 20 μg/ml working concentration. Bacterial grade 24-well plates (Beckon Dickinson) were coated with 625 μl of the working streptavidin concentration and incubated overnight at 4 ºC. Wells were then washed twice with PBS and 10 μM of VN-HBD peptide incubated for 2 h at room temperature, after which wells were washed again and 1 ml of mTeSR^{TM}1 supplemented with 10 μM Rock inhibitor (Y27632) (Calbiochem) according to the study by Klim *et al.* (Klim *et al.* 2010) . The use of Y27632 markedly increases the survival of dissociated-induced cell death as demonstrated by Watanabe *et al.* (Watanabe *et al.* 2007). Coated plates were used immediately for the crystal violet cell adhesion assay (Section 2.2.6).

3.2.2. Heparinase digestion and heparin-inhibition of HES-3 cells

To efficiently remove cell surface HS for the study of cell attachment, heparinase I, II and III were employed. Heparinase I (E.C. 4.2.2.7), heparinase II (no E.C. number) and heparinase III (E.C. 4.2.2.8) were purchased from Sigma Aldrich,

resuspended in digestion buffer (20 mM Tris-HCL, 50 mM NaCl, 4 mM $CaCl_2$ and 0.01 % BSA, pH 7.5) and used within 1 freeze-thaw cycle. HES-3 single cells at 1 x 10^6 cells per well were resuspended in 100 μl of DMEM/F12 media (Invitrogen) containing heparinase I (10 milli international units (mIU)), heparinase II (5 mIU) and heparinase III (10 mIU). The cell suspensions were incubated at 37 ^oC for 1 h, with mixing every 10 min. The cells were then spun at 12,000 rpm and surface HS expression analyzed by FACS.

Soluble heparin (Sigma Aldrich) was preincubated with cells and served as a competitor to the surface-bound HS with the peptide surface. Similarly, cells (1 x 10^6) were resuspended in 100 μl DMEM/F12 media (Invitrogen), incubated with soluble heparin at 500 μg/ml concentrations for 1 h, with mixing after every 10 min. Cells were then analysed for binding to VN-HBD surfaces with the crystal violet assay (Section 2.2.6).

Both the heparinase-digested cells and cells incubated with soluble heparin were seeded onto the prepared 10 μM of VN-HBD peptide surface (as described above) or positive control VN5 in 96-well plates (as described in Chapter 2). Plates were left to incubate for 45 min to allow attachment, and crystal violet cell adhesion assays performed as described in Section 2.2.6. Streptavidin-coated surfaces served as a negative control and data was normalized to the absorbance of VN5.

3.2.3. FACS analysis of heparinase-digested cells

To ensure enzymatic digestion effectively removed exogenous HS chains from HES-3 cells, FACS analysis using both the 10E4 and 3G10 antibody was performed. The 10E4 antibody recognizes common N-sulfated and N-acetylated glucosamine sugar units in native HS sugar chains on cell surfaces (van den Born *et al.* 2005) and

the 3G10 antibody specifically binds to de-saturated uronic acid residues that remain after digestion of HS with heparinase (David *et al.* 1992). Live staining was done on ice to prevent cell death. Digested cells at a density of 2.5 x 10^5 were washed with 1 % BSA and 200 µl of either 10E4 or the 3G10 (1:100) antibodies (Seikagaku) added for 1 h. Respective isotype controls (10 µg/ml) (DAKO) for the primary antibodies were used to stain cells to account for non-specific antibody binding. Cells were then washed and stained with FITC-conjugated goat anti-mouse secondary antibody (DAKO) (1:500) for 30 min. Exogenous HS expression was then determined using a FACS Calibur (Becton Dickinson) and the results analyzed with FlowJo software. Gating was done at the point of intersection between the isotype control and 10E4/3G10 expression.

3.2.4. Peptide binding assay with ^{3}H-heparin

To confirm the binding ability of the synthesized VN-HBD peptide to heparin, the ^{3}H-heparin binding assay was employed in the manner of Baird *et al.* (Baird *et al.* 1988). Biotinylated VN-HBD peptide (Biotin-PRPSLAKKQRFRHRNRRKGYRSQRGHSRGRNQNSRR) was serially diluted in PBS (0, 12.5, 25, 50 and 100 µg peptide) and individually spotted onto 0.2 µM nitrocellulose membranes (Biorad). Peptide was left to dry on the membrane for 1 h at room temperature and heated to 80 ^{o}C for 30 min. The membrane was then washed three times with PBS, where upon 1 ml of 0.1 µCi of ^{3}H-heparin (Perkin Elmer) in 4 % BSA (Sigma Aldrich) was added, and the membrane incubated overnight at room temperature with agitation. Next day, the membrane was washed three times with PBS and 1 ml of Ultima Gold scintillation cocktail (Perkin Elmer) was added in a 20 ml glass scintillation vial (Perkin Elmer). The vial was analyzed in a liquid

scintillation Tri-carb 2800TR counter (Perkin Elmer, Massachusetts, USA) for 1 min, three times. The counts-per-minute readings were averaged and plotted.

3.2.5. Affinity chromatography

To isolate the VN binding variants from starting porcine intestinal mucosal HS (HS^{pm}) material, affinity chromatography using biotinylated VN-HBD peptide as the capture ligand was performed. Saturating amounts of biotinylated VN-HBD peptide (3 mg) were coupled to a 1 ml streptavidin column (GE Healthcare) as assessed by the detection of unbound peptide at 280 nm in the flowthrough. To ensure peptide is firmly bound to the column, a 1.5 M high salt buffer wash was performed. When no traces at 280 nm were detected, the column was equilibrated with low salt buffer and was ready for HS loading.

Crude HS (HS^{pm}) (Celsus Laboratories) was dissolved in low salt buffer (20 mM phosphate buffer, 150 mM NaCl, pH 7.2) at a concentration of 1 mg/ml. A total of 100 mg HS^{pm} solution was loaded in a total of 30 separate injections in low-salt buffer (Biologic-Duoflow chromatography system; Bio-Rad) at a flow rate of 0.2 ml/min, and the column washed with the same buffer until the baseline reached zero. The bound HS was eluted with a one step gradient of 1.5 M high salt (20 mM phosphate buffer, 1.5 M NaCl), the bound and unbound variants collected (monitored at A_{232} nm), and the column re-equilibrated with low-salt buffer. The eluent ($HS9^{+ve}$) and flow-through ($HS9^{-ve}$) peak samples were collected separately, freeze-dried, and stored at -20 ^{o}C. Both the $HS9^{+ve}$ and the $HS9^{-ve}$ variants were then separately dissolved in 10 ml of HPLC grade water (Sigma Aldrich) and desalted once on a HiPrep 26/10 desalting column (Amersham Biosciences) at a flow rate of 10 ml/min. The different HS variants were then collected, freeze-dried, and stored at – 20 ^{o}C.

3.2.6. Dot Blotting

To analyze the different HS variants for binding affinity to VN, dot blotting was conducted. Nitrocellulose membranes were rinsed with TBST and assembled into the Biorad dot blot apparatus according to manufacturer's instructions. The edges of the membrane were marked to help in reassembling the membrane sandwich after blocking. VN (1 μg) was added into the wells and the assembly put under vacuum. The membrane was removed and blocked with 5 % BSA for 1 h. After blocking the membrane was assembled back into the dot blot apparatus in the same configuration.

The GAGs (2 mg) were initially biotinylated using biotin-LC-hydrazide (60 μl of a 2 mg/ml solution) (Thermo Scientific) dissolved in 1 ml of 0.1 M MES buffer, pH 5.5. Briefly, EDC (1.5 mg) was added to the mixture and incubated for 2 h before the addition of another 1.5 mg of EDC after which unincorporated biotin was removed with a Fast Desalting (PD 10) Column (GE Healthcare). These biotinylated GAGs (1 μg) were added into the wells of the dot blot apparatus, left for 10 min and then aspirated off with a pipette. After incubation, the membrane was then washed with TBST. Streptavidin-HRP (2 ml) was added onto the membrane for 10 min, and washed again with TBST. Finally, the membrane was exposed to the LumiGLO chemiluminescent substrate (Kirkegaard & Perry Laboratories) and exposed to X-ray film (Amersham) in the dark.

3.2.7. Heparin-Sepharose bead competition assay

Heparin-Sepharose bead competition assays were performed to investigate the binding affinity of each desalted HS variant (Heparin, HS^{pm}, $HS9^{+ve}$ and $HS9^{-ve}$) to VN and other ECM proteins according to Ono *et al. (Ono et al. 1999)*. The assay was done at room temperature and a "master mix" of bead slurry was prepared to reduce

error. For each reaction, 20 µl of heparin-Sepharose beads (Sigma Aldrich) were mixed with 20 µl of Biogel P10 (Biorad). The total volumes of beads and Biogel for the required reactions were calculated and brought together to form a master mix. The height of the suspension was marked for later resuspension. The bead suspension was washed 3 times with 1 ml of 1% BSA, and the beads allowed to settle to the bottom of the tube between washes. After the last wash, beads were left to settle and resuspended back to the original height using the initial marked height. From the master mix, aliquots (40 µl) of bead slurry were separated into individual 1.5 ml Eppendorf tubes for binding experiments. Excess liquid was removed by pipette, leaving the beads at the bottom of the tube.

Optimization of the amount of protein needed to achieve sub-optimal binding to beads was first conducted. Varying concentrations of ECM proteins (VN, LN, and FN) were added to the beads in 100 µl volume. The suspension was incubated for 30 min under constant rotation, after which the beads were spun down at 2000 rpm for 1 min, and washed twice with 1 ml of 1% BSA and with 1 ml of 0.02 % Tween20 (Sigma Aldrich) in PBS. Excess wash buffer was removed from the last wash. The corresponding anti-ECM antibody (100 µl) (Millipore) prepared in PBS (250 ng/ml anti-VN, 5 µg/ml anti-LN, 2 µg/ml anti-FN), was added and, the mixture incubated for another 30 min with constant rotation. The beads were washed again as previously described and 100 µl of the HRP-conjugated goat anti-mouse antibodies (1:10,000) in PBS was added to each reaction, under rotation for 30 min. Finally, the beads were washed, 100 µl of TMB substrate (Thermo Scientific) added and colour allowed to develop. The reaction was stopped at 30 min by adding 50 µl of 2 M H_2SO_4. Beads were centrifuged at 2000 rpm and 100 µl of the supernatant removed and added into a

96-well plate (NUNC) to be read at 450 nm. Results were plotted and sub-optimal concentrations of each ECM protein used for the subsequent competition assay.

The binding affinities of the GAGs to ECM proteins were next investigated using the competition assay. Different concentrations (0, 5, 50 and 100 μg) of GAGs were pre-incubated with the individual ECM protein in 100 μl for 30 min with rotation. The reaction was then added into the washed 40 μl of bead slurry as previously prepared. Results were expressed as "percentage bound" by normalizing to readings from control, uncompeted beads.

To confirm the results from the competition assay, immunoblotting was performed. After the competition, the beads were washed and boiled at 95 ^{o}C with 30 μl of Laemmli buffer (Sigma Aldrich). The beads were spun and the supernatant loaded into SDS-PAGE gels (Invitrogen) at 180 V for 40 min and transferred to nitrocellulose membranes at 100 V for 90 min. The membrane was then probed with the corresponding primary antibody in 5 % BSA at 4 ^{o}C overnight. Membranes were washed with TBST 3 times for 5 min each. Then, HRP-conjugated goat anti-mouse secondary antibody (Jackson Immunoresearch) (1:10000) in 5 % BSA was incubated for 1 h at room temperature. Membranes were finally washed and exposed to LumiGLO Reserve^{TM} chemiluminescent substrate (Kirkegaard & Perry Laboratories) to visualise the bands on X-ray films.

3.2.8. Glycosaminoglycan ELISA

To further examine the VN binding affinities of each HS variant, GAG ELISA was performed. This assay was based on the immobilization of HS variants onto the glycosaminoglycan-binding 96-well plates (Iduron) by electrostatic interactions and

the VN binding ability assessed by antibodies as per manufacturer's recommendations.

Wells were incubated overnight at room temperature with 200 µl of 5 µg/ml GAGs (Heparin, HS^{pm}, $HS9^{+ve}$ and $HS9^{-ve}$), heparin disaccharides standards (dp2 to dp12) or selectively desulfated heparin standards prepared in standard assay buffer (SAB). SAB was prepared with 100 mM NaCl, 50 mM NaAc, (v/v) 0.2 % Tween 20, pH 7.2. Wells were then washed with 200 µl of SAB three times and blocked (0.4 % (w/v) fish gelatin in SAB), for 1 h at 37 ^{o}C. Wells were washed with SAB three times and VN at different concentrations (0 - 1 µg/ml, 200 µl each) was added into the wells and incubated at 37 ^{o}C for 2 h. Wells were again washed (3 times) and 200 µl of anti-VN antibodies (250 ng/ml) (Millipore) added into the wells and incubated at 37 ^{o}C for 1 h. Wells were washed (3 times) to remove unbound antibody and 200 µl of 250 ng/ml goat anti-mouse biotinylated antibody (Sigma Aldrich) added for 1 h at 37 ^{o}C. After incubation, wells were washed again (3 times) and ExtrAvidin (200 µl of 220 ng/ml) (Sigma Aldrich) added for 30 min for 37 ^{o}C. Wells were finally washed (3 times) and 200 µl of SIGMA*FAST*™ p-Nitrophenyl phosphate (Sigma Aldrich) added into the wells with incubation at room temperature for 40 min. Colourimetric absorbance was read at 405 nm with a Victor multiplate reader (Perkin Elmer, Massachusetts, USA).

3.2.9. Capillary electrophoresis

To investigate the different molar percentages of each disaccharide present in the heparinase-polymerized HS variants, capillary electrophoresis (CE) was performed. CE is a sensitive technique to separate the samples based on charge and molecular weight. Heparin, HS^{pm}, $HS9^{+ve}$ and $HS9^{-ve}$ variants (200 µg) were all

digested with heparinase I, II and III (Iduron) in digestion buffer (100 μl) to give 2 mg/ml stock. Digestion buffer consisted of 50 mM NaAc, 1 mM calcium acetate and 100 μg/ml BSA, pH 7. Heparin was first digested with 4 mIU of heparinase I and II each for 3 h at 30 ^{o}C, and later 1 mIU of heparinase II for another 60 min to complete the digestion. HS samples were digested with 4 mIU heparinase I for 30 min and later 4 mIU heparinase II and III each for another 3.5 h at 30 ^{o}C. Absorbances at 232 nm were measured throughout the digestion process to ensure complete digestion; this was recognized by the lack of further increases in absorbance. Absorbance was performed at 232 nm because of the C=C bonds created in the uronic acid after digestion can be detected at this wavelength. Reactions were terminated by denaturing the enzymes at 95 ^{o}C for 1 min. Solutions were centrifuged at 10,000 rpm and supernatants used for the CE analysis.

The quantification of each disaccharide in the depolymerized samples were completed by diluting the stock (2 mg/ml) to 1 mg/ml with MilliQ water and 25 μl of a 1 mg/ml internal standard (4UA-2S ® GlcNCOEt-6S) (Iduron) Δ-disaccharide added. This internal standard was added because it had a migration time distinct from the Δ-disaccharide standards and could thus be utilized for the determination of each disaccharide unit from its relative migrational shift. The depolymerized sample was then injected into the CE system to generate the electropherogram. The area-under-the-peak was then measured and compared to a standard curve to derive the concentrations. Molar percentages of each sample were then calculated from the molecular weight of each standard and compared in a table.

To generate the standard migration profile for comparison, commercially available, digested heparin disaccharide (Δ-disaccharide) standards (Iduron) as shown in Figure 1.12 were separated at 250 μg/ml, with the exception of IVA. These

standards were used for the generation of the electropherogram to identify the migration time; from these the quantification of each disaccharide unit in the digested GAGs samples became possible. By using 7 different concentrations (undiluted (1 mg/ml), 1x, 2x, 4x, 8x, 12x and 16x dilution) of each standard to generate a calibration curve based on its area-under-the-peak, the standard curve of area against concentration was plotted.

CE was performed on a P/ACE MDQ instrument equipped with a diode array detector (Beckman instrument) at 25 ^{o}C. Membrane-filtered (0.22 μm) 60 mM formic acid solution (pH 3.4) (Sigma Aldrich) was used as the running buffer. Separations were carried out in uncoated fused-silica capillaries, with a length of 60 cm and a 75 μm internal diameter (Beckman instrument). Capillaries were first pre-treated with 1 M NaOH for 30 min and rinsed with MilliQ water for another 20 min. The capillary was than conditioned with formic acid buffer for 60 min in readiness for sample injection. The cycles were programmed for 5 min water rinses, 3 min 1M NaOH, 5 min buffer washes and 5 sec sample injection (0.5 pound force per square inch (p.s.i.) and reverse polarity of -15 kV), so that disaccharides would migrate from cathode to anode due to their electrophoretic mobility (EM) against the electro-osmotic flow (EOF) of the buffer. Disaccharides were separated for 40 min and individual peaks were detected at 232 nm. This cycle was repeated for the next injection.

To ensure reproducibility of migration times and peak areas (expressed as relative standard deviation, R.S.D.), 5 replicates of the heparin standards were performed daily. Digestion buffer was also run through the system to ensure no interference to the sample peaks.

3.2.10. Sodium hydroxide etching of polystyrene surface

The first strategy was to immobilize HS with a chemical method to covalently anchor it onto surfaces. The generation of a positively charged surface is first needed for such an immobilization reaction. Habardzumyan *et al.* reported the successful oxidation of polystyrene substrates using NaOH (Hambardzumyan *et al.* 2002). Therefore NaOH was employed for the etching of polystyrene surfaces to expose the maximal number of carboxyl groups.

White-wall transparent bottomed 96-well TCPS plates (Corning) were used for NaOH etching. Following Habardzumyan *et al.*, a solution of 4: 1 (v/v) NaOH (4 N): methanol was prepared and 250 µl added into each well at the nominated time points (day 0 to day 7) at 37 ^{o}C. After 7 days, the wells were washed with 10 % citric acid (Sigma Aldrich) for 1 h and used for subsequent ^{3}H-GAG grafting assays.

3.2.11. Fluorescamine Assay

To compare the amount of primary amines in various GAGs (heparin, HS^{pm}, $HS9^{+ve}$ and $HS9^{-ve}$), a fluorescamine protein dye assay was conducted. The dye reacts rapidly with primary amines and, when activated at 365 nm, emits at 470 nm; thus it is particularly suitable for the quantification of minute amounts of GAG. Fresh stocks of fluorescamine (Sigma Aldrich) (3 mg/ml) were prepared with dimethyl sulfoxide (DMSO) in an amber tube with vigorous mixing. Two GAG concentrations (0.5 and 1 mg/ml) were utilized. GAG solutions (90 µl) were added to 30 µl of the stock fluorescamine solution and mixed by pipeting. The reaction was allowed to proceed at room temperature for 15 min, after which the reaction was thoroughly mixed and read using an Infinite® 200 Multimode Microplate Reader (Tecan, Switzerland).

Standard curves were generated from the two-fold dilutions of BSA (from 500 μg/ml) standards. The 90 μl standards were mixed with 30 μl of dye at room temperature for 15 min and read. Concentrations of primary amines were quantified by comparison to the standard curve.

3.2.12. Covalent binding of GAG to TCPS with EDC

To physically link HS onto NaOH-etched PS and TCPS surfaces, covalent immobilization using EDC was explored. The carboxyl groups on the plates were utilised to form stable amide bonds with the free amine groups on the GAGs. The 1-ethyl-3-[3-dimethylaminopropyl] carbodiimide hydrochloride (EDC) (Sigma Aldrich) is a soluble, zero-length carbodiimide crosslinker that activates carboxyl groups into a reactive ester for the spontaneous reaction with primary amines. Preliminary experiments aimed at optimizing the concentration of EDC required to crosslink amine of ^{3}H-lysine (Perkin Elmer) yielded a working concentration of 50 mg/ml. This EDC concentration was dissolved in 0.1 M MES buffer, pH 6, and 200 μl of this solution was added into a well of the white-wall transparent bottomed 96-well TCPS plates to react for 1 h at room temperature with agitation. EDC reacts with the carboxyl group on the plate to form an amine-reactive *O*-acylisourea ester intermediate. This intermediate forms an amide bond when it encounters a primary amine; if not, it hydrolyzes and regenerates the carboxyl group. After 60 min, the plate was first washed with 0.1 M MES buffer and then with water, twice each. This removes the excess reagents and cross-linking by-products. Different concentrations of ^{3}H-heparin and ^{3}H-HS (0 to 100 mg/ml) in PBS (100 μl) were added into triplicate wells and incubated at room temperature for 2 h with agitation. Finally, the wells were washed twice with 10 x PBS (10 min each), once with water (10 min) and three more

times with water (5 min each). This excessive washing removes any unbound reagent. Scintillation liquid (200 µl) was added into each well and radioactive counts (1 min) monitored on a MicroBeta counter (Perkin Elmer, Massachusetts, USA).

3.2.13. Poly-L-lysine coating

A simpler method of creating a positively charged surface is by the coating of poly-L-lysine on TCPS. This allowed electrostatic binding between the positively charged surface and the negatively charged HS. The 0.01 % PLL solution (Sigma Aldrich) (50 µl) was added into each well of the white-wall transparent bottomed 96-well TCPS plates or 300 µl into each well of 24-well plate for 5 min at room temperature with agitation. Excess unbound PLL solution was removed and the surface washed twice with PBS. The plate was air-dried for 3 h. The poly-L-lysine coated positive charged surfaces were then utilized for the immobilization of GAGs (5 µg/ml) and subsequent cell culture.

3.2.14. Screening of PLL surface with HES-3 cells

To ensure the suitability of PLL surfaces for stem cell culture, a cell attachment assay was performed with HES-3. PLL-pre-coated 24-well plates were coated with 400 µl of GAG (heparin, HS^{pm}, $HS9^{+ve}$, $HS9^{-ve}$) (5 µg/ml) in PBS for 2 h at room temperature. Wells were washed with PBS and subsequently coated with VN2.5 or VN5 (300 µl per well) in PBS overnight at 4 ^{o}C. Wells were named according to which GAG and what VN concentration was used i.e.; PLL+GAG+VN.

HES-3 cells were routinely maintained on TCPS coated with VN5 in mTeSR^{TM}1 media (Stem Cell Technologies). Differentiated cells were removed by manual pipetting and the rest were dissociated mechanically. Cells (3 x 10^5) were

seeded into each PLL+GAG+VN well and cell growth was observed at the end of day 7.

3.2.15. Allylamine plasma polymerization and analysis

To robustly generate positively charge TCPS surfaces for electrostatic immobilization of negative charged GAGs, plasma polymerization using allylamine monomer (Sigma Aldrich) was employed. The plasma reactor is made up of a cylindrical stainless steel vacuum vessel (~ 100 L volume) with an internal electrode at one end. Polystyrene plates (96-well or 24-well) (SARSTEDT) and an aluminium foil were placed in the chamber under vacuum overnight to remove any air prior to the next day's plasma coating. The reactor was evacuated to a base pressure of less than 5 x 10^{-4} mbar, using a two-stage rotary pump coupled to a liquid nitrogen cold trap. The flow of the monomer into the chamber was controlled with a needle valve.

Allylamine monomer was degassed over several freeze-thaw cycles to remove dissolved gases before use. A monomer flow rate of ~ 5 standard cubic centimetres per minute (sccm) (Mahoney *et al.* 2004) was tuned with the needle valve and allowed to stabilise before deposition. To achieve the different percentages of the AA-coated plates, the flow was mixed with different ratios of allylamine and octa-1, 7-diene. The monomer ratios used were 100% allylamine, 90% allylamine: 10% octa-1, 7-diene, 80% allylamine: 20% octa-1, 7-diene, 50% allylamine: 50% octa-1, 7-diene and 100% octa-1, 7-diene. The flow rate was calculated using this formula based on Robinson *et al.* (Robinson *et al.* 2008):

(Pressure after isolating the chamber at the end of 30 sec – pressure before isolating the chamber)/ 30 *1251

Plasma was then ignited with a radio frequency generator (Coaxial Power System Ltd, UK) at 13.56 MHz and 5 Watts of power. The plasma was turned on for 40 min after which the chamber was pumped back to base pressure. The plates were removed and lids were replaced to maintain sterility. These sterile plates were then used for the experiments involving immobilization of GAGs for cell culture. The aluminium foil in the chamber was read by a XPS equipped with an aluminium anode and wide-scan analysis to confirm the density of amines deposited onto the plates (Mawson Institute, University of South Australia). Results were analyzed with CasaXPS software. The nitrogen: carbon (N: C) ratios were calculated from the area underneath the N and C peaks to obtained the relative amount of AA on the surface. Immobilized GAGs on the various percentages of AA coated 96-well plates were analysed for its binding ability to VN using the GAG ELISA assay method as described in Section 3.2.8.

3.2.16. Quantification of ^{3}H-heparin and ^{3}H-HS^{pm}

To determine the amount of GAG bound to the 100 % AA-polymerized 96-well plate, binding assays using ^{3}H-heparin (Perkin Elmer) and ^{3}H-HS^{pm} (radiolabelled by RC TRITEC, Switzerland) were employed. Ascending concentrations (0, 1.25, 2.5 and 5 μg/ml) of mixtures of 90 % un-labelled heparin or HS^{pm} : 10% of ^{3}H-heparin and ^{3}H-HS^{pm} radioactive solution were prepared in PBS. Each GAG solution (200 μl) was incubated on the surfaces to be tested (TCPS, PLL, AA) overnight at room temperature. The next day, wells were washed with PBS three times, 200 μl of scintillation cocktail added, and the plates read three times in a MicroBeta liquid scintillation counter for 1 min each. A standard curve was generated

with known amounts of ^{3}H-GAG and surface densities of heparin and HS^{pm} were determined.

3.2.17. ^{125}I-VN quantification on surfaces

To quantify the amount of VN bound to the different 96-well plates (TCPS, PLL+$HS9^{+ve}$ and 100 % AA polymerized surfaces coated with $HS9^{+ve}$ (AA+$HS9^{+ve}$)), a highly sensitive radiolabelling study using radioactive-labelled VN was employed. Surfaces were previously coated with 5 μg/ml of $HS9^{+ve}$ at 300 μl per well. VN was labelled with ^{125}I isotope (Perkin Elmer) using Thermo Scientific Pierce Iodination Beads and quantification was conducted as described in section 2.2.14.

3.2.18. Statistical analysis

All data values are reported as the mean $\pm$ standard error taken from three individual experiments with triplicate runs each. One-way ANOVA was performed to compare differences across the groups, and $P < 0.05$ was considered as significant. A two-tailed student's t-test was performed to determine the differences between two sample groups. Graphs were plotted and data transformed using Sigma plot software.

3.3. Results

3.3.1. Surface heparan sulfate is important for attachment to VN-HBD substrate

As endogenous GAGs could be part of the attachment apparatus to VN (Klim *et al.* 2010), I first sought to investigate the role of surface HS in cell attachment. Braam *et al.* have previously shown that αVβ5 integrin is required for hESCs to adhere to full-length VN (Braam *et al.* 2008). Another study by Klim *et al.* demonstrated that surface GAG is important for hESCs to bind VN-HBD, which lack RGD motif, after digestion with chrondroitinase ABC. Together both studies reported the involvement of integrins and endogenous CS in attachment.

However, chrondroitinase ABC digests primarily chondroitin sulfate (CS), rather than the most abundant GAG on stem cell surfaces, HS. Therefore, to investigate the functional role of surface HS on cell attachment to VN-coated TCPS, the enzymes heparinase I, II and III were first used to specifically digest cell surface HS. When used in combination, the enzymes can remove > 90 % of endogenous HS (Manton *et al.* 2007). After digestion, the cells were analyzed by FACS to confirm the absence of surface HS with both the 10E4 and 3G10 antibodies (Fig. 3.1). The 10E4 antibody binds to intact HS and 3G10 antibody binds to depolymerized HS chains. Before digestion, the cells expressed high levels (> 90 %) of intact 10E4-reactive HS and low levels (< 2 %) of digested 3G10-reactive HS. After heparinase digestion, intact HS chains were removed, so revealing > 95 % 3G10-reactive de-saturated uronic acid residues on the cell surface (Fig. 3.1). This confirmed the absence of endogenous HS after heparinase digestion.

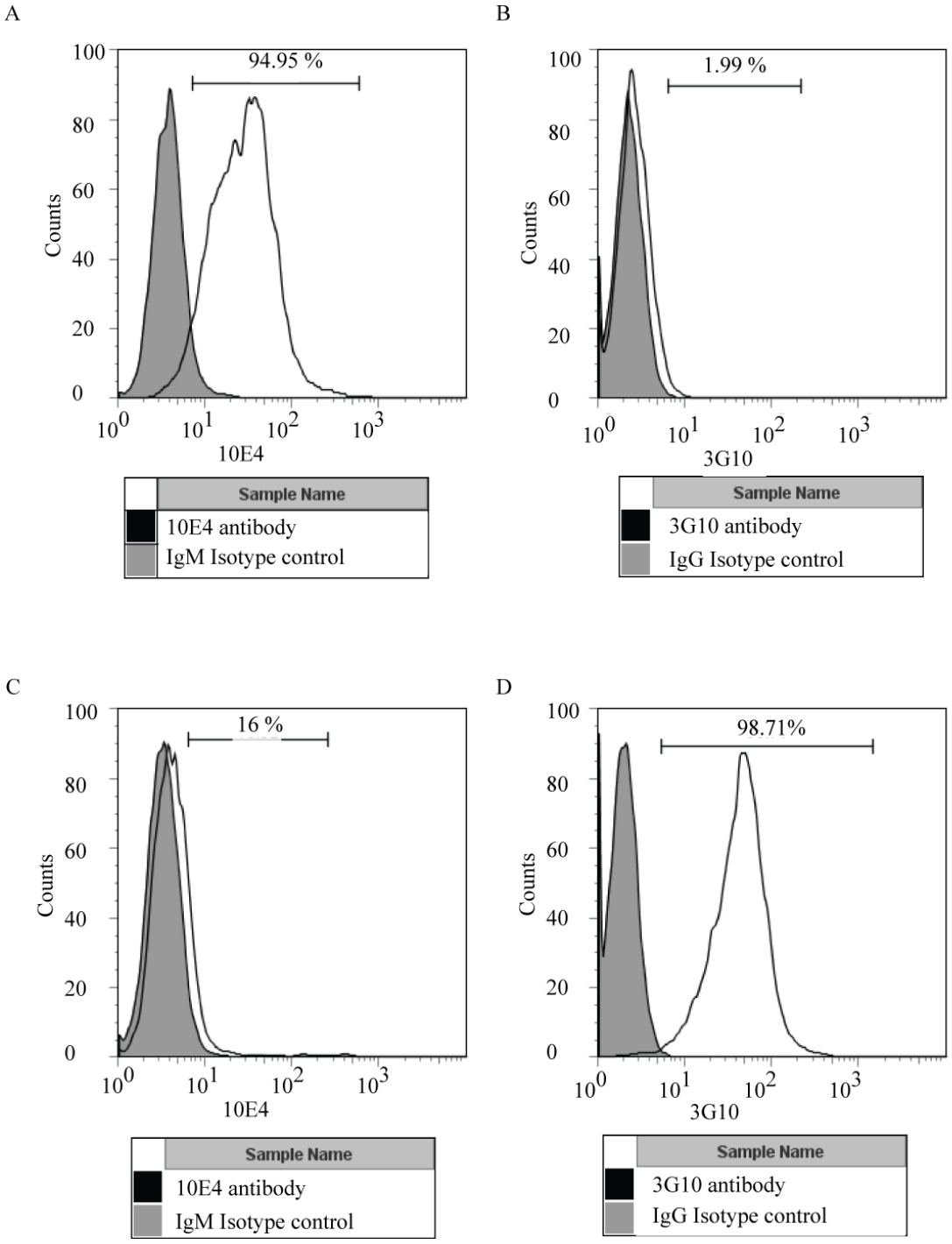

Figure 3.1. FACS analysis of HES-3 cells before and after heparinase I, II and III digestion. (A) 10E4 (B) 3G10 antibody staining of cells before enzyme digestion. Cells expressed high levels of intact HS chains, and low levels of digested HS chains. (C) 10E4 and (D) 3G10 antibody staining of cells after enzyme digestion. Cells expressed low levels of intact HS chains and high levels of digested HS chains.

The digested cells were then seeded onto VN or VN-HBD surfaces and their attachment was measured. Data clearly showed that the binding ability to this peptide surface was reduced for digested cells but not affected for untreated cells (Fig. 3.2). Pre-incubation of cells with soluble heparin also reduce its binding (~ 40 %) implying that heparin was able to compete with endogenous HS in binding to peptide. Taken together, this showed that the cells bind to VN-HBD peptide via endogenous HS. In contrast, cells in either treatment did not have their binding reduced on the VN5 surface, which is similar to untreated cells. Therefore, this suggested that surface HS was not critical for the binding to full length VN, a binding for which cells mainly use αVβ5 integrin.

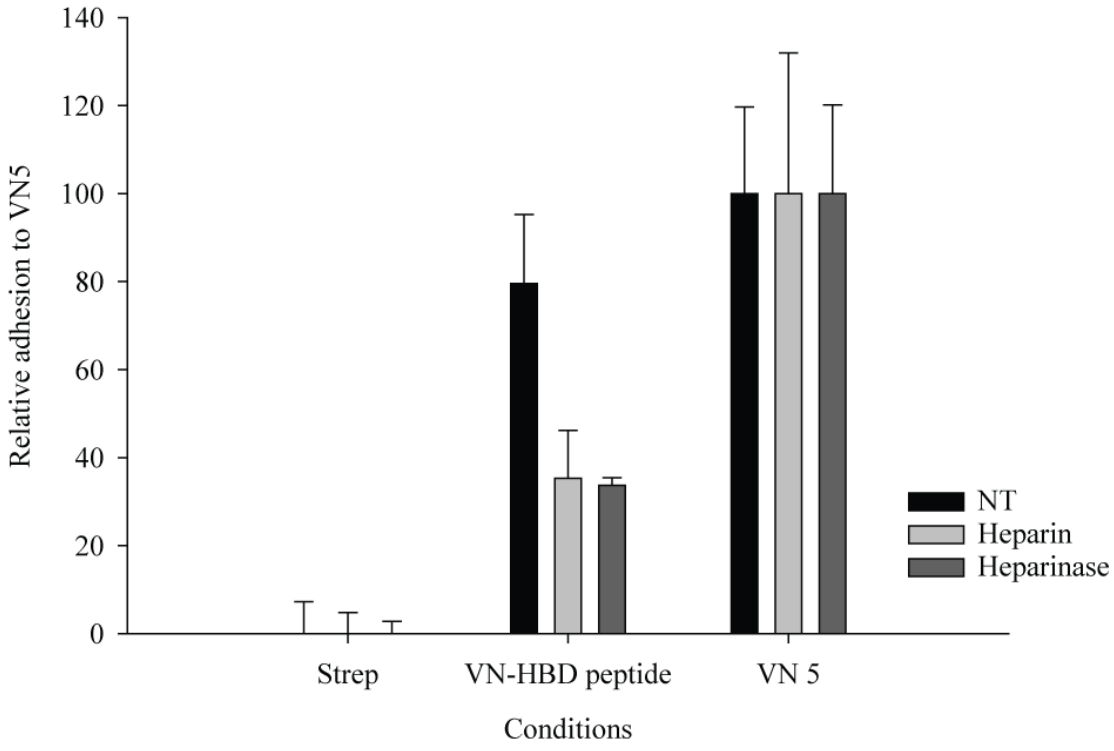

Figure 3.2. Heparinase I, II and III-digested HES-3 cell adhesion assay. Intact cells, cells pre-incubated with heparin, and heparinase-digested cells were analyzed by the crystal violet cell adhesion assay. Cells were seeded onto streptavidin control surfaces, VN-HBD peptide surfaces or VN5 surfaces. The adhesion to VN-HBD peptide was reduced by ~ 40 % after heparin and heparinase treatment, while the cells' ability to bind VN5 was not affected. Thus cell surface HS is important for the binding of hESCs to the VN-HBD.

3.3.2. Isolation of HS9^{+ve} variant

Following the findings that endogenous HS participated in cell binding, we next explored the possibility of isolating an HS variant with high VN binding affinity. To confirm the heparin binding ability of the synthesized biotinylated VN-HBD peptide, a ^{3}H-heparin radioactivity binding assay was first performed. It was adapted from a publication by Baird *et al.* who enzymatically digested FGF-2 into peptides and investigated its binding to ^{3}H-heparin (Baird *et al.* 1988). The assay was performed on nitrocellulose membranes and the data showed that the peptides were able to bind to ^{3}H-heparin in a concentration-dependent manner (Fig. 3.3), suggesting that this sequence in VN is indeed heparin-binding and could be used for affinity chromatography.

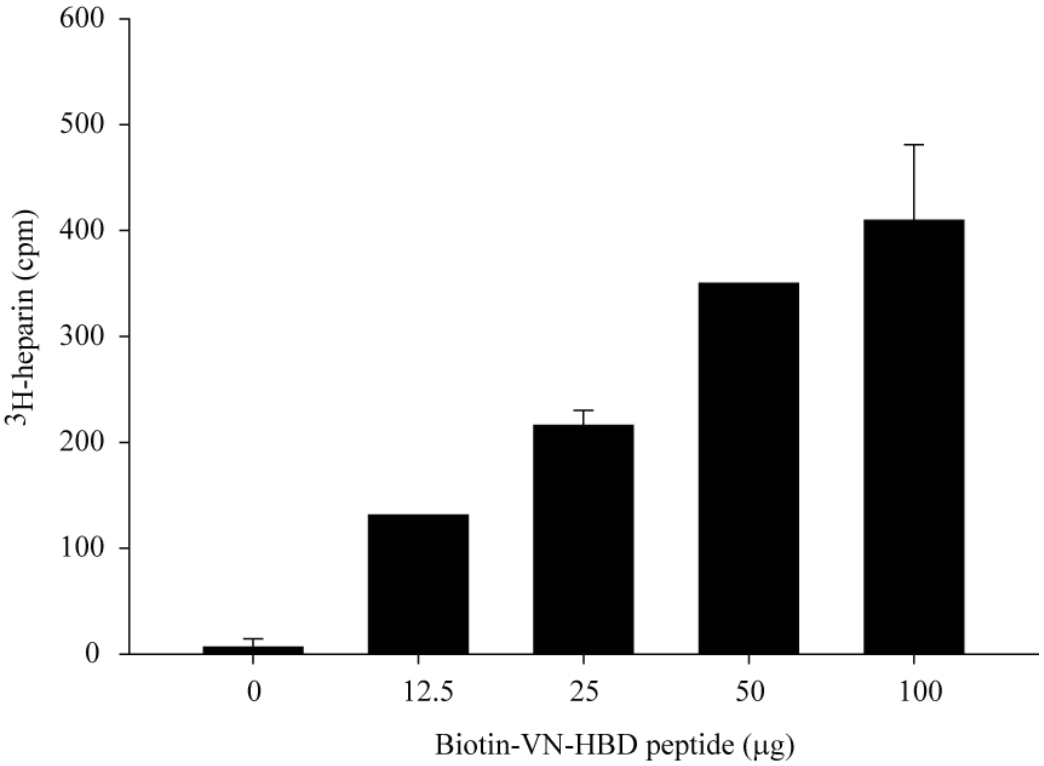

Figure 3.3. Binding ability of VN-HBD to ^{3}H-heparin. VN-HBD peptides were spotted onto nitrocellulose membranes, air dried and incubated with ^{3}H-heparin. Bound ^{3}H-heparin was determined by liquid scintillation.

As the peptide was able to bind heparin, it was then used to derivatise streptavidin columns for affinity chromatography. The column was first saturated with biotin-peptide until excess peptide (green trace) was observed in the flowthrough at 280 nm (Fig.3.4). To assess the binding affinity between streptavidin and biotin-peptide, the column was washed with 1.5 M high salt buffer (red trace). No peptide was eluted off the column, indicating that the column is saturated with strongly bound peptides that will not dissociate during the later elution of HS variants. The column was equilibrated with low salt buffer in readiness for the loading of the commercial preparation of HS^{pm} (Fig. 3.5). Collected variants that did not bind to the peptide (blue trace) were designated as the $HS9^{-ve}$ variant. Bound variants were eluted from the column using a one-step 1.5 M NaCl elution (red trace) and collected as the $HS9^{+ve}$ variant (blue trace). The NaCl was removed by a desalting step using HiPrep 26/10 desalting columns (Fig. 3.6). From the 100 mg of starting HS^{pm}, 19.6 mg (19.6 %) of $HS9^{+ve}$ and 43.4 mg (43.4 %) of $HS9^{-ve}$ were isolated; the rest of the weight was constituted by NaCl. An interesting observation was the presence of a lag time to reach maximum elution in $HS9^{+ve}$ during the high salt washes. This suggested that there is a heterogeneous population of high- to low-binding affinity species in $HS9^{+ve}$ variant. A modification to the elution buffer, involving a step-wise elution with a different molarity buffer to separate the different species in $HS9^{+ve}$ is a future possibility. The binding ability of the $HS9^{+ve}$ and $HS9^{-ve}$ fractions to VN were determined prior to further characterization.

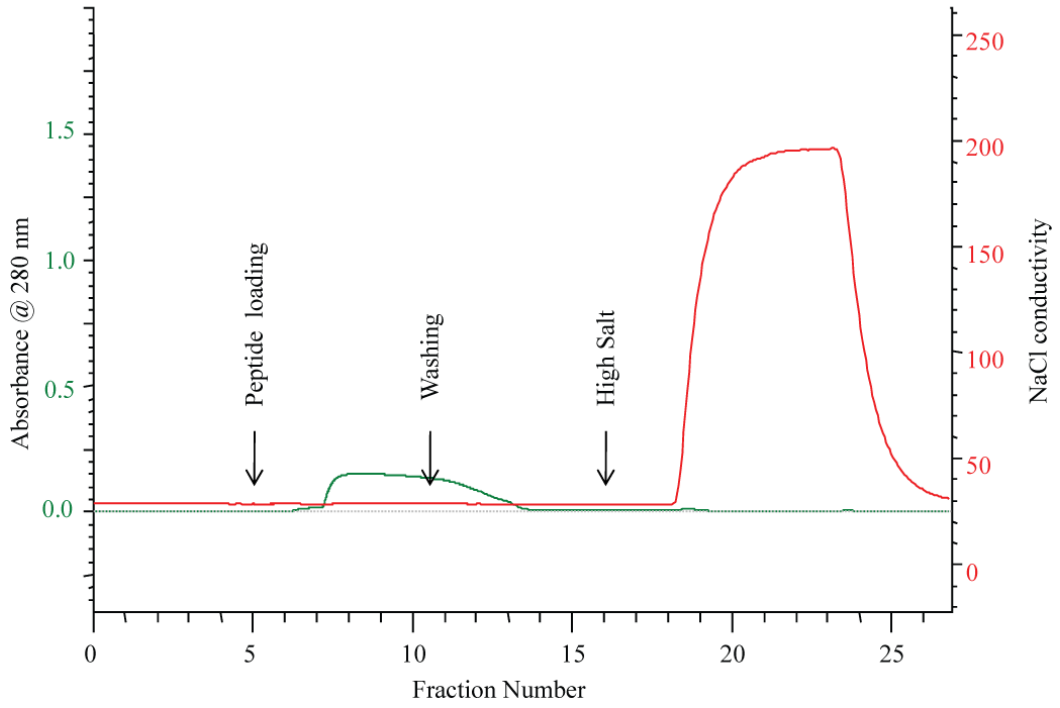

Figure 3.4. Chromatogram of biotinylated VN-HBD peptide loading. Peptide was loaded into the column and excess peptide that flows out of the column was monitored at 280 nm. Column was washed with 1.5 M high salt buffer to ensure peptide is tightly bound to the column.

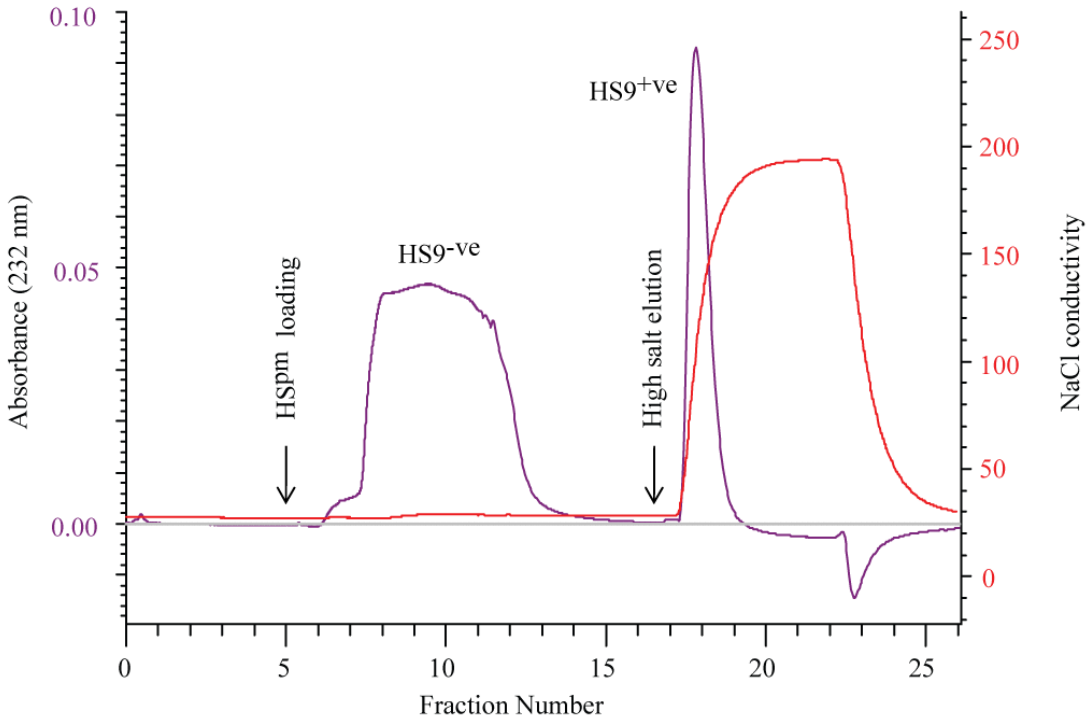

Figure 3.5. Chromatogram depicting HS9^{+ve} isolation. HS9^{+ve} variant were isolated from the starting HS^{pm} mixture using streptavidin column pre-bound with VN-HBD peptide. A high salt wash (1.5 M) (red trace) released the HS9^{+ve} variant (blue trace) and was collected.

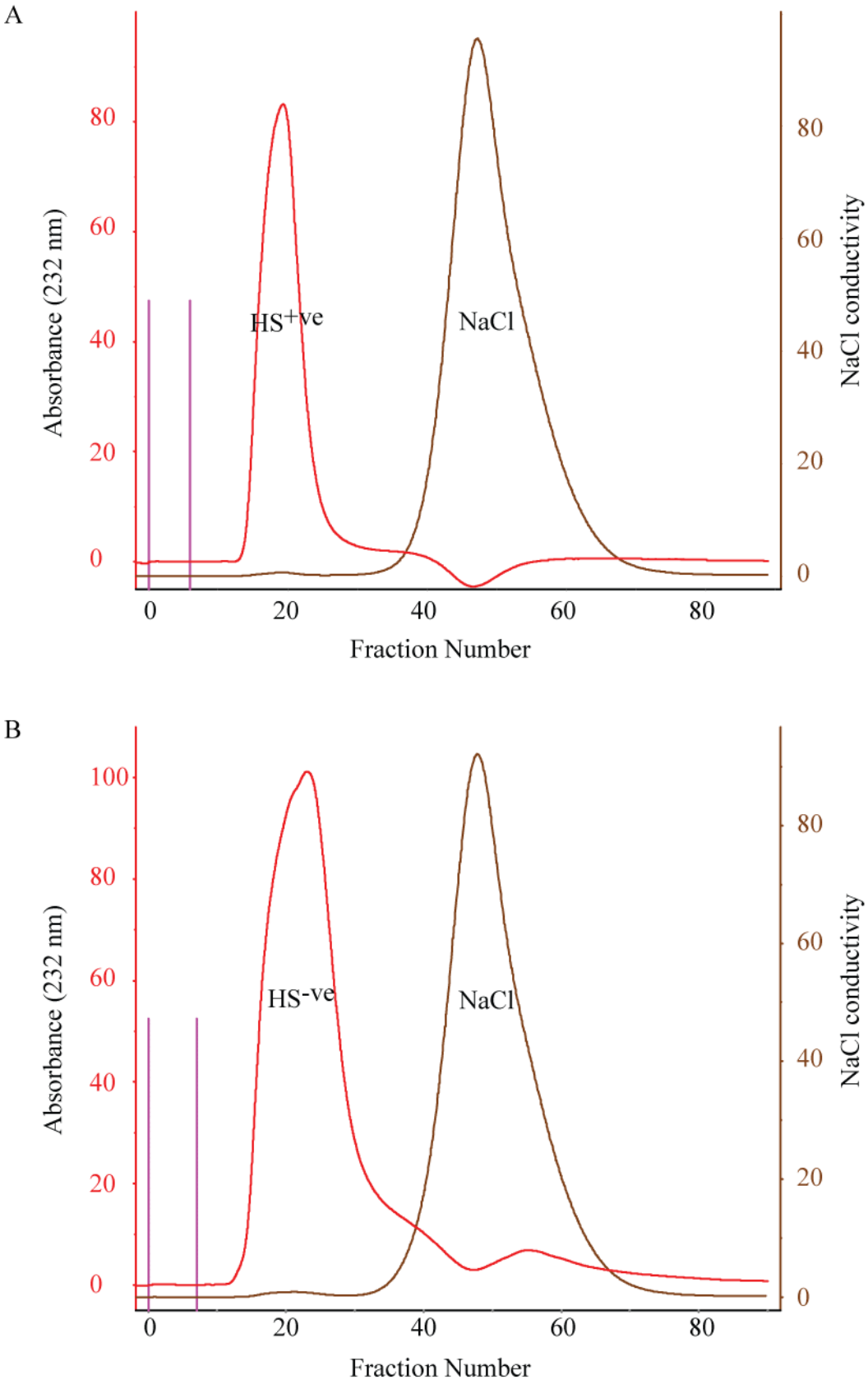

Figure 3.6. Elution profile of desalted HS variants. The high molecular weight HS eluted first, while the smaller NaCl eluted last. (A) Elution profile of $HS9^{+ve}$ variant (B) Elution profile of the $HS9^{-ve}$ variant.

3.3.3. HS variants characterization

To further investigate the binding affinity of heparin, starting material (HS^{pm}), bound variant ($HS9^{+ve}$) and unbound variant ($HS9^{-ve}$), dot blotting, heparin-Sepharose bead assays and GAG microtiter plate assays were conducted. These assays used different strategies to assess their VN binding affinity, either by immobilizing VN or GAG, or a competition for VN binding to heparin beads.

3.3.3.1. Dot blotting

An immunoblot using nitrocellulose-immobilized VN, followed by biotinylated GAG, was used to verify the binding ability of each HS variant. No non-specific binding of the GAGs was detected as shown by the absence of spots in negative control (Fig. 3.7). In the positive control, heparin was found to bind strongly to VN, producing an intense spot on the film. As for the rest of the variants, $HS9^{+ve}$ bound to VN better than $HS9^{-ve}$ variants, and HS^{pm} was found to have an intermediate binding ability. This was expected, as we surmised HS^{pm} contained mixtures of HS, and thus highly variable degrees of binding ability.

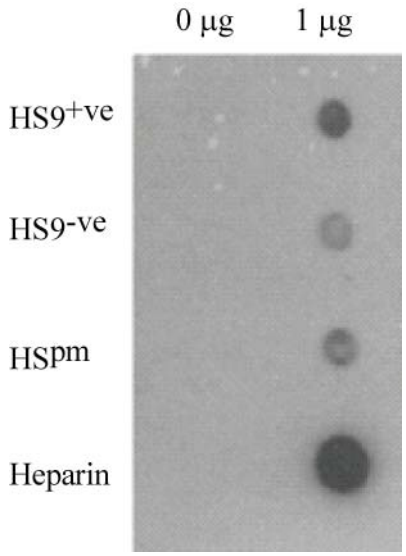

Figure 3.7. Dot blots binding profile of the different HS variants. VN was spotted onto the membrane and incubated with different GAGs ($HS9^{+ve}$, $HS9^{-ve}$, HS^{pm} and heparin). $HS9^{+ve}$ variants have a higher binding capacity for heparin than the $HS9^{-ve}$ variants; HS^{pm} has only intermediate binding ability. Heparin serves as a positive control.

3.3.3.2. Heparin-Sepharose bead competition assay

To more fully explore the relative affinity of each of the HS variants to VN, a heparin-Sepharose bead assay was employed. This assay measures the ability of the HS variants to inhibit the binding of VN to heparin beads. Heparin, having a net negative charge, will bind to VN with the highest affinity. Therefore, the binding ability of heparin for VN was challenged with the different HS variants. A successful challenge would result in lower VN binding to the beads, suggesting that the HS variant binds to VN with higher affinity, as measured by ELISA.

To show that VN did bind to the heparin beads, and to determine a good working concentration for VN, various amounts of VN were utilized (0 – 80 ng) and detected using this ELISA method. A good working concentration of VN will require suboptimal VN levels to prevent any false positive results arising from the excess VN binding to the beads. The VN saturation curve revealed that VN bound in a concentration-dependent manner, with maximal binding occurring at 40 ng of VN.

The sub-optimal VN amount identified from the curve was 20 ng (Fig. 3.8). The inserts in Figure 3.8 depict the immunoblot bands, which visualize the amount of VN on the beads. As a control, absorbance from the VN (20 ng) was used as the 100 % VN bound to the beads. The subsequent competition was done with the same amount of VN and results expressed in % bound relative to this 100 % level.

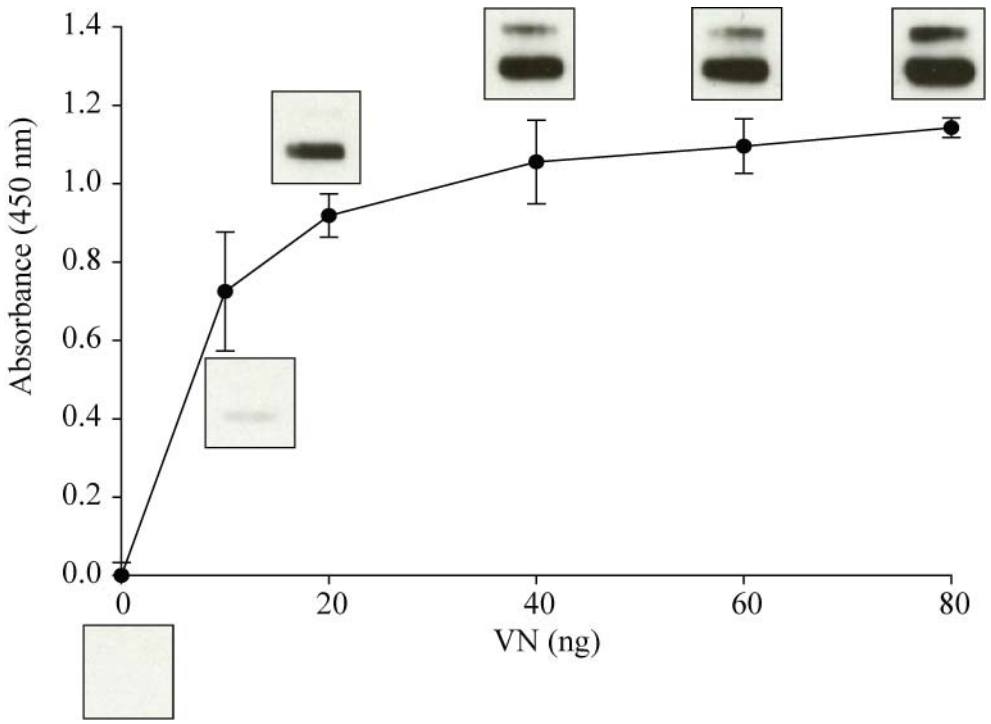

Figure 3.8. VN binding profile on heparin beads. Beads were incubated with different amounts of VN, and visualized with HRP. To prevent non-specific binding, sub-optimal amounts of VN were used as probes. The small insert shows the immunoblot images of the respective amounts of VN.

After establishing the sub-optimal VN concentration, competition with heparin beads was performed. The assay was done with pre-incubation of VN with soluble heparin (as a positive control), HS^{pm}, $HS9^{+ve}$ or $HS9^{-ve}$ variants, each at 5, 50 and 100 µg. Results were normalized to the absorbance of 100 % VN-bound beads as measured previously, and plotted as % bound to beads (Fig. 3.9A). In this procedure,

the HS variants that specifically bind to VN would competitively inhibit the binding of the VN to the heparin beads. Soluble heparin (100 μg) could almost completely inhibit VN binding (< 10 % binding) to the heparin beads as confirmed by the lack of detection of bound VN. The $HS9^{-ve}$ variant had the weakest binding affinity for VN as shown by the high absorbances detected. Increasing amounts of $HS9^{-ve}$ even to 100 μg could not inhibit the interactions between VN and the heparin beads, thus a higher amount (~ 50 %) remained bound on the beads. In contrast, with the increasing amount of $HS9^{+ve}$ variant, a concentration-dependent inhibition of VN binding to the beads was observed. The $HS9^{+ve}$ variant had a much greater binding affinity for VN than $HS9^{-ve}$, because it can strongly inhibit VN from binding to the beads as indicated by the lesser amount of VN detected (~ 10 % bound at 100 μg VN). An intermediate binding affinity was detected from HS^{pm} as suggested by the intermediary inhibition (~ 30 % bound at 100 μg VN) to the VN-bead interaction. Together, these findings suggested that the binding affinity of the $HS9^{+ve}$ variant is higher than the $HS9^{-ve}$ variant, and that HS^{pm} has an intermediate affinity.

To further understand the requirements of HS-VN binding, the ionic strength of the binding buffer was also systemically varied. Immunoblotting results revealed that desalted HS^{pm} could inhibit VN-bead binding, as indicated by the decrease in band intensity. However, NaCl-containing HS^{pm} could not bind to VN, as confirmed by the strong band intensity (Fig. 3.9B). This was expected because the cations in the NaCl-containing buffer will bind to the negative charges on HS and mask its VN binding domains. Therefore only physiological buffers such as PBS were used for subsequent binding experiments.

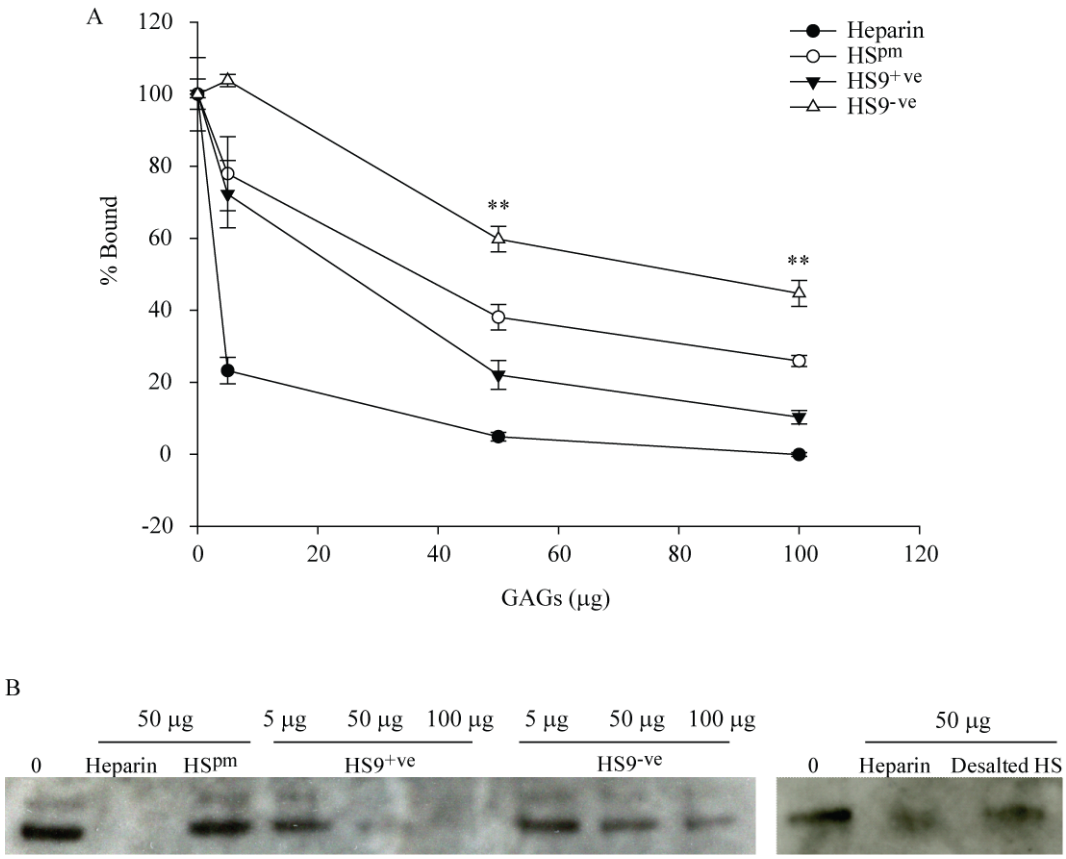

Figure 3.9. Inhibitory effects of various HS variants on the binding of VN to heparin beads. (A) The competition assay was performed with soluble heparin (as a positive control), or the HS variants. Soluble heparin binds to most avidly to VN, followed by $HS9^{+ve}$, HS^{pm} and $HS9^{-ve}$. (B) Immunoblot images of the VN left on the beads after competition. Note that desalted HS^{pm} binds to VN better than NaCl containing HS^{pm}. ** = $P < 0.05$

In order to confirm the relative specificity of $HS9^{+ve}$ for VN, the affinity of $HS9^{+ve}$ for other ECM proteins (FN and LN) was also investigated. Similarly, the suboptimal working amount of each ECM protein was predetermined, before the competition assays were performed. The saturating binding profiles of FN and LN showed that the sub-optimal amounts were 200 ng and 1 µg respectively (Fig. 3.10). These determined amounts were utilized for the subsequent competition assays and for the normalization of competition data to achieve % bound on beads.

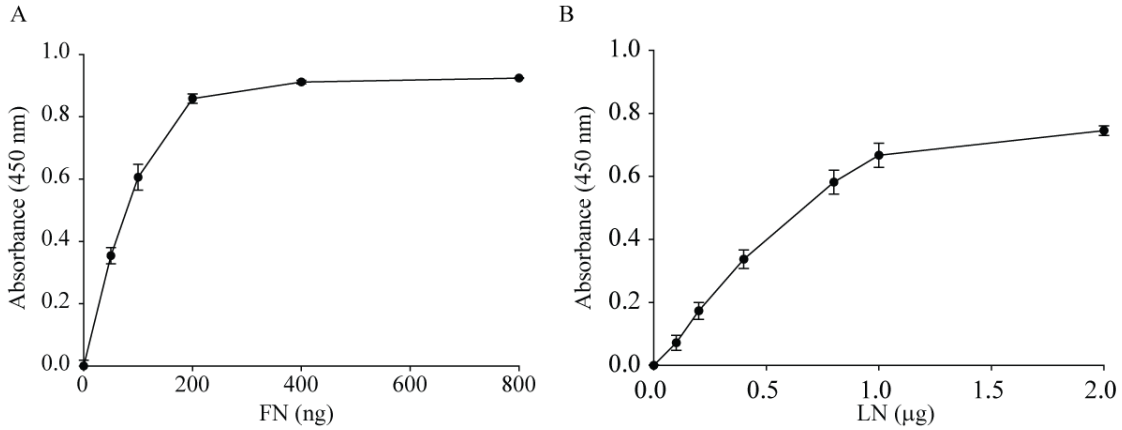

Figure 3.10. Binding profiles of FN and LN to heparin beads. Binding profile of each protein (A) FN and (b) LN on heparin beads. Beads bound to increasing amount of protein and reached saturation at 200 ng for FN and 1 μg for LN.

Increasing concentrations of soluble the HS9^{+ve} variant were used to competitively inhibit the binding of the different ECM proteins to the heparin beads, and the amount of protein left on the beads measured with their respective antibody (Fig. 3.11A). The HS9^{+ve} variant dose-dependently inhibited the binding of VN to heparin beads, leading to a lower level of VN detected, but did not inhibit the binding of FN and LN to heparin beads. This was indicated by the lack of dose-dependent decrease in protein bound even at 100 μg of HS9^{+ve}, suggesting that HS9^{+ve} have specificity for VN. Concurrently, the HS9^{-ve} variant was also used to inhibit VN binding to heparin beads (Fig. 3.11B). The data showed that HS9^{-ve} variant was able to inhibit FN binding to the beads better than VN or LN. This suggested that that the HS9^{-ve} variant was enriched for FN-binding sequences. Further isolation of an FN-binding HS is thus justifiable.

In order to ensure that this competitive inhibition procedure is reliable, soluble heparin was used as the competitor (Fig. 3.11C). Heparin inhibited all three ECM proteins to varying degrees, with VN inhibition better than FN and LN in binding to heparin beads (Fig. 3.11C). Collectively these findings in heparin-Sepharose bead

assays clearly show that HS9 variants have a graded binding affinity to VN: heparin > $HS9^{+ve}$ > HS^{pm} > $HS9^{-ve}$. Also, the $HS9^{+ve}$ variant avidly bind more VN than the $HS9^{-ve}$ variant. This highlighted the practical use of affinity chromatography to separate better VN-binding HS variants from a mixture HS^{pm}.

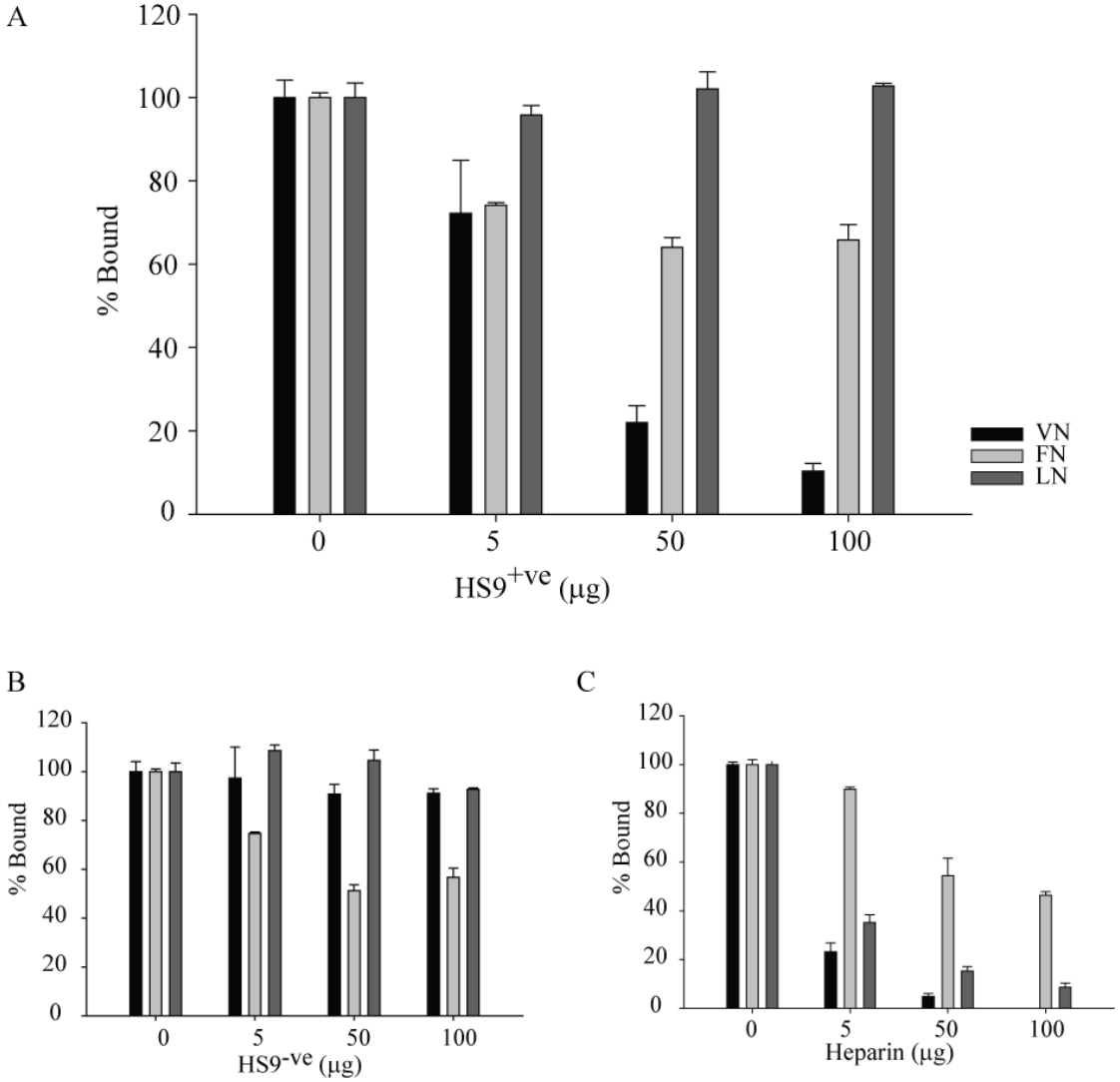

Figure 3.11. Inhibitory effect of HS variants on the binding of VN, FN and LN to heparin beads. (A) Different concentrations of $HS9^{+ve}$ were used to compete with heparin beads for binding to VN, FN and LN. $HS9^{+ve}$ variants inhibited VN rather than to FN and LN in binding to heparin beads. (B) $HS9^{-ve}$ had higher affinity to FN than VN and LN. (C) Heparin was used as positive control. Heparin was able to bind VN, FN and LN in a concentration-dependent manner with varying affinities.

3.3.3.3. Glycosaminoglycan ELISA

To provide another independent validation of HS9 variant binding affinity, an ELISA based on GAG binding to VN was investigated. The initial experiments were designed to optimize the concentrations of GAGs (heparin, HS^{pm}, $HS9^{+ve}$ and $HS9^{-ve}$) needed to completely saturate the plate surface. Wells were coated with 1, 5 and 10 μg/ml of each GAG and the binding affinity for VN explored (Fig. 3.12). At the various heparin concentrations, a dose-dependent increase in VN binding was observed (Fig. 3.12A). For HS^{pm} coatings, a marked difference was observed from 1 μg/ml and 5 μg/ml, while the increase in VN binding was less compared to the 5 μg/ml and 10 μg/ml HS^{pm} solutions (Fig. 3.12B). Similar trends were also observed with the $HS9^{+ve}$ and $HS9^{-ve}$ variants (Fig. 3.12 C and D). As significant differences were observed between the 1 and 5 μg/ml of GAGs, no further increase in VN binding was seen between 5 and 10 μg/ml. This suggested that 5 μg/ml of a GAG solution was sufficient to completely saturate the wells; this saturating concentration was therefore used for the rest of the experiments.

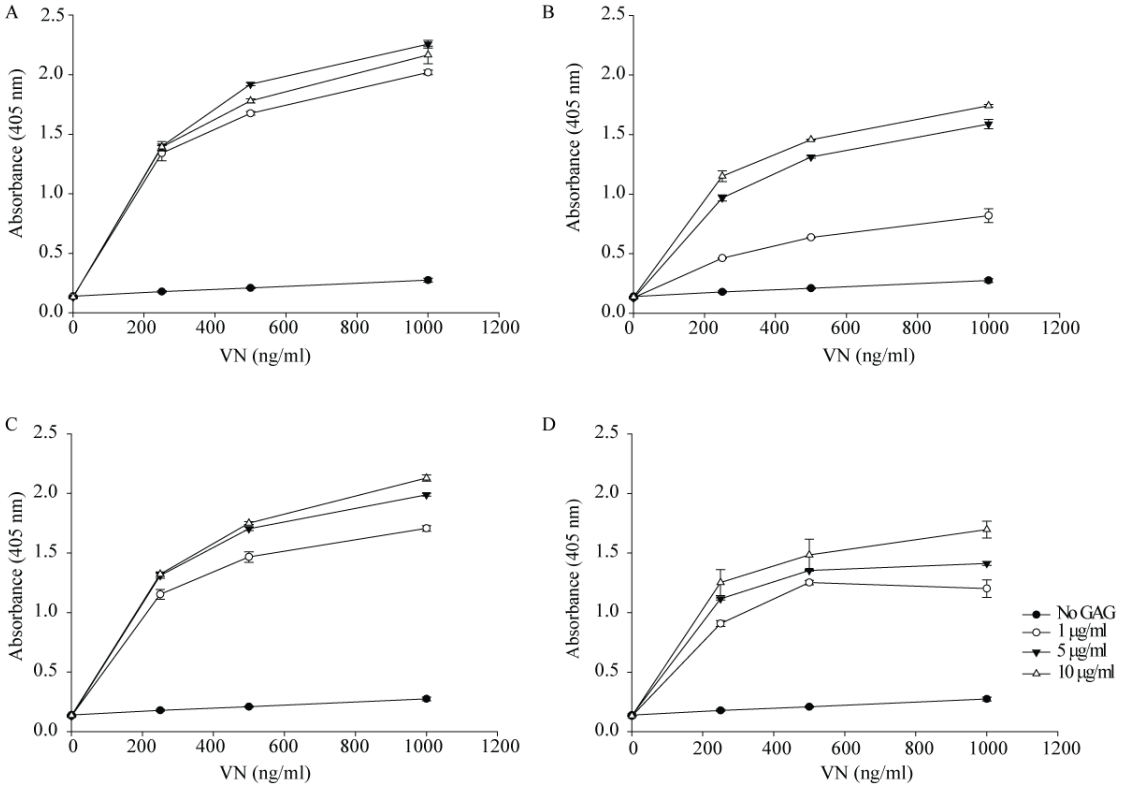

Figure 3.12. Determination of saturating amounts of GAGs with GAG ELISA. Differing concentrations of (A) heparin, (B) HS^{pm}, (C) $HS9^{+ve}$ and (D) $HS9^{-ve}$ were coated onto the wells and their ability to bind VN analyzed. No significant difference was observed in either 5 or 10 µg/ml; therefore 5 µg/ml was the saturating concentration. Uncoated wells served as the negative control.

After determining the saturating GAG concentration (5 µg/ml), GAGs were coated overnight and investigated for their binding affinity to VN (Fig. 3.13). The binding curve showed that, irrespective of GAGs, there was a dose-dependent increase in VN binding. $HS9^{+ve}$ had a significantly higher affinity for VN than starting material HS^{pm} and flowthrough $HS9^{-ve}$ variants. Heparin, being the most negatively charged variant, was bound to VN at significantly higher levels than the rest. This reinforced the results of the heparin beads competition assay, showing that the $HS9^{+ve}$ variants have a higher affinity for VN.

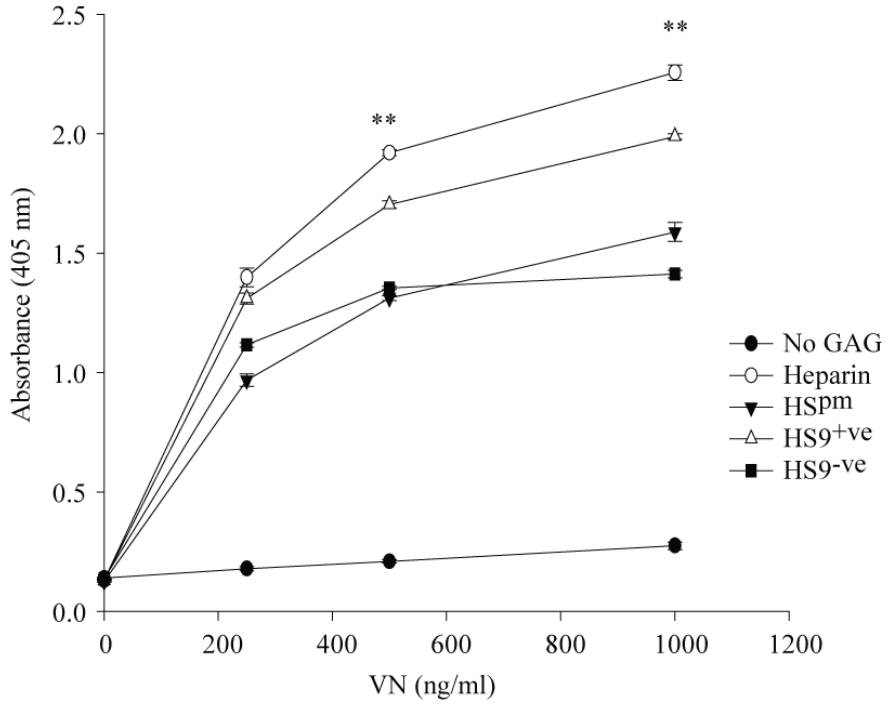

Figure 3.13. Binding profile of various GAGs to VN by GAG-ELISA. Heparin, HS^{pm}, $HS9^{+ve}$ and $HS9^{-ve}$ variants were coated onto wells and different concentrations of VN used to determine the binding ability of each GAG variant. $HS9^{+ve}$ variants had a significantly higher affinity for VN than the HS^{pm} and $HS9^{-ve}$ variants. Heparin served as a positive control. ** = $P < 0.05$

Because HS binding is in part the result of negatively charged sulfate residues along the disaccharide chain, understanding the structural composition of HS that is likely to interact with VN was next explored. To understand the necessary sulfation motifs for VN binding, selectively desulfated heparin standards were immobilized onto the ELISA surfaces (Fig. 3.14). Heparin that had been selectively de-N-sulfated or de-6-O-sulfated was found to have significantly reduced levels of binding to VN. In contrast, chains lacking 2-O sulfation were unaffected, and strongly bound to VN in a manner comparable to that of the intact heparin chains. In analogous experiments, heparin standards of varying length, from 2 disaccharides (degree of polymerization (dp2)) to 12 disaccharides (dp12), were used to look for the minimum size needed for VN binding (Fig. 3.15). There was a significant lack of binding from the dp2 and dp4

chains. For chains with more than 3 repeating units, there was similar binding affinity for VN. These results strongly suggest therefore that N- and 6-O-sulfation on chains of at least 3 repeating disaccharide units are necessary for VN binding to heparin. As heparin and HS share roughly similar disaccharide composition, this conclusion may also be valid for HS. A detailed CE analysis of the composition of $HS9^{+ve}$ and $HS9^{-ve}$ variants will be used to further quantitate such differences.

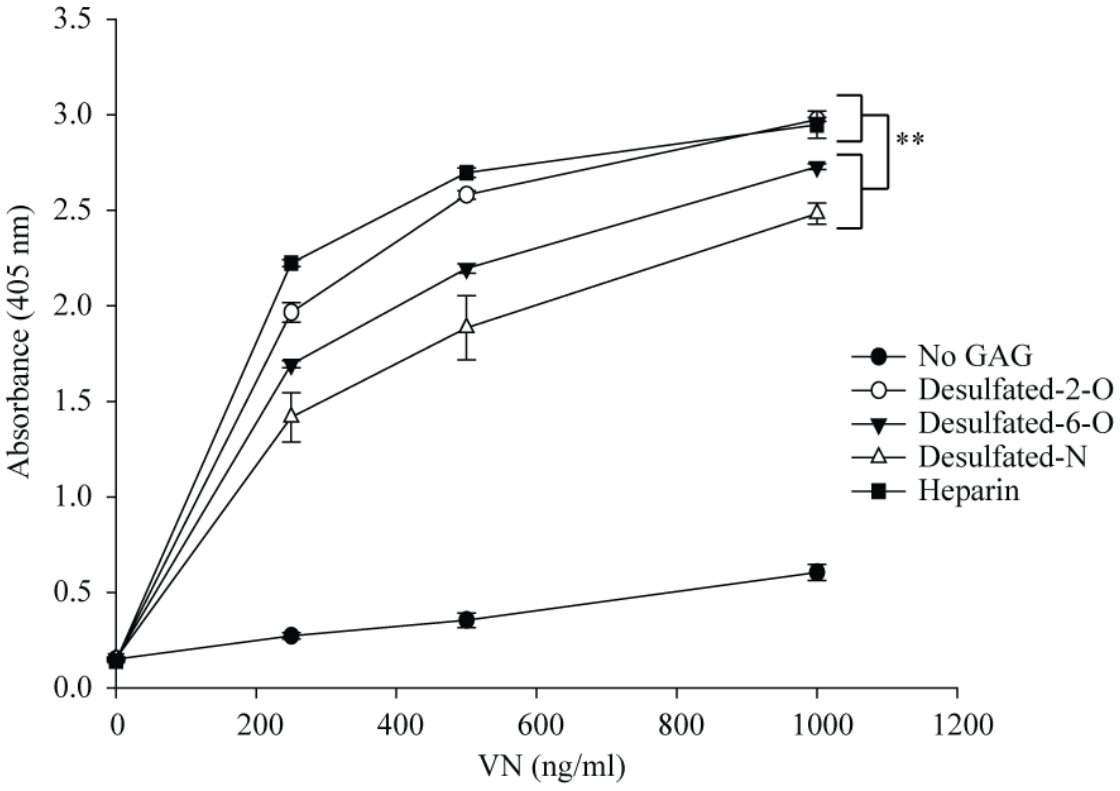

Figure 3.14. Binding profile of various de-sulfated heparin to VN by GAG-ELISA. Desulfated 2-O, 6-O and N- standards were coated onto the wells and investigated for their binding affinity to VN. Variants without 6-O and N sulfation had significantly reduced binding, and variants without 2-O sulfation had no effect on VN binding. Heparin served as a positive control. ** = $P < 0.05$

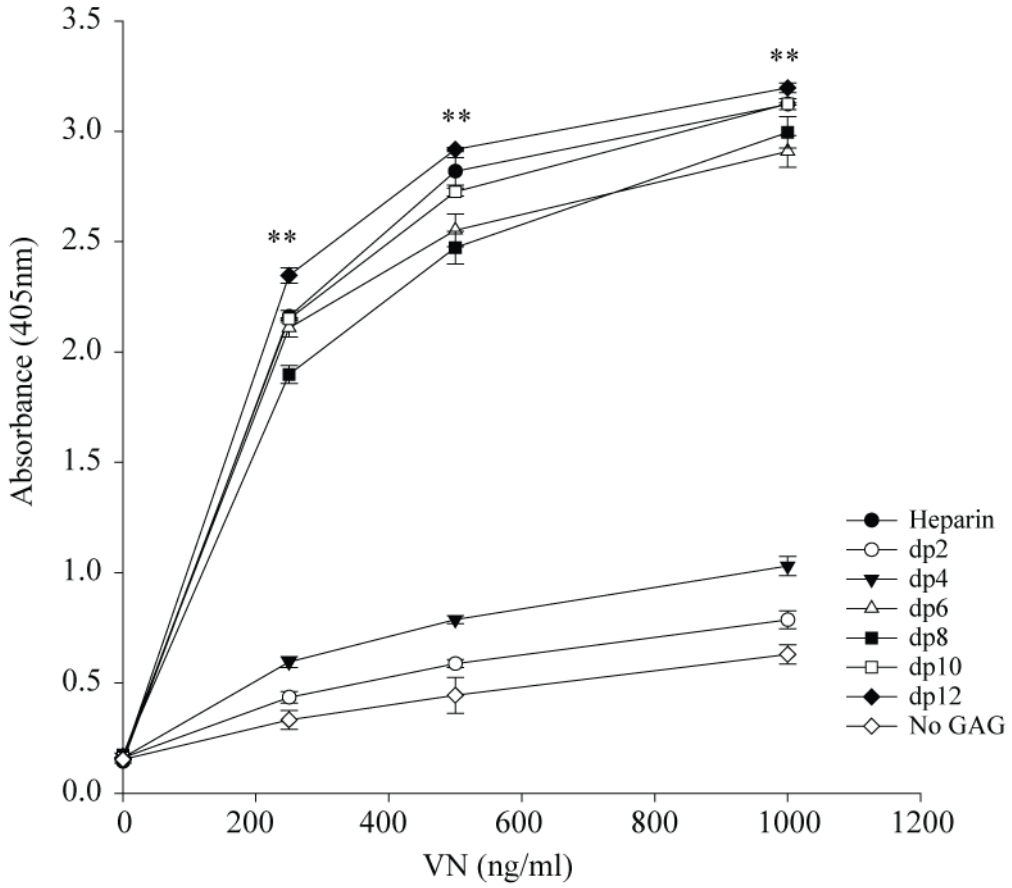

Figure 3.15. Binding profile of various length of heparin to VN by GAG-ELISA. Lengths of heparin varying from dp2 to dp12 were coated onto the wells. GAGs of dp2 and dp4 were not able to bind VN, but dp6 units and longer were able to bind to VN. ** = $P < 0.05$

3.3.3.4. Capillary electrophoresis

Capillary electrophoresis is a sensitive and powerful technique for the separation of individual heparin disaccharides based on size and charge. This method was employed for the further analysis of each of the generated HS variants. Ruiz-Calero *et al.* demonstrated that this could be attained with the separation and quantification of 8 heparin disaccharide species using a formic acid buffer, 15 kV reverse polarity and pH 3 (Ruiz-Calero *et al.* 1998). Using this protocol, the separation of 7 heparin disaccharide standards was completed, and is depicted in Figure 3.16. Δ-disaccharide standard IS designation represents Δ UA2S(1→4)-D-

GlcNS6S containing 2O-, 6O- and N-sulfation; IIS represents Δ UA(1→4)-D-GlcNS6S containing 6O- and N-sulfation; IIIS represents Δ UA2S(1→4)-D-GlcNS containing 2O- and N-sulfation; IVS represents Δ UA(1→4)-D-GlcNS containing only N-sulfation; IA represents Δ UA2S(1→4)-D-GlcNAc6S containing 2O- and 6O-sulfation; IIA represents Δ UA(1→4)-D-GlcNAc6S containing only 6O-sulfation and IIIA represents Δ UA2S(1→4)-D-GlcNAc containing only 2O-sulfation. All these structures are shown in Figure 1.12.

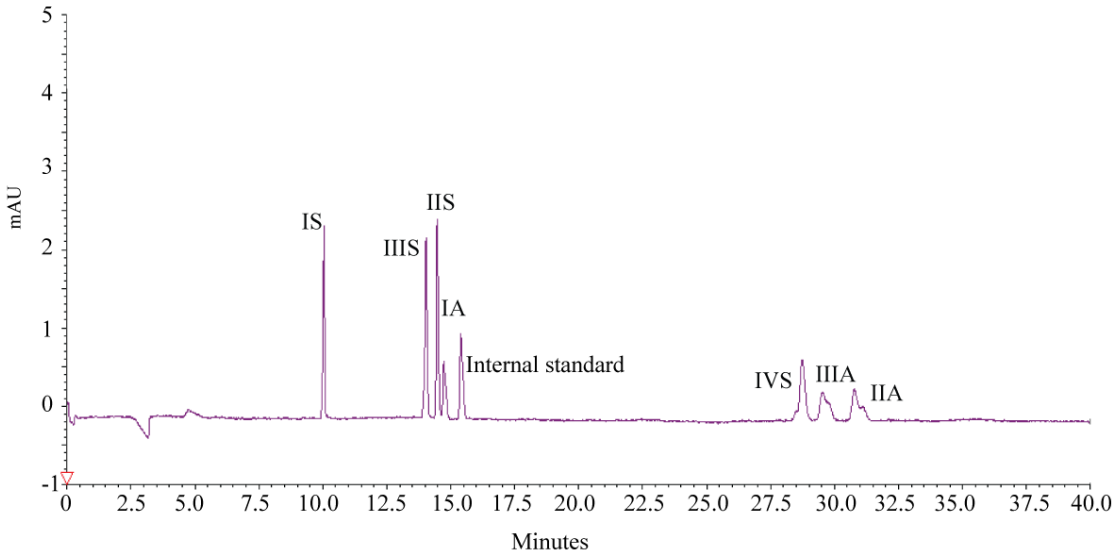

Figure 3.16. Electropherogram of Δ-disaccharide standards. Standards were individually separated with distinct peaks.

The electropherogram generated from this study has a similar profile to the one presented by Ruiz-Calero *et al.* (Fig. 1.13). The last peak (IVA) could not be detected even when the recommended 0.5 per square inch (p.s.i.) pressure gradient was applied for a further 30 min after the completion of the run. Thus IVA is omitted from this study. The observed differences in the detection times from Ruiz-Calero *et al.* might be due to the different equipment used, or the inability to achieve 0.5 p.s.i.;

nevertheless the peaks were well separated from each other. An internal standard was added to assist in the identification of the various peaks in the digested samples.

To achieve reproducible results and account for the variations in the samples, 5 replicates of the Δ-disaccharide standards were separated. The migration time and peak areas were expressed as relative standard deviation (R.S.D.) (Table 3.1). R.S.D. was considered reliable when area standard deviations were < 5 %, and migration time standard deviations of < 1 % were achieved. The R.S.D. was calculated and confirmed the reproducible results.

Table 3.1. Relative standard deviation (R.S.D.) of Δ-disaccharide standards. RT represents retention time.

	RSD (%)	
Δ-disaccharide	Area	RT
IS	2.2	0.4
IIIS	2.3	0.4
IA	2.2	0.5
IIS	2.3	0.4
IVS	2.2	0.5
IIIA	3.2	0.5
IIA	2.1	0.5
Internal	2.2	0.5

The measurement standard (R.S.D.) allowed for the generation of calibration curves for each Δ-disaccharide standard. These curves were constructed by using different dilutions of the stock (1 mg/ml), from undiluted control to 1, 2, 4, 8, 12 and 16 times dilution. The individual peak areas were determined, plotted and regression lines generated; the working linear concentrations have a goodness-of-fit (R^2) > 0.99

(Fig. A1). These calibration curves were then used for the quantification of the molar concentration (mol %) of each disaccharide.

Following the generation of a standard curve, the electropherogram profiles of depolymerized heparin, HS^{pm}, $HS9^{+ve}$ or $HS9^{-ve}$ variants were generated. Before CE analysis, the depolymerization of each HS variant was monitored at 232 nm. The undigested samples had an absorbance of 0.01 and increased to ~ 1.1, and when no further increase was seen the depolymerization was be deemed to be complete. The samples were injected into the system for 5 sec, and peaks detected at 232 nm. Electropherograms showing each sample profile are shown in Figure 3.17. Three replicates were run and average areas-under-the-peak calculated and compared to the standard curve. The identity of each peak was determined from the relative shift from the internal standard added into the mixture. Moreover, the migration time of each peak was also consistent with the standards' migration time. Due to the almost undetectable peak for IIIA, its identity was confirmed by adding IIIA Δ-disaccharide standard into the depolymerized HS sample. The increase in the height of that peak from the original sample confirmed it to be the IIIA variant.

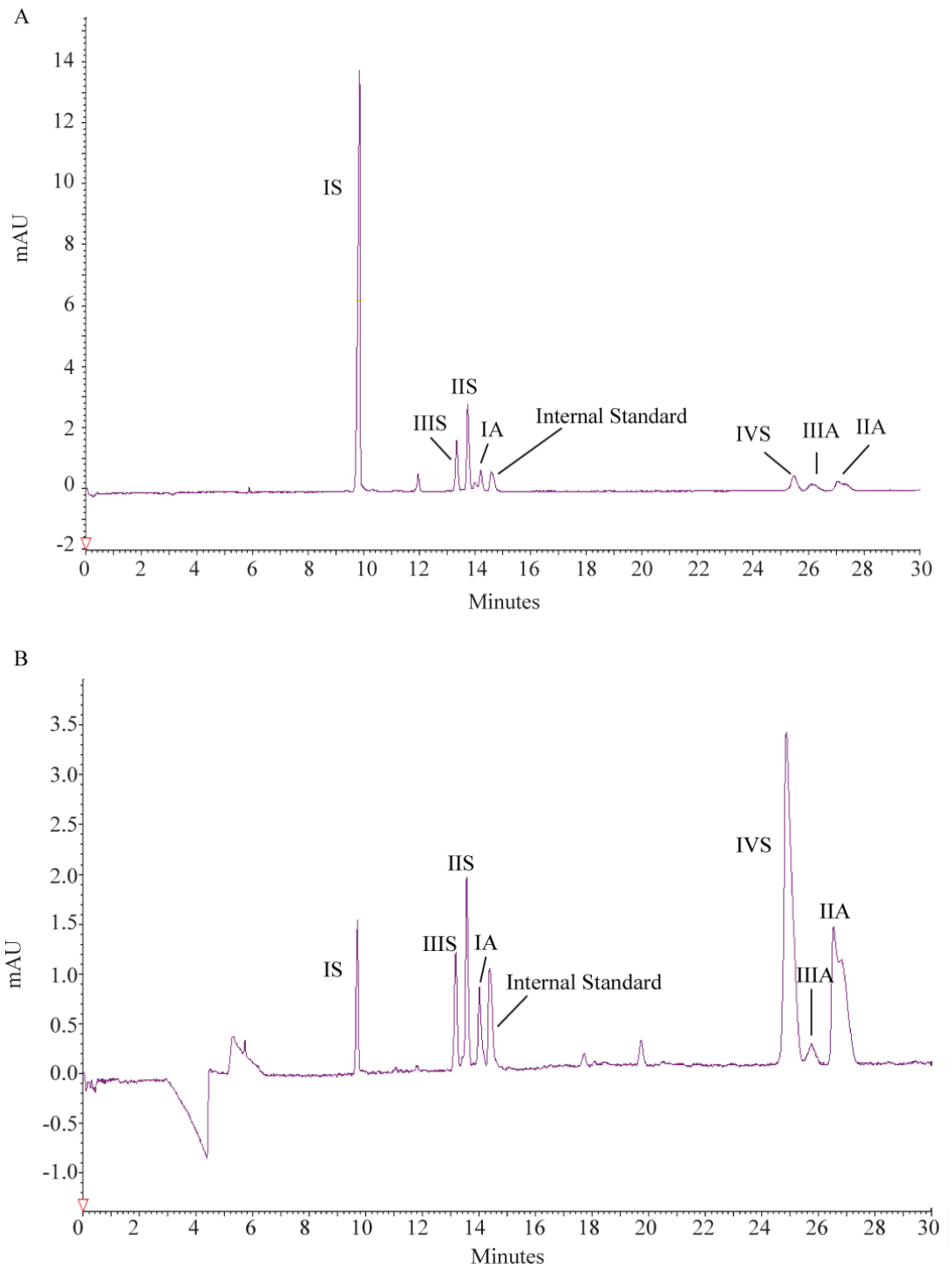
A
mAU
IS
IIS
IIIS
IA
Internal Standard
IVS
IIIA
IIA
Minutes
B
mAU
IS
IIS
IIIS
IA
Internal Standard
IVS
IIA
IIIA
Minutes

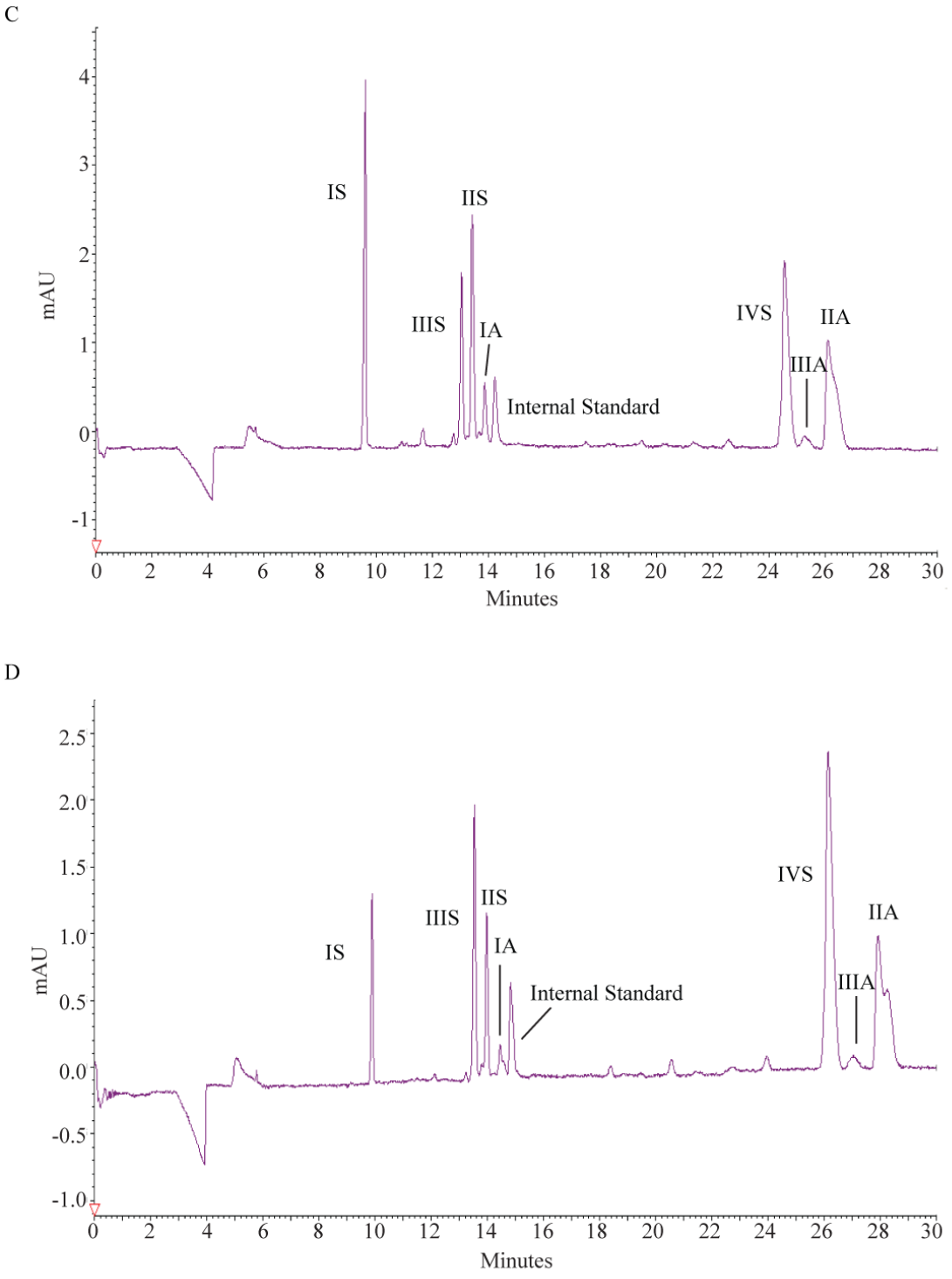

Figure 3.17. Electropherograms of the depolymerized samples. (a) Heparin, (b) HS^{pm}, (c) $HS9^{+ve}$ and (d) $HS9^{-ve}$. IS: ΔUA2S(1→4)-D-GlcNS6S (2S, NS, 6S); IIIS: ΔUA2S(1→4)-D-GlcNS (2S, NS); IIS: ΔUA(1→4)-D-GlcNS6S (NS, 6S); IA: ΔUA2S(1→4)-D-GlcNAc6S (2S, 6S); IVS: ΔUA(1→4)-D-GlcNS (NS); IIIA: ΔUA2S(1→4)-D-GlcNAc (2S); IIA: ΔUA(1→4)-D-GlcNAc6S (6S) Internal standard helped in identifying each peak.

A comparison of the disaccharide composition of each digested HS variant is shown in Table 3.2. The results revealed that the major units in heparin are the trisulfated (2S, 6S and NS) IS and disulfated (6S and NS) IIS at 66.1% and 20.8 % respectively. In contrast, the major units in HS^{pm} are the monosulfated (NS) IVS and disulfated (6S and NS) IIS (36.8 % and 23.7 % respectively). The large decrease in trisulfated (2S, 6S and NS) IS observed in HS^{pm} is likely because of the lower sulfation in HS. It was also observed that after the affinity chromatography step, the $HS9^{+ve}$ variant was enriched for trisulfated (2S, 6S and NS) IS and disulfated (6S and NS) IIS (26.0 % and 30.6 % each), and whereas the $HS9^{-ve}$ variant most prominently possessed monosulfated (NS) IVS (33.3 %) as its major disaccharide unit.

Table 3.2. Comparison of the different composition of depolymerized GAG samples.

Disaccharides	Molar percentage (mol%)			
	Heparin	HS^{pm}	$HS9^{+ve}$	$HS9^{-ve}$
IS	66.1	10.5	26.0	13.0
IIIS	5.5	6.3	10.0	14.7
IIS	20.8	23.7	30.6	19.8
IA	1.1	2.1	1.75	1.1
IVS	2.6	36.8	18.0	33.3
IIIA	1.5	2.2	1.20	1.45
IIA	2.4	18.4	12.5	16.6

Clearly the most notable point is the presence of the higher proportions of the trisulfated (2S, 6S and NS) IS and disulfated (6S and NS) IIS Δ-motifs in $HS9^{+ve}$ than in $HS9^{-ve}$ variants. This clearly suggests that a combination of 6O- and N-sulfation is very important for HS binding to VN, a result also supported by the GAG-ELISA in Figure 3.14. Lack of enrichment of monosulfated (NS) IVS and monosulfated (6S)

IIA in $HS9^{+ve}$ variants as compared to starting HS^{pm} material suggests that neither domain alone are sufficient for VN binding. Instead, a combination of 6O- and N-sulfation seems to be critical for VN binding. In contrast, 2O-sulfation is clearly not essential for the binding of HS to VN, as evidenced by the lack of enrichment of the monosulfated (2S) IIIA, disulfated (2S, 6S) IA and disulfated (2S and NS) IIIS Δ-disaccharide units in $HS9^{+ve}$. Also, in GAG ELISA assay, removal of 2O-sulfation did not reduce VN binding. The other disaccharide units appear to be of less importance for the $HS9^{+ve}$ and $HS9^{-ve}$ variants.

Collectively, the results in this section demonstrate that the highly 6O- and N-sulfated $HS9^{+ve}$ variant isolated by VN affinity chromatography has a higher capacity for VN than either the HS^{pm} starting material or the $HS9^{-ve}$ flow-through. It also has a greater capacity to bind VN than either LN or FN, suggesting that the specificity of the $HS9^{+ve}$ has increased. This clearly demonstrated that affinity chromatography is a powerful technique for isolating VN-binding HS forms from a heterogeneous HS mixture. Following this characterization study, and with the aim of using HS9 as a substrate to capture and present sufficient VN for hESC culture, the following section will delineate the different methods for immobilizing the $HS9^{+ve}$ variant for cell culture.

3.3.4. Immobilization of HS9 variants

As $HS9^{+ve}$ demonstrated high binding affinity to VN as compared to the rest of the HS variants, strategies to immobilize it efficiently onto surfaces for the presentation of unmodified VN for cell culture using covalent and electrostatic methods were explored. The first was to use the covalent EDC method to chemically link the amine groups on HS to the carboxyl groups on surfaces. The second was to create a net positively charged surface with poly-L-lysine and lastly to use plasma polymerization to create high net positive charges for electrostatic interactions between surfaces and HS.

3.3.4.1. Covalent EDC chemistry

In order to provide an optimal substrate to immobilize HS variants, NaOH was utilized to etch surfaces to create free carboxyl groups on low carboxylated polystyrene (PS) surfaces. The coupling of the primary amine groups in HS and carboxyl groups on etched PS surfaces was accomplished with EDC chemistry. It was previously shown by Plante *et al.* that EDC chemistry could be used to tether disaccharide units through their free amine ends to surface carboxyl groups (Plante *et al.* 2001). Therefore, NaOH-treated PS, together with TCPS surfaces, was both analyzed for their ability to be derivatized with HS variants (Fig. 3.18).

An optimization of EDC concentrations (10, 50 and 100 mg/ml) was first required. ^{3}H-lysine was used, because every molecule contains 2 primary amines for coupling so that the amine will not be the limiting factor. The results demonstrated that 24 h of NaOH treatment was sufficient to etch the maximum levels of the carboxyl groups on PS surfaces. However, TCPS yielded better grafting than NaOH-treated PS; thus TCPS was used for the subsequent reactions. A concentration-

dependent increase in grafting of ^{3}H-lysine was observed with 10 and 50 mg/ml. However, no significant increase from 50 to 100 mg/ml of EDC was observed, suggesting that the grafting concentration saturated at 50 mg/ml. Therefore the EDC concentration was settled at 50 mg/ml.

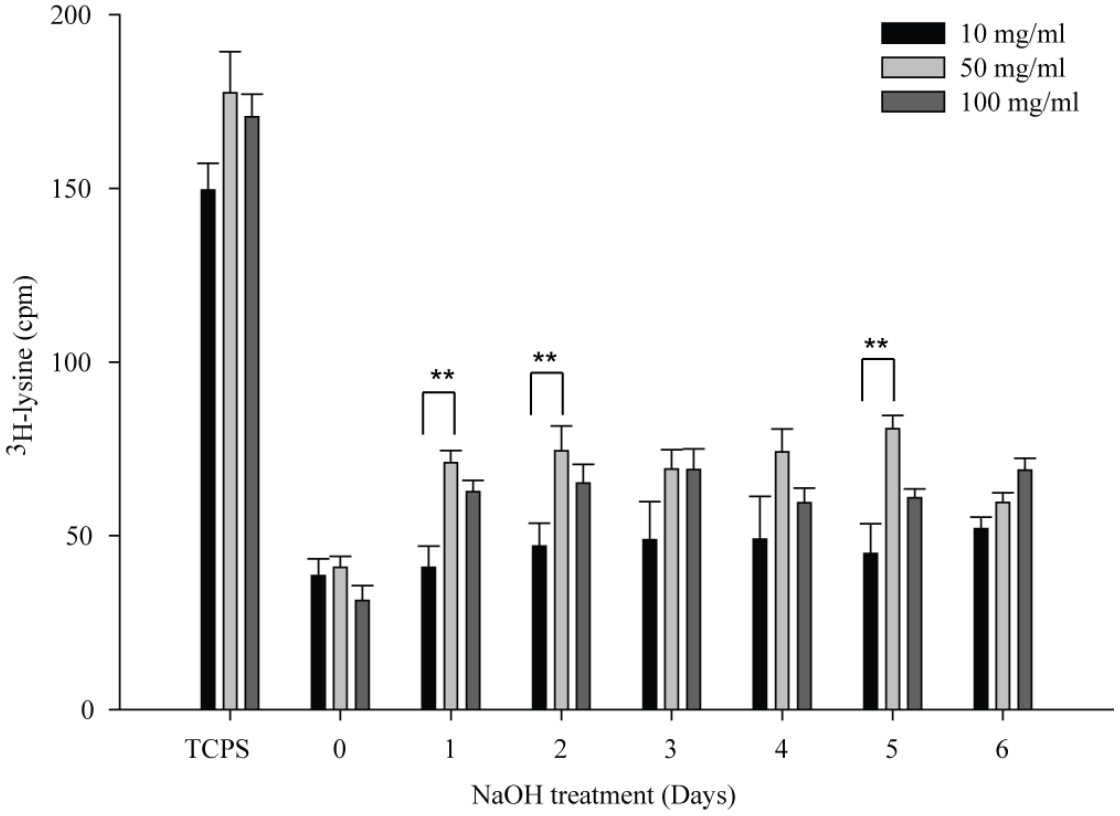

Figure 3.18. Optimizations of surface and EDC concentration for covalent grafting. ^{3}H-lysine was used as a read-out for the EDC grafting ability on the different surfaces. NaOH was used to etch the PS surface for 6 days to produce different densities of carboxyl groups. TCPS gives the highest grafting ability as compared to NaOH-treated surfaces, regardless of how many days etching was carried out. The optimized EDC concentration was 50 mg/ml. ** = $P < 0.05$

Another parameter that required consideration was the amount of primary amines in heparin and HS^{pm}. To confirm these levels, a fluorescamine protein assay was employed (Fig. 3.19). The dye binds to primary amines and has an excitation wavelength at 365 nm and an emission wavelength at 470 nm. The relative levels of primary amines can then be deduced using a BSA standard curve. Using two

concentrations of each GAG (0.5 and 1 mg/ml); the results confirmed as expected that there are more (> 60 %) primary amines present in HS^{pm} than in heparin. By comparing 1 mg/ml heparin and the HS^{pm} variants, it was shown that there are $\sim 3 \times 10^{16}$ amines present in heparin and $\sim 5 \times 10^{14}$ amines present in HS^{pm}, a difference of > 60 %. This difference was less (~ 40 %) in heparin compared to HS9 variants (~ 2×10^{16} amines), suggesting some compositional differences in both of them after affinity chromatography, confirming the data obtained previously with CE. Thus, the number of amines in GAGs directly affects the EDC grafting efficiency.

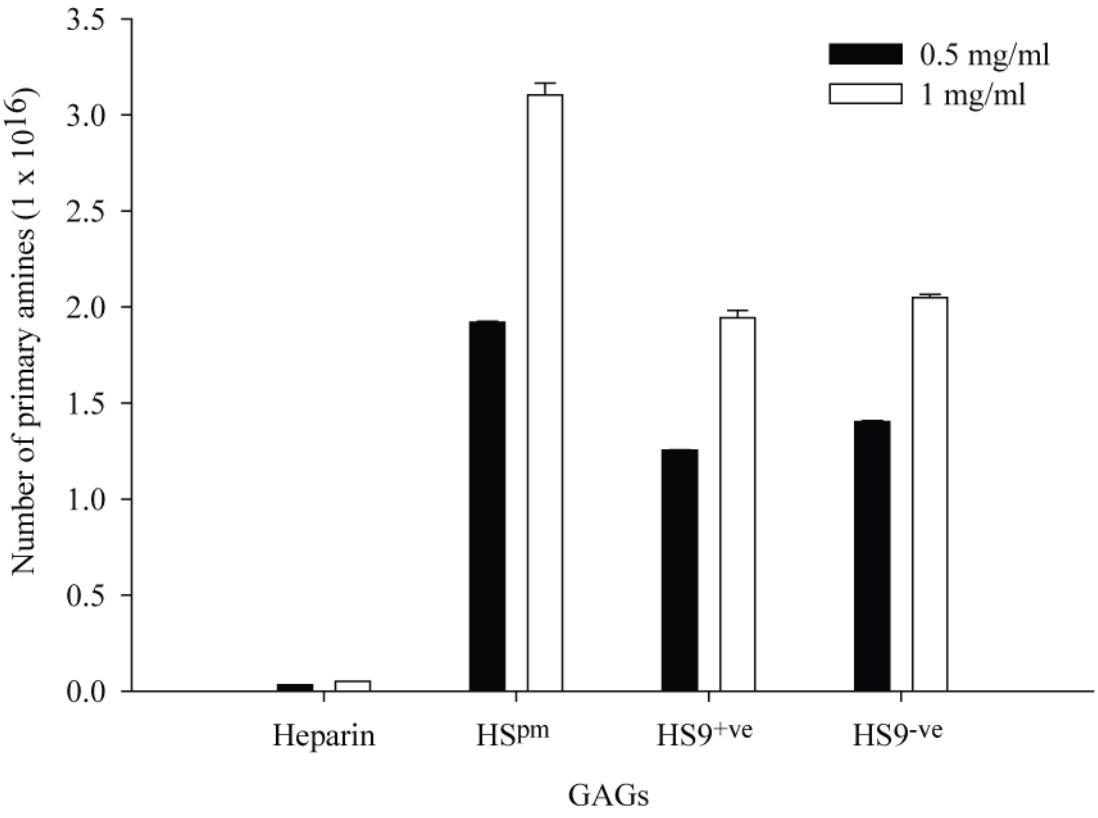

Figure 3.19. Number of primary amines in GAGs by fluorescamine protein assay. Increase in number of amines from 0.5 mg/ml to 1 mg/ml GAGs. A > 60 % difference in the number of primary amines at 1 mg/ml of HS and heparin.

Having established the suitable surface, optimal EDC concentration and number of amines in GAGs, ^{3}H-heparin and ^{3}H-HS^{pm} were grafted onto TCPS surfaces (Fig. 3.20). Concentration-dependent increases in ^{3}H-GAG binding were observed, with the surface densities of ^{3}H-GAGs measured by comparison to standard curves (Fig. A2). The surface density of ^{3}H-HS^{pm} was notably higher than ^{3}H-heparin at all concentrations tested. This was expected, because heparin has > 80 % N-sulfates and the number of free amines is lower than in HS^{pm} (Table 1.2).

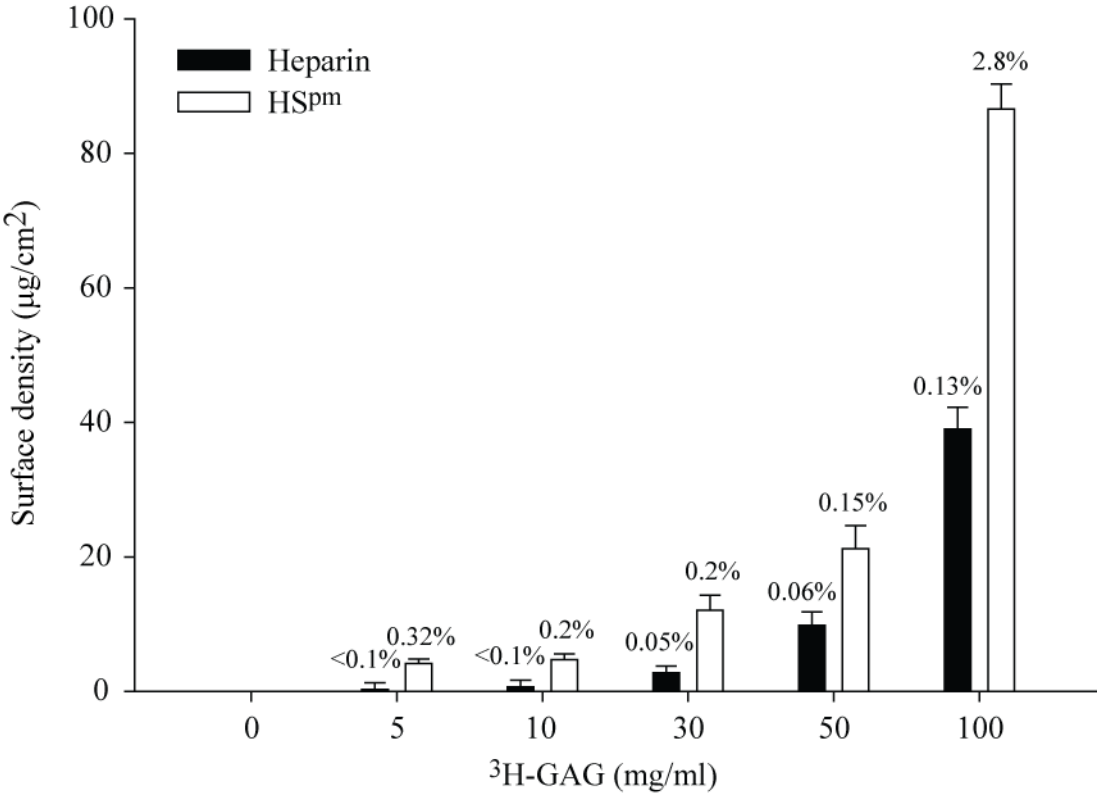

Figure 3.20. Surface density of heparin and HS^{pm} on EDC grafted surfaces. Concentration-dependent increase in ^{3}H-GAG grafting onto surfaces. The percentages represent the grafting efficiency. This low efficiency is not feasible for further studies.

Although this method does immobilize GAGs onto surfaces, the overall grafting is inefficient. For example, by using 30 mg/ml of ^{3}H-GAG at 3mg per well (0.32 cm^2), only ~ 1.5 μg of ^{3}H-heparin and ~ 6 μg of ^{3}H-HS^{pm} were detectable on the surfaces, which equates to a 0.05 % and 0.2 % grafting efficiency respectively. At such low efficiencies, these methods are not suitable for further applications. Moreover, a study by Roy *et al.* has shown that covalently binding GAGs to surfaces carries significant disadvantages. In particular, utilizing the N-domains for coupling compromises the biological activities of GAGs (Roy *et al.* 2011). Therefore, better and more efficient strategies need to be uncovered.

3.3.4.2. Poly-L-lysine coatings

As covalent immobilization is not efficient, strategies exploiting the electrostatic interactions between the negatively charged HS and positively charged surfaces were employed. Poly-L-lysine (PLL) has been used successfully as a substrate for many types of stem cells, but not for hESCs on TCPS (Cai *et al.* 2012a, Cai *et al.* 2012b, Galli *et al.* 2011). Therefore to test such surfaces, PLL-coated TCPS plates were subjected to overnight coating with different concentrations of ^{3}H-heparin and ^{3}H-HS^{pm} (Fig. 3.21). The surface density of each GAG was then determined: 1 μg of ^{3}H-GAG solution yielded a surface density of ~ 200 ng/cm^2, with density increasing to ~ 800 ng/cm^2 and 400 ng/cm^2 respectively at 2 μg of ^{3}H-heparin and ^{3}H-HS^{pm}. The higher density of ^{3}H-heparin observed was due to its higher overall negative charge. Interestingly, differences in surface density were observed in heparin and HS^{pm} only at 2 μg, suggesting an inferior binding of GAGs onto PLL surfaces at lower GAG concentrations. Therefore, 2 μg was subsequently used for the immobilization of GAGs on PLL surfaces.

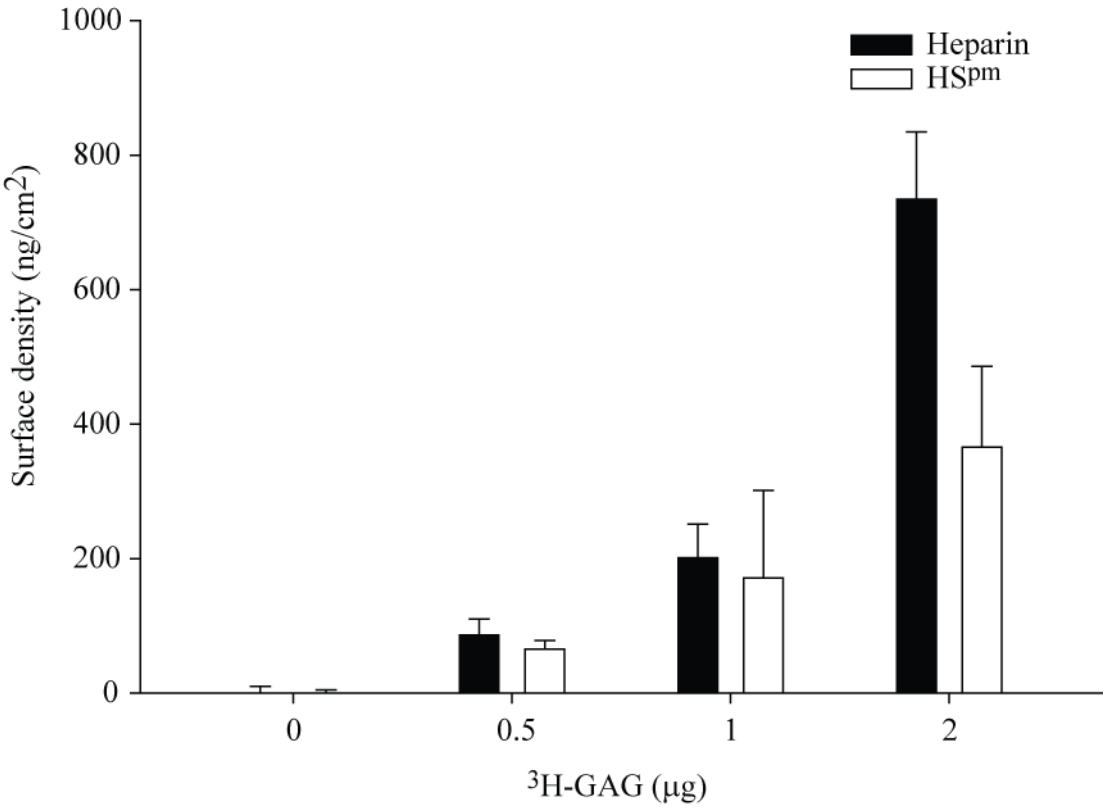

Figure 3.21. Surface density of heparin and HS^{pm} on PLL surfaces. Different GAG concentrations were used for overnight coating of PLL surfaces. Increasing surface density was observed with increasing solution concentrations. The surface density of ^{3}H-heparin and ^{3}H-HS^{pm} after exposure to 2 μg of coating solution was ~ 800 ng/cm^2 and 400 ng/cm^2 respectively.

To further analyze the utility of the PLL surface for cell culture, hESCs (HES-3) were screened for cell proliferation on PLL-coated GAG (PLL+GAG) surfaces (Fig. 3.22). VN2.5 and VN5 was coated onto PLL+GAG surfaces, and HES-3 cells seeded and allowed to grow for 7 days. Photomicrographs at the end of one week revealed that the cells had not spread well on these surfaces, with the exception of those on PLL+heparin+VN5. This suggested that PLL-coated surfaces are not optimal for hESC culture. Therefore a third strategy that of exploiting plasma polymerization was next explored.

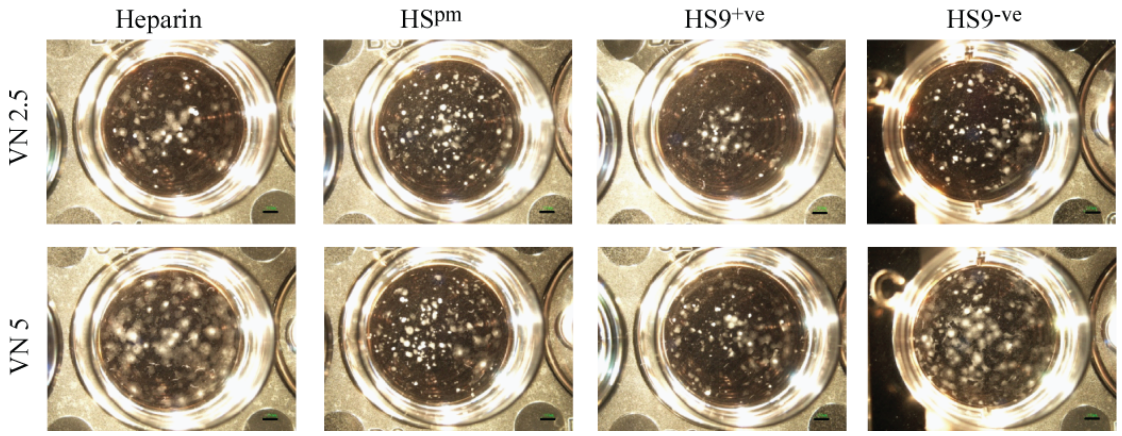

Figure 3.22. HES-3 cell images after 7 days of culture on PLL+GAG+VN surfaces. Cells did not spread, or reach confluence, suggesting that PLL surfaces are not suitable. Scale bar = 0.3 mm.

3.3.4.3. Allylamine polymerization

As the previous two methods (EDC covalent grafting, PLL coating) failed to address the key characteristics (cost, simplicity, safety and efficacy) required of an engineered substrate; another surface is clearly needed to immobilize GAGs for long-term cell propagation. Professor Short's laboratory at the University of South Australia has developed a method for immobilizing GAG via the plasma polymerization of allylamine (AA) monomers onto plastic surfaces. The AA monomer is positively charged, and, when polymerized onto surfaces, gives the surface a net positive charge that persists over time (Whittle *et al.* 2000).

To assess the optimal AA density for immobilizing HS on surfaces, different percentages of AA surfaces were generated to determine which density has the highest functional binding ability for GAGs as assessed by ELISA. Surface densities were controlled with a neutral octa-1, 7-diene monomer. Density varied from 0% AA: 100% octa-1, 7-diene, 50% AA: 50% octa-1, 7-diene, 80% AA: 20% octa-1, 7-diene, 90% AA: 10% octa-1, 7-diene to 100% AA: 0% octa-1, 7-diene. The results revealed that the 100% AA surfaces bound the highest amount of functional GAG, followed by

the 90% AA surface (Fig. 3.23). It was interesting to note that the GAGs bound to 80 % AA surface no longer retained their capability to bind VN, instead having a negative effect. This was almost certainly due to the high background observed in the blank wells, which may have been because of the ineffective blocking of the fish gelatin. The 50% AA surface could not trigger any VN binding, suggesting that insufficient GAG was immobilized by it onto the surface. Thus, the 100% AA polymerized surface gave by far the best binding and was used for all further analysis.

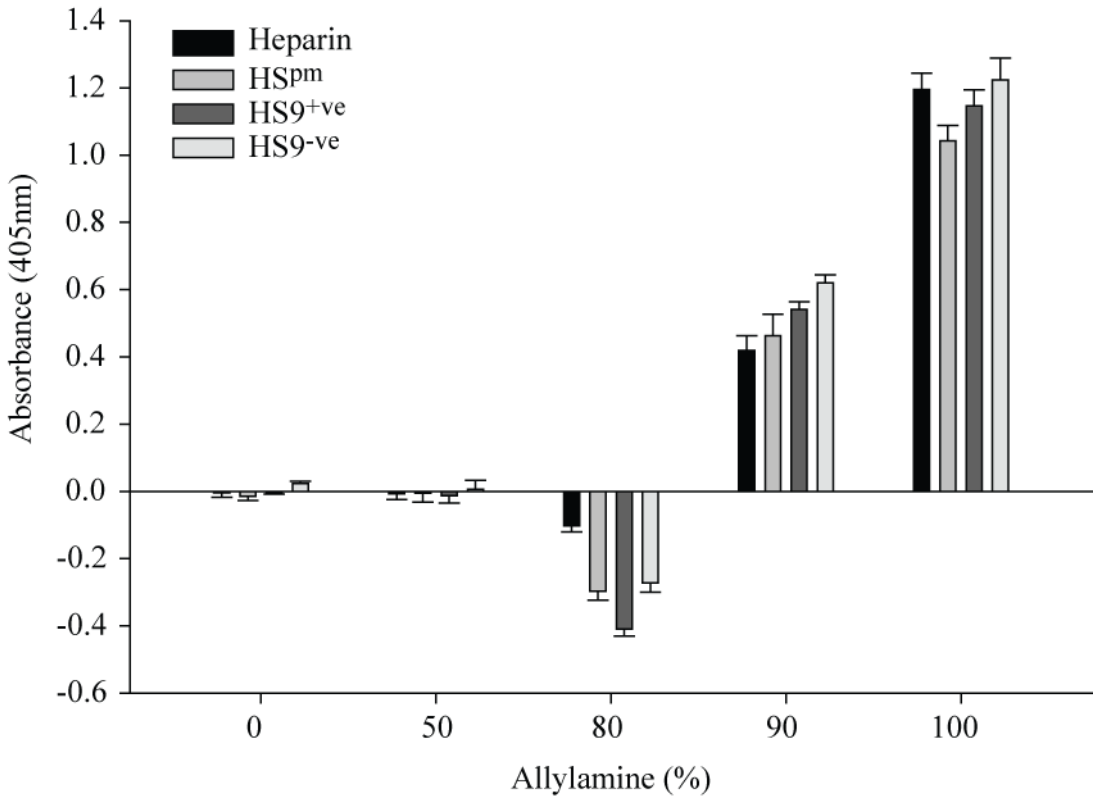

Figure 3.23. GAG binding profile on the different allylamine surface by ELISA. GAG (5 μg/ml) was coated onto the different AA density surfaces (0, 50, 80, 90 and 100%) followed by binding of 500 ng/ml of VN. The AA surface at 100 % density binds the highest amount of VN while densities < 100 % no longer bind the optimal amount of GAG.

In order to confirm the presence of AA polymer on the surface, an XPS analysis was performed to determine the oxygen (O), nitrogen (N) and carbon (C) content of the AA polymerized aluminium foil surfaces placed together in the plasma reactor chamber. The readings on the foil reflected the amount of each atom on the plate surface (Robinson *et al.* 2012). The 50% AA surface gave readings of C (92.5%), N (4.56 %) and O (2.93 %); the 80% AA surface produced C (85.2 %), N (12.14 %) and O (2.7 %); the 90 % AA surface produced C (80.7 %), N (15.3 %) and O (4 %); the 100% AA surface had C (79.2 %), N (16.4 %) and O (4.34 %) (Fig. 3.24). A consistent nitrogen: carbon (N: C) ratio of 0.18 to 0.22 was observed for several batches of the 100% AA plates (Table 3.3). It is summarized to show the various N: C ratios of the AA surfaces in Table 3.3. This all demonstrated the reproducibility of the plasma polymerization reaction, which was also consistent with the study done in Professor Short's laboratory (Mahoney *et al.* 2004, Robinson *et al.* 2012). Thus an N: C ratio of 0.18 to 0.22 was optimal for functional HS9 binding and was used subsequently for immobilization of unmodified VN.

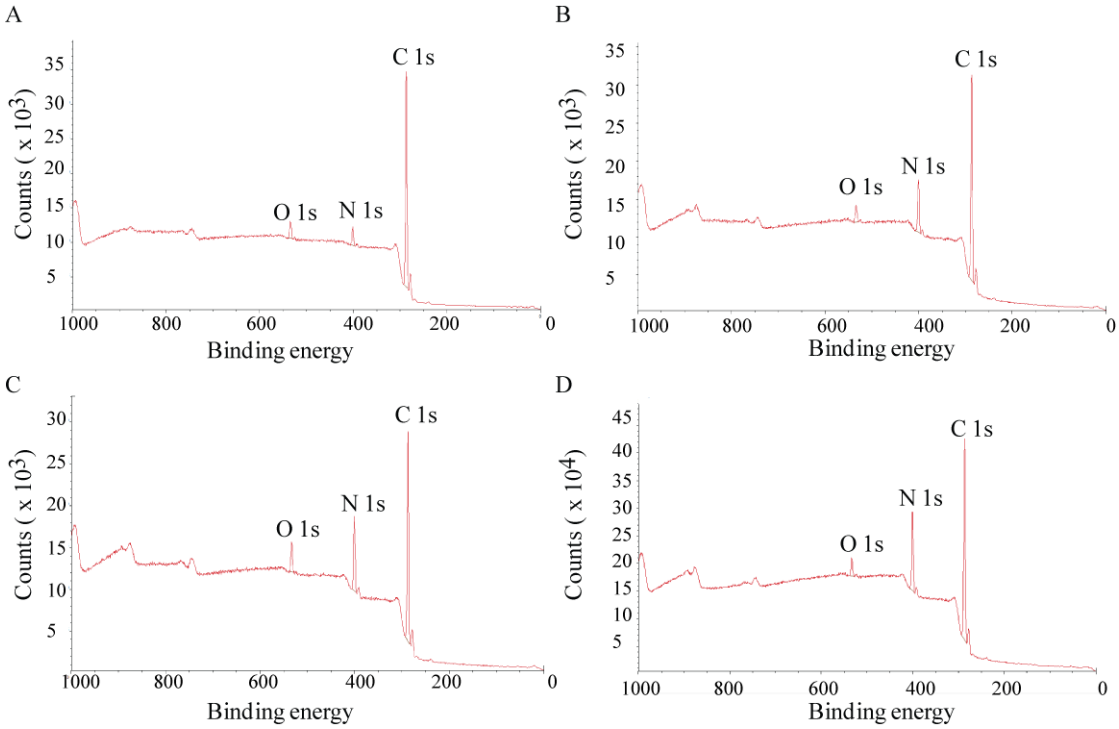

Figure 3.24. Representative XPS binding energy profile of 0-100% AA plates. The amount of O, N and C atoms on the surfaces of plates were read from the aluminium foil placed in the reaction chamber. Results were analyzed with CasaXPS software to determine the area of the peaks and N: C ratio was calculated. (A) 50% AA: 50% octa-1, 7-diene (B) 80% AA: 20% octa-1, 7-diene (C) 90% AA: 10% octa-1, 7-diene (D) 100% AA: 0% octa-1, 7-diene. The 100% AA surface has C (79.2 %), N (16.4 %) and O (4.34 %).

Table 3.3. Summary of the N: C ratios of 0, 50, 80, 90 and 100% AA surfaces.

Allylamine (%)	N: C
0	0
50	0.03 ± 0.02
80	0.12 ± 0.02
90	0.17 ± 0.02
100	0.20 ± 0.02

Following the success of HS immobilization, the ability of each GAG variant to bind VN was assessed by ELISA (Fig.3.25). Irrespective of the GAG, there was a concentration-dependent increase in absorbance. Wells without GAG served as the negative control, indicating no non-specific interactions. Binding data revealed that the heparin and $HS9^{+ve}$ variants had the highest affinity for VN, and that the flowthrough $HS9^{-ve}$ variant and starting HS^{pm} had the weakest. Moreover, the $HS9^{+ve}$ variant produced a higher absorbance than the $HS9^{-ve}$ variant, indicating a significant higher affinity for VN. This result is similar to that which employed the GAG-ELISA (Fig. 3.13), suggesting the higher binding affinity in the $HS9^{+ve}$.

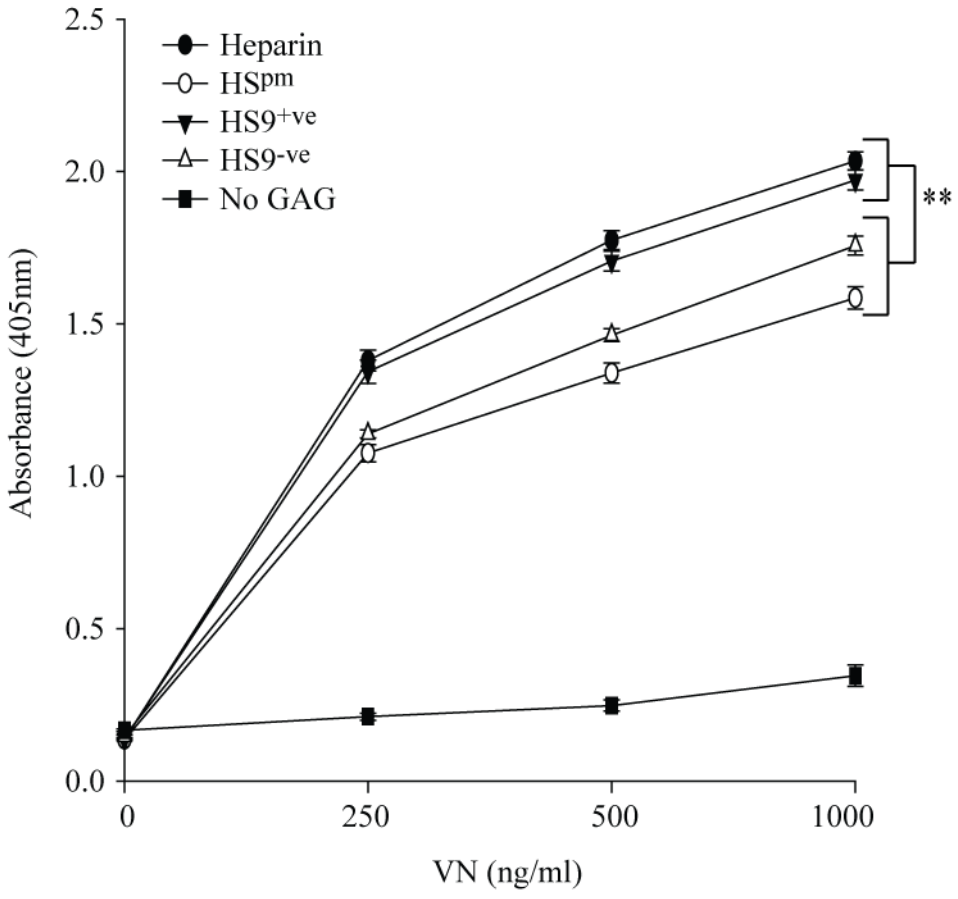

Figure 3.25. VN binding profile on the 100% AA surface. GAGs were coated onto the AA surface and the binding profiles of different concentrations of VN analyzed by ELISA. The $HS9^{+ve}$ variants bind VN significantly better than the $HS9^{-ve}$ variants. Uncoated wells and heparin-coated wells served as the negative and positive control respectively. ** = $P < 0.05$

To confirm the presence of GAGs on the AA surfaces, the surface density of ^{3}H-heparin and ^{3}H-HS^{pm} was determined. ^{3}H-GAG was immobilized onto the surface overnight, washed and read in a scintillation counter. Counts were compared to the standard curve, and a surface density determined (Fig. 3.26). There was a concentration-dependent increase in surface density, with a higher density seen for heparin than for HS^{pm}. When 1 μg of GAG was used for coating, the ^{3}H-heparin yielded a surface density of ~ 250 ng/cm^{2}; ^{3}H-HS^{pm} yielded only ~ 100 ng/cm^{2}. This corresponds to immobilization efficiencies of ~ 8 % and ~ 3.2 % respectively, which was a significant increase over the use of covalent EDC immobilization chemistry depicted in Figure 3.19. It was expected that heparin would bind better to the surfaces because of its higher density of negative charge per unit length. Thus, this simple and robust AA+GAG surface was used for all further immobilization of VN.

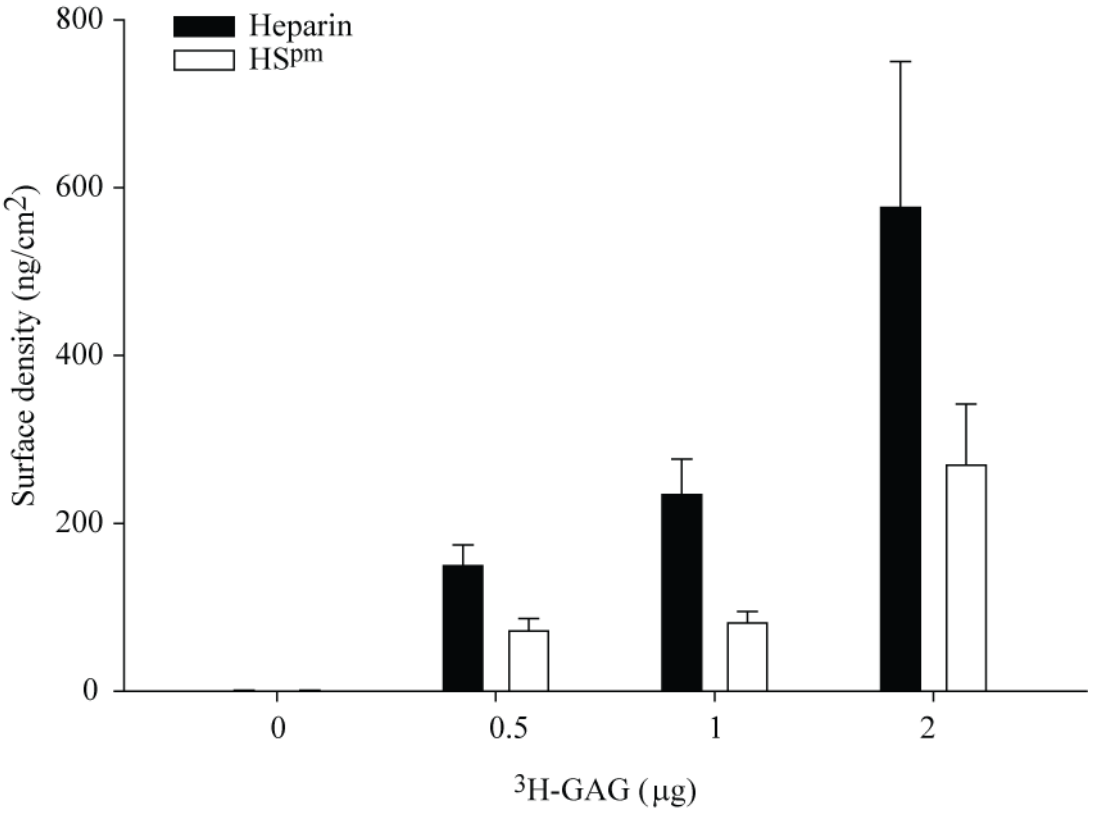

Figure 3.26. Surface densities of heparin and HS^{pm} on the 100% AA surface. GAG binds to AA surface in a concentration-dependent manner with the heparin density higher than HS^{pm}. ^{3}H-GAG (1 μg) was used for coating; the final surface density of ^{3}H-heparin was ~250 ng/cm^2 and of the ^{3}H-HS^{pm} ~ 100 ng/cm^2.

3.3.5. ^{125}I-VN surface density

Chapter 2 demonstrated that the threshold density for successful maintenance of hESCs on VN-adsorbed TCPS surfaces is 250 ng/cm^2. The question now became whether an HS with tuned affinity for VN can be used as a substrate to capture and present VN in an efficient way. The surface densities of VN on TCPS, AA+HS9^{+ve} and PLL+HS9^{+ve} substrates were measured and compared. Increasing concentrations (0, 1.25, 2.5 and 5 μg/ml) of ^{125}I-VN were incubated on the different surfaces, and the amounts measured by scintillation and compared to a standard curve (Fig. 3.27). All surfaces showed a concentration-dependent increase in binding of the ^{125}I-VN, with the lowest VN surface density recorded on the PLL+HS9^{+ve} surface and the highest on TCPS surface. There was insufficient VN on the surface for cells to attach and proliferate on the PLL+HS9^{+ve} surface, presumably explaining the HES-3 cell response seen in Figure 3.22. Thus, establishing this surface density profile on the various substrates was useful for the determination of the density most suitable for hESC culture in the next chapter.

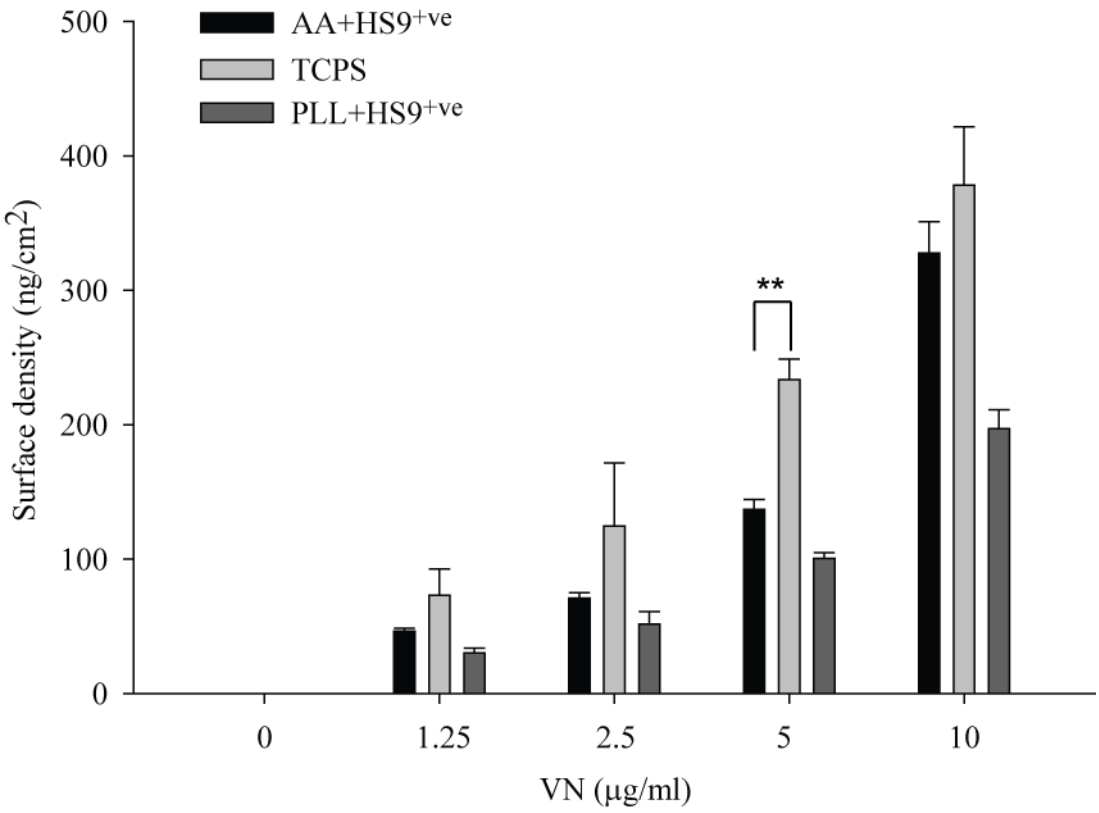

Figure 3.27. ^{125}I-VN surface density on TCPS-, AA+HS9^{+ve}- and PLL+HS9^{+ve}-coated surfaces. The highest VN density was measured on TCPS, followed by the AA+HS9^{+ve} surface, with the lowest density on PLL+ HS9^{+ve} across all the VN concentrations used. ** = $P < 0.05$

3.4. Discussion

Glycosaminoglycans are an important structural and functional component of the ECM (Gandhi & Mancera 2008). Previously studies have shown that cell surface HSPGs are crucial for cell adhesion to a FN heparin-binding peptide, as shown after soluble heparin and heparinase treatment (Drake *et al.* 1992, Mahalingam *et al.* 2007). A study by Klim *et al.* showed that digesting hESCs with chrondroitinase ABC impaired the binding ability of cells to VN-HBD surfaces, suggesting that surface GAGs were important for cell binding (Klim *et al.* 2010). One of most abundant GAGs on stem cell surfaces is HS, with CS predominant in the ECM of mature bone, cartilage and heart valve (Gandhi & Mancera 2008). Thus, to extend these findings, heparinase digestion of surface HS was employed to determine its importance for cell binding to VN-HBD. The results showed that cells could bind to VN-HBD peptide via surface HS, but that they are not critical if the RGD motif is present. Several studies have also shown that heparin and HS are able to support hESC self-renewal and growth (Furue *et al.* 2008, Sasaki *et al.* 2008). Following this, we aimed to isolate a high affinity VN binding HS variant from a mixture, to present VN efficiently.

The isolation of a VN-binding HS variant via VN-HBD peptide affinity chromatography has allowed us to engineer a novel hESC culture platform. The binding ability of the different variants was compared using a combination of dot blot, ELISA and heparin bead competition assays. To check the apparent specificity of the $HS9^{+ve}$ variant for VN binding, it was compared to the binding of LN and FN. Together these results confirmed that the $HS9^{+ve}$ variant binds VN with relative specificity and certainly better than the HS^{pm} and $HS9^{-ve}$ variants. This result suggests the possibility of isolating a library of HS variants tuned to other ECM proteins for generating a range of specific substrates.

Affinity-separated heparin variants have been isolated before, but by employing whole native protein during the affinity step. Thus, heparin variants with high affinity to fibronectin (Falcone & Salisbury 1988), heparin co-factor II (Kim & Linhardt 1989), tissue plasminogen activator (Andradegordon & Strickland 1986), FGF-1 (Barzu *et al.* 1989, Sudhalter *et al.* 1989) and anti-thrombin III (Hook *et al.* 1976, Scully *et al.* 1988) have been isolated. However, the use of whole protein is both impractical and costly, especially at this scale. McCaffrey and colleagues subsequently demonstrated that two variants, with high and low TGF-β binding affinity, could be isolated from heparin mixtures with a synthetic peptide that mimicked the TGF-β HBD (McCaffrey *et al.* 1992). Their study used heparin as the starting material, a molecule not suitable for clinical applications.

Understanding the compositional make-up of the variants is clearly important for the future design of a synthetic HS9. As evidenced by the low R.S.D. values with all the depolymerized samples, the compositional analysis of heparin and HS can be considered reliable. The percentages of disaccharides in heparin were consistent with those published by other groups (Ampofo *et al.* 1991, Desai *et al.* 1993a, Jandik *et al.* 1994, Karamanos *et al.* 1996, Ruiz-Calero *et al.* 1998, Scapol *et al.* 1996). The molar percentages of the major disaccharides in porcine intestinal mucosa heparin, are IS and IIS, which range from 50 % to 68 % and from 10 % to 20 % respectively. No compositional studies have been done with the porcine mucosa HS; however, a previous comparison between HS from other sources such as bovine kidney revealed a similar trend, with the monosulfated IVS disaccharide unit having a higher molar percent ratio compared to the other units (Ampofo *et al.* 1991, Militsopoulou *et al.* 2002).

The elucidation of the anti-coagulant pentasaccharide sequence in heparin revealed that 3O-sulfation is essential for its anti-coagulant effects (Lindahl *et al.* 1980); in a similar manner, FGF-2 binding to HS requires 2O-sulfation (Faham *et al.* 1996, Maccarana *et al.* 1993) whereas 6O- and N- sulfation impair binding (Ernst *et al.* 1995); FGF-1 interaction with HS in contrast requires the 6O-sulfate group (Fromm *et al.* 1997). FGF-4 requires both 2O- and 6O-sulfation for binding and signalling (Ashikari-Hada *et al.* 2009, Guimond *et al.* 1993) and hepatocyte growth factor requires 6O-sulfation (Lyon *et al.* 1994). Falcone *et al.* and Mahalingam *et al.* demonstrated that an avid heparin-binding variant for FN appeared particularly highly charged, with 7 to 8 N-sulfated disaccharides being required, and a larger domain (> 14 residues) than unfractionated heparin (Falcone & Salisbury 1988, Mahalingam *et al.* 2007). Ling *et al.* also showed that N-sulfation in heparin contributes to the binding and activity of Wnt3a ligands for its osteogenic activity (Ling *et al.* 2010). These studies support the idea that differentially modified HS motifs confer distinct protein recognition properties on HS. The GAG ELISA and CE analysis both directly and indirectly revealed that the 6O- and N-sulfation of the glucosamine residue, and that at least 3 disaccharide units, are required for VN binding to HS. Removal of N-sulfation from the heparin standards also reduced the level of binding to VN, indicating that N-sulfation together with 6O-sulfation is crucial. This is the first report of an essential sulfation motif within HS important for VN binding.

In the search for an effective and efficient way to immobilize $HS9^{+ve}$ variants onto TCPS, the results demonstrated that the low proportion of primary amines in HS renders the EDC coupling method inefficient. This also accounts for the lack of proliferation on VN-coated PLL surfaces revealed in the ^{125}I-VN binding assay. The low VN surface density on PLL surfaces was also not sufficient to support robust

culture of hESCs. As shown in Chapter 2, the minimum VN surface density required on TCPS is at least 250 ng/cm^2 (Yap *et al.* 2011). Therefore, of the various approaches, AA plasma polymerization was the most efficient and effective method. AA polymerized cell culture surfaces have been studied by Punzon-Quijorna *et al.* and Schroder *et al.* to culture mesenchymal stem cells on both polycaprolactone (PCL) (Punzon-Quijorna *et al.* 2011) and titanium surfaces (Schroder *et al.* 2010). Although AA surfaces have been used for cell culture, this thesis is particularly interested in the culture of hESCs, which are known to be very demanding in their choice of substrate.

An interesting observation about the surface density of VN was that the amount of VN was in the order: TCPS > AA > PLL. VN (P04004) contains a similar number of negatively (66) and positively (56) charged residues (calculated from data on the ExPASy website, www.expasy.com), which might explain VN binding to both of the negative and positive charged surfaces. Thus I posit that the hydrophilic, net negatively charged TCPS surface is favourable for VN binding, while the highly positively charged AA surface supports more VN binding than PLL. PLL might not uniformly coat the surface, so that less positive charge is deposited, explaining the lower VN density. Such patchy coating might also translate into an inability of stem cells to proliferate on the PLL+HS9^{+ve} surfaces.

3.5. Summary

The aim of this chapter was to develop a substrate capable of binding unmodified VN based on its affinity for heparan glycosaminoglycans. An avid VN-binding variant (HS9^{+ve}) derived from HS^{pm} was isolated using affinity chromatography. Comparison of the HS9^{+ve}, HS9^{-ve} and HS^{pm} variants revealed that

the HS9^{+ve} variant had a higher binding propensity for VN, suggesting that affinity chromatography is a powerful technique for the separation of active GAG variants tuned to specific adhesive proteins. The HS9^{+ve} specificity for VN rather than FN and LN proteins was confirmed using ELISA.

Compositional analysis with CE confirmed an enrichment of trisulfated (2S, 6S and NS) IS and disulfated (6S and NS) IIS disaccharides in the HS9^{+ve} variant. Together with the GAG-ELISA results, it can thus be concluded that 6O-sulfation together with N-sulfation on glucosamine residue and at least 3 disaccharide units are critical for HS9^{+ve} binding to VN.

A consistent 100 % AA polymerized surface was generated by plasma. This surface was able to bind to functional GAG, which in turn was able to bind sufficient amounts of VN for successful cell culture as depicted in Figure 3.28. This layer-by-layer approach was used for the subsequent long-term culture of hESCs. The surface density of the various layers, from HS to VN, was determined and subsequently used for later quantification. This chapter thus demonstrated the process development of a robust, simple and cost effective substrate for the presentation of unmodified VN.

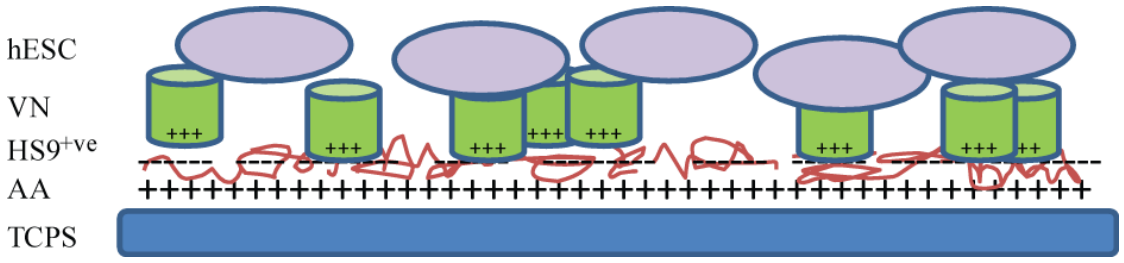

Figure 3.28. Summary of novel substrate for hESC culture. TCPS surfaces were first polymerized with positively-charged AA, than coated with negatively-charged HS9^{+ve} variants and VN for hESC culture.

CHAPTER 4 : CELL CULTURE STUDIES ON HS9 SUBSTRATES

4.1 Introduction

Previous chapter described a successful method for culturing hESCs on different concentrations of VN, and established a threshold surface density of 250 ng/cm^2 as being necessary. However, the method of immobilizing VN was based on passive adsorption onto TCPS surface, and as such was inefficient and non-specific. There is thus a major opportunity to replace this poorly defined method by using a tuned VN-binding HS variant (HS9^{+ve}) isolated by utilizing the affinity chromatography platform. To immobilize the HS9^{+ve} variant, an allylamine (AA) polymerized surface was utilized. In order to assess this surface for the capture of sufficient unmodified VN and provide for the long-term culture of hESC, this chapter will describe several biological assays.

The most widely used microenvironment to cultivate hESCs unfortunately still relies on Matrigel^{TM} of mouse origin. To achieve such defined substrates, other "defined" contituents including ECM proteins (LN, VN, FN, and collagen), peptides (biotinylated VN-HBD) and synthetic compounds (PMEDSAH, APMAAm, PMVE-alt-MA) (Table 1.1) have been studied. However, the exact surface density of these coatings for the successful long-term culture of hESC remains unknown.

To evaluate a surface as suitable for hESC expansion, criteria encompassing cell attachment, cell proliferation, pluripotent marker expression, chromosomal stability and differentiation capability need to be assessed (Yap *et al.* 2011). Two different hESC cells (HES-3 and H7) were used here to ensure the robustness of these assays. From the cell responses, a minimal functional VN surface density was deduced as being optimal for the successful long-term stem cell culture.

4.2. Materials and Methods

4.2.1. Preparation of AA cell culture surfaces

Based on the earlier findings that AA-polymerized TCPS surfaces demonstrated superior HS binding, these were utilized for the investigation of hESC bio-responses. AA-polymerized 24-well plates were coated with 5 μg/ml of GAG (heparin, HS^{pm}, $HS9^{+ve}$, $HS9^{-ve}$) (400 μl, 2 μg per well) overnight at room temperature. Wells were washed twice with PBS, and 300 μl of the various VN solutions (from 0 to 10 μg/ml) added, with a further incubation at 4 ^{o}C overnight. The coated substrate are referred to as AA+GAG+VN, depending on which GAG (heparin, HS^{pm}, $HS9^{+ve}$, $HS9^{-ve}$) and which VN concentration was used to coat the surface. The coated substrate was then named accordingly: for example, surfaces pre-coated with AA and $HS9^{+ve}$ variants for the capture of 5 μg/ml VN solution concentration are named AA+$HS9^{+ve}$+VN5.

4.2.2. Cell culture on AA surface

HES-3 (ES Cell International) or H7 (WiCell Research Institute) cells were maintained on AA surfaces for > 8 weeks in mTeSR^{TM}1 media. Routine maintenance of cells by weekly mechanical passaging using a 1:10 passage ratio was performed on cells cultured on control TCPS surfaces coated with VN5.

4.2.3. Adhesion, differentiation and FACS assays

To assess cell responses on the AA surfaces, various assays were performed. For the study of cell attachment efficiency, a crystal violet adhesion assay was utilized as described in Section 2.2.6. The *in vitro* (EB differentiation) and *in vivo* (teratoma formation) differentiation potential of both cells at week 5 was analyzed according to

the techniques introduced in Sections 2.2.7 and 2.2.8 respectively. For the study of pluripotent marker (OCT-4 and Tra1-60) expression, weekly staining of cells and analysis with FACS was performed as described in Section 2.2.10.

4.2.4. Cell growth analysis

To determine the doubling time of cells, a 7 day growth curve was generated with daily cell counts. Cultured cells were dissociated mechanically, counted with the nucleocounter NC-3000 and seeded (3×10^5 cells) into AA-polymerized 24-well surfaces in mTeSR™1 medium. Cells were left to proliferate for 7 days and counted daily by dissociation with TrypLE™ express (Invitrogen). Total viable cell numbers were plotted against time, and the specific growth rate determined from the calculated gradients during exponential phases of growth. The doubling time was calculated in the manner of the study by Ding *et al.* (Ding *et al.* 2010):

$$\text{Doubling time} = \ln 2 / \sigma, \text{ where } \sigma \text{ is the specific growth rate}$$

4.2.5. Immunocytochemistry

In order to assess changes in pluripotency during culture, antibodies were utilized to stain the target pluripotent proteins OCT-4 and Tra1-60. Staining was performed at room temperature with agitation. After approximately 24 – 48 h, cells were fixed with 4 % paraformaldehyde (Sigma Aldrich) for 1 h, washed 3 times with 0.1 % Triton-X100 (Biorad) in PBS for 5 min and blocked with 5% BSA for 1 h. Cells were then reacted with either anti-OCT-4 (1:30) or anti-Tra1-60 (1:150) each diluted in 1 % BSA for 1 h. Cells were then washed, and probed with Alexa (647)-tagged anti-mouse $IgG2_b$ (1:500) for OCT-4 or Alexa (633)-tagged anti-mouse IgM (1:500) for Tra1-60 for 30 min. Secondary antibodies were all from Invitrogen. Cells

were then washed with PBS to remove unbound antibodies and counterstained with SlowFade Gold anti-fade reagent with DAPI (Invitrogen) to visualise nuclei.

4.2.6. Quantitative real time PCR

Real time PCR (qRT-PCR) was employed to quantitate mRNA transcript levels for cells cultured on AA+HS9^{+ve} substrates. Total RNA was extracted and 1 μg reversed transcribed to cDNA. SYBR® green-based (Applied Biosystems) PCR was then performed using 5 μM of both forward and reverse primers for the three germ lineages (endo-, meso- and ectoderm). To detect the endoderm lineage, AFP and GATA binding factor 6 (GATA6) primers were used. For the mesoderm lineage, HAND1 and Nkx2.5 primers were used and for the ectoderm lineage, paired box protein 6 (PAX6) and microtubule-associated protein 2 (MAP2) primers were utilised. Nanog and OCT-4 primers were used as the pluripotent markers, with GAPDH as the internal control. Primer sequences are shown in Table A1. Total RNA was extracted in a similar manner from undifferentiated cells for comparative purposes. Reactions were measured in an ABI PRISM® 7500 PCR machine, which analyzed the optical absorption from each well. Cycling conditions were: 10 min at 95 ^{o}C, 45 cycles of a three-step amplification including 20 sec at 95 ^{o}C, 10 sec at 55 ^{o}C and 30 sec at 60 ^{o}C, followed by a final extension for 40 sec at 72 ^{o}C. Fold induction was calculated relative to GAPDH using the ΔΔCt method.

4.2.7. Karyotype stability

Genetic stability is an important factor to ensure that the cells are not adversely affected by the culturing on various substrates. The stability of hESCs cultured on AA surfaces for > 5 passages was analyzed by the Cytogenetic Laboratories at the Department of Obstetrics and Gynaecology, Kandang Kerbau Women's and Children's Hospital, Singapore. Karyotyping analysis was performed using BrdU/colcemid with 20 cells being analyzed per condition. Cells with more than 2 abnormal chromosomes were considered karyotypically unstable.

4.2.8. Statistical analysis

All data values are reported as the mean $\pm$ standard error taken from three individual experiments with triplicate runs each. When appropriate, one-way ANOVA was performed to compare differences across the groups, and $P < 0.05$ was considered as significant. The two-tailed student's t-test was performed to determine the differences between two sample groups. Graphs were plotted and data transformed using Sigma plot software.

4.3. Results

4.3.1. Cell adhesion on AA substrates

To determine the suitability of the substrate coating that consisted of AA+GAG+VN for serial culturing, hESC growth was assessed over a 7 day period. Surfaces that were pre-coated with AA and GAGs (heparin, HS^{pm}, $HS9^{+ve}$ and $HS9^{-ve}$) were used to immobilize different concentrations (0, 2, 2.5 and 5 μg/ml) of VN. Surfaces were screened for HES-3 attachment. Photomicrographs taken after 7 days revealed that, irrespective of the surface, cells attached to an overlay of VN5 (Fig. 4.1). However, cell attachment and proliferation on VN2 and VN2.5 was only supported with the heparin and $HS9^{+ve}$ pre-coatings. In many ways this finding was to be expected, given the previously identified VN surface density in Section 3.3.5. Clearly, higher amounts of VN were adsorbed on the heparin and $HS9^{+ve}$ substrates as compared to the HS^{pm} and $HS9^{-ve}$ substrates (Fig. 3.27) at these concentrations. This confirmed that the affinity chromatography was able to separate 'tuned' HS with a higher VN-binding affinity from low binding $HS9^{-ve}$ and medium binding HS^{pm}. According to the VN surface densities previously identified with ^{125}I-VN (Fig. 3.27), the densities on AA+$HS9^{+ve}$+VN2.5 and AA+$HS9^{+ve}$+VN5 were 80 ng/cm^2 and 150 ng/cm^2 respectively. Notably, after 2 weeks of continuous passaging, HES-3 cells were unable to maintain their growth on AA+$HS9^{+ve}$+VN2. This VN concentration was therefore deemed as not suitable, and was excluded from further study.

As heparin binds strongly to a wide range of ECM proteins, it was utilized as a positive control for the experiments. Although heparin can support HES-3 cells at low VN concentration (VN2), it is not a suitable pre-coating for future therapy because of its adverse clinical side effects (Gandhi & Mancera 2008).

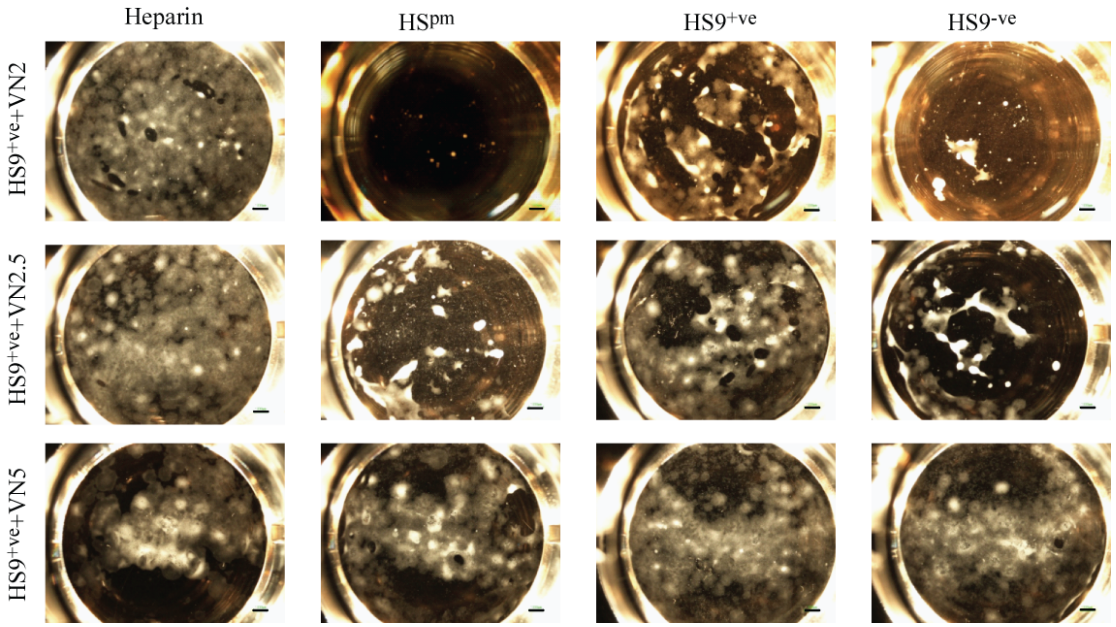

Figure 4.1. Photomicrographs of HES-3 cells on AA surfaces. Cells attached to VN5 regardless of the underlying GAG substrate, but selectively attached to heparin and $HS9^{+ve}$ surfaces coated with VN2.5 and VN2. Therefore $AA+HS^{pm}$ and $AA+HS9^{-ve}$ substrates were not viable for further cell culture. Cells detached from $HS9^{+ve}$+VN2 after 2 passages and this coating was also excluded from the study. Scale bar = 1 mm

4.3.2. Characterization of HES-3 cells on AA+$HS9^{+ve}$+VN substrates

After screening AA+GAG, it was concluded that VN concentrations of $\geq$ 2.5 μg/ml would be suitable for all subsequent long-term pluripotent cell-based assays. Thus, HES-3 cells cultured on either AA+HS9 substrates coated with either VN5 or VN2.5, or control TCPS surfaces coated with VN at 5 μg/ml (VN5), were subjected to adhesion assays, cell growth analysis, pluripotent marker expression and chromosomal stability analysis.

4.3.2.1. Crystal violet adhesion and cell growth assay

To assess the attachment efficiency of HES-3 cells on surfaces (AA+HS9^{+ve} and AA+HS9^{-ve}) coated with VN2.5 or VN5, a crystal violet cell adhesion assay was performed (Fig. 4.2A). An AA+HS9^{-ve}-coated surface was included in this attachment assay as a comparison. Irrespective of the surface, cells attached in a concentration-dependent manner, reaching saturation at VN5. Cells preferentially bound to AA+HS9^{+ve} rather than the AA+HS9^{-ve} substrate, which was consistent with the previous data. Results were normalized to the absorbance from cells attached to VN5. Even though the % bound to AA surface was less than VN5, the cell growth curve and doubling times were similar (Fig. 4.2B). A 7 day cell growth curve was then constructed for TCPS coated with 2.5 μg/ml VN solution (VN2.5), VN5, AA+HS9^{+ve}+VN2.5 and AA+HS9^{+ve}+VN5. Cells attached and proliferated on all substrates, although initially having a lag phase (day 0 to day 2) for cell adaptation followed by an exponential growth phase from day 2 to day 5, with saturation reached after day 5. Similar cell numbers were seen at the end of 7 days for all the cultures, and the doubling times calculated from the exponential phase of the growth curve were similar at ~ 32 h (Table 4.1). These results thus suggested that AA+HS9^{+ve} surfaces were at least comparable to TCPS surfaces.

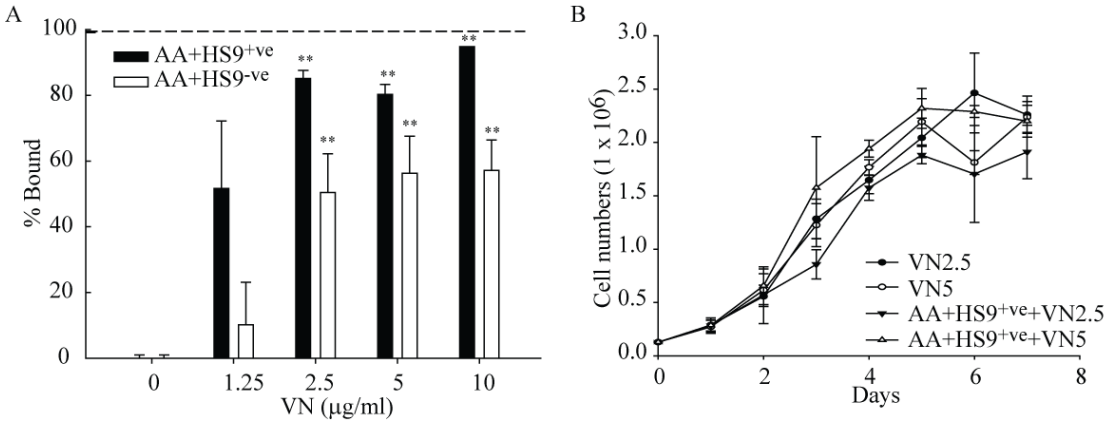

Figure 4.2. HES-3 adhesion and cell growth assay. (A) Adhesion assay on AA+HS9^{+ve} and AA+HS9^{-ve} surfaces with 0, 1.25, 2.5 and 5 μg/ml VN solution. Results were normalized to the absorbance of VN5. Cells bind preferentially to AA+HS9^{+ve} rather than AA+HS9^{-ve} substrates. Thus the former surface was better for cell culture. (B) Cell growth analysis on VN2.5, VN5, AA+HS9^{+ve}+VN2.5 and AA+HS9^{+ve}+VN5 substrates. Similar cell numbers were achieved at the end of 7 days. ** = $P < 0.05$

Table 4.1. Doubling time of HES-3 and H7 cells. Cells cultured on VN5, VN2.5, AA+HS9^{+ve}+VN2.5 and AA+HS9^{+ve}+VN5 substrates had a similar doubling time of ~ 33 h on all surfaces.

	HES-3	H7
VN2.5	31 h	34 h
VN5	32 h	33 h
AA+HS9^{+ve}+VN2.5	33 h	34 h
AA+HS9^{+ve}+VN5	31 h	32 h

To determine the pluripotency marker expression levels of HES-3 cells, FACS was applied to cells cultured AA+HS9^{+ve}+VN2.5 and AA+HS9^{+ve}+VN5 substrates for 8 passages. Cells were > 95 % positive for the Tra1-60 and OCT-4 markers of pluripotency (Fig. 4.3A). The FACS analysis across the 8 passages is summarized in Table A2. Immunostaining of colonies also revealed that all colonies stained positive for Tra1-60 and OCT-4 (Figs. 4.3 B and C). Thus, the similar pluripotency marker expression levels on the cells cultured on control VN5 substrates suggest that they are at the very least an equally viable surface for cell culture.

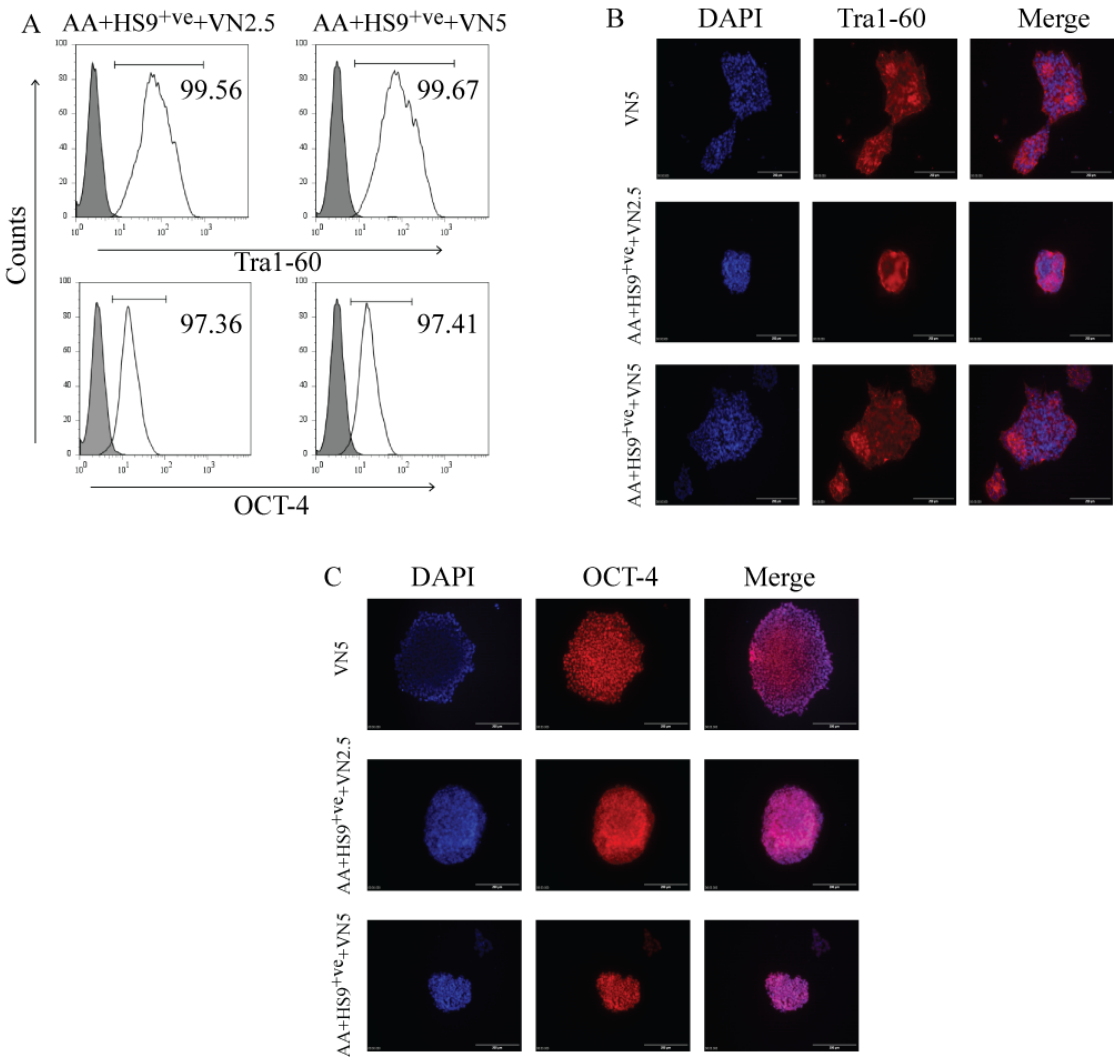

Figure 4.3. FACS analysis and immunostaining of HES-3 cells. Cells were cultured on VN5, AA+HS9^{+ve}+VN2.5 and AA+HS9^{+ve}+VN5 substrates. (A) Tra1-60 and OCT-4 FACS analysis at passage 6. Cells express high levels of the pluripotency markers (> 95%). Merged cell images of the DAPI and (B) OCT-4 or (C) Tra1-60 markers. The OCT-4 and Tra1-60 antigens appear red and nuclei appear blue. Colonies expressed comparable levels of pluripotency markers to cells cultured on control VN5 substrates.

4.3.2.2. Karyotyping

To assess whether cells underwent culture-adaptation, chromosomal stability was determined with karyotyping. Long-term (passage 5) cells cultured on VN5 or AA+HS9^{+ve}+VN2.5 and AA+HS9^{+ve}+VN5 substrates were analyzed and shown to retain normal diploid chromosomes when cultured on AA+HS9^{+ve}+VN5 (Fig. 4.4A). However, 3 out of 20 of the cells cultured on AA+HS9^{+ve}+VN2.5 substrates were abnormal. These 3 cells were found to have a terminal deletion of the long arm of chromosome 7 at band 7q32 (Fig. 4.4B). This is of interest because the changes observed here are different from the changes seen in the large scale study with 125 hESC and 11 iPSC lines analyzed by the International Stem Cell Initiative (Amps *et al.* 2011). They reported changes in chromosomes 1, 12, 17 and 20, rather than chromosome 7, with > 20 % of the abnormal cells having amplifications in chromosome 20q11.21. A strong candidate for driving culture-adaptation in ESC is the BCL2L1 gene located in chromosome 20. To confirm this, another independent study with HES-3 cells cultured on the same surface (AA+HS9^{+ve}+VN2.5) for 5 passages showed normal karyotype. This suggests that this particular change could be spontaneous and random. Although cells cultured on AA+HS9^{+ve}+VN2.5 have higher propensity for slight variations in their chromosome structure, further downstream characterization was still done.

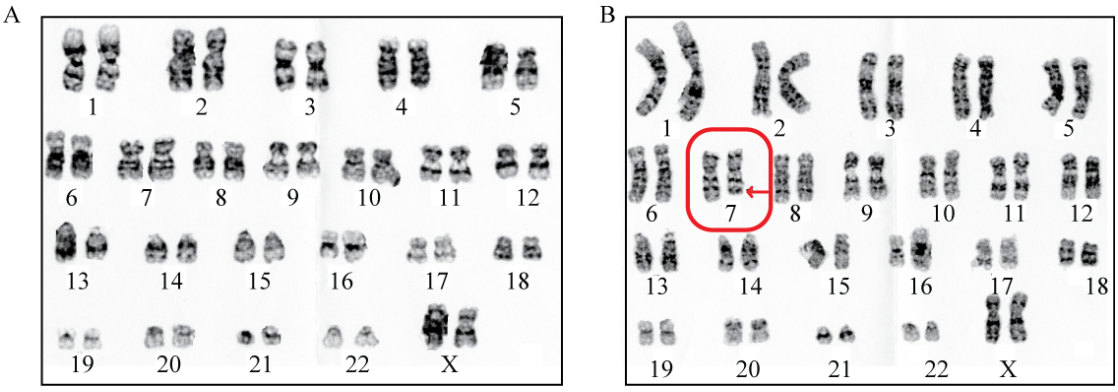

Figure 4.4. Karyogram of HES-3 cells. (A) Cells cultured on the AA+HS9^{+ve}+VN5 surface for 5 passages were analyzed for genetic instability. Results showed that the cells remained normal, with diploid chromosomes. (B) Cells cultured on AA+HS9^{+ve}+VN2.5 surfaces showed at a rate of 3 out of 20 a deletion on chromosome 7; the other 17 of the cells have normal diploid chromosomes.

4.3.2.3. *In vitro* and *in vivo* differentiation

Other than pluripotent marker expression, the key "trademark" of pluripotent cells is the ability of cells to differentiate into the 3 germ layers (endo-, meso- and ectoderm). Cells cultured on AA+HS9^{+ve}+VN2.5 or AA+HS9^{+ve}+VN5 substrates were thus triggered into *in vitro* and *in vivo* differentiation. When pluripotent hESCs were lifted from the culture surface and allowed to form embryoid bodies (EB), they randomly differentiated into all 3 germ layers. Thus, i*n vitro* EB differentiation was induced here in HES-3 cells at passage 6, with the various germ layer gene expression patterns analyzed by quantitative real-time PCR (Fig. 4.5). Endoderm (AFP and GATA6), mesoderm (Hand1 and Nkx2.5) and ectoderm (Pax6 and MAP2) genes were upregulated and pluripotent genes (Nanog and OCT-4) were downregulated after differentiation.

Finally, HES-3 cells were tested for *in vivo* teratoma differentiation by injecting the treated cells into SCID mice. If the cells remained pluripotent, they should form tumours consisting of cells from all 3 germ layers. Teratomas formed by

7 weeks, and all possess the characteristic structures of all 3 germ layers (Fig. 4.6). Cells differentiated along the ectoderm lineage formed neural rosettes, those along the mesoderm lineages formed cartilage and bone and those along the endoderm lineages formed gut epithelium structures. Collectively, these differentiation assays confirmed the continuing pluripotency status of the cells cultured on the AA+HS9^{+ve}+VN2.5 and AA+HS9^{+ve}+VN5 substrates.

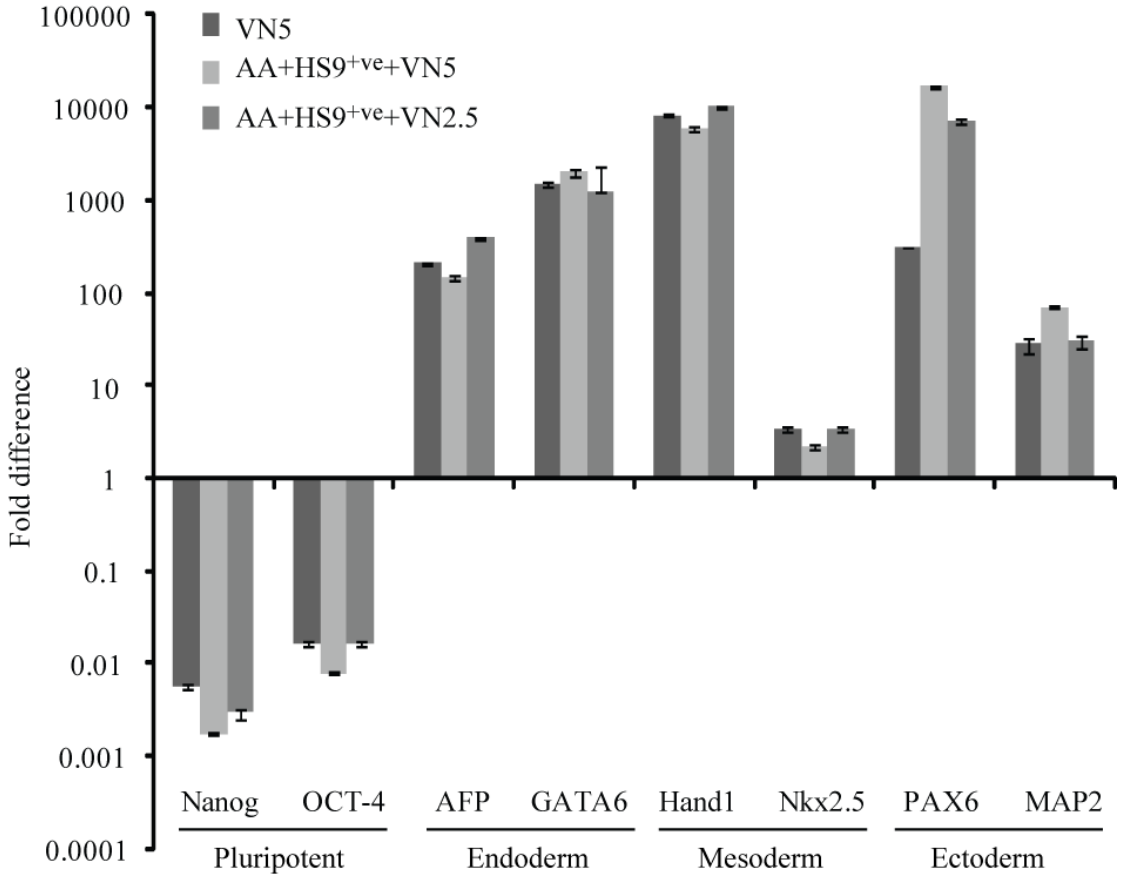

Figure 4.5. mRNA transcripts expression in HES-3 cells after EB differentiation. Complementary DNA was generated from HES-3 cells before and after EB differentiation and then probed by qRT-PCR for the genes from the 3 germ layers. AFP and GATA6 represented the endoderm markers; Hand1 and Nkx2.5 represented the mesoderm markers and PAX6 and MAP2 represented the ectoderm markers. C_t values were normalized to those before EB differentiation and expressed as fold difference. Cells upregulate genes from all the 3 germ layers and downregulate pluripotent genes (Nanog and OCT4).

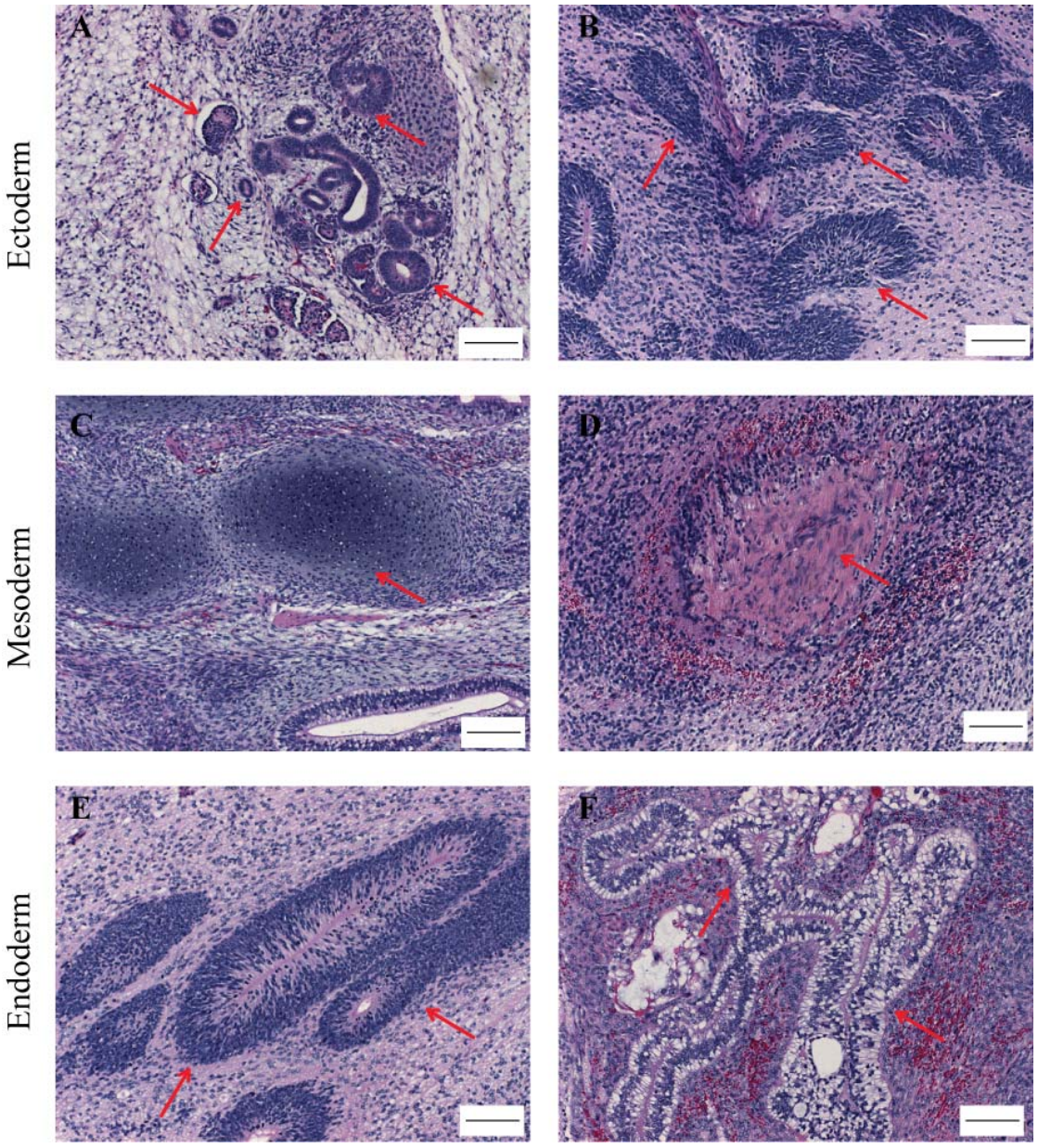

Figure 4.6. Representative structures in teratomas from HES-3 cells stained with haematoxylin and eosin. Teratomas formed from HES-3 cells cultured on AA+HS9^{+ve}+VN2.5 surfaces show (A) neural rosettes, (C) cartilage and (E) gut epithelium, which corresponds to the endo-, meso- and ectoderm lineages. Similarly, cells cultured on AA+HS9^{+ve}+VN5 surfaces show (B) neural rosettes, (D) bone and (F) gut epithelium, indicating that cells differentiated along the endo-, meso- and ectoderm lineages respectively. Scale bar = 100 μm

From the earlier ^{3}H-HS^{pm} and ^{125}I-VN surface measurements made on AA+HS9 surfaces (Fig. 3.26 and 3.27), it was determined that 2 μg HS coating solution gives rise to a 300 ng/cm^2 HS density. The AA+HS9^{+ve}+VN2.5 and AA+HS9^{+ve}+VN5 substrates captured 80 ng/cm^2 and 150 ng/cm^2 of VN respectively. These VN densities were much lower than the ones measured with VN5 (250 ng/cm^2). This indicates that AA+HS9^{+ve} surfaces can successfully modulate the function of VN at much lower threshold densities. Although there is more VN adsorbed onto TCPS, it appears that this extra VN is not functional. It can be thus surmised that protein needs to be immobilized in the correct conformation to maintain its function, because simply having more VN on TCPS does not translate into higher biological activity. Marson *et al.* showed that protein immobilized on surfaces can lose function by steric hindrance or conformational perturbation (Marson *et al.* 2005). These data strongly suggested that the appropriate immobilized GAGs were contributing positively to the VN structure-function relationship in terms of bioactivation.

4.3.3. Characterization of H7 cells cultured on AA+HS9^{+ve}+VN substrate

To ensure the robustness of these results for the general culture of pluripotent hESCs on AA+HS9^{+ve}+VN substrates, another hESC (H7) line was tested. The initial photomicrographs at day 7 of AA+GAG substrates were taken. As seen previously, heparin and HS9^{+ve} surfaces (AA+HS9^{+ve}+VN2.5 and AA+HS9^{+ve}+VN5) were the only ones able to support H7 cell attachment (Fig. 4.7).

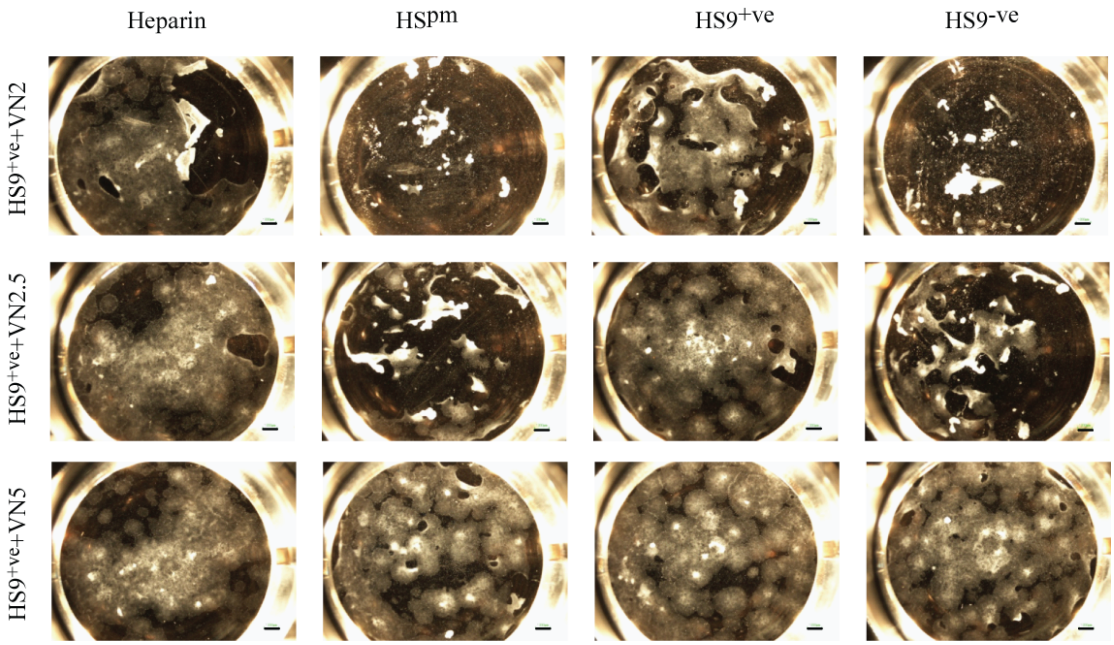

Figure 4.7. H7 cell attachment on various AA surfaces. Irrespective of underlying coating, wells coated with 5 μg/ml of VN (VN5) could support cell attachment and proliferation to confluence. However, cells preferentially bind and proliferate on AA+heparin+VN2.5 and AA+HS9^{+ve}+VN2.5 but not the other surfaces. Scale bar = 1 mm.

Similarly, H7 cells have a similar growth curve and doubling time (~ 33 h) (Table 4.1) on VN5 (Fig. 4.8A). FACS analysis of cells also revealed high levels of Tra1-60 and OCT-4 marker expression (Table A2). It is worth noting that the karyotype of H7 cells on both surfaces remained normal. This confirms the idea that there are wide variations between hESC lines.

Differentiation potential was also determined, by both EB and teratoma formation. Together these results revealed that AA+HS9^{+ve}+VN2.5 and AA+HS9^{+ve}+VN5 surfaces are able to support the robust, long-term pluripotent status of hESCs in culture. As HES-3 cells have higher propensity for chromosomal changes at AA+HS9^{+ve}+VN2.5, the AA+HS9^{+ve}+VN5 surface was selected as the most viable surface. Therefore, I conclude that the potential minimum threshold indentified for the successful long-term culture of hESCs is at least 150 ng/cm^2 VN coated over 300 ng/cm^2 HS9^{+ve}.

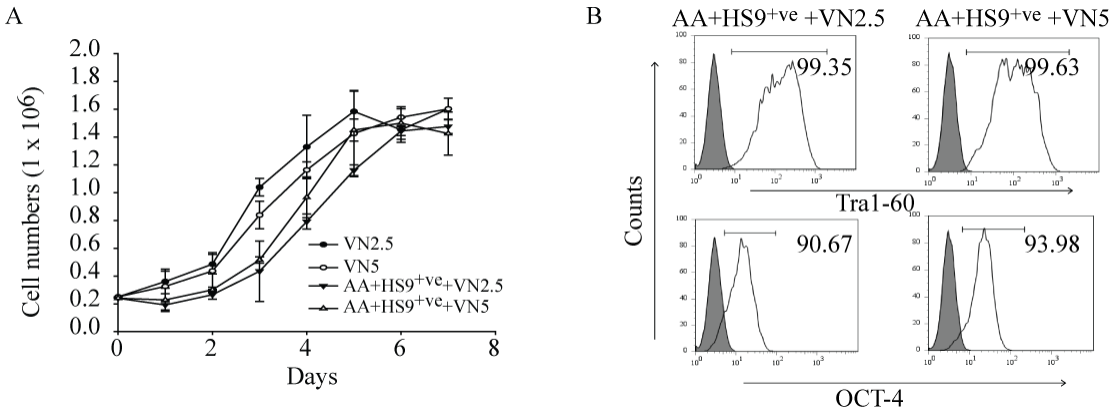

Figure 4.8. Growth curve and FACS analysis of H7 cells. (A) The 7 day cell growth analysis on the various surfaces showed similar growth kinetics, with a doubling time of ~ 33 h. (B) High expression levels of Tra1-60 and OCT-4 pluripotent markers revealed by FACS analysis.

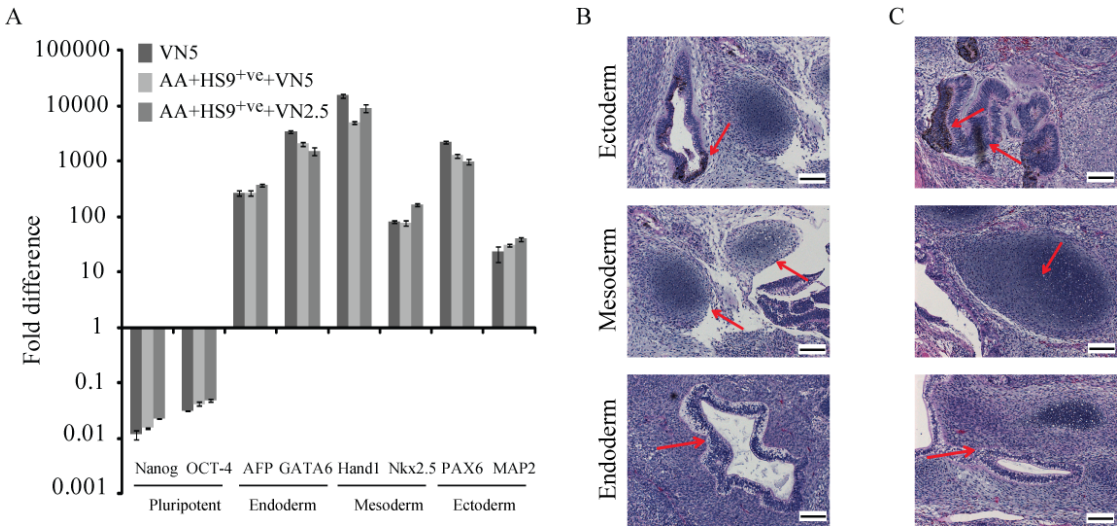

Figure 4.9. Differentiation potential of H7 cells. (A) qRT-PCR analysis of cells after EB differentiation. mRNA transcripts from the 3 germ layers were upregulated and pluripotency genes (Nanog and OCT-4) were downregulated. Teratomas formed from cells cultured on (B) AA+HS9^{+ve}+VN2.5 and (C) AA+HS9^{+ve}+VN5 substrates contained structures from all the 3 germ layers. Ectoderm lineage is represented by pigmented epithelium; mesoderm lineage is represented by the formation of cartilage and the endoderm lineage shows gut epithelium structures. Scale bar = 100 μm

4.4. Discussion

It has become clear that to fulfill the potential that hESC have for clinical application, defined culture surfaces will need to be rigorously specified to allow for the maximum propagation with minimal differentiation. I believe that VN is a promising candidate, and that understanding the surface threshold requirements that stem cells have for it will help to reduce the cost of culturing them in large-scale bioreactors. However, hESCs, unlike other stem cells, are particularly demanding. They do not attach and grow on bare TCPS, and are in fact extremely sensitive to the ECM components they will tolerate.

Here I employed a novel attachment strategy: using plasma-polymerized AA substrates to immobilize a VN-tuned HS variant, on the premise that the optimized presentation of VN will prove a great advantage for the culture of hESCs. The platform affinity chromatography technology is well suited for a scale-up of the

isolation of a avid VN binding variant ($HS9^{+ve}$) as shown from the preferential binding of hESCs for it as compared to the flowthrough ($HS9^{-ve}$) or starting HS (HS^{pm}) (Fig. 4.1 and 4.7). These data suggests that this compound substrate could sufficiently mimic the essential features of stem cell ECM, where GAGs and proteins are known to combine to support cell attachment and growth *in vivo*.

Chromosomal stability was used to check the quality of the cultured cells on the substrate variations. Karyotypic instability was found in HES-3 cells, but not in H7 cells, when they were cultured on AA+$HS9^{+ve}$+VN2.5 substrates. This confirms the intrinsic differences between stem cell lines. Indeed, differences in growth rate, genetic and epigenetic changes between different hESC lines in culture have long been reported (Carpenter *et al.* 2003, Carpenter *et al.* 2004, Hoffman & Carpenter 2005b). As the H7 cells remained karyotypically normal on the AA+$HS9^{+ve}$+VN2.5 surface, they appear better adapted to it than HES-3 cells. We therefore chose to continue with the apparently safer VN density of 150 ng/cm^2.

The VN density differences seen between the AA+$HS9^{+ve}$+VN2.5 combination and the AA+$HS9^{+ve}$+VN5 are very significant, from 80 ng/cm^2 to 150 ng/cm^2. The actual threshold must lie between these two densities, and further fine-tuning might reveal an even lower VN threshold. This surface density is at least 30 % lower than the one initially identified for VN5 (250 ng/cm^2). This significant reduction in surface requirement is a potentially important cost saving for any cell culture scale-up using VN as a regimen.

What is most interesting was the comparison of surface densities from VN absorbed onto TCPS at VN2.5 and AA+$HS9^{+ve}$+VN5 surfaces. Both surfaces have a similar density of ~ 150 ng/cm^2. However, cells cultured on VN2.5 did not form teratomas after their injection into mice (Chapter 2), unlike cells cultured on the

AA+HS9^{+ve}+VN5 surface. This suggested that the absorbed VN on TCPS is not as biological active. Indeed, it is possible that the immobilized HS plays a role in the multimerization of plasma VN, transforming the inactive monomer into active heparin-binding multimers. Izumi *et al.* and Seiffert *et al.* both demonstrated that plasma VN exists in these two structurally and functionally distinct forms (Izumi 1989, Seiffert & Schleef 1996). Upon VN binding to HS, via its HBD, the complex becomes allosterically stabilized (Francois *et al.* 1999). These structural changes within VN expose additional binding sites within it, enabling the binding of additional proteins (Morris *et al.* 1994, Seiffert & Smith 1997). Thus the binding of VN to GAGs presumably anchors it onto the culture surface, and opens up new complexing opportunities. VN's RGD sequences are located at its N-terminal, whereas the HBD is located at its C-terminal. In the first proposed model of VN-HBD engagement (Fig. 1.4), the structural changes induced in VN upon HS binding causes cryptic sites at N-terminal to be revealed, exposing loci for other ligands. Seiffert *et al.* demonstrated that these cryptic sites contained extra RGD cell adhesion motifs, so promoting integrin-mediated cell binding (Seiffert & Smith 1997). It was also demonstrated by Noble *et al.* that breast cancer cell migration is enhanced when insulin growth factor-II is bound to surface-adsorbed VN, rather than when it is left in solution, again suggesting a complex conformational activation. As is the case for LN and FN, both proteins which require conformational activation by pre-binding to heparin, it is clear that VN belongs to the same class of large, multi-domain ECM proteins that are designed to cross-link collagens, proteoglycans, adhesive glycoproteins and cell surface integrins into large informational networks. Thus it is hardly surprising that VN requires similar HS binding to reach the zenith of its

potential activity. Thus, we conclude that the HS-functionalized surface permits VN to adopt a more optimal configuration for hESC attachment.

In attempts to further delineate the lower VN density required on HS-functionalized surfaces as compared to TCPS surfaces, the inherent properties of the VN protein need to be considered. Plasma-derived VN exists mainly in an inactive monomeric form, with only a small proportion existing in the active, RGD-exposed multimeric form (Francois *et al.* 1999, Gibson & Peterson 2001, Izumi 1989, Schvartz *et al.* 1999b). As plasma-derived VN was used here, it was to be expected that more inactive VN was absorbed onto the TCPS surfaces. The VN adsorption itself might add to this intrinsic steric hindrance, thus further compounding the loss of activity. Mei *et al.* has also shown that adsorbed VN protein needs to interact with an appropriate surface to be able to adopt a conformation that can promote colony formation (Mei *et al.* 2010).

The successful attachment of cells to a substrate via integrin receptors leads to the formation of focal adhesion contacts; these surface complexes conduct cues from ECM into the cells (Askari *et al.* 2009, Hynes 2009, Zou *et al.* 2007). Integrin signalling is critical for cell survival and proliferation. It has been observed that optimal cell stimulation with various growth factors is itself dependent on integrin-mediated cell attachment to an appropriate ECM (Giancotti & Ruoslahti 1999). Integrin clustering triggered by sufficient binding becomes associated with the cytoskeleton through talin-vinculin binding, which in turn mostly through FAK (focal adhesion kinase) leads to the formation of integrin-growth factor receptor complexes (Askari *et al.* 2010, Calderwood *et al.* 1999, Hynes 2009, Mostafavi-Pour *et al.* 2003). Such an example of molecular cooperation is the activation of the EGF receptor by integrin-mediated pancreatic cancer cell migration and chemoresistance (Danilov *et*

al. 2011). Such integrin activation by ECM binding in turn lowers the threshold for growth factor receptor signalling. The stable bioresponses of hESCs to the substrate combinations tested here implies that just such stable FAK interactions are themselves promoting long term stem cell survival and pluripotency. This remains to be proven.

Vitronectin is known to synergize with several growth factors in such a way as to maintain both embryonic and adult stem cells in an undifferentiated state. Parker *et al.* reported that VN, together with IGF-1 and transforming growth factor 1 (TGF-1), could modulate human mesenchymal stem cell activity (Parker *et al.* 2009). Studies by Upton and colleagues demonstrated the ability of VN and IGF-1, together with IGF binding protein (IGFBP) or a chimeric VN: IGF-1 protein, as adjuvant to the serum-free cell culture medium could support the successful culture of hESCs (Manton *et al.* 2010, Richards *et al.* 2008). Mutagenic studies have shown that the HBDs in IGFBP-3 and IGFBP-5 are also involved in the enhancement of IGF-1 binding to VN (Firth *et al.* 1998, Nam *et al.* 1997), which is necessary for the growth factor's activities (Clemmons *et al.* 1999, Grulich-Henn *et al.* 2002, Rees & Clemmons 1998). These growth factors can induce markedly different mitotic rates in embryonic and adult stem cells (Ghule *et al.* 2008). The mTeSR^{TM}1 medium used in this study contains FGF-2, TGFβ-1 and BSA, markedly different growth factors that all require HS. Moreover Levenstein *et al.* have shown that MEFs secrete HSPGs which help to stabilize and extend the half-life of FGF-2, a key growth factor for cells to remain pluripotent (Levenstein *et al.* 2008). Thus, the HS-VN substrate is generally beneficial for the activities of these important growth factors.

A study by Doran *et al.* reported a method of creating substrates with high ECM-derived protein content on a layer-by-layer, self-assembled surface of HA and chitosan (Doran *et al.* 2010). Both the ability of the hESCs to initially attach to such

surfaces and the ability of mesenchymal stem cells to differentiate down the osteogenic lineage were studied. They employed NHS/EDC chemistry to covalently link 3 layers of the ECM protein to the 5 pre-coated bilayers of the HA/chitosan surface, resulting in > 50 % of the protein becoming bound, a very high proportion under such circumstances. The technique resulted in ~ 3 $\mu g/cm^2$ recombinant VN and ~ 5 $\mu g/cm^2$ recombinant FN being coupled for cell culture. However, the method employed to quantify the protein was only indirect, being a measurement from the difference between the concentration of the input solution and the output unbound solution and based on the relatively insensitive Bio-rad Protein assay. The high VN density reported is above the threshold density (150 ng/cm^2) measured in this study with the much more accurate ^{125}I-VN binding assay. In terms of using VN in systems for large-scale cell culturing, their technique is neither cost-effective, nor scalable.

Using EDC to tightly and covalently link ECM proteins clearly poses the risk of altering their protein structure, and thus affecting their function. The high density of measured protein might not translate to full activity on such immobilized surfaces. I believe that the most economical and effective way to immobilize a protein, without affecting its conformation or function, is through non-covalent methods. Even though a culture surface is constantly modified by proteins from both the cell culture media and secreted by the cells, this merely reflects the extraordinarily dynamic environment to which cells become exposed. Embryonic stem cells naturally exist within the complex 3-D environment within blastocysts; shifting them suddenly onto a 2-D surface is a particularly harsh change. Therefore, it can be posited that a dynamic surface, with conformationally better presented adhesive factors, will better mimic the natural environment for such cells.

A recent study by Peng *et al.* showed that decellularized human fibroblast matrix was able to propagate hPSC (Peng *et al.* 2012). The surface was generated using dextran sulfate as a macromolecular crowder to increase the ECM deposition from fibroblasts. However, not all every fibroblast cell lines are suitable and this highly complex substrate is not defined. Specific staining of the matrix showed the presence of HS, collagens and FN. It is interesting to note that VN is not present in this decellularized substrate and Matrigel™, which indicates that in the presence of a combination of different ECM components, VN is not essential (Hughes *et al.* 2011). However without the complex matrix, a single component VN is sufficient to propagate hPSCs. These results supported our hypothesis that by using HS and VN can recapitulate the function of the natural ECM.

Development in hPSC culture surfaces has increase expoenentially leading to various commercial products. Study by Melkoumian *et al.* led to the development of synthemax® by Corning® that require high RGD peptide density and the peptide conjugation reaction is limited by EDC/NHS efficiency. Study by Nagaoka *et al.* led to the development of StemAdhere™ by Stemcell™ Technologies that used colorimetric measurement to determine E-cadherin surface density which is not a specific methodology. Human recombinant laminin-511 surfaces demonstrated by Rodin *et al.* led to the development of recombinant coating by BioLamina. The surface was made active by passive adsorption of peptide onto culture surfaces. PuraMatrix™ substrate by BD Biosciences, PuraMatrix™ is a hydrogel that require optimization with additional ECM protein or growth factor to be functional, thus utilizing it for hPSC culture is cumbersome. Therefore, the substrate developed in this thesis contributes to the field by establishing a defined surface density of HS and VN without any modification or optimization for the long-term propagation of hPSCs.

4.5. Summary

The previous chapter demonstrated that $HS9^{+ve}$ variants have significantly higher affinity to VN than $HS9^{-ve}$ variants, and that the novel engineered $HS9^{+ve}$-functionalized AA surfaces could serve as an effective ECM replacement for the long-term culture of hESCs. Among all the HS9 variant-AA surfaces, only AA+$HS9^{+ve}$+VN2.5 and AA+$HS9^{+ve}$+VN5 could support cell growth. Thus, a full characterization of pluripotency of HES-3 and H7 cells with the combination of FACS, EB differentiation potential and teratoma formation was conducted for AA+$HS9^{+ve}$+VN2.5 and AA+$HS9^{+ve}$+VN5 surfaces. Cells cultured on AA+$HS9^{+ve}$+VN2.5 were found to be relatively karyotypically unstable, even though they were able to form teratomas *in vivo*. Thus this surface was not considered suitable for further development.

Such results allowed me to conclude that an HS surface density of 300 ng/cm^2 and VN surface density of 150 ng/cm^2 on HS-derviatised AA surfaces are the threshold levels for successful long-term hESC culture. This study distinguishes itself from earlier attempts in that a real unmodified functional VN surface density was defined. A significant, cost-saving density reduction of at least 30 % was achieved with the tuned HS9 variant as compared to mere passive adsorption onto TCPS surfaces.

CHAPTER 5 : CONCLUSIONS AND RECOMMENDATIONS

5.1. Conclusions

The aim of this thesis is to engineer an effective substrate capable of binding and presenting unmodified VN, without compromising its biological utility, for the culture of pluripotent hESCs. Such a defined set of components should allow for the identification of appropriate threshold surface densities suitable for the long-term propagation of clinically relevant cells such as hPSCs. Such mixtures would allow for faster rates of progress in the improvement of industrial stem cell culture. The basis of the novel surface was the "tuned" $HS9^{+ve}$ variant, purified from HS starting mixture, through an inexpensive and quick affinity chromatography step, on its ability to bind to the heparin-binding domain of vitronectin. The minimum HS-supplemented VN threshold surface density was identified, and compared for its efficacy against the standard passive adsorption of VN onto TCPS. Based on this study, the following conclusions were derived:

(1) The relatively specific VN-tuned HS variant can be isolated from crude HS material with reproducible confidence. This $HS9^{+ve}$ variant bind VN with significantly higher affinity than the other HS variants; furthermore, the 6O- and N-sulfation motifs and a length of at least 6 disaccharide units on HS appear to be crucial for this association.

(2) Plasma-polymerized AA films are a particularly suitable substrate for the immobilization of HS. The hESCs are able to attach and thrive on AA+$HS9^{+ve}$+VN substrates for > 8 passages, and remain pluripotent.

(3) Defined surface densities need to be carefully identified, as in this study. An N: C ratio of 1.8 to 2.2 is optimal for HS binding. When 300 ng/cm^2 of

HS is combined with 150 ng/cm^2 of VN on the engineered substrate, it allows for the successful long-term culture of hESCs in a pristine state.

(4) Even at this early stage of optimization, a significant cost savings (~ 30 %) can be achieved with this novel engineered substrate, as compared to the widely practiced, standard passive adsorption of VN onto TCPS. This novel technique can easily be scaled-up for even greater cost savings.

This thesis thus propose that the data presented here concerning this defined platform more than justifies a proper trailing for the large scale culturing of pluripotent stem cells to meet the unmet clinical demand. Higher densities of hESCs and their differentiated progenies are required for those future applications that cannot be achieved with conventional 2D culture systems. It has long been known that 3-D suspension culture systems are more effective for the generation of high cell densities because of the larger surface growth areas per volume offered by bioreactors (Oh *et al.* 2009). Several groups have addressed this issue by culturing cells in suspension culture as pluripotent aggregates, or by using microcarriers (MCs) (Amit *et al.* 2011, Chen *et al.* 2011, Heng *et al.* 2012, Larijani *et al.* 2011, Oh *et al.* 2009, Steiner *et al.* 2010, Zweigerdt *et al.* 2011). As this thesis reports only on the successful culture of hESCs in a 2D system, it will be very interesting to see whether the technology can be up-scaled onto bioreactor MCs.

Bioreactors present a viable and industrially scalable means to generate large quantities of such cells. Due to its capacity for automation of the large scale batch processing of cell culture in a controlled and reliable manner, bioreactor MC technology has stimulated much interest recently (Chen *et al.* 2011, Heng *et al.* 2012, Storm *et al.* 2010). MC culture is a well established technology in the pharmaceutical

industry, which employs it extensively for the culture of mammalian cells which synthesize commercially important vaccines and enzymes (Braeckmans *et al.* 2002). Chen *et al.* demonstrated that conventional MCs that had proven successful for mammalian cells were not suitable for hESCs, and reported that either Matrigel^{TM} or laminin coating seemed necessary for the latter's culture on beads (Chen *et al.* 2011). Recently, Heng *et al.* showed that VN-coated MCs allowed for the 3-D culture of hESCs at a VN surface density of 450 ng/cm^2 (Heng *et al.* 2012). The MC coating method was the usual overnight passive absorption of protein, which presumably explains the high concentration of VN required. Obviously I surmise that AA+HS9^{+ve} MCs would coincidentally reduce the surface density of VN needed for cell culture by a significant amount, and improve the quality and numbers of cells.

Few studies have addressed the cost-benefits of improved cell adhesion technology for the large scale manufacturing of stem cells. The overall costs involve many factors. If it is assumed that 1 mg of recombinant human VN costs USD1400 (from Millipore), then, according to Chen *et al.*, a 1 litre bioreactor contains 1 - 4 mg/ml of polystyrene MCs with a total surface area of approximately 4000 - 7000 cm^2. Based on a minimum VN threshold identified on TCPS for hESC culture of 250 ng/cm^2 (described in Chapter 2), this translates to ~ 1 - 1.75 mg of effective surface VN after passive adsorption, costing between USD1400 - 2450 (Chen *et al.* 2011).

On the basis of the results reported here for the AA+HS substrate, I believe a savings of at least USD 420 to 735 per litre, a 30 % reduction. This is even before a thorough optimization at scale, where even greater efficiencies can be expected. The cost of building a plasma reactor to polymerize surfaces with AA is relatively low, and affinity chromatography purification is well established commercially as one of

the cheapest and easiest purification technologies now available. In large scale manufacturing plants, where bioreactors with capacities of hundreds of litres are used, significant efficiencies can be envisaged.

In conclusion, the process development reported in this thesis from isolating a high VN binding affinity HS variant and immobilizing it onto surfaces to capture functional VN for hESC culture is novel. Moreover, the generation of the AA+HS9^{+ve}+VN substrate fulfilled the key features include cost, simplicity, safety and efficacy. Finally, the technology of obtaining a 'tuned' HS variant, isolated from a heterogeneous population of HS by affinity binding to a HBD-VN peptide, clearly demonstrated the applicability for the isolation of other 'tuned' HS variants aimed at specific ECM components

5.2 Recommendations for future research

5.2.1. Physical characteristics of AA+GAG+VN surface

A detailed physical characterization of TCPS coated with VN was completed by employing XPS, AFM, colloidal gold staining and VN adsorption/desorption kinetics. To further analyze the AA+GAG+VN surface, a physical characterization could also be attempted. Material properties such as surface topology can be measured by AFM, XPS and water contact angle. Water contact angle analysis would provide wetability details, which would help define the hydrophobicity-hydrophilicity of the surface. Li *et al.* have shown that a substrate water contact angle of 65^{o} is optimal for HES-3 culture (Li *et al.* 2010). High-throughput methods such as AFM and XPS would reveal the surface morphology and its elemental composition. These would be useful as they would better define the structure-function relationship

between the material properties of the surface and its subsequent biological performance.

5.2.2 The 3-dimensional (3-D) culturing of hPSCs on synthetic polymers

Translating the use of hPSCs from the bench into the clinic is a multi-faceted problem. Reliance on the culturing of cells on 2-D TCPS is inefficient; thus other scalable methods need to be explored. As the AA plasma polymerization method can be applied to most surfaces, carriers made of any cell culture-friendly material, including cellulose and polystyrene, can be so derivatized, and thus further coated with the $HS9^{+ve}$ variant and VN, or any other HS-ECM protein combination. I envisage an AA-coated material that can be produced commercially and made available off-the-shelf, so that the end-user has merely to coat surfaces with the appropriate ECM protein tuned-HS. This again should translate to major cost savings and a more effective manufacturing process.

5.2.3 Further fine-tuning of $HS9^{+ve}$ variants

I also envisage a "second generation" $HS9^{+ve}$ variant with an increased binding avidity for VN. This idea was generated from the observation that a delay in $HS9^{+ve}$ variant elution in high salt buffer suggested that a mixture of binding HSs could be present (Fig.3.4).The affinity chromatography method can be fine-tuned to include either a slow gradient, or a more gradual step-wise NaCl series of washes, instead of the single 1.5 M NaCl wash described here. A more gradual increase in ionic strength would more effectively remove the weaker binding $HS9^{+ve}$ variants, and leave the stronger binding (more avid) HS bound to the peptide. The stronger-binding $HS9^{+ve}$ variant would be eluted at the highest ionic strength buffer. Presumably this more specific variant would allow even better VN activity at less concentration.

The results from the GAG-binding ELISA indicated that 6 disaccharide units was the minimum length that the HS must possess for effective VN binding. Thus a third generation $HS9^{+ve}$ variant could also be separated based on the basis of its minimum size; that is, it should be possible to remove HS of less than 6 repeats. Such procedures will generate an even more potent VN-binding variant. Such advanced purification procedures should simplify the job of sequencing the disaccharides that make up the VN-binding domain. This is turn would bring us a step closer to generating fully synthetic HS molecules for stem cell application.

5.2.4 Extension of HS isolating technology to other ECM proteins

Regarding the isolation of other ECM-specific HS variants, such as those against FN or LN, the affinity chromatography technique is also clearly applicable. A library of different ECM-binding HS species could be generated with relative ease, and used for the culturing of many other clinically relevant cell types, including mesenchymal or endothelial stem cells. Heydarkhan-Hagvall *et al.* recently showed that 3D scaffolds coated with either LN or VN support murine ESC differentiation into cardiac progenitor cells (Heydarkhan-Hagvall *et al.* 2012). Thus, isolating ECM-binding HS species could potentially improve the function of many different varieties of tissue-specific ECM protein, thereby promoting the specific differentiation capacities needed in such specialized areas as cardiovascular or connective tissue engineering.

BIBLIOGRAPHY

Abraham S, Riggs MJ, Nelson K, Lee V, Rao RR. 2010. Characterization of human fibroblast-derived extracellular matrix components for human pluripotent stem cell propagation. *Acta Biomaterialia* 6: 4622-33

Akopian V, Andrews PW, Beil S, Benvenisty N, Brehm J, et al. 2010. Comparison of defined culture systems for feeder cell free propagation of human embryonic stem cells. *In Vitro Cell. Dev. Biol.-Anim.* 46: 247-58

Alper J. 2009. Geron gets green light for human trial of ES cell-derived product. *Nat. Biotechnol.* 27: 213-14

Amabile G, Meissner A. 2009. Induced pluripotent stem cells: current progress and potential for regenerative medicine. *Trends in Molecular Medicine* 15: 59-68

Amit M, Carpenter MK, Inokuma MS, Chiu CP, Harris CP, et al. 2000. Clonally derived human embryonic stem cell lines maintain pluripotency and proliferative potential for prolonged periods of culture. *Developmental Biology* 227: 271-78

Amit M, Itskovitz-Eldor J. 2006. Maintenance of human embryonic stem cells in animal serum- and feeder layer-free culture conditions. *Human Embryonic Stem Cell Protocols* 331: 105-13

Amit M, Laevsky I, Miropolsky Y, Shariki K, Peri M, Itskovitz-Eldor J. 2011. Dynamic suspension culture for scalable expansion of undifferentiated human pluripotent stem cells. *Nat. Protoc.* 6: 572-79

Amit M, Margulets V, Segev H, Shariki K, Laevsky I, et al. 2003. Human feeder layers for human embryonic stem cells. *Biol. Reprod.* 68: 2150-56

Ampofo SA, Wang HM, Linhardt RJ. 1991. Disaccharide compositional analysis of heparin and heparan-sulfate using capillary zone electrophoresis *Anal. Biochem.* 199: 249-55

Amps K, Andrews PW, Anyfantis G, Armstrong L, Avery S, et al. 2011. Screening ethnically diverse human embryonic stem cells identifies a chromosome 20 minimal amplicon conferring growth advantage. *Nat. Biotechnol.* 29: 1132-U113

Andradegordon P, Strickland S. 1986. Interaction of heparin with plasminogen activators and plasminogen-effects on the activation of plasminogen *Biochemistry* 25: 4033-40

Aoi T, Yae K, Nakagawa M, Ichisaka T, Okita K, et al. 2008. Generation of pluripotent stem cells from adult mouse liver and stomach cells. *Science* 321: 699-702

Ashikari-Hada S, Habuchi H, Sugaya N, Kobayashi T, Kimata K. 2009. Specific inhibition of FGF-2 signaling with 2-O-sulfated octasaccharides of heparan sulfate. *Glycobiology* 19: 644-54

Askari JA, Buckley PA, Mould AP, Humphries MJ. 2009. Linking integrin conformation to function. *Journal of Cell Science* 122: 165-70

Askari JA, Tynan CJ, Webb SED, Martin-Fernandez ML, Ballestrem C, Humphries MJ. 2010. Focal adhesions are sites of integrin extension. *J. Cell Biol.* 188: 891-903

Aumailley M, Gayraud B. 1998. Structure and biological activity of the extracellular matrix. *J. Mol. Med.* 76: 253-65

Avilion AA, Nicolis SK, Pevny LH, Perez L, Vivian N, Lovell-Badge R. 2003. Multipotent cell lineages in early mouse development depend on SOX2 function. *Genes & Development* 17: 126-40

Baird A, Schubert D, Ling N, Guillemin R. 1988. Receptor-binding and heparin-binding domains of basic fibroblast growth-factor *Proc. Natl. Acad. Sci. U. S. A.* 85: 2324-28

Baker DEC, Harrison NJ, Maltby E, Smith K, Moore HD, et al. 2007. Adaptation to culture of human embryonic stem cells and oncogenesis in vivo. *Nat. Biotechnol.* 25: 207-15

Barry JJA, Silva M, Shakesheff KM, Howdle SM, Alexander MR. 2005. Using plasma deposits to promote cell population of the porous interior of three-dimensional poly(D,L-lactic acid) tissue-engineering scaffolds. *Adv. Funct. Mater.* 15: 1134-40

Barzu T, Lormeau JC, Petitou M, Michelson S, Choay J. 1989. Heparin-derived oligosaccharides - Affinity for acidic fibroblast growth-factor and effect on its growth-promoting activity for human-endothelial cells *J. Cell. Physiol.* 140: 538-48

Beck AJ, Candan S, Short RD, Goodyear A, Braithwaite NSJ. 2001. The role of ions in the plasma polymerization of allylamine. *J. Phys. Chem. B* 105: 5730-36

Ben-Hur T, Idelson M, Khaner H, Pera M, Reinhartz E, et al. 2004. Transplantation of human embryonic stem cell-derived neural progenitors improves behavioral deficit in Parkinsonian rats. *Stem Cells* 22: 1246-55

Bertozzi CR, Kiessling LL. 2001. Chemical glycobiology. *Science* 291: 2357-64

Best CH. 1959. Preparation of heparin and its use in the 1st clinical cases. *Circulation* 19: 79-86

Bienkowski MJ, Conrad HE. 1985. Structural characterization of the oligosaccharides formed by depolymerization of heparin with nitrous acid *J. Biol. Chem.* 260: 356-65

Bishop JR, Schuksz M, Esko JD. 2007. Heparan sulphate proteoglycans fine-tune mammalian physiology. *Nature* 446: 1030-37

Boston CG. 2001. High potential diagnosis in stem cell research. *http://www.slideshare.net/MedicineAndHealth14/stem-cells-sweden*

Boucas RI, Trindade ES, Tersariol ILS, Dietrich CP, Nader HB. 2008. Development of an enzyme-linked immunosorbent assay (ELISA)-like fluorescence assay to investigate the interactions of glycosaminoglycans to cells. *Anal. Chim. Acta* 618: 218-26

Bowles J, Schepers G, Koopman P. 2000. Phylogeny of the SOX family of developmental transcription factors based on sequence and structural indicators. *Developmental Biology* 227: 239-55

Braam SR, Zeinstra L, Litjens S, Ward-van Oostwaard D, van den Brink S, et al. 2008. Recombinant vitronectin is a functionally defined substrate that supports human embryonic stem cell self-renewal via alphavbeta5 integrin. *Stem Cells* 26: 2257-65

Bradford MM. 1976. A Rapid and Sensitive Method for the Quantitation of Microgram Quantities of Protein Utilizing the Principle of Protein-Dye Binding. *Anal. Biochem.* 72: 248-54

Braeckmans K, De Smedt SC, Leblans M, Pauwels R, Demeester J. 2002. Encoding microcarriers: Present and future technologies. *Nat. Rev. Drug Discov.* 1: 447-56

Brafman DA, Chang CW, Fernandez A, Willert K, Varghese S, Chien S. 2010. Long-term human pluripotent stem cell self-renewal on synthetic polymer surfaces. *Biomaterials* 31: 9135-44

Bramono DS, Murali S, Rai B, Ling L, Poh WT, et al. 2012. Bone marrow-derived heparan sulfate potentiates the osteogenic activity of bone morphogenetic protein-2 (BMP-2). *Bone* 50: 954-64

Bramono DS, Rider DA, Murali S, Nurcombe V, Cool SM. 2011. The Effect of Human Bone Marrow Stroma-Derived Heparan Sulfate on the Ex Vivo Expansion of Human Cord Blood Hematopoietic Stem Cells. *Pharm. Res.* 28: 1385-94

Brickman YG, Ford MD, Small DH, Bartlett PF, Nurcombe V. 1995. Heparan sulfates mediate the binding of basic fibroblast growth-factor to a specific receptor on neural precursor cells *J. Biol. Chem.* 270: 24941-48

Bushuev VN, Metsis ML, Morozkin AD, Ruuge EK, Sepetov NF, Koteliansky VE. 1985. A comparative-study of structural-properties of fibronectin and its 180 KDa fragment *FEBS Lett.* 189: 276-80

Cai L, Lu J, Sheen V, Wang SF. 2012a. Optimal Poly(L-lysine) Grafting Density in Hydrogels for Promoting Neural Progenitor Cell Functions. *Biomacromolecules* 13: 1663-74

Cai L, Lu J, Sheen V, Wang SF. 2012b. Promoting Nerve Cell Functions on Hydrogels Grafted with Poly(L-lysine). *Biomacromolecules* 13: 342-49

Calderwood DA, Zent R, Grant R, Rees DJG, Hynes RO, Ginsberg MH. 1999. The talin head domain binds to integrin beta subunit cytoplasmic tails and regulates integrin activation. *J. Biol. Chem.* 274: 28071-74

Caldwell EEO, Nadkarni VD, Fromm JR, Linhardt RJ, Weiler JM. 1996. Importance of specific amino acids in protein binding sites for heparin and heparan sulfate. *Int J. Biochem. Cell Biol.* 28: 203-16

Capila L, Linhardt RJ. 2002. Heparin-proteins interactions. *Angew Chem Int Ed Engl* 41: 390-412

Cardin AD, Weintraub HJR. 1989. Molecular modeling of protein-glycosaminoglycan interactions *Arteriosclerosis* 9: 21-32

Carpenter MK, Rosler E, Rao MS. 2003. Characterization and differentiation of human embryonic stem cells. *Cloning Stem Cells* 5: 79-88

Carpenter MK, Rosler ES, Fisk GJ, Brandenberger R, Ares X, et al. 2004. Properties of four human embryonic stem cell lines maintained in a feeder-free culture system. *Dev. Dyn.* 229: 243-58

Castner DG, Ratner BD. 2002. Biomedical surface science: Foundations to frontiers. *Surf. Sci.* 500: 28-60

Casu B, Lindahl U. 2001. Structure and biological interactions of heparin and heparan sulfate In *Advances in Carbohydrate Chemistry and Biochemistry, Vol 57*, pp. 159-206. San Diego: Elsevier Academic Press Inc

Chai WG, Hounsell EF, Bauer CJ, Lawson AM. 1995. Characterization by LSI-MS and H-1-NMR spectroscopy of tetra-saccharides, hexa-saccharides, and octa-saccharides of porcine intestinal heparin *Carbohydrate Research* 269: 139-56

Chai WG, Luo JL, Lim CK, Lawson AM. 1998. Characterization of heparin oligosaccharide mixtures as ammonium salts using electrospray mass spectrometry. *Anal. Chem.* 70: 2060-66

Chambers I, Colby D, Robertson M, Nichols J, Lee S, et al. 2003. Functional expression cloning of Nanog, a pluripotency sustaining factor in embryonic stem cells. *Cell* 113: 643-55

Chambers I, Silva J, Colby D, Nichols J, Nijmeijer B, et al. 2007. Nanog safeguards pluripotency and mediates germline development. *Nature* 450: 1230-U8

Champe PC, Harvey RA. 1994. *Biochemistry*. Lippencott - Raven Publishers.

Chatelier RC, Drummond CJ, Chan DYC, Vasic ZR, Gengenbach TR, Griesser HJ. 1995a. Theory of contact angles and the free-energy of formation of ionizable surfaces - Application to heptylamine radiofrequency plasma-deposited films *Langmuir* 11: 4122-28

Chatelier RC, Hodges AM, Drummond CJ, Chan DYC, Griesser HJ. 1997. Determination of the intrinsic acid-base dissociation constant and site density of ionizable surface groups by capillary rise measurements. *Langmuir* 13: 3043-46

Chatelier RC, Xie XM, Gengenbach TR, Griesser HJ. 1995b. Effects of plasma modification conditions on surface restructuring *Langmuir* 11: 2585-91

Chen AKL, Chen XL, Choo ABH, Reuveny S, Oh SKW. 2011. Critical microcarrier properties affecting the expansion of undifferentiated human embryonic stem cells. *Stem Cell Res.* 7: 97-111

Chillakuri CR, Jones C, Mardon HJ. 2010. Heparin binding domain in vitronectin is required for oligomerization and thus enhances integrin mediated cell adhesion and spreading. *FEBS Lett.* 584: 3287-91

Chin ACP, Padmanabhan J, Oh SKW, Choo ABH. 2010. Defined and Serum-Free Media Support Undifferentiated Human Embryonic Stem Cell Growth. *Stem Cells Dev.* 19: 753-61

Choo A, Padmanabhan J, Chin A, Fong WJ, Oh SK. 2006. Immortalized feeders for the scale-up of human embryonic stem cells in feeder and feeder-free conditions. *Journal of biotechnology* 122: 130-41

Choo AB, Tan HL, Ang SN, Fong WJ, Chin A, et al. 2008. Selection against undifferentiated human embryonic stem cells by a cytotoxic antibody recognizing podocalyxin-like protein-1. *Stem Cells* 26: 1454-63

Choo ABH, Padmanabhan J, Chin ACP, Oh SKW. 2004. Expansion of pluripotent human embryonic stem cells on human feeders. *Biotechnol. Bioeng.* 88: 321-31

Clemmons DR, Horvitz G, Engleman W, Nichols T, Moralez A, Nickols GA. 1999. Synthetic alpha V beta 3 antagonists inhibit insulin-like growth factor-I-stimulated smooth muscle cell migration and replication. *Endocrinology* 140: 4616-21

Conrad HE. 1998. Heparin-Binding Proteins. *San Diego CA: Academic press*

Couchman JR, Chen LG, Woods A. 2001. Syndecans and cell adhesion. *Int.Rev.Cytol.* 207: 113-50

Cox DA, Anderson PG, Roubin GS, Chou CY, Agrawal SK, Cavender JB. 1992. Effect of local-delivery of heparin and methotrexate on neointimal proliferation in stented porcine coronary-arteries *Coronary Artery Dis.* 3: 237-48

D'Amour KA, Bang AG, Eliazer S, Kelly OG, Agulnick AD, et al. 2006. Production of pancreatic hormone-expressing endocrine cells from human embryonic stem cells. *Nat. Biotechnol.* 24: 1392-401

Danilov AV, Neupane D, Nagaraja AS, Feofanova EV, Humphries LA, et al. 2011. DeltaNp63alpha-Mediated Induction of Epidermal Growth Factor Receptor Promotes Pancreatic Cancer Cell Growth and Chemoresistance. *PLoS One* 6: 15

Darr H, Mayshar Y, Benvenisty N. 2006. Overexpression of NANOG in human ES cells enables feeder-free growth while inducing primitive ectoderm features. *Development* 133: 1193-201

David G, Bai XM, Vanderschueren B, Cassiman JJ, Vandenberghe H. 1992. Developmental-changes in heparan-sulfate expression - insitu detection with mAbs *J. Cell Biol.* 119: 961-75

de Paz JL, Angulo J, Lassaletta JM, Nieto PM, Redondo-Horcajo M, et al. 2001. The activation of fibroblast growth factors by heparin: Synthesis, structure, and biological activity of heparin-like oligosaccharides. *Chembiochem* 2: 673-85

de Paz JL, Spillmann D, Seeberger PH. 2006. Microarrays of heparin oligosaccharides obtained by nitrous acid depolymerization of isolated heparin. *Chem. Commun.*: 3116-18

Declerck PJ, Demol M, Alessi MC, Baudner S, Paques EP, et al. 1988. Purification and characterization of plasminogen-activator inhibitor-1 binding-protein from human-plasma - Identification as a multimeric form of S-protein (Vitronectin) *J. Biol. Chem.* 263: 15454-61

Delgass WN, Hughes TR, Fadley CS. 1970. X-ray photoelectron spectroscopy - A tool for research in catalysis *Catalysis Reviews* 4: 179-&

Derda R, Li LY, Orner BP, Lewis RL, Thomson JA, Kiessling LL. 2007. Defined substrates for human embryonic stem cell growth identified from surface arrays. *ACS chemical biology* 2: 347-55

Desai UR, Wang HM, Ampofo SA, Linhardt RJ. 1993a. Oligosaccharide composition of heparin and low-molecular-weight heparins by capillary electrophoresis *Anal. Biochem.* 213: 120-27

Desai UR, Wang HM, Linhardt RJ. 1993b. Specificity studies on the heparin lyases from Flavobacterium-heparinum *Biochemistry* 32: 8140-45

Desaire H, Leary JA. 2000. Detection and quantification of the sulfated disaccharides in chondroitin sulfate by electrospray tandem mass spectrometry. *J. Am. Soc. Mass Spectrom.* 11: 916-20

Ding VMY, Ling L, Natarajan S, Yap MGS, Cool SM, Choo ABH. 2010. FGF-2 Modulates Wnt Signaling in Undifferentiated hESC and iPS Cells Through Activated PI3-K/GSK3 beta Signaling. *J. Cell. Physiol.* 225: 417-28

Doran MR, Frith JE, Prowse ABJ, Fitzpatrick J, Wolvetang EJ, et al. 2010. Defined high protein content surfaces for stem cell culture. *Biomaterials* 31: 5137-42

Douglas JF, Johnson HE, Granick S. 1993. A Simple Kinetic Model of Polymer Adsorption and Desorption. *Science* 262: 2010-12

Drake SL, Klein DJ, Mickelson DJ, Oegema TR, Furcht LT, McCarthy JB. 1992. Cell-surface phosphatidylinositol-anchored heparan-sulfate proteoglycan initiates mouse melanoma cell-adhesion to a fibronectin-derived, heparin-binding synthetic peptide *J. Cell Biol.* 117: 1331-41

Eliceiri BP. 2001. Integrin and growth factor receptor crosstalk. *Circ.Res.* 89: 1104-10

Ernst S, Langer R, Cooney CL, Sasisekharan R. 1995. Enzymatic degradation of glycosaminoglycans *Crit. Rev. Biochem. Molec. Biol.* 30: 387-444

Evans MJ, Kaufman MH. 1981. Establishment in culture of pluripotential cells from mouse embryos *Nature* 292: 154-56

Evseenko D, Schenke-Layland K, Dravid G, Zhu YH, Hao QL, et al. 2009. Identification of the Critical Extracellular Matrix Proteins that Promote Human Embryonic Stem Cell Assembly. *Stem Cells Dev.* 18: 919-27

Faham S, Hileman RE, Fromm JR, Linhardt RJ, Rees DC. 1996. Heparin structure and interactions with basic fibroblast growth factor. *Science* 271: 1116-20

Falcone DJ, Salisbury BGJ. 1988. Fibronectin stimulates macrophage uptake of low-density lipoprotein-heparin-collagen complexes *Arteriosclerosis* 8: 263-73

Fally F, Doneux C, Riga J, Verbist JJ. 1995. Quantification of the functional-groups present at the surface of plasma polymers deposited from propylamine, allylamine and propargylamine *J. Appl. Polym. Sci.* 56: 597-614

Feng WY, Zhao LH, Wang KY. 2004. Interaction of polysaccharides with interferon-gamma using an improved ELISA approach. *Carbohydrate Polymers* 58: 89-94

Ferro DR, Provasoli A, Ragazzi M, Casu B, Torri G, et al. 1990. Conformer populations of L-Iduronic acid residues in glycosaminoglycan sequences *Carbohydrate Research* 195: 157-67

Firth SM, Ganeshprasad U, Baxter RC. 1998. Structural determinants of ligand and cell surface binding of insulin-like growth factor-binding protein-3. *J. Biol. Chem.* 273: 2631-38

Folkman J, Klagsbrun M, Sasse J, Wadzinski M, Ingber D, Vlodavsky I. 1988. A heparin-binding angiogenic protein - Basic fibroblast growth-factor - is stored within basement membrane *Am. J. Pathol.* 130: 393-400

Foxall C, Holme KR, Liang WH, Wei Z. 1995. An enzyme-linked-immunosorbent-assay using biotinylated heparan-sulfate to evaluate the interactions of heparin-like molecules and basic fibroblast growth-factor *Anal. Biochem.* 231: 366-73

France RM, Short RD, Dawson RA, MacNeil S. 1998. Attachment of human keratinocytes to plasma co-polymers of acrylic acid octa-1,7-diene and allyl amine octa-1,7-diene. *J. Mater. Chem.* 8: 37-42

Francois PP, Preissner KT, Herrmann M, Haugland RP, Vaudaux P, et al. 1999. Vitronectin interaction with glycosaminoglycans - Kinetics, structural determinants, and role in binding to endothelial cells. *J. Biol. Chem.* 274: 37611-19

Fromm JR, Hileman RE, Weiler JM, Linhardt RJ. 1997. Interaction of fibroblast growth factor-1 and related peptides with heparan sulfate and its oligosaccharides. *Arch. Biochem. Biophys.* 346: 252-62

Funderburgh JL. 2000. Keratan sulfate: structure, biosynthesis, and function. *Glycobiology* 10: 951-58

Furue MK, Na J, Jackson JP, Okamoto T, Jones M, et al. 2008. Heparin promotes the growth of human embryonic stem cells in a defined serum-free medium. *Proc. Natl. Acad. Sci. U. S. A.* 105: 13409-14

Galli D, Benedetti L, Bongio M, Maliardi V, Silvani G, et al. 2011. In vitro osteoblastic differentiation of human mesenchymal stem cells and human dental pulp stem cells on poly-L-lysine-treated titanium-6-aluminium-4-vanadium. *J. Biomed. Mater. Res. Part A* 97A: 118-26

Gancarz I, Bryjak J, Bryjak M, Pozniak G, Tylus W. 2003. Plasma modified polymers as a support for enzyme immobilization 1. Allyl alcohol plasma. *Eur. Polym. J.* 39: 1615-22

Gandhi NS, Mancera RL. 2008. The Structure of Glycosaminoglycans and their Interactions with Proteins. *Chem. Biol. Drug Des.* 72: 455-82

Gao CY, Guan JJ, Zhu YB, Shen JC. 2003. Surface immobilization of bioactive molecules on polyurethane for promotion of cytocompatibility to human endothelial cells. *Macromol. Biosci.* 3: 157-62

Genbacev O, Krtolica A, Zdravkovic P, Zdravkovic T, Brunette E, et al. 2005. Serum-free derivation of human embryonic stem cell lines on human placental fibroblast feeders. *Fertility and Sterility* 83: 1517-29

Gengenbach TR, Chatelier RC, Griesser HJ. 1996. Correlation of the nitrogen 1s and oxygen 1s XPS binding energies with compositional changes during oxidation of ethylene diamine plasma polymers. *Surf. Interface Anal.* 24: 611-19

Gengenbach TR, Xie XM, Chatelier RC, Griesser HJ. 1994. Evolution of the surface-composition and topography of perfluorinated polymers following ammonia-plasma treatment *J. Adhes. Sci. Technol.* 8: 305-28

Germer M, Kanse SM, Kirkegaard T, Kjoller L, Felding-Habermann B, et al. 1998. Kinetic analysis of integrin-dependent cell adhesion on vitronectin - The inhibitory potential of plasminogen activator inhibitor-1 and RGD peptides. *Eur. J. Biochem.* 253: 669-74

Ghule PN, Dominski Z, Yang XC, Marzluff WF, Becker KA, et al. 2008. Staged assembly of histone gene expression machinery at subnuclear foci in the abbreviated cell cycle of human embryonic stem cells. *Proc. Natl. Acad. Sci. U. S. A.* 105: 16964-69

Giancotti FG, Ruoslahti E. 1999. Transduction - Integrin signaling. *Science* 285: 1028-32

Gibson AD, Lamerdin JA, Zhuang P, Baburaj K, Serpersu EH, Peterson CB. 1999. Orientation of heparin-binding sites in native vitronectin - Analyses of ligand binding to the primary glycosaminoglycan-binding site indicate that putative secondary sites are not functional. *J. Biol. Chem.* 274: 6432-42

Gibson AD, Peterson CB. 2001. Full-length and truncated forms of vitronectin provide insight into effects of proteolytic processing on function. *Biochim. Biophys. Acta-Protein Struct. Molec. Enzym.* 1545: 289-304

Globus RK, Plouet J, Gospodarowicz D. 1989. Cultured bovine bone-cells synthesize basic fibroblast growth-factor and store it in their extracellular-matrix *Endocrinology* 124: 1539-47

Goldring CEP, Duffy PA, Benvenisty N, Andrews PW, Ben-David U, et al. 2011. Assessing the Safety of Stem Cell Therapeutics. *Cell Stem Cell* 8: 618-28

Gospodarowicz D, Delgado D, Vlodavsky I. 1980. Permissive effect of the extracellular-matrix on cell-proliferation in vitro. *Proceedings of the National Academy of Sciences of the United States of America-Biological Sciences* 77: 4094-98

Gospodarowicz D, Greenburg G, Birdwell CR. 1978. Determination of cellular shape by extracellular matrix and its correlation with control of cellular growth *Cancer Res.* 38: 4155-71

Grulich-Henn J, Ritter J, Mesewinkel S, Heinrich U, Bettendorf M, Preissner KT. 2002. Transport of insulin-like growth factor-I across endothelial cell monolayers and its binding to the subendothelial matrix. *Exp. Clin. Endocrinol. Diabet.* 110: 67-73

Grunert M, Dombrowski C, Sadasivam M, Manton K, Cool SM, Nurcombe V. 2007. Isolation of a native osteoblast matrix with a specific affinity for BMP2. *J Mol Histol* 38: 393-404

Guimond S, Maccarana M, Olwin BB, Lindahl U, Rapraeger AC. 1993. Activating and inhibitory heparin sequences for FGF-2 (Basic FGF) - Distinct requirements for FGF-1, FGF-2, and FGF-4 *J. Biol. Chem.* 268: 23906-14

Hagihara K, Watanabe K, Chun J, Yamaguchi Y. 2000. Glypican-4 is an FGF2-binding heparan sulfate proteoglycan expressed in neural precursor cells. *Dev. Dyn.* 219: 353-67

Hakala H, Rajala K, Ojala M, Panula S, Areva S, et al. 2009. Comparison of Biomaterials and Extracellular Matrices as a Culture Platform for Multiple,

Independently Derived Human Embryonic Stem Cell Lines. *Tissue Eng. Part A* 15: 1775-85

Halme DG, Kessler DA. 2006. FDA regulation of stem-cell-based therapies. *N. Engl. J. Med.* 355: 1730-35

Hambardzumyan A, Biltresse S, Dufrene Y, Marchand-Brynaert J. 2002. An unprecedented surface oxidation of polystyrene substrates by wet chemistry under basic conditions. *J Colloid Interface Sci* 252: 443-9

Hampson IN, Gallagher JT. 1984. Separation of radiolabeled glycosaminoglycan oligosaccharides by polyacrylamide-gel electrophoresis *Biochem. J.* 221: 697-705

Harris EN, Weigel JA, Weigel PH. 2008. The human hyaluronan receptor for endocytosis (HARE/Stabilin-2) is a systemic clearance receptor for heparin. *J. Biol. Chem.* 283: 17341-50

Hasan M, Najjam S, Gordon MY, Gibbs RV, Rider CC. 1999. IL-12 is a heparin-binding cytokine. *J. Immunol.* 162: 1064-70

Hay DC, Sutherland L, Clark J, Burdon T. 2004. Oct-4 knockdown induces similar patterns of endoderm and trophoblast differentiation markers in human and mouse embryonic stem cells. *Stem Cells* 22: 225-35

Hayashi M, Akama T, Kono I, Kashiwagi H. 1985. Activation of vitronectin (serum spreading factor) binding of heparin by denaturing agents *J. Biochem.* 98: 1135-38

Hayman EG, Pierschbacher MD, Ohgren Y, Ruoslahti E. 1983. Serum spreading factor (vitronectin) is present at the cell-surface and in tissues *Proceedings of the National Academy of Sciences of the United States of America-Biological Sciences* 80: 4003-07

Helledie T, Dombrowski C, Rai B, Lim ZX, Hin IL, et al. 2012. Heparan sulfate enhances the self-renewal and therapeutic potential of mesenchymal stem cells from human adult bone marrow. *Stem Cells Dev* 21: 1897-910

Heng BC, Li J, Chen AKL, Reuveny S, Cool SM, et al. 2012. Translating Human Embryonic Stem Cells from 2-Dimensional to 3-Dimensional Cultures in a Defined Medium on Laminin- and Vitronectin-Coated Surfaces. *Stem Cells Dev.* 21: 1701-15

Heydarkhan-Hagvall S, Gluck JM, Delman C, Jung M, Ehsani N, et al. 2012. The effect of vitronectin on the differentiation of embryonic stem cells in a 3D culture system. *Biomaterials* 33: 2032-40

Higai K, Suzuki C, Imaizumi Y, Xin X, Azuma Y, Matsumoto K. 2011. Binding Affinities of NKG2D and CD94 to Sialyl Lewis X-Expressing N-Glycans and Heparin. *Biol. Pharm. Bull.* 34: 8-12

Hoffman LM, Carpenter MK. 2005a. Characterization and culture of human embryonic stem cells. *Nat Biotechnol* 23: 699-708

Hoffman LM, Carpenter MK. 2005b. Human embryonic stem cell stability. *Stem Cell Rev.* 1: 139-44

Holley RJ, Pickford CE, Rushton G, Lacaud G, Gallagher JT, et al. 2011. Influencing Hematopoietic Differentiation of Mouse Embryonic Stem Cells using Soluble Heparin and Heparan Sulfate Saccharides. *J. Biol. Chem.* 286: 6241-52

Hook M, Bjork I, Hopwood J, Lindahl U. 1976. Anticoagulant activity of heparin - separation of high-activity and low-activity heparin species by affinity chromatography on immobilized antithrombin *FEBS Lett.* 66: 90-93

Huangfu D, Maehr R, Guo W, Eijkelenboom A, Snitow M, et al. 2008. Induction of pluripotent stem cells by defined factors is greatly improved by small-molecule compounds. *Nat. Biotechnol.* 26: 795-97

Hughes CS, Radan L, Betts D, Postovit LM, Lajoie GA. 2011. Proteomic analysis of extracellular matrices used in stem cell culture. *Proteomics* 11: 3983-91

Hynes R. 1985. Molecular-biology of fibronectin *Annu. Rev. Cell Biol.* 1: 67-90

Hynes RO. 2009. The Extracellular Matrix: Not Just Pretty Fibrils. *Science* 326: 1216-19

Hyslop, Armstrong L., Stojkovic M., M. L. 2005a. Human embryonic stem cells: biology and clinical applications. *Expert Reviews in Molecular Medicine* 7: 1-21

Hyslop L, Stojkovic M, Armstrong L, Walter T, Stojkovic P, et al. 2005b. Downregulation of Nanog induces differentiation of human embryonic stem cells to extraembryonic lineages. *Stem Cells* 23: 1035-43

Irwin EE, Gupta R, Dashti DC, Healy KE. 2011. Engineered polymer-media interfaces for the long-term self-renewal of human embryonic stem cells. *Biomaterials* 32: 6912-19

Isik FF, Gibran NS, Jang YC, Sandell L, Schwartz SM. 1998. Vitronectin decreases microvascular endothelial cell apoptosis. *J. Cell. Physiol.* 175: 149-55

Itano N. 2008. Simple primary structure, complex turnover regulation and multiple roles of hyaluronan. *J. Biochem.* 144: 131-37

Izumi M, Yamada, K. M., and Hayashi, M. . 1989. Vitronectin exists in two structurally and functionally distinct forms in human plasma. *Biochim ica et Biophysica A cta* 990: 101-08

Jackson RL, Busch SJ, Cardin AD. 1991. Glycosaminoglycans - molecular-properties, protein interactions, and role in physiological processes *Physiol. Rev.* 71: 481-539

Jandik KA, Gu KA, Linhardt RJ. 1994. Action pattern of polysaccharide lyases on glycosaminoglycans *Glycobiology* 4: 289-96

Jones JL, Walker RA. 1999. Integrins: a role as cell signalling molecules. *J. Clin. Pathol.-Mol. Pathol.* 52: 208-13

Judson RL, Babiarz JE, Venere M, Blelloch R. 2009. Embryonic stem cell-specific microRNAs promote induced pluripotency. *Nat. Biotechnol.* 27: 459-61

Karamanos NK, Vanky P, Tzanakakis GN, Hjerpe A. 1996. High performance capillary electrophoresis method to characterize heparin and heparan sulfate disaccharides. *Electrophoresis* 17: 391-95

Karamanos NK, Vanky P, Tzanakakis GN, Tsegenidis T, Hjerpe A. 1997. Ion-pair high-performance liquid chromatography for determining disaccharide composition in heparin and heparan sulphate. *J. Chromatogr. A* 765: 169-79

Kato S, Sugiura N, Kimata K, Kujiraoka T, Toyoda J, Akamatsu N. 1995. Chondroitin sulfate immobilized onto culture substrates modulates DNA-synthesis, tyrosine aminotransferase induction, and intercellular communication in primary rat hepatocytes *Cell Struct. Funct.* 20: 199-209

Kern B, Shen JH, Starbuck M, Karsenty G. 2001. Cbfa1 contributes to the osteoblast-specific expression of type I collagen genes. *J. Biol. Chem.* 276: 7101-07

Khan MY, Medow MS, Newman SA. 1990. Unfolding transitions of fibronectin and its domains - stabilization and structural alteration of the N-terminal domain by heparin *Biochem. J.* 270: 33-38

Khoo KH, Morris HR, McDowell RA, Dell A, Maccarana M, Lindahl U. 1993. FABMS derivatization strategies for the analysis of heparin-dervied oligosaccharides *Carbohydrate Research* 244: 205-23

Kim YS, Linhardt RJ. 1989. Structural features of heparin and their effect of heparin cofactor-II mediated inhibition of thrombin *Thromb. Res.* 53: 55-71

Kimura E, Akita M, Matsuyama S, Mizushima S. 1991. Determination of a region in seca that interacts with presecretory proteins in escharichia-coli *J. Biol. Chem.* 266: 6600-06

Kingshott P, Thissen H, Griesser HJ. 2002. Effects of cloud-point grafting, chain length, and density of PEG layers on competitive adsorption of ocular proteins. *Biomaterials* 23: 2043-56

Kiskinis E, Eggan K. 2010. Progress toward the clinical application of patient-specific pluripotent stem cells. *Journal of Clinical Investigation* 120: 51-59

Klim JR, Li LY, Wrighton PJ, Piekarczyk MS, Kiessling LL. 2010. A defined glycosaminoglycan-binding substratum for human pluripotent stem cells. *Nat. Methods* 7: 989-U72

Kolhar P, Kotamraju VR, Hikita ST, Clegg DO, Ruoslahti. 2008. Synthetic Surfaces for Human Embryonic Stem Cell Culture. *Journal of biotechnology* doi:10.1016/j.jbiotec.2010.01.016

Kopp JL, Ormsbee BD, Desler M, Rizzino A. 2008. Small increases in the level of Sox2 trigger the differentiation of mouse embryonic stem cells. *Stem Cells* 26: 903-11

Lamari F, Militsopoulou M, Gioldassi X, Karamanos NK. 2001. Capillary electrophoresis: a superior miniaturized tool for analysis of the mono-, di-, and oligosaccharide constituents of glycan moieties in proteoglycans. *Fresenius J. Anal. Chem.* 371: 157-67

Lane DAaL, U. 1989. Heparin, Chemical and Biological Properties, Clinical Applications. *CRC Press, Inc., Boca Raton, FL.*

Larijani MR, Seifinejad A, Pournasr B, Hajihoseini V, Hassani SN, et al. 2011. Long-Term Maintenance of Undifferentiated Human Embryonic and Induced Pluripotent Stem Cells in Suspension. *Stem Cells Dev.* 20: 1911-23

Lassen B, Malmsten M. 1997. Competitive protein adsorption at plasma polymer surfaces. *J. Colloid Interface Sci.* 186: 9-16

Laurent TC, Lauret UB, Fraser JR. 1996. The structure and fucntion of hyaluronan: an overview. *Immunol Cell Biol* 74: A1-A7

Lavon N, Yanuka O, Benvenisty N. 2004. Differentiation and isolation of hepatic-like cells from human embryonic stem cells. *Differentiation* 72: 230-38

Lee S, Kim J, Park TJ, Shin Y, Lee SY, et al. 2011. The effects of the physical properties of culture substrates on the growth and differentiation of human embryonic stem cells. *Biomaterials* 32: 8816-29

Levenstein ME, Berggren WT, Lee JE, Conard KR, Llanas RA, et al. 2008. Secreted Proteoglycans Directly Mediate Human Embryonic Stem Cell-Basic Fibroblast Growth Factor 2 Interactions Critical for Proliferation. *Stem Cells* 26: 3099-107

Li J, Bardy J, Yap LYW, Chen A, Nurcombe V, et al. 2010. Impact of vitronectin concentration and surface properties on the stable propagation of human embryonic stem cells. *Biointerphases* 5: FA132-FA42

Li Y, Powell S, Brunette E, Lebkowski J, Mandalam R. 2005. Expansion of human embryonic stem cells in defined serum-free medium devoid of animal-derived products. *Biotechnol. Bioeng.* 91: 688-98

Liang OD, Rosenblatt S, Chhatwal GS, Preissner KT. 1997. Identification of novel heparin-binding domains of vitronectin. *FEBS Lett.* 407: 169-72

Lim JWE, Bodnar A. 2002. Proteome analysis of conditioned medium from mouse embryonic fibroblast feeder layers which support the growth of human embryonic stem cells. *Proteomics* 2: 1187-203

Lincoff AM, Furst JG, Ellis SG, Tuch RJ, Topol EJ. 1997. Sustained local delivery of dexamethasone by a novel intravascular eluting stent to prevent restenosis in the porcine coronary injury model. *J. Am. Coll. Cardiol.* 29: 808-16

Lindahl U, Backstrom G, Hook M, Thunberg L, Fransson LA, Linker A. 1979. Structure of the antithrombin-binding site in heparin *Proc. Natl. Acad. Sci. U. S. A.* 76: 3198-202

Lindahl U, Backstrom G, Thunberg L, Leder IG. 1980. Evidence for a 3-O-sulfated D-glucosamine residue in the antithrombin-binding sequence of heparin. *Proceedings of the National Academy of Sciences of the United States of America-Biological Sciences* 77: 6551-55

Lindahl U, Kjellen L. 1991. Heparin or heparan-sulfate - what is the difference *Thromb. Haemost.* 66: 44-48

Lindahl U, Kusche-Gullberg M, Kjellen L. 1998. Regulated diversity of heparan sulfate. *J. Biol. Chem.* 273: 24979-82

Ling L, Dombrowski C, Foong KM, Haupt LM, Stein GS, et al. 2010. Synergism between Wnt3a and heparin enhances osteogenesis via a phosphoinositide 3-kinase/Akt/RUNX2 pathway. *J Biol Chem* 285: 26233-44

Linhardt RJ, Ampofo SA, Fareed J, Hoppensteadt D, Mulliken JB, Folkman J. 1992. Isolation and characterization of human heparin *Biochemistry* 31: 12441-45

Linker A, Hoffman P, Sampson P, Meyer K. 1958. Heparitin sulfate *Biochimica Et Biophysica Acta* 29: 443-44

Liu Y, Wang X, Kaufman DS, Shen W. 2011. A synthetic substrate to support early mesodermal differentiation of human embryonic stem cells. *Biomaterials* 32: 8058-66

Ludwig TE, Bergendahl V, Levenstein ME, Yu JY, Probasco MD, Thomson JA. 2006a. Feeder-independent culture of human embryonic stem cells. *Nat. Methods* 3: 637-46

Ludwig TE, Levenstein ME, Jones JM, Berggren WT, Mitchen ER, et al. 2006b. Derivation of human embryonic stem cells in defined conditions. *Nat Biotechnol* 24: 185-7

Lynn GW, Heller WT, Mayasundari A, Minor KH, Peterson CB. 2005. A model for the three-dimensional structure of human plasma vitronectin from small-angle scattering measurements. *Biochemistry* 44: 565-74

Lyon M, Deakin JA, Mizuno K, Nakamura T, Gallagher JT. 1994. Interaction of hepatocyte growth-factor with heparan-sulfate - Elucidation of the major heparan-sulfate structural determinants. *J. Biol. Chem.* 269: 11216-23

Lyon M, Rushton G, Askari JA, Humphries MJ, Gallagher JT. 2000. Elucidation of the structural features of heparan sulfate important for interaction with the Hep-2 domain of fibronectin. *J. Biol. Chem.* 275: 4599-606

Maccarana M, Casu B, Lindahl U. 1993. Minimal sequence in hepain heparan-sulfate required for binding of basic fibroblast growth-factor *J. Biol. Chem.* 268: 23898-905

Mahalingam Y, Gallagher JT, Couchman JR. 2007. Cellular adhesion responses to the heparin-binding (HepII) domain of fibronectin require heparan sulfate with specific properties. *J. Biol. Chem.* 282: 3221-30

Mahoney DJ, Mulloy B, Forster MJ, Blundell CD, Fries E, et al. 2005. Characterization of the interaction between tumor necrosis factor-stimulated gene-6 and heparin - Implications for the inhibition of plasmin in extracellular matrix microenvironments. *J. Biol. Chem.* 280: 27044-55

Mahoney DJ, Whittle JD, Milner CM, Clark SJ, Mulloy B, et al. 2004. A method for the non-covalent immobilization of heparin to surfaces. *Anal. Biochem.* 330: 123-29

Malavaki CJ, Theocharis AD, Lamari FN, Kanakis I, Tsegenidis T, et al. 2011. Heparan sulfate: biological significance, tools for biochemical analysis and structural characterization. *Biomed. Chromatogr.* 25: 11-20

Mallis LM, Wang HM, Loganathan D, Linhardt RJ. 1989. Sequence-analysis of highly sulfated, heparin-dervied oligosaccharides using fast atom bombardment mass-spectrometry *Anal. Chem.* 61: 1453-58

Manton KJ, Leong DF, Cool SM, Nurcombe V. 2007. Disruption of heparan and chondroitin sulfate signaling enhances mesenchymal stem cell-derived osteogenic differentiation via bone morphogenetic protein signaling pathways. *Stem Cells* 25: 2845-54

Manton KJ, Richards S, Van Lonkhuyzen D, Cormack L, Leavesley D, Upton Z. 2010. A Chimeric Vitronectin: IGF-I Protein Supports Feeder-Cell-Free and Serum-Free Culture of Human Embryonic Stem Cells. *Stem Cells Dev.* 19: 1297-305

Marion RM, Strati K, Li H, Murga M, Blanco R, et al. 2009. A p53-mediated DNA damage response limits reprogramming to ensure iPS cell genomic integrity. *Nature* 460: 1149-U119

Marson A, Rock MJ, Cain SA, Freeman LJ, Morgan A, et al. 2005. Homotypic fibrillin-1 interactions in microfibril assembly. *J. Biol. Chem.* 280: 5013-21

Martin GR. 1981. Isolation of a pluripotent cell-line from early mouse embryos cultured in medium conditioned by teratocarcinoma stem-cells *Proceedings of the National Academy of Sciences of the United States of America-Biological Sciences* 78: 7634-38

Mason M, Vercruysse KP, Kirker KR, Frisch R, Marecak DM, et al. 2000. Attachment of hyaluronic acid to polypropylene, polystyrene, and polytetrafluoroethylene. *Biomaterials* 21: 31-36

Masui S, Nakatake Y, Toyooka Y, Shimosato D, Yagi R, et al. 2007. Pluripotency governed by Sox2 via regulation of Oct3/4 expression in mouse embryonic stem cells. *Nature Cell Biology* 9: 625-U26

Matin MM, Walsh JR, Gokhale PJ, Draper JS, Bahrami AR, et al. 2004. Specific knockdown of Oct4 and beta 2-microglobulin expression by RNA interference in human embryonic stem cells and embryonic carcinoma cells. *Stem Cells* 22: 659-68

McCaffrey TA, Falcone DJ, Du BH. 1992. Transforming growth factor-beta-1 is a heparin-binding protein - Identification of putative heparin-binding regions and isolation of heparins with varying affinity for TGF-beta-1 *J. Cell. Physiol.* 152: 430-40

Mei Y, Saha K, Bogatyrev SR, Yang J, Hook AL, et al. 2010. Combinatorial development of biomaterials for clonal growth of human pluripotent stem cells. *Nat. Mater.* 9: 768-78

Melkoumian Z, Weber JL, Weber DM, Fadeev AG, Zhou Y, et al. 2010. Synthetic peptide-acrylate surfaces for long-term self-renewal and cardiomyocyte differentiation of human embryonic stem cells. *Nat. Biotechnol.* 28: 606-U95

Mera K, Nagai M, Brock JWC, Fujiwara Y, Murata T, et al. 2008. Glutaraldehyde is an effective cross-linker for production of antibodies against advanced glycation end-products. *J. Immunol. Methods* 334: 82-90

Meyer-Plath AA, Finke B, Schroder K, Ohl A. 2003. Pulsed and cw microwave plasma excitation for surface functionalization in nitrogen-containing gases. *Surf. Coat. Technol.* 174: 877-81

Meyer E. 1992. Atomic force microscopy *Prog. Surf. Sci.* 41: 3-49

Mikhailov D, Linhardt RJ, Mayo KH. 1997. NMR solution conformation of heparin-derived hexasaccharide. *Biochem. J.* 328: 51-61

Milis L, Morris CA, Sheehan MC, Charlesworth JA, Pussell BA. 1993. Vitronectin-mediated inhibition of complement - Evidence for binding-sites for C5B-7 and C9 *Clin. Exp. Immunol.* 92: 114-19

Militsopoulou M, Lamari FN, Hjerpe A, Karamanos NK. 2002. Determination of twelve heparin- and heparan sulfate-derived disaccharides as 2-aminoacridone derivatives by capillary zone electrophoresis using ultraviolet and laser-induced fluorescence detection. *Electrophoresis* 23: 1104-09

Mitsui K, Tokuzawa Y, Itoh H, Segawa K, Murakami M, et al. 2003. The homeoprotein Nanog is required for maintenance of pluripotency in mouse epiblast and ES cells. *Cell* 113: 631-42

Miyazaki T, Futaki S, Hasegawa K, Kawasaki M, Sanzen N, et al. 2008. Recombinant human laminin isoforms can support the undifferentiated growth of human embryonic stem cells. *Biochemical and biophysical research communications* 375: 27-32

Moore H. 2006. The medium is the message. *Nat. Biotechnol.* 24: 160-61

Morris CA, Underwood PA, Bean PA, Sheehan M, Charlesworth JA. 1994. Relative topography of biologically-active domains of human vitronectin - Evidence from monoclonal-antibody epitope and denaturation studies *J. Biol. Chem.* 269: 23845-52

Mostafavi-Pour Z, Askari JA, Parkinson SJ, Parker PJ, Ng TTC, Humphries MJ. 2003. Integrin-specific signaling pathways controlling focal adhesion formation and cell migration. *J. Cell Biol.* 161: 155-67

Muguruma H, Hiratsuka A, Karube I. 2000. Thin-film glucose biosensor based on plasma-polymerized film: Simple design for mass production. *Anal. Chem.* 72: 2671-75

Muller M, Oehr C. 1999. Plasma aminofunctionalisation of PVDF microfiltration membranes: comparison of the in plasma modifications with a grafting method using ESCA and an amino-selective fluorescent probe. *Surf. Coat. Technol.* 116: 802-07

Mummery C, Ward-van Oostwaard D, Doevendans P, Spijker R, van den Brink S, et al. 2003. Differentiation of human embryonic stem cells to cardiomyocytes - Role of coculture with visceral endoderm-like cells. *Circulation* 107: 2733-40

Nadesalingam J, Bernal AL, Dodds AW, Willis AC, Mahoney DJ, et al. 2003. Identification and characterization of a novel interaction between pulmonary surfactant protein D and decorin. *J. Biol. Chem.* 278: 25678-87

Nagaoka M, Si-Tayeb K, Akaike T, Duncan SA. 2010. Culture of human pluripotent stem cells using completely defined conditions on a recombinant E-cadherin substratum. *BMC Dev. Biol.* 10: 12

Najjam S, Gibbs RV, Gordon MY, Rider CC. 1997. Characterization of human recombinant interleukin 2 binding to heparin and heparan sulfate using an ELISA approach. *Cytokine* 9: 1013-22

Nam TJ, Busby W, Clemmons DR. 1997. Insulin-like growth factor binding protein-5 binds to plasminogen activator inhibitor-I. *Endocrinology* 138: 2972-78

Nasonkin IO, Koliatsos VE. 2006. Nonhuman sialic acid Neu5Gc is very low in human embryonic stem cell-derived neural precursors differentiated with B27/N2 and noggin: Implications for transplantation. *Experimental Neurology* 201: 525-29

Ng VY, Ang SN, Chan JX, Choo AB. 2010. Characterization of epithelial cell adhesion molecule as a surface marker on undifferentiated human embryonic stem cells. *Stem Cells* 28: 29-35

Nishioka S, Aikawa J, Ida M, Matsumoto I, Street M, et al. 2007. Ligand-binding activity and expression profile of annexins in Caenorhabditis elegans. *J. Biochem.* 141: 47-55

Nurcombe V, Cool SM. 2007. Heparan sulfate control of proliferation and differentiation in the stem cell niche. *Crit. Rev. Eukaryot. Gene Expr.* 17: 159-71

Oh SKW, Chen AK, Mok Y, Chen XL, Lim UM, et al. 2009. Long-term microcarrier suspension cultures of human embryonic stem cells. *Stem Cell Res.* 2: 219-30

Oh SKW, Choo ABH. 2008. Advances and perspectives in human and mouse embryonic stem cell bioprocessing. Drug Discov Today: Technol doi: 10.1016/j.ddtec.2008.10.001

Ono K, Hattori H, Takeshita S, Kurita A, Ishihara M. 1999. Structural features in heparin that interact with VEGF(165) and modulate its biological activity. *Glycobiology* 9: 705-11

Ori A, Wilkinson MC, Fernig DG. 2008. The heparanome and regulation of cell function: structures, functions and challenges. *Frontiers in Bioscience* 13: 4309-38

Orner BP, Derda R, Lewis RL, Thomson JA, Kiessling LL. 2004. Arrays for the combinatorial exploration of cell adhesion. *Journal of the American Chemical Society* 126: 10808-09

Parkar AA, Day AJ. 1997. Overlapping sites on the Link module of human TSG-6 mediate binding to hyaluronan and chondroitin-4-sulphate. *FEBS Lett.* 410: 413-17

Parker T, Upton Z, Leavesley D. 2009. Vitronectin Modulates Human Mesenchymal Stem Cell Response to Insulin-like Growth Factor-I and Transforming Growth Factor Beta 1 in a Serum-free Environment. *Tissue Eng. Part A* 15: 1415-26

Parslow TG, Blair DL, Murphy WJ, Granner DK. 1984. Structure of the 5' ends of immunoglobin genes - A novel conserved sequence *Proceedings of the National Academy of Sciences of the United States of America-Biological Sciences* 81: 2650-54

Pellegrini L, Burke DF, von Delft F, Mulloy B, Blundell TL. 2000. Crystal structure of fibroblast growth factor receptor ectodomain bound to ligand and heparin. *Nature* 407: 1029-34

Peng Y, Bocker MT, Holm J, Toh WS, Hughes CS, et al. 2012. Human fibroblast matrices bio-assembled under macromolecular crowding support stable propagation of human embryonic stem cells. *Journal of tissue engineering and regenerative medicine* 6: e74-86

Phillips BW, Hentze H, Rust WL, Chen Q-P, Chipperfield H, et al. 2007. Directed differentiation of human embryonic stem cells into the pancreatic endocrine lineage. *Stem Cells Dev.* 16: 561-78

Plante OJ, Palmacci ER, Seeberger PH. 2001. Automated solid-phase synthesis of oligosaccharides. *Science* 291: 1523-27

Podor TJ, Singh D, Chindemi P, Foulon DM, McKelvie R, et al. 2002. Vimentin exposed on activated platelets and platelet microparticles localizes vitronectin and plasminogen activator inhibitor complexes on their surface. *J. Biol. Chem.* 277: 7529-39

Preissner KT, May AE, Wohn KD, Germer M, Kanse SM. 1997. Molecular crosstalk between adhesion receptors and proteolytic cascades in vascular remodelling. *Thromb. Haemost.* 78: 88-95

Preissner KT, Mullerberghaus G. 1987. Neutralization and binding of heparin by S-protein vitronectin in the inhibition of Factor-Xa by antithrombin-III-involvement of an inducible heparin-binding domain of S protein/vitronectin *J. Biol. Chem.* 262: 12247-53

Prowse ABJ, Doran MR, Cooper-White JJ, Chong F, Munro TR, et al. 2010. Long term culture of human embryonic stem cells on recombinant vitronectin in ascorbate free media. *Biomaterials* 31: 8281-88

Punzon-Quijorna E, Sanchez-Vaquero V, Noval AM, Perez DG, Font AC, et al. 2011. Optimized allylamine deposition for improved pluripotential cell culture. *Vacuum* 85: 1071-75

Rademacher TW, Parekh RB, Dwek RA. 1988. Glycobiology *Annu. Rev. Biochem.* 57: 785-838

Rees C, Clemmons DR. 1998. Inhibition of IGFBP-5 binding to extracellular matrix and IGF-1-stimulated DNA synthesis by a peptide fragment of IGFBP-5. *J. Cell. Biochem.* 71: 375-81

Rees SG, Wassell DTH, Shellis RP, Embery G. 2004. Effect of serum albumin on glycosaminoglycan inhibition of hydroxyapatite formation. *Biomaterials* 25: 971-77

Reubinoff BE, Itsykson P, Turetsky T, Pera MF, Reinhartz E, et al. 2001. Neural progenitors from human embryonic stem cells. *Nat. Biotechnol.* 19: 1134-40

Reubinoff BE, Pera MF, Fong CY, Trounson A, Bongso A. 2000. Embryonic stem cell lines from human blastocysts: somatic differentiation in vitro (vol 18, pg 402, 2000). *Nat. Biotechnol.* 18: 559-59

Rhomberg AJ, Ernst S, Sasisekharan R, Biemann K. 1998. Mass spectrometric and capillary electrophoretic investigation of the enzymatic degradation of heparin-like glycosaminoglycans. *Proc. Natl. Acad. Sci. U. S. A.* 95: 4176-81

Richards S, Leavesley D, Topping G, Upton Z. 2008. Development of defined media for the serum-free expansion of primary keratinocytes and human embryonic stem cells. *Tissue Engineering Part C-Methods* 14: 221-32

Rinsch CL, Chen XL, Panchalingam V, Eberhart RC, Wang JH, Timmons RB. 1996. Pulsed radio frequency plasma polymerization of allyl alcohol: Controlled deposition of surface hydroxyl groups. *Langmuir* 12: 2995-3002

Robinson DE, Buttle DJ, Short RD, McArthur SL, Steele DA, Whittle JD. 2012. Glycosaminoglycan (GAG) binding surfaces for characterizing GAG-protein interactions. *Biomaterials* 33: 1007-16

Robinson DE, Marson A, Short RD, Buttle DJ, Day AJ, et al. 2008. Surface gradient of functional heparin. *Advanced Materials* 20: 1166-+

Rodin S, Domogatskaya A, Strom S, Hansson EM, Chien KR, et al. 2010. Long-term self-renewal of human pluripotent stem cells on human recombinant laminin-511. *Nat. Biotechnol.* 28: 611-U102

Rowland TJ, Miller LM, Blaschke AJ, Doss EL, Bonham AJ, et al. 2010. Roles of Integrins in Human Induced Pluripotent Stem Cell Growth on Matrigel and Vitronectin. *Stem Cells Dev.* 19: 1231-40

Roy S, Lai HC, Zouaoui R, Duffner J, Zhou H, et al. 2011. Bioactivity screening of partially desulfated low-molecular-weight heparins: A structure/activity relationship study. *Glycobiology* 21: 1194-205

Ruiz-Calero V, Puignou L, Galceran MT. 1998. Use of reversed polarity and a pressure gradient in the analysis of disaccharide composition of heparin by capillary electrophoresis. *J. Chromatogr. A* 828: 497-508

Ruoslahti E. 1988. Fibronectin and its receptors *Annu. Rev. Biochem.* 57: 375-413

Saito A, Munakata H. 2005. Factor H is a dermatan sulfate-binding protein: Identification of a dermatan sulfate-mediated protease that cleaves factor H. *J. Biochem.* 137: 225-33

Salmivirta M, Lidholt K, Lindahl U. 1996. Heparan sulfate: A piece of information. *Faseb J.* 10: 1270-79

Sano S, Kato K, Ikada Y. 1993. Introduction of functional-groups onto the surface of polyethylene for protein immobilization *Biomaterials* 14: 817-22

Sasaki N, Okishio K, Ui-Tei K, Saigo K, Kinoshita-Toyoda A, et al. 2008. Heparan sulfate regulates self-renewal and pluripotency of embryonic stem cells. *J. Biol. Chem.* 283: 3594-606

Scapol L, Marchi E, Viscomi GC. 1996. Capillary electrophoresis of heparin and dermatan sulfate unsaturated disaccharides with triethylamine and acetonitrile as electrolyte additives. *J. Chromatogr. A* 735: 367-74

Schlessinger J. 2000. Cell signaling by receptor tyrosine kinases. *Cell* 103: 211-25

Schroder K, Finke B, Ohl A, Luthen F, Bergemann C, et al. 2010. Capability of Differently Charged Plasma Polymer Coatings for Control of Tissue Interactions with Titanium Surfaces. *J. Adhes. Sci. Technol.* 24: 1191-205

Schvartz I, Seger D, Shaltiel S. 1999a. Vitronectin. *Int J Biochem Cell Biol* 31: 539-44

Schvartz I, Seger D, Shaltiel S. 1999b. Vitronectin. *Int J. Biochem. Cell Biol.* 31: 539-44

Schwartz SD, Hubschman JP, Heilwell G, Franco-Cardenas V, Pan CK, et al. 2012. Embryonic stem cell trials for macular degeneration: a preliminary report. *Lancet* 379: 713-20

Scully MF, Ellis V, Kakkar VV. 1988. Heparan-sulfate with no affinity for antithrombin-III and the control of hemostasis. *FEBS Lett.* 241: 11-14

Seiffert D, Schleef RR. 1996. Two functionally distinct pools of vitronectin (Vn) in the blood circulation: identification of a heparin-binding competent population of Vn within platelet alpha-granules. *Blood* 88: 552-60

Seiffert D, Smith JW. 1997. The cell adhesion domain in plasma vitronectin is cryptic. *J. Biol. Chem.* 272: 13705-10

Serruys PW, Emanuelsson H, vanderGiessen W, Lunn AC, Kiemeney F, et al. 1996. Heparin-coated Palmaz-Schatz stents in human coronary arteries - Early outcome of the Benestent-II pilot study. *Circulation* 93: 412-22

Serruys PW, van Hout B, Bonnier H, Legrand V, Garcia E, et al. 1998. Randomised comparison of implantation of heparin-coated stents with balloon angioplasty in selected patients with coronary artery disease (Benestent II). *Lancet* 352: 673-81

Shi Y, Desponts C, Do JT, Hahm HS, Schoeler HR, Ding S. 2008. Induction of Pluripotent Stem Cells from Mouse Embryonic Fibroblasts by Oct4 and Klf4 with Small-Molecule Compounds. *Cell Stem Cell* 3: 568-74

Shively JE, Conrad HE. 1976. Formation of anhydrosugars in chemical depolymerization of heparin *Biochemistry* 15: 3932-42

Shriver Z, Sundaram M, Venkataraman G, Fareed J, Linhardt R, et al. 2000. Cleavage of the antithrombin III binding site in heparin by heparinases and its implication in the generation of low molecular weight heparin. *Proc. Natl. Acad. Sci. U. S. A.* 97: 10365-70

Skidmore M, Atrih A, Yates E, Turnbull J. 2009. Labelling heparan sulfate saccharides with chromophore, fluorescence and mass tag for HPLC and MS separations. *Methods in Molecular biology* 534: 157-69

Skottman H, Dilber MS, Hovatta O. 2006. The derivation of clinical-grade human embryonic stem cell lines. *FEBS Lett.* 580: 2875-78

Solem M, Helmrich A, Collodi P, Barnes D. 1991. Human and mouse S-protein messenger-RNA detected in northern blot experiments and evidence for the gene coding S-protein in mammals by southern blot analysis *Mol. Cell. Biochem.* 100: 141-49

Son YS, Park JH, Kang YK, Park JS, Choi HS, et al. 2005. Heat shock 70-kDa protein 8 isoform 1 is expressed on the surface of human embryonic stem cells and downregulated upon differentiation. *Stem Cells* 23: 1502-13

Stanley KK. 1986. Homology with hemopexin suggests a possible scavenging function for S-protein vitronectin. *FEBS Lett.* 199: 249-53

Steffen HJ, Schmidt J, Gonzalez-Elipe A. 2000. Biocompatible surfaces by immobilization of heparin on diamond-like carbon films deposited on various substrates. *Surf. Interface Anal.* 29: 386-91

Steiner D, Khaner H, Cohen M, Even-Ram S, Gil Y, et al. 2010. Derivation, propagation and controlled differentiation of human embryonic stem cells in suspension. *Nat. Biotechnol.* 28: 361-U88

Stochaj WR, Berkelman T, Laird N. 2006. Staining membrane-bound proteins with colloidal gold. *CSH Protoc* 2006

Storm MP, Orchard CB, Bone HK, Chaudhuri JB, Welham MJ. 2010. Three-Dimensional Culture Systems for the Expansion of Pluripotent Embryonic Stem Cells. *Biotechnol. Bioeng.* 107: 683-95

Sudhalter J, Folkman J, Svahn CM, Bergendal K, Damore PA. 1989. Importance of size, sulfation, and anticoagulant activity in the potentiation of acidic fibroblast growth-factor by heparin *J. Biol. Chem.* 264: 6892-97

Sukhishvili SA, Granick S. 1998. Kinetic regimes of polyelectrolyte exchange between the adsorbed state and free solution. *J. Chem. Phys.* 109: 6869-78

Sukhishvili SA, Granick S. 1999. Adsorption of human serum albumin: Dependence on molecular architecture of the oppositely charged surface. *J. Chem. Phys.* 110: 10153-61

Summit Sc. 2007. http://www.stemcellsummit.com/2007/stem-cell-fact-sheet.pdf.

Suzuki S, Pierschbacher MD, Hayman EG, Nguyen K, Ohgren Y, Ruoslahti E. 1984. Domain-structure of vitronectin - Alignment of active-sites *J. Biol. Chem.* 259: 5307-14

Swaraj S, Oran U, Lippitz A, Friedrich JF, Unger WES. 2005. Study of influence of external plasma parameters on plasma polymerised films prepared from organic molecules (acrylic acid, allyl alcohol, allyl amine) using XPS and NEXAFS. *Surf. Coat. Technol.* 200: 494-97

Taipale J, Keskioja J. 1997. Growth factors in the extracellular matrix. *Faseb J.* 11: 51-59

Takahashi K, Tanabe K, Ohnuki M, Narita M, Ichisaka T, et al. 2007. Induction of pluripotent stem cells from adult human fibroblasts by defined factors. *Cell* 131: 861-72

Takahashi K, Yamanaka S. 2006. Induction of pluripotent stem cells from mouse embryonic and adult fibroblast cultures by defined factors. *Cell* 126: 663-76

Thomson JA, Itskovitz-Eldor J, Shapiro SS, Waknitz MA, Swiergiel JJ, et al. 1998. Embryonic stem cell lines derived from human blastocysts. *Science* 282: 1145-47

Timpl R, Brown JC. 1994. The laminins *Matrix Biol.* 14: 275-81

Timpl R, Rohde H, Robey PG, Rennard SI, Foidart JM, Martin GR. 1979. Laminin - Glycoprotein from basement membranes *J. Biol. Chem.* 254: 9933-37

Trowbridge JM, Gallo RL. 2002. Dermatan sulfate: new functions from an old glycosaminoglycan. *Glycobiology* 12: 117R-25R

Turnbull JE, Fernig DG, Ke YQ, Wilkinson MC, Gallagher JT. 1992. Identification of the basic fibroblast growth-factor binding sequence in fibroblast heparan-sulfate. *J. Biol. Chem.* 267: 10337-41

Turnbull JE, Hopwood JJ, Gallagher JT. 1999. A strategy for rapid sequencing of heparan sulfate and heparin saccharides. *Proc. Natl. Acad. Sci. U. S. A.* 96: 2698-703

Turnbull JE, Powell A, Guimond S. 2001. Heparan sulfate: decoding a dynamic multifunctional cell regulator. *Trends Cell Biol.* 11: 75-82

Uhm JH, Dooley NP, Kyritsis AP, Rao JS, Gladson CL. 1999. Vitronectin, a glioma-derived extracellular matrix protein, protects tumor cells from apoptotic death. *Clin. Cancer Res.* 5: 1587-94

Unger C, Skottman H, Blomberg P, Dilber MS, Hovatta O. 2008. Good manufacturing practice and clinical-grade human embryonic stem cell lines. *Hum. Mol. Genet.* 17: R48-R53

Uygun BE, Stojsih SE, Matthew HWT. 2009. Effects of Immobilized Glycosaminoglycans on the Proliferation and Differentiation of Mesenchymal Stem Cells. *Tissue Eng. Part A* 15: 3499-512

Vallier L, Alexander M, Pedersen RA. 2005. Activin/Nodal and FGF pathways cooperate to maintain pluripotency of human embryonic stem cells. *Journal of Cell Science* 118: 4495-509

van den Born J, Salmivirta K, Henttinen T, Ostman N, Ishimaru T, et al. 2005. Novel heparan sulfate structures revealed by monoclonal antibodies. *J. Biol. Chem.* 280: 20516-23

Varki A. 1999. The essential of Glycobiology. *Cold Spring Harbor, New York: Cold Spring Habor Laboratory Press*

Venkataraman G, Shriver Z, Raman R, Sasisekharan R. 1999. Sequencing complex polysaccharides. *Science* 286: 537-42

Villa-Diaz LG, Nandivada H, Ding J, Nogueira-De-Souza NC, Krebsbach PH, et al. 2010. Synthetic polymer coatings for long-term growth of human embryonic stem cells. *Nat. Biotechnol.* 28: 581-83

Vlodavsky I, Lui GM, Gospodarowicz D. 1980. Morphological appearance, growth-behavior and migratory activity of human-tumor cells maintained on extracellular-matrix versus plastic *Cell* 19: 607-16

Vynios DH, Karamanos NK, Tsiganos CP. 2002. Advances in analysis of glycosaminoglycans: its application for the assessment of physiological and pathological states of connective tissues. *J. Chromatogr. B* 781: 21-38

Wang L, Schuiz TC, Sherrer ES, Dauphin DS, Shin S, et al. 2007. Self-renewal of human embryonic stem cells requires insulin-like growth factor-1 receptor and ERBB2 receptor signaling. *Blood* 110: 4111-19

Ward AJ, Short RD. 1993. A time-of-flight secondary-ion mass-spectrometry and X-ray photoelectron-spectroscopy investigation of the structure of plasma polymers prepared from the methacrylate series of monomers *Polymer* 34: 4179-85

Ward AJ, Short RD. 1995. A TOF SIMS and XPS investigation of the structure of plasma polymers prepared from the methacrylate series of monomers 2. The influence of the W/F parameter on structural and functional-group retention *Polymer* 36: 3439-50

Watanabe K, Ueno M, Kamiya D, Nishiyama A, Matsumura M, et al. 2007. A ROCK inhibitor permits survival of dissociated human embryonic stem cells. *Nat Biotechnol* 25: 681-6

Whateley JG, Knox P. 1980. Isolation of a serum component that stimulates the spreading of cells in culture. *The Biochemical journal* 185: 349-54

Whittle JD, Short RD, Douglas CWI, Davies J. 2000. Differences in the aging of allyl alcohol, acrylic acid, allylamine, and octa-1,7-diene plasma polymers as studied by X-ray photoelectron spectroscopy. *Chem. Mat.* 12: 2664-71

Wobus AM, Holzhausen H, Jakel P, Schoneich J. 1984. Characterization of a pluripotent stem-cell line derived from a mouse embryo *Exp. Cell Res.* 152: 212-19

Wong LS, Khan F, Micklefield J. 2009. Selective Covalent Protein Immobilization: Strategies and Applications. *Chemical Reviews* 109: 4025-53

Xie XM, Gengenbach TR, Griesser HJ. 1992. Changes in wettability with time of plasma-modified perfluorinated polymers *J. Adhes. Sci. Technol.* 6: 1411-31

Xu CH, Inokuma MS, Denham J, Golds K, Kundu P, et al. 2001a. Feeder-free growth of undifferentiated human embryonic stem cells. *Nat Biotechnol* 19: 971-4

Xu D, Baburaj K, Peterson CB, Xu Y. 2001b. Model for the three-dimensional structure of vitronectin: Predictions for the multi-domain protein from threading and docking. *Proteins* 44: 312-20

Yang BH, Yang BL, Goetinck PF. 1995. Biotinylated hyaluronic-acid as a probe for identifying hyaluronic acid-binding proteins *Anal. Biochem.* 228: 299-306

Yap LYW, Li J, Phang IY, Ong LT, Ow JaZ-E, et al. 2011. Defining a Threshold Surface Density of Vitronectin for the Stable Expansion of Human Embryonic Stem Cells. *Tissue Engineering Part C-Methods* 17: 193-207

Zaehres H, Lensch MW, Daheron L, Stewart SA, Itskovitz-Eldor J, Daley GQ. 2005. High-efficiency RNA interference in human embryonic stem cells. *Stem Cells* 23: 299-305

Zanetti A, Conforti G, Hess S, Martinpadura I, Ghibaudi E, et al. 1994. Clustering of vitronectin and RGD peptides on microspheres leads to engagement of integrins on the luminal aspect of endothelial-cell membrane *Blood* 84: 1116-23

Zhang HL, Bremmell K, Kumar S, Smart RSC. 2004. Vitronectin adsorption on surfaces visualized by tapping mode atomic force microscopy. *J. Biomed. Mater. Res. Part A* 68A: 479-88

Zhang Z, Knoll W, Forch R. 2005. Amino-functionalized plasma polymer films for DNA immobilization and hybridization. *Surf. Coat. Technol.* 200: 993-95

Zhang ZH, Chen Q, Knoll W, Foerch R, Holcomb R, Roitman D. 2003. Plasma polymer film structure and DNA probe immobilization. *Macromolecules* 36: 7689-94

Zhao C, Sun YL, Kirk RL, Thoreson AR, Jay GD, et al. 2010. Effects of a lubricin-containing compound on the results of flexor tendon repair in a canine model in vivo. *J Bone Joint Surg Am* 92: 1453-61

Zhao X-y, Li W, Lv Z, Liu L, Tong M, et al. 2009. iPS cells produce viable mice through tetraploid complementation. *Nature* 461: 86-U88

Zhou W, Freed CR. 2009. Adenoviral Gene Delivery Can Reprogram Human Fibroblasts to Induced Pluripotent Stem Cells. *Stem Cells* 27: 2667-74

Zhuang P, Chen AI, Peterson CB. 1997. Native and multimeric vitronectin exhibit similar affinity for heparin - Differences in heparin binding properties induced upon denaturation are due to self-association into a multivalent form. *J. Biol. Chem.* 272: 6858-67

Zor T, Seliger Z. 1996. Linearization of the bradford protein assay increases its sensitivity: Theoretical and experimental studies. *Anal. Biochem.* 236: 302-08

Zou ZY, Chen H, Schmaier AA, Hynes RO, Kahn ML. 2007. Structure-function analysis reveals discrete beta 3 integrin inside-out and outside-in signaling pathways in platelets. *Blood* 109: 3284-90

Zweigerdt R, Olmer R, Singh H, Haverich A, Martin U. 2011. Scalable expansion of human pluripotent stem cells in suspension culture. *Nat. Protoc.* 6: 689-700

APPENDIX A: SUPPLEMENTARY FIGURES AND TABLES

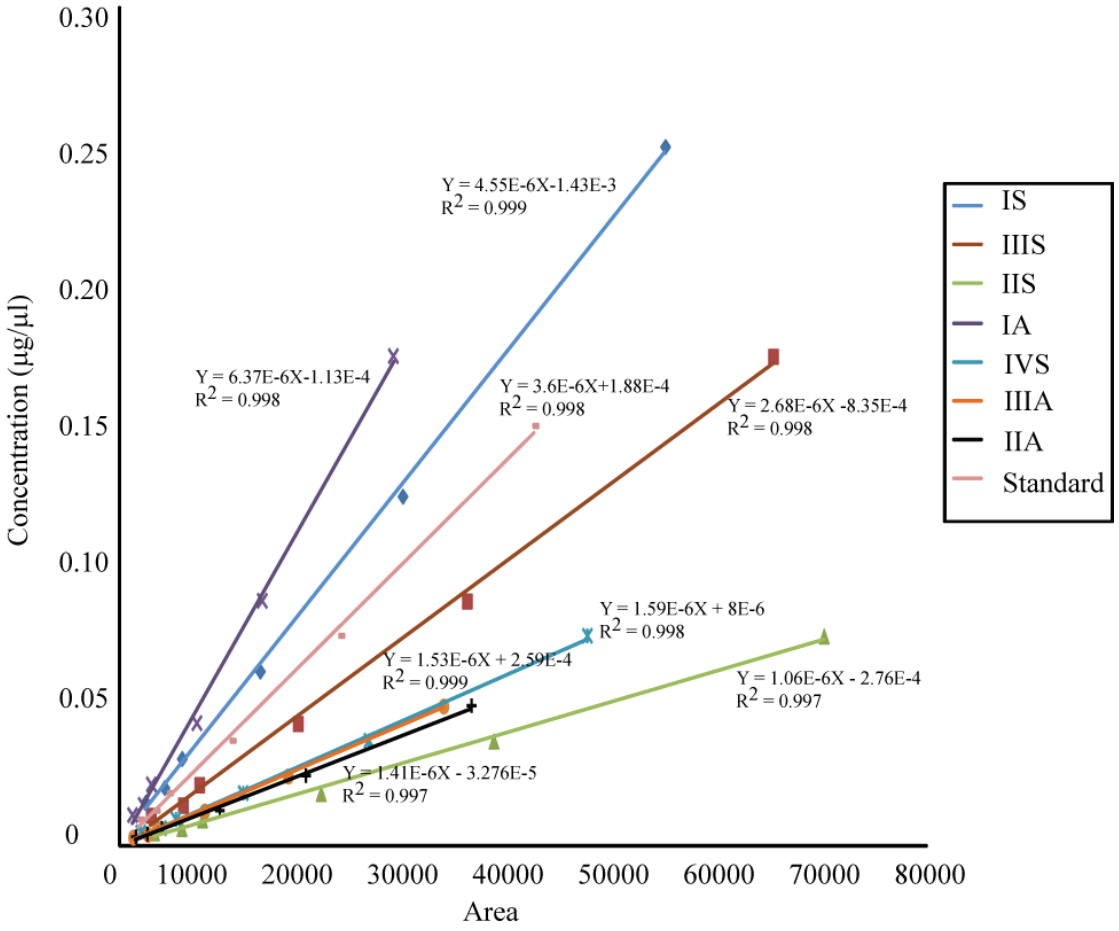

Figure A1. Δ-disaccharide standard curve. Different dilutions of each standard were separated by CE, area-under-the curve determined and standard curve plotted.

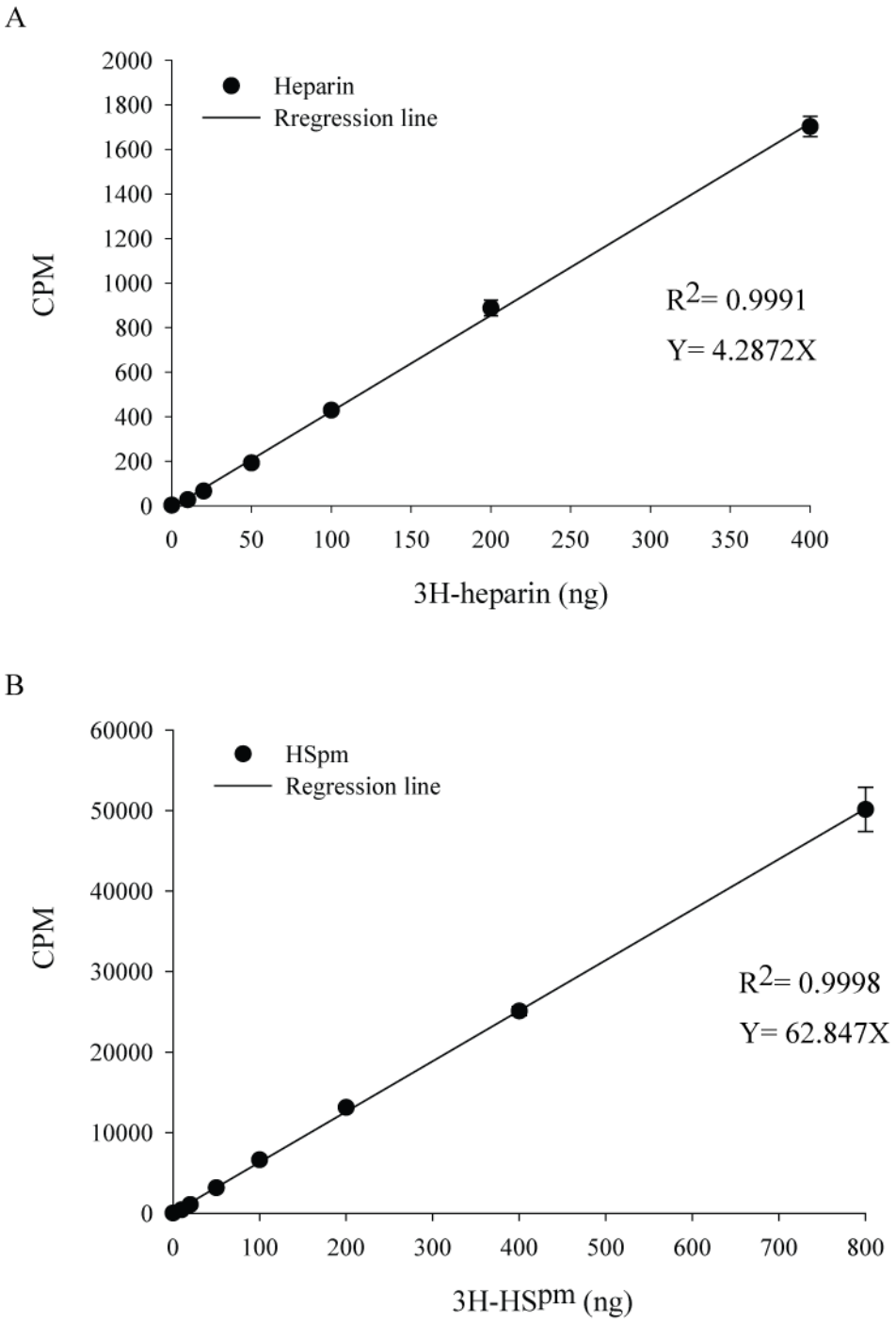

Figure A2. Standard curves of (A) ^{3}H-heparin and (B) ^{3}H-HS^{pm} on surfaces.

Table A1. PCR primer sequences

Target gene	Ascension No.	Forward (5'-3')	Reverse (5'-3')
AFP	NM_001134	TCC CTC CTG CAT TCT CTG ATG	CCT GAG CTT GGC ACA GAT CC
GATA6	NM_005257	GCG GCT TGG ATT GTC CTG T	TGC GCC ATA AGG TGG TAG TTG
MSX1	NM_002448	CCT TCC CTT TAA CCC TCA CAC	CCG ATT TCTTG CGC TTT TC
Nkx2.5	NM_004387	TCC CCT GGA TTT TGC ATT CA	AGG ATC ACT CAT TGC ACG CTG
HAND1	NM_004821	CCA CCC TTT TGG AGC GAA TT	AAT TAG AGA AGA CGG CGT CGG
NFH	NM_021076	TGA ACA CAG ACG CTA TGC GCT CAG	CAC CTT TAT GTG AGT GGA CAC AGA
PAX6	NM_0011276	CCA GCT TCA CCA TGG CAA AT	GGC AGC ATG CAG GAG TAT GAG
MAP2	NM_002374	TAT CCC AGG ACC CCT CAC AC	TCA CTC GGC ACC AAG ATG G
Nanog	NM_024865	GAA AAA CAA CTG GCC GAA GAAT	GGT GCT GAG GCC TTC TGC
OCT-4	NM_002701	AAC GAC CAT CTG CCG CTT T	GGC CGC AGC TTA CAC ATG TT
GAPDH	NM_002046	GTC GGA GTC AAC GGA TTT GG	AAA AGC AGC CCT GGT GAC C

Table A2. FACS analysis of Tra1-60 and OCT-4 pluripotent marker expression in (A) HES-3 and (B) H7 cells for 8 continuous passages.

A

	Tra1-60		OCT-4	
VN (μg/ml)	2.5	5	2.5	5
P1	95.3	97.9	97.9	96.7
P3	98.9	99.3	98.4	98.2
P6	99.7	99.6	97.4	97.4
P8	98.5	96.8	97.8	93.3

B

	Tra1-60		OCT-4	
VN (μg/ml)	2.5	5	2.5	5
P1	99.3	98.7	98.5	97.7
P3	99.3	95.4	95.0	99.4
P6	99.6	99.4	90.4	94.0
P8	98.1	98.6	86.5	90.2

APPENDIX B: SUPPLEMENTARY INFORMATION FOR MATERIAL AND METHODS

General chemicals and reagents

0.01% poly-l-lysine (Cat No. P4707, Sigma Aldrich, MO, USA)

1-Ethyl-3-[3-dimethylaminopropyl]carbodiimide hydrochloride (EDC) powder (Cat. No. N2770, Sigma Aldrich, MO, USA)

2-(N-Morpholino)ethanesulfonic acid (MES) powder (Cat. No. M3670, Sigma Aldrich, MO, USA)

3,3′,5,5′-Tetramethylbenzidine (TMB) substrate (Cat No. 34021, Thermo Fisher Scientific Inc, IL, USA)

Acetic acid (Cat. No.1.00063.2500, Merck Millipore, Darmstadt, Germany)

Agarose powder (Cat. No. 10975-035, Invitrogen, Life Technologies Corporation, CA, USA)

Allyamine monomer (Cat. No. 14,583-1, Sigma Aldrich, MO, USA)

Bio-Gel® P-10 Gel (Cat No. 150-4144, Biorad Laboratories, Hercules, USA)

Biotin-LC-hydrazide (Cat No. 21340, Thermo Fisher Scientific Inc, IL, USA)

Bovine serum albumin (BSA) (Cat No. A7906, Sigma Aldrich, MO, USA)

Bradford reagent (Cat. No. B6916, Sigma Aldrich, MO, USA)

Calcium acetate ($Ca(OAc)_2$) (Cat. No.C-1000, Sigma Aldrich, MO, USA)

Calcium chloride ($CaCl_2$) (Cat No. C5670, Sigma Aldrich, MO, USA)

Colloidal Gold Total Protein Stain (Cat. No. 170-6527, Biorad Laboratories, Hercules, USA)

Crystal violet powder (Cat. No. C3886, Sigma Aldrich, MO, USA)

Dimethyl sulfoxide (DMSO) (Cat.No. D2438 , Sigma Aldrich, MO, USA)

Ethanol (Cat. No. 1.00983.2500, Merck Millipore, Darmstadt, Germany)

Ethidium bromide (Cat No. 161-0433, Biorad Laboratories, Hercules, USA)

ExtrAvidin® - Alkaline phosphatase (Cat No. E2636, Sigma Aldrich, MO, USA)

Fish gelatin powder (Cat. No. G7041, Sigma Aldrich, MO, USA)

Fluorescamne protein dye (Cat. No. F9015, Sigma Aldrich, MO, USA)

Formic acid (Cat. No.06450, Sigma Aldrich, MO, USA)

Gelatin from porcine skin Type A (Cat No. G1890, Sigma Aldrich, MO, USA)

Glycine (Cat. No. 161-0718, Biorad Laboratories, Hercules, USA)

Heparan sulfate sodium salt from porcine intestinal mucosa (HS^{pm}) (Cat No. HO-03103, Celsus Laboratories Inc, Ohio, USA)

Heparin Sepharose beads (Cat. No. H6508, Sigma Aldrich, MO, USA)

Heparin sodium salt from porcine intestinal mucosa (Cat. No. H3149, Sigma Aldrich, MO, USA)

HPLC grade water (Cat. No. 95304, Sigma Aldrich, MO, USA)

Laemmli buffer (Cat. No. S3401, Sigma Aldrich, MO, USA)

LumiGLO chemiluminescent substrate (Cat. No. 54-61-01, Kirkegaard & Perry Laboratories, Gaithersburg, USA)

LumiGlo Reserve™ chemiluminescent substrate (Cat. No. 54-71-01, Kirkegaard & Perry Laboratories, Gaithersburg, USA)

Methanol (Cat. No. 1.06009.2500, Merck Millipore, Darmstadt, Germany)

MilliQ water (MilliQ Integral water purification system, Merck Millipore, Darmstadt, Germany)

Mitomycin-C (Cat. No. M4287, Sigma Aldrich, MO, USA)

MOPS SDS running buffer (20 X) (Cat No. NP 0001-02, Invitrogen)

Octa-1,7-diene monomer (Cat. No. 02501, Sigma Aldrich, MO, USA)

Paraformaldehyde (Cat. No. P6148, Sigma Aldrich, MO, USA)

Ponceau S staining solution (Cat. No. P7170, Sigma Aldrich, MO, USA)

Precision Plus protein standards (Cat No. 161-0373, Biorad Laboratories, Hercules, USA)

SIGMAFAST™ p-Nitrophenyl phosphate tablets (Cat. No. N2770, Sigma Aldrich, MO, USA)

Sodium acetate (NaAc) (Cat No. 71185, Sigma Aldrich, MO, USA)

Sodium chloride (NaCl) (Cat No. 73575, Sigma Aldrich, MO, USA)

Sodium dodecyl sulfate (SDS) powder (Cat. No. 1.13760.1000, Merck Millipore, Darmstadt, Germany)

Sodium hydroxide (NaOH) (Cat. No. S8045, Sigma Aldrich, MO, USA)

Streptavidin-HRP (Cat No. 21324, Thermo Fisher Scientific Inc, IL, USA)

Sulfuric acid (H_2SO_4) (Cat No. 87003 – 234, VWR, USA)

Triton X100 (Cat No. 161-0407, Biorad Laboratories, Hercules, USA)

Triza® base minimum 99.9 % (Cat No. T1503, Sigma Aldrich, MO, USA)

Tween 20 (Cat. No. P1379, Sigma Aldrich, MO, USA)

Ultima Gold scintillation cocktail (Cat. No. 6013321, Perkin Elmer, Massachusetts, USA.)

Other materials

0.2 μM nitroceullose membrane (Cat No. 162-0112, Biorad Laboratories, Hercules, USA)

20 ml glass scintillation vials (Cat No. 6000128, Perkin Elmer, Massachusetts, USA.)

GE PD Minitrap™ G-10 (Cat No. 28-9180-0, GE Healthcare)

GE PD Minitrap™ PD-10 (Cat No. 17-0851-01, GE Healthcare)

Glycosaminoglycan 96-well binding plates (Cat No. H/G Plates, Iduron Ltd, Manchester, UK)

Iodination beads (Cat. No. 28665, Thermo Fisher Scientific Inc, IL, USA)

NUPAGE® 4-12% Bis-Tris gel SDS-PAGE gel (Cat No. NP0335PK2, Invitrogen, Life Technologies Corporation, CA, USA)

X-ray film (Cat No. 28906844, GE Healthcare)

Radiochemicals

^{125}I isotope (17.4 Ci/mg) (Cat. No. NEZ 033A, Perkin Elmer, Massachusetts, USA.)

^{3}H-heparin (0.35 mCi/mg) (Cat. No. NET476, Perkin Elmer, Massachusetts, USA.)

^{3}H-lysine (105.4 Ci/mmol) (Cat. No. NET376, Perkin Elmer, Massachusetts, USA.)

Tritiation of HS^{pm} done by RC TRITEC AG, Teufen, Switzerland.

Heparin standards

Heparin disaccharide standards (ΔUA,2S – GlcNS,6S; ΔUA,2S – GlcNS, ΔUA,2S – GlcNAc,6S, ΔUA – GlcNS,6S, ΔUA – GlcNS, ΔUA – GlcNAc, ΔUA,2S – GlcNAc, ΔUA – GlcNAc,6S, ΔUA-2S ® GlcNCOEt-6S, ΔUA,2S – GlcN, ΔUA,2S – GlcN,6S, ΔUA – GlcN,6S, ΔUA – GlcN) (Cat No. HD001 to HD013, , Iduron Ltd, Manchester, UK)

Heparin Oligosaccharides (dp4, dp6, dp8, dp10, dp12) (Cat. No. HO04, HO06, HO08, HO10, HO12)

Selectively desulfated heparin standards (2-O, 6-O and N- desulfated heparin) (Cat No. DSH001/2, DSH002/6, DSH003/N, Iduron Ltd, Manchester, UK)

Enzymes

Heparinase I (Cat No. H2519, Sigma Aldrich, MO, USA)

Heparinase I (Cat. No. HEP-ENZ I, Iduron Ltd, Manchester, UK)

Heparinase II (Cat No. H6512, Sigma Aldrich, MO, USA)

Heparinase II (Cat. No. HEP-ENZ II, Iduron Ltd, Manchester, UK)

Heparinase III (Cat No. H8891, Sigma Aldrich, MO, USA)

Heparinase III (Cat. No. HEP-ENZ III, Iduron Ltd, Manchester, UK)

Superscript II reverse transcriptase (Cat No. 18064-014, Invitrogen, Life Technologies Corporation, CA, USA)

Kits

Fix and Perm kit (Cat No. GAS003, Invitrogen, Life Technologies Corporation, CA, USA)

RNA extraction kit (Cat No. 74104, Qiagen, Hilden, Germany)

Primers

Oligo dT primers (Cat No. 18418-020, Invitrogen, Life Technologies Corporation, CA, USA)

Primers for PCR and qRT-PCR synthesized by Sigma Aldrich, MO, USA, sequences in Table A1

SYBR green PCR master mix (Cat No. 4309155, Applied Biosystems, BV, USA)

Antibodies

Alexa(633) anti-mouse IgM (Cat No. A-21046, Invitrogen, Life Technologies Corporation, CA, USA)

Alexa(647) goat anti-mouse IgG2b (Cat No. A-21242, Invitrogen, Life Technologies Corporation, CA, USA)

Anti- ΔHS 3G10 antibody (Cat No. 37026, Seikagaku corporation, Tokyo, Japan)

Anti-fibronectin (Cat No. MAB 1932, Merck Millipore, Darmstadt, Germany)

Anti-heparan sulfate 10E4 antibody (Cat No.370255, Seikagaku Corporation, Tokyo, Japan)

Anti-laminin (Cat No. MAB 88918, Merck Millipore, Darmstadt, Germany)

Anti-OCT-4 (Cat No. sc5279, Santa Cruz, USA)

Anti-Tra1-60 (Cat No.MAB4360, Merck Millipore, Darmstadt, Germany)

Anti-vitronectin (Cat No. MAB1945, Merck Millipore, Darmstadt, Germany)

Chromogen DAB (Cat No. K400711, DAKO, Denmark)

Desmin clone 33 (Cat. No. M076001, DAKO, Denmark)

EnVision+ horse-radish peroxidase (HRP) anti-rabbit (Cat No. K4002, DAKO, Denmark)

EnVision+HRP anti-mouse (Cat No. K4000, DAKO, Denmark)

FITC-conjugated goat anti-mouse secondary antibody (Cat No. F0479, DAKO, Denmark)

Goat anti-mouse biotinylated antibody (Cat No. ab 6788, Abcam, Cambridge, UK)

HRP-conjugated goat anti-mouse Ig G (H+L) antibody (Cat No. 115-035-062, Jackson Immunoresearch laboratories Inc, PA, USA)

Mouse IgG2 isotype control (Cat No. X0943, DAKO, Denmark)

Mouse IgM isotype control (Cat No. X0942, DAKO, Denmark)

Polyclonal rabbit anti-cytokeratin (Cat No. Z0622, DAKO, Denmark)

Rabbit anti-Glial fibrillary acidic protein (GFAP) (Cat. No. Z033401, DAKO, Denmark)

SlowFade Gold anti-fade reagent with DAPI (Cat No. S36938, Invitrogen, Life Technologies Corporation, CA, USA)

Cell lines

H1 and H7 hESCs from WiCell Research Institute, WI, USA.

HES-3 hESCs from ES Cell International, Singapore, http://escellinternational.com),

Media and solutions for cell culture

0.25 % Trypsin-EDTA (Cat No. 25200, Invitrogen, Life Technologies Corporation, CA, USA)

24-well non-TCPS plates (Cat No. 351147, Beckon Dickinson, Frankin Lakes, NJ.)

24-well TCPS plates (Cat No. 142475, NUNC, Denmark)

2-mercaptoethanol (Cat No. 21985-023, Invitrogen, Life Technologies Corporation, CA, USA)

60 mm center-well organ culture (OCD) dishes (Cat No. 353037, Beckon Dickinson, Frankin Lakes, NJ.)

96-well non-TCPS white-walled transparent bottom plates (Cat No. 265302, NUNC, Denmark)

96-well TCPS plates (Cat No. 167008, NUNC, Denmark)

96-well TCPS white-walled transparent bottom plates (Cat No. 3610, Corning)

BD Matrigel^{TM} (Cat No. 354234, Beckon Dickinson, Frankin Lakes, NJ.)

Collagenase IV, (Cat No. 17104-019, Invitrogen, Life Technologies Corporation, CA, USA)

DMEM high glucose (Cat. No.11960, Invitrogen, Life Technologies Corporation, CA, USA)

DMEM/F12 (Cat No. 11039, Invitrogen, Life Technologies Corporation, CA, USA)

Fetal bovine serum (FBS) (Cat No. 10270, Invitrogen, Life Technologies Corporation, CA, USA)

FGF-2 (Cat No. 13256-029, Invitrogen, Life Technologies Corporation, CA, USA)

Fibronectin (Cat No. F2006 from Sigma Aldrich, MO, USA)

Iscove's Modified Dulbecco's Medium (IMDM) (Cat No. 12440-046, Invitrogen, Life Technologies Corporation, CA, USA)

Knock-out Dulbecco's Modified Eagle's medium (KO-DMEM) (Cat. No. 10829018, Invitrogen, Life Technologies Corporation, CA, USA)

Knock-out serum replacer (Cat. No. 10828-028, Invitrogen, Life Technologies Corporation, CA, USA)

Laminin (Cat No. AG56P, Merck Millipore, Darmstadt, Germany)

L-glutamine (Cat No. 25030-081, Invitrogen, Life Technologies Corporation, CA, USA)

mTeSR™1 media (Cat No. 05850 from Stem Cell Technologies, BC, Canada)

Nonessential amino acids (Cat No. 11140-050, Invitrogen, Life Technologies Corporation, CA, USA)

Penicillin-Streptomycin (Cat. No. 15140, Invitrogen, Life Technologies Corporation, CA, USA)

Phosphate buffered saline (PBS) (Cat No. 14190, Invitrogen, Life Technologies Corporation, CA, USA)

Rock inhibitor (Y27632) (Cat. No. 688002, Merck Millipore, Darmstadt, Germany)

Streptavidin (Cat No. Z02043, Genescript, NJ, USA)

TrypLE™ express (Cat No.12604-021, Invitrogen, Life Technologies Corporation, CA, USA)

Vitronectin (Cat No. CC080, Merck Millipore, Darmstadt, Germany)

Preparation of media and solutions

MEF culture media

90 % (v/v) DMEM high glucose, 10% FBS, 2 mM L-glutamine, 25 Units/ml penicillin and 25 μg/ml streptomycin.

Mitomycin C

2 mg of mitomycin C powder dissolved in 2 ml of PBS to generate 1 mg/ml stock solution, filtered through 0.22 μM sterile filter (Sartorius) and stored at 4 ^{o}C.

FGF buffer

10 mM Tris, 0.1 % BSA, sterilize through 0.22 μM filter and stored in 4 ^{o}C.

Collagenase IV solution

Prepare 500 μg/ml of collagenase IV in KO-DMEM, 0.22 μM sterile filter (Sartorius) and stored at 4 ^{o}C.

Conditioned media

85 % KO-DMEM and 15 % KO serum replacer supplemented with 1 mM L-glutamine, 1 % nonessential amino acids, 0.1 mM 2-mercaptoethanol, 25 U/ml Penicillin, 25 μg/ml streptomycin and 10 ng/ml FGF-2.

mTeSR^{TM}1 media preparation

Thaw 5 x supplement and add into basal medium, 0.22 μM sterile filter (Nalgene) and stored at 4 ^{o}C.

Heparinase digestion buffer (Sigma)

20 mM Tris-HCL, 50 mM NaCl, 4 mM $CaCl_2$ and 0.01 % BSA, pH 7.5.

Heparinase digestion buffer (Iduron)

50 mM NaAc, 1 mM ($Ca(OAc)_2$) and 100 μg/ml BSA at pH 7.

Matrigel™

Matrigel™ was thaw at 4 °C overnight and diluted (1:30) in cold KO-DMEM

0.1 % gelatin-coated plates

Weigh out 2.5 g gelatin from porcine skin Type A and dissolve in 25 ml MilliQ water, 0.22 μM sterile filter (Sartorius) and stored at 4 °C.

Low salt affinity chromatography buffer

20 mM phosphate buffer, 150 mM NaCl, pH 7.2

High salt affinity chromatography buffer

20 mM phosphate buffer, 1.5 M NaCl, pH 7.2

0.1 M MES buffer

Weigh 1.952 g MES powder and dissolve in 100 ml MilliQ water.

PBST

30 ml 5 M NaCl, 66 ml 1.5 M Tris, 1ml Tween 20 and 990 ml MilliQ water

1 x Transfer buffer

For 1 L, add 24.22 g of Triza® base, 112.6 g glycine and top up with MilliQ water

Standard assay buffer (SAB)

100 mM NaCl, 50 mM NaAc, (v/v) 0.2 % Tween 20, pH 7.2

APPENDIX C: PUBLICATIONS

TISSUE ENGINEERING: Part C
Volume 17, Number 2, 2011

DOI: 10.1089/ten.tec.2010.0328

Defining a Threshold Surface Density of Vitronectin for the Stable Expansion of Human Embryonic Stem Cells

Lynn Y.W. Yap, B.Sc.,[1,2] Jian Li, Ph.D.,[3] In Yee Phang, Ph.D.,[3] Lay Ting Ong, M.Sc.,[3] Jo'an Zhu-En Ow, B.Eng.,[4] James C.H. Goh, Ph.D.,[5] Victor Nurcombe, Ph.D.,[1,6] Jonathan Hobley, Ph.D.,[3] Andre B.H. Choo, Ph.D.,[4] Steve K.W. Oh, Ph.D.,[4] Simon M. Cool, Ph.D.,[1,6] and William R. Birch, Ph.D.[3]

Current methodology for pluripotent human embryonic stem cells (hESCs) expansion relies on murine sarcoma basement membrane substrates (Matrigel™), which precludes the use of these cells in regenerative medicine. To realize the clinical efficacy of hESCs and their derivatives, expansion of these cells in a defined system that is free of animal components is required. This study reports the successful propagation of hESCs (HES-3 and H1) for >20 passages on tissue culture-treated polystyrene plates, coated from 5 μg/mL of human plasma-purified vitronectin (VN) solution. Cells maintain expression of pluripotent markers Tra1-60 and OCT-4 and are karyotypically normal after 20 passages of continuous culture. *In vitro* and *in vivo* differentiation of hESC by embryoid body formation and teratoma yielded cells from the ecto-, endo-, and mesoderm lineages. VN immobilized on tissue culture polystyrene was characterized using a combination of X-ray photoemission spectroscopy, atomic force microscopy, and quantification of the VN surface density with a Bradford protein assay. Ponceau S staining was used to measure VN adsorption and desorption kinetics. Tuning the VN surface density, via the concentration of depositing solution, revealed a threshold surface density of 250 ng/cm^2, which is required for hESCs attachment, proliferation, and differentiation. Cell attachment and proliferation assays on VN surface densities above this threshold show the substrate properties to be equally viable.

Introduction

Human embryonic stem cells (hESCs) are self-renewing, pluripotent cells. They are isolated from the inner cell mass of blastocysts and have the ability to differentiate into all three germ layers, thus holding the promise of applications in tissue repair and drug development.[1] Early methods of culturing hESCs relied on co-culture with inactivated mouse embryonic fibroblasts (MEFs).[1] This method, however, is not suitable for the development of clinical-grade hESCs, partly due to the xenogenic risks it introduces. Although human feeders have been reported to successfully replace MEFs,[2,3] these cells may carry-over during hESC removal and thus adversely affect hESC purity.

Other than cell-based feeder layers, Matrigel™, a gelatinous basement membrane extract secreted by mouse Engelbreth-Holm-Swarm tumor cells and distributed by Becton Dickinson Biosciences, is now routinely used as a substrate for maintaining the pluripotency of cultured hESCs. However, a medium conditioned by MEFs is usually used in combination with Matrigel to maintain pluripotent hESCs. Matrigel is known to contain a diverse number of factors that include laminin-111, entactin, heparan sulfate proteoglycans, and multiple growth factors.[4] Importantly, in a move toward a more defined culture platform, Hakala *et al.* recently compared the use of Matrigel with different feeder-free hESC culture substrates (biomaterials, human extracellular matrix [ECM] proteins, and human and animal sera matrices) and reported that Matrigel was superior in terms of the maximum passage number attained, as well as hESC morphology and pluripotent marker expression.[5] Despite these advances in feeder-free systems, the use of Matrigel is limited by batch to batch variability, complex protein mixtures, and the possibility of transferring nonhuman sialic acid, Neu5Gc, to the hESCs.[6] Neu5Gc is an immunogenic molecule and can

[1]Stem Cells and Tissue Repair Group, Institute of Medical Biology, Agency for Science, Technology and Research (A*STAR), Singapore, Singapore.
[2]Graduate School for Integrative Sciences and Engineering, National University of Singapore, Singapore, Singapore.
[3]Institute of Materials Research and Engineering, Agency for Science, Technology and Research (A*STAR), Singapore, Singapore.
[4]Stem Cell Group, Bioprocessing Technology Institute, Agency for Science, Technology and Research (A*STAR), Singapore, Singapore.
[5]Tissue Engineering Program, Department of Orthopedic Surgery, National University of Singapore, Singapore, Singapore.
[6]Department of Orthopaedic Surgery, Yong Loo Lin School of Medicine, National University of Singapore, Singapore, Singapore.

limit the industrial scale up of this technology for clinical applications. These results have driven the exploration of several routes to develop a defined system suitable for culturing hESCs.

Defined model surfaces in the form of immobilized peptide arrays have been used as substrates for hESC adhesion and expansion.[7,8] Although dilution is used to tune the peptide surface density, the latter is not quantified or otherwise measured. Rather, this study identifies a peptide surface density threshold that promotes cell adhesion. Further, the analysis of hESC pluripotency is limited to detecting endogenous alkaline phosphatase and *OCT-4*, without examining karyotypic stability or differentiation potential of the expanded hESCs. In a more recent study by Kolhar *et al.*, immobilized cyclic arginine, glycine and asparigine (RGD) peptide sequences where shown to promote hESCs attachment and propagation.[9] Using this platform, hESCs were cultured for >10 passages, without adversely affecting karyotypic stability or differentiation potential. Although an estimate of peptide surface density (10–30 fmol/cm^2) was obtained from fluorescence measurements and enzyme-linked immunosorbent assay, no direct quantification of the peptide surface density or other surface characterization was carried out.

Recent advances in synthetic surfaces by Melkoumian *et al.* describe synthetic peptide-acrylate surfaces that are able to sustain the propagation of pluripotent hESCs for >20 passages in a xeno-free environment.[10] This study detects surface-immobilized peptides by fluorescence, and while solution concentration is used to tune the conjugated peptide surface density, the surface density was not reported. Villa-Diaz *et al.* report the propagation of hESCs on a fully synthetic polymer (without immobilized biomolecules) with tunable surface wettability and Young's modulus.[11] This surface successfully propagates H9 hESCs in StemPro defined medium, but was not reported to be robust across cell lines and with the mTeSR-defined cell culture medium.

A further development of a defined hESC culture platform was described by Ludwig *et al.*, who reported that a combination of human collagen IV, fibronectin, laminin, and vitronectin (VN) was able to support several passages of hESCs when combined with a xeno-free culture medium (TeSR1).[12] However, this platform relies on a combination of four human matrix protein substrates that adds significant cost to the scale-up of hESCs. Moreover, the cells were found to be karyotypically abnormal,[12] which may explain their adaptation to this platform. In other approaches, hESCs have been shown to propagate on separate matrices of fibronectin, laminin, laminin-511, and VN,[13–16] highlighting that a defined, scalable substrate on which to propagate hESCs may be a realistic possibility. Also, induced pluripotent stem cells (iPSC) have recently been successfully propagated on plasma-purified VN,[17] suggesting that VN, of the various ECM proteins being investigated, may be universally applicable for the propagation of pluripotent stem cells.

VN is an abundant glycoprotein that is found in the ECM. It promotes cell adhesion and spreading, but inhibits the complement pathway that can compromise hESC viability. It is secreted as a single molecule (75 kDa),[18] which may be approximated by a cylinder with a radius of 30.3 ± 0.6 Å and a length of 110 Å.[19] Braam *et al.* reported the successful culture for at least 10 passages of hESCs on 5 μg/mL of recombinant VN and identified αVβ5 integrin as VN receptor.[15] Rowland *et al.* also reported similar results with 10 μg/mL of plasma-purified VN with iPSCs.[17] However, neither of these reports determined the threshold amount of VN necessary for the long-term propagation of hESCs. As such, there is a need to better characterize and quantify VN substrates for hESC expansion so as to provide a defined platform for the scale-up of stem cell cultures.[20–22]

In the present study, we adsorb VN onto tissue culture polystyrene (TCPS) and determined the effect of VN surface density on the adhesion, proliferation, and long-term maintenance of hESCs compared to Matrigel.[12] This simplified VN substrate also provided an opportunity to tune the relevant surface properties for promoting hESC adhesion and propagation. VN surface density was characterized by a combination of Ponceau S staining, Bradford assay, X-ray photoemission spectroscopy (XPS), and the physical roughness of the surface determined by atomic force microscopy (AFM). Although AFM has previously been used to study VN adsorption on smooth mica surfaces,[23] the present study examined VN adsorbed to TCPS, a surface demonstrated to be successful for the long-term propagation of hESCs.

We show that the bioresponse of cultured hESCs to adsorbed VN correlates with VN surface density. Further, we establish a minimum threshold of surface-bound VN that is required for the maintenance of hESC pluripotency.

Materials and Methods

Biological response

Coating of TCPS with VN or Matrigel. A 5 μg/mL working solution of VN was prepared by diluting stock VN solution (1 mg/mL) (Millipore) with 1×phosphate-buffered saline (PBS). This solution (300 μL) was added into 60 mm center-well organ culture dishes (Becton Dickinson Biosciences), which are made from TCPS. After overnight incubation (15 h) at 4°C, the VN-coated plates, referred to as VN5, were rinsed once with PBS and then immediately used for cell seeding. For surface characterization, the coated TCPS substrates were rinsed twice in MilliQ water (Milli Q Gradient A10; Millipore) and dried under a nitrogen flow. Matrigel™ (Becton Dickinson Biosciences), used as a control cell culture surface, was diluted in cold knock-out (KO) Dulbecco's modified Eagle's medium (Invitrogen) at 1:30 ratio and allowed to coat TCPS overnight at 4°C before washing and cell seeding.

hESCs and matrices. HES-3 (46, XX) and H1 (46, XY) cells were obtained from ES Cell International and WiCell, respectively. They were cultured on Matrigel or VN-coated culture dishes with conditioned medium (CM) from ΔE-MEF[24] or in mTeSR®1 serum-free defined growth medium, with bovine serum albumin (BSA) as the only animal-derived component (Stem Cell Technologies) at 37°C/5% CO_2. The CM used for culturing hESCs contained 85% KO-Dulbecco's modified Eagle's medium and 15% KO serum replacer, supplemented with 1 mM L-glutamine, 1% nonessential amino acids, 0.1 mM 2-mercaptoethanol, 25 U/mL penicillin, 25 μg/mL streptomycin (Gibco), and 10 ng/mL fibroblast growth factor-2 (Invitrogen). This medium was

conditioned overnight on ΔE-MEF as described above, sterilized with a 0.22 mm filter, and again supplemented with 10 ng/mL fibroblast growth factor-2 before adding into hESCs culture. Cells were grown on the matrix for 7 days with a daily change of CM or mTeSR1. mTeSR1 medium was prepared according to the manufacturer's instructions.

hESC cultures were passaged following Choo *et al.*[3] Briefly, cells grown on Matrigel were treated with collagenase IV (200 U/mL) for 5 min at 37°C and differentiated cells removed by pipetting. Cells were then dissociated into small clumps by scraping and repeated pipetting. Harvested cells were split at 1:4 ratio and seeded into fresh Matrigel-coated tissue culture dishes. For cells grown on VN, mechanical passaging was employed. Colonies that appeared differentiated were removed by manual pipetting and the remaining cells scraped into small clumps. Cells were then seeded into freshly coated VN culture dishes at a 1:6 passage ratio.

Fluorescence-activated cell sorting analysis. Flow cytometry was performed with the cell surface marker *Tra1-60* and transcription factor *OCT-4* with an appropriate isotype control for hESCs grown on the various platforms. Cells were first trypsinized with 0.25% trypsin/ethylenediaminetetraacetic acid to a single cell suspension and then fixed and permeabilized with a Fix and Perm kit (Caltag Laboratories, Invitrogen), used according to the manufacturer's instructions. During the 15 min permeabilization step, *OCT-4* (1:20; Santa Cruz) or *Tra1-60* (1:50; Chemicon) mouse monoclonal antibodies were incubated together with the kit's Reagent B. Cells were then washed with 1% BSA/PBS followed by 15 min incubation in the dark with fluorescein isothiocyanate-conjugated goat anti-mouse antibody at 1:500 dilution (Dako). Finally, cells were washed and resuspended with 1% BSA in PBS for analysis on a fluorescence-activated cell sorting (FACS) Calibur (Becton-Dickinson). Results were analyzed with FlowJo software, with gating selected at the point of intersection between the marker and isotype control curves.[25]

Adhesion assay. Flat-bottom 96-well TCPS plates (Thermo Fisher Scientific) were coated with VN solutions at concentrations of 0, 2.5, 5, 10, 15, and 20 μg/mL, as described above, yielding VN coated TCPS surfaces that are referred to as VN0, VN2.5, VN5, VN10, and VN20, respectively, (in triplicates). The wells were then blocked with 2% BSA (1 h, 20°C) and a single cell suspension of HES-3 cells (3×10^5 per well), dissociated with TrypLE™ (Invitrogen), was seeded into the wells. The cells were incubated for 45 min at 37°C/5% CO_2. TCPS substrates coated from the same VN solution and similarly blocked were used as blanks. After 45 min, the wells were washed three times with Iscove's modified Dulbecco's medium (Invitrogen), supplemented with 0.35% BSA, and then rinsed once with PBS to remove nonadherent cells. Cells on TCPS were fixed with 100% ethanol for 5 min and stained with 0.4% crystal violet in methanol for another 5 min at room temperature. Cells were then washed with deionized water three times, followed by the addition of 40 μL of 1% sodium dodecyl sulfate to solubilize the dye. The plates were left on an orbital shaker until a uniform color in the well was observed. Cell adhesion was determined by measuring the optical density at 570 nm with results normalized to Matrigel (100%).

Cell growth. A solution containing 3×10^5 cells was used to seed the TCPS surface of organ culture dishes, coated with different concentrations of VN (VN0, VN2.5, VN5, and VN10), in triplicates. Cells were counted on days 1 and 7. Briefly, cultures were washed with 1× PBS and cells dissociated with 0.25% trypsin/ethylenediaminetetraacetic acid (Invitrogen). The total cell number was determined using a nucleocounter NC-100 (ChemoMetec).

In vitro differentiation assay (embryoid body formation) and reverse transcribed-polymerase chain reaction analysis. To determine whether HES-3 cells cultured on VN with mTeSR1 media retain their ability to differentiate into the three germ layers, confluent HES-3 cells grown on VN were removed using a cell scraper to form random-sized embryoid bodies (EBs). These were grown in suspension for 7 days and replated on 0.1% gelatinized plates for 14 days with a media change every 2 days. Total ribonucleic acid (RNA) was extracted from EBs after 21 days culture using an RNA extraction kit (Qiagen) in accordance with the manufacturer's instructions. Purity and concentration of RNA was quantified using an ND-1000 Spectrophotometer (Nanodrop Technologies). The RNA was reverse transcribed with polymerase chain reaction (RT-PCR) using oligo dT primers and superscript II reverse transcriptase (Promega) into complementary DNA. PCR (Biorad) was carried out with primers specific to the three germ layers. The endodermal lineage was represented by alpha-feto protein (*AFP*), the mesodermal lineage by Msh homeobox 1, heart- and neural crest derivatives-expressed protein 1 (MSX1), and the ectoderm lineage by neurofilament heavy chain (*NFH*). *OCT-4* (undifferentiated marker) and *GAPDH* (house keeping gene) were used as controls (Table 1). In parallel, RNA was harvested from undifferentiated HES-3 cells for comparison to differentiated cells. The amplified products were observed with ethidium bromide-stained 1% agarose gels.

In vivo differentiation assay (teratoma analysis). To confirm the pluripotentiality of hESCs cultured on the various substrates, an intramuscular injection of cells was given to SCID mice and the formation of tumors determined 10 weeks post injection. Briefly, HES-3 cells cultured on VN for 18 passages with either CM or mTeSR1 media were harvested by trypsin, and an intramuscular injection (hamstring muscle) of 5×10^6 cells in 50 μL of sterile PBS was delivered to 4-week-old female SCID mice with a sterile 22G needle. After 10 weeks, mice were sacrificed and the tumors dissected, fixed in 10% formalin, embedded in paraffin, and then sectioned and stained with hematoxylin and eosin (H&E). The presence of germ layers (ectoderm, mesoderm, and endoderm) in the tumors was assessed by immunohistochemistry, using the primary antibodies: polyclonal rabbit anti-cytokeratin (1:250), Desmin Clone 33 (1:100), and Rabbit anti-glial fibrillary acidic protein (*GFAP*) (1:250) (Dako) with matching undiluted secondary antibodies: EnVision+HRP anti-rabbit and EnVision+HRP anti-mouse (Dako). Sections were then incubated with Chromogen DAB (Dako) and counter stained with hematoxylin.

Table 1. Primer Sequences for Reverse Transcribed Polymerase Chain Reaction

Target gene	*Ascension no.*	*Forward (5′–3′)*	*Reverse (5′–3′)*	*Size (bp)*
AFP	NM_001134	AAA TGC GTT TCT CGT TGC	CAG CCT CAA GTT GTT CCT CT	428
MSX1	NM_002448	CCT TCC CTT TAA CCC TCA CAC	CCG ATT TCT CTG CGC TTT TC	287
NFH	NM_021076	TGA ACA CAG ACG CTA TGC GCT CAG	CAC CTT TAT GTG AGT GGA CAC AGA	398
HAND1	NM_004821	TGC CTG AGA AAG AGA ACC AG	ATG GCA GGA TGA ACA AAC AC	274
Nanog	NM_024865	ACC AGA ACT GTG TTC TCT TCC ACC	GGT TGC TCC AGG TTG AAT TGT TCC	330
OCT-4	NM_002701	CGR GAA GCT GGA GAA GGA GAA GCT G	AAG GGC CGC AGC TTA CAC ATG TTC	242
GAPDH	NM_002046	TGG TAT CGT GGA AGG ACT CA	CCT GCT TCA CCA CCT TCT TG	250

Karyotypic stability. To assess chromosomal stability of hESCs cultured on VN for more than five passages, karyotyping of 20 colonies using BrdU/colcemid was performed by the Cytogenetics Laboratories at the Department of Obstetrics and Gynaecology, Kandang Kerbau Women's and Children's Hospital, Singapore.

Surface characterization

Adsorption and desorption kinetics were measured by Ponceau S staining. VN-coated organ culture dishes: VN0, VN2.5, VN5, VN10, and VN20, prepared as described above for the cell culture substrates, were exposed to Ponceau S staining solution (Sigma-Aldrich) for 15 h at room temperature.[26,27] After three rinses in water and blow-drying, 400 μL of 0.1 M NaOH (Goodrich Chemical Enterprise) were added to each TCPS substrate. The samples were then shaken gently for 20 min, allowing desorption of bound Ponceau S stain from the sample surface.[27] TCPS samples were run in triplicates, yielding six 200 μL aliquots per VN concentration. Each aliquot was placed in a flat-bottom 96-well plate and neutralized with 15 μL of 50% acetic acid (J.T. Baker). Colorimetric adsorption was measured at 515 nm on an Infinite® 200 Multimode Microplate Reader (Tecan). This was compared with a standard curve generated using Ponceau S concentrations ranging from 0 to 10 μg/mL in 5% (w/v) acetic acid. The Ponceau S solution density was converted into molarity, which was used to calculate density of stain adsorbed to TCPS-immobilized VN. Ponceau S staining was similarly used to determine VN adsorption kinetics at 4°C, where TCPS samples were incubated with 5 μg/mL VN for different times. For VN desorption, TCPS samples were coated with 5 μg/mL VN solution overnight (15 h) at 4°C. Samples were then rinsed once with water and blow-dried. They were then incubated with 1 mL of PBS at 37°C at different times and subsequently stained with Ponceau S, as described above.

Quantification of VN adsorbed on TCPS by Bradford assay. VN adsorbed to TCPS was quantified by its depletion from the depositing solution by using a modified Bradford assay[28,29] to measure the VN concentration in PBS before and after coating of TCPS. Dye reagent was prepared according to Bradford[28] and TCPS substrates were incubated with VN solutions at concentrations of 0, 5, 10, 15, and 20 μg/mL for 15 h at 4°C, as described above. After coating, 100 μL VN in PBS supernatant from triplicate samples for each concentration were combined into one 1.5 mL glass vial and 1.2 mL of Bradford dye reagent solution was added. The contents were mixed for 5 min and six 200 μL aliquots of each solution were then pipetted into a flat-bottom 96-well plate to measure their absorbance at 590 nm (A590) and 450 nm (A450) on a Tecan plate reader. This process was carried out within 10–20 min, to minimize nonspecific adsorption of VN during handling of the protein solution. For each well, the A590/A450 ratio mitigates fluctuations arising from differences in solution volume. This was normalized by subtracting the average A590/A450 value for PBS (0 μg/mL).[29] An assay of VN solutions with concentrations of 0, 5, 10, 15, and 20 μg/mL was used to plot the standard curve of A590/A450 versus VN concentrations. The VN solution concentrations before TCPS coating were taken as 0, 5, 10, 15, and 20 μg/mL. The A590/A450 values obtained from VN solutions used to coat TCPS were compared with the standard curve, yielding the depletion in VN solution concentration. These values were then used to calculate VN adsorbed to TCPS and its corresponding surface density. For the latter, the coated surface area of the 60 mm center-well organ culture dishes was estimated at 3.5 cm^2, which includes the base and a rim extending 1.5 mm above it.

XPS measurements. VN0, VN2.5, VN5, VN10, and VN20 were prepared as described above. Their surface chemical composition was determined using a Theta Probe X-ray photoelectron spectrometer (Thermo Fisher Scientific), equipped with an aluminium anode (15 kV, 100 W), and a quartz monochromator. The latter was set to a 50° take-off angle, measured from the normal to the plane of the sample surface, yielding a probing depth of ~5 nm. Detailed scans of the N1s, O1s, and C1s peaks were performed on each sample, taking data from a 400 μm^2 spot and using a pass energy of 40 eV. Detailed scans were repeated as follows: 20 times for C1s, 15 times for O1s, and 20 times for N1s. A wide scan (binding energy from 0 to 1300 eV) was then performed with pass energy of 200 eV. Peaks were fitted with a mixed Lorentz-Gaussian function. Deconvolution of the C1s signal reveals five peaks: aromatic C (284.8–284.9 eV), C-C (285 eV), C-NH_2 (285.5–286.0 eV), C-O (287.6–288.4 eV), and C=O (287.6–288.4 eV).

AFM measurements. Surface topography was assessed by AFM profilometry, as a measure of the hESC responses to VN-coated TCPS. Bare TCPS and VN0, VN2.5, VN5, VN10, and VN20 were measured after blow-drying in ambient conditions using a Bioscope I microscope equipped with a NanoScope IIIa controller and a low noise scanner (Digital Instruments; Veeco Metrology Group). PointProbe® Plus

noncontact high resonance frequency (PPP-NCH) silicon cantilevers (Nanosensors) were used for intermittent-contact (also known as tapping) mode operation to obtain high-resolution images of the samples. Scan rates ranged from 0.75 to 1 Hz, and free amplitude (A_0) setpoint values were ~1.6 V. Images of the TCPS surface morphology and the corresponding VN-coated surfaces were taken at 85%–90% of the free amplitude. Roughness analysis was performed by Nanoscope software version v5.12rb. Briefly, two-dimensional AFM height maps can be used to determine the arithmetic roughness (R_a) of the bare and VN-coated TCPS surfaces. The arithmetic roughness, R_a, describes the absolute

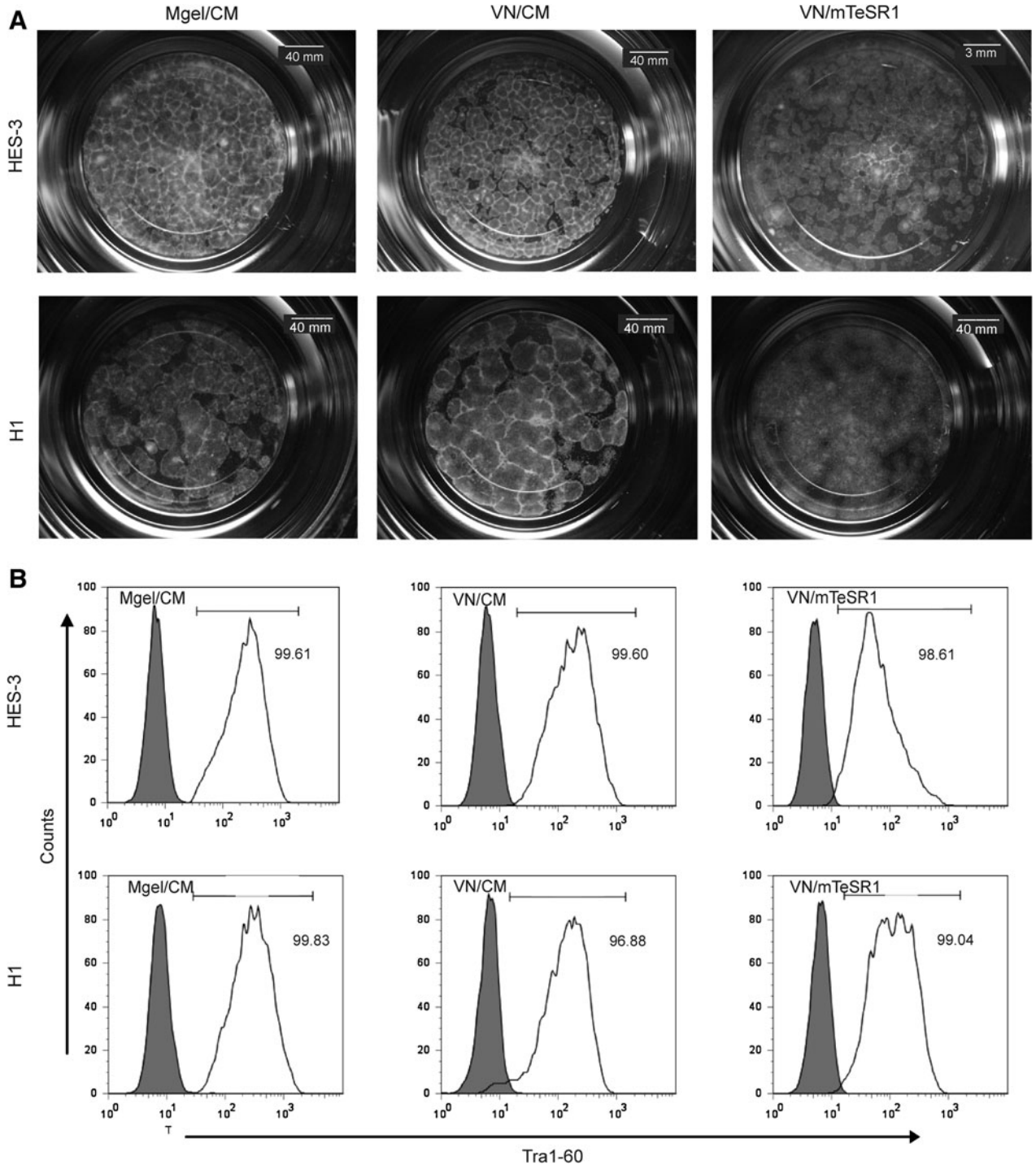

FIG. 1. Characterization of HES-3 and H1 cells cultured on VN5 in either conditioned medium (CM) or mTeSR1 medium at passage 15. **(A)** Representative pictures after 1 week of culture; cells retained the typical stem cells morphology and **(B)** fluorescence-activated cell sorting analysis of *Tra1-60* surface marker and cells were grown on Matrigel as a positive control. Shaded bar represents isotype control expression and unshaded bar represents *Tral-60* marker expression. Both cell lines expressed >90% positive for *Tra1-60* markers, demonstrating that cells are able to adapt to VN coating.

value of the surface height, measured relative to a two-dimensional plane, set at the average sample height. R_a was calculated from the entire ($4\times4\,\mu m$) image or several smaller areas ($2\times2\,\mu m$) within the image. Phase data records variations in the cantilever oscillation, reflecting changes in surface rigidity and viscoelasticity. This was used to improve the contrast between adsorbed VN aggregates and the TCPS substrate surface. Bearing analysis was carried out using Nanoscope software version v5.12rb.

Colloidal gold staining of VN adsorbed to TCPS. To evaluate the uniformity of VN adsorbed to TCPS over length scales of mm–cm, the surface-bound protein was detected by the Colloidal Gold Total Protein Stain (Bio-Rad). VN0, VN2.5, VN5, VN10, and VN20 were prepared as described above. After rinsing and blow-drying, the surfaces were incubated overnight in Colloidal Gold stain at room temperature. They were then rinsed with water, blow-dried, and photographed.

Statistical analysis. Data values are reported as a mean and a standard deviation. Graphs were plotted and data were transformed using Sigmaplot software. One-way analysis of variance was applied to compare differences across the groups and $p < 0.05$ was considered as significant.

Results

Stable expansion and analysis of HES-3 and H1 cells cultured on VN5

The development of a defined matrix to support long-term hESC expansion is important for potential therapeutic applications. To determine whether VN is a suitable substrate, HES-3 and H1 cells were cultured for >10 passages on VN5 in either CM or mTeSR1 media. Cells grown on Matrigel in CM served as a positive control. Images of cells cultured at passage 15 showed that both hESC lines retained an undifferentiated morphology that was characterized by the formation of compact colonies with distinct boundaries and a high nucleus to cytoplasmic ratio (Fig. 1A). Cells cultured with mTeSR1 appeared to have less distinct boundaries as compared to cells cultured in CM. However, this difference was not reflected in the expression level of the pluripotent marker *Tra1-60* (Fig. 1B) and *OCT-4*, with >90% positive expression after 12 passages (Table 2). Quantitative RT-PCR of HES-3 cells cultured on VN5 and Matrigel at passage 20 revealed similar levels of *Nanog* and *OCT-4* mRNA expression, which confirms their pluripotency (Supplementary Fig. S1 and Supplementary Table S1, available online at www.liebertonline.com). The population doubling time of HES-3 cells was assessed from the exponential region of a growth curve, measured over 7 days (Supplementary Fig. S2, available online at www.liebert online.com). Refer to supplemental materials and methods section for the description of quantitative PCR and population doubling time analysis. Results show that the doubling times are 32 and 25 h for VN5 and Matrigel, respectively.

Karyotype analysis was performed on HES-3 (46, XX) at passage 9 and H1 (46, XY) at passage 5 from the VN5 in mTeSR1 platform and the cells were found to be of a normal diploid karyotype (Fig. 2A). Moreover, FACS and karyotype analyses were also repeated on passage 30 hESC, with >90% of the cells continuing to express *Tra1-60* and *OCT-4* with a normal diploid karyotype (data not shown).

A robust tri-germ layer differentiation potential is also a hallmark of pluripotent hESCs. After VN propagation for 25 passages, HES-3 cells were induced to differentiate through EBs and the presence of ectoderm, mesoderm, and endoderm probed by PCR (Fig. 2B). After 21 days of differentiation, HES-3 express the mRNA transcripts for *AFP* (endoderm), *NFH* (ectoderm), and *MSX1* (mesoderm) that are absent in undifferentiated cells (Fig. 2B). As expected, expression of the pluripotent markers *Nanog* and *OCT-4* were suppressed when the cells were induced to differentiate.

As a final test of pluripotency, the tumorgenicity of HES-3 was investigated *in vivo*. When cultured on VN5 for 18 passages in mTeSR1 medium and then injected into the muscle of SCID mice, a teratoma formed contained structures from all three germ layers, as determined by H&E and immunohistochemical staining (Fig. 2C, D). Ectoderm (neural epithelium and pigmented epithelium), mesoderm (bone and cartilage), and endoderm (gut epithelium) were clearly visible by H&E. Similarly, the presence of *GFAP*-positive intermediate filaments (ectoderm), desmin-positive muscle (mesoderm), and cytokeratin-positive epithelium (endoderm) was confirmed by immunohistochemistry.

Taken together, these data suggest that VN5 combined with mTeSR1 medium is able to support the long-term propagation of undifferentiated, pluripotent hESCs. Notably, similar results were also found for induced pluripotent stem cell (IMR90) that could be readily propagated on VN5 mTeSR1 medium for over five passages (data not shown).

Table 2. Tra1-60 and OCT-4 Marker Expression for HES-3 on VN5

	Tra1-60			*OCT-4*		
Passage	*Matrigel/CM*	*VN/CM*	*VN/mTeSR1*	*Matrigel/CM*	*VN/CM*	*VN/mTeSR1*
P2	91.0	96.0	97.0	93.8	93.5	96.3
P4	98.9	93.0	98.0	89.8	90.7	91.9
P6	94.2	98.0	95.2	98.8	93.0	95.9
P8	95.0	99.2	98.6	89.4	97.4	92.7
P10	96.0	97.6	97.0	95.3	96.6	96.2
P12	94.0	98.3	99.0	97.1	93.4	95.3

Cells maintain >90% positive for both markers expression for 12 passages.
CM, conditioned medium; VN, vitronectin.

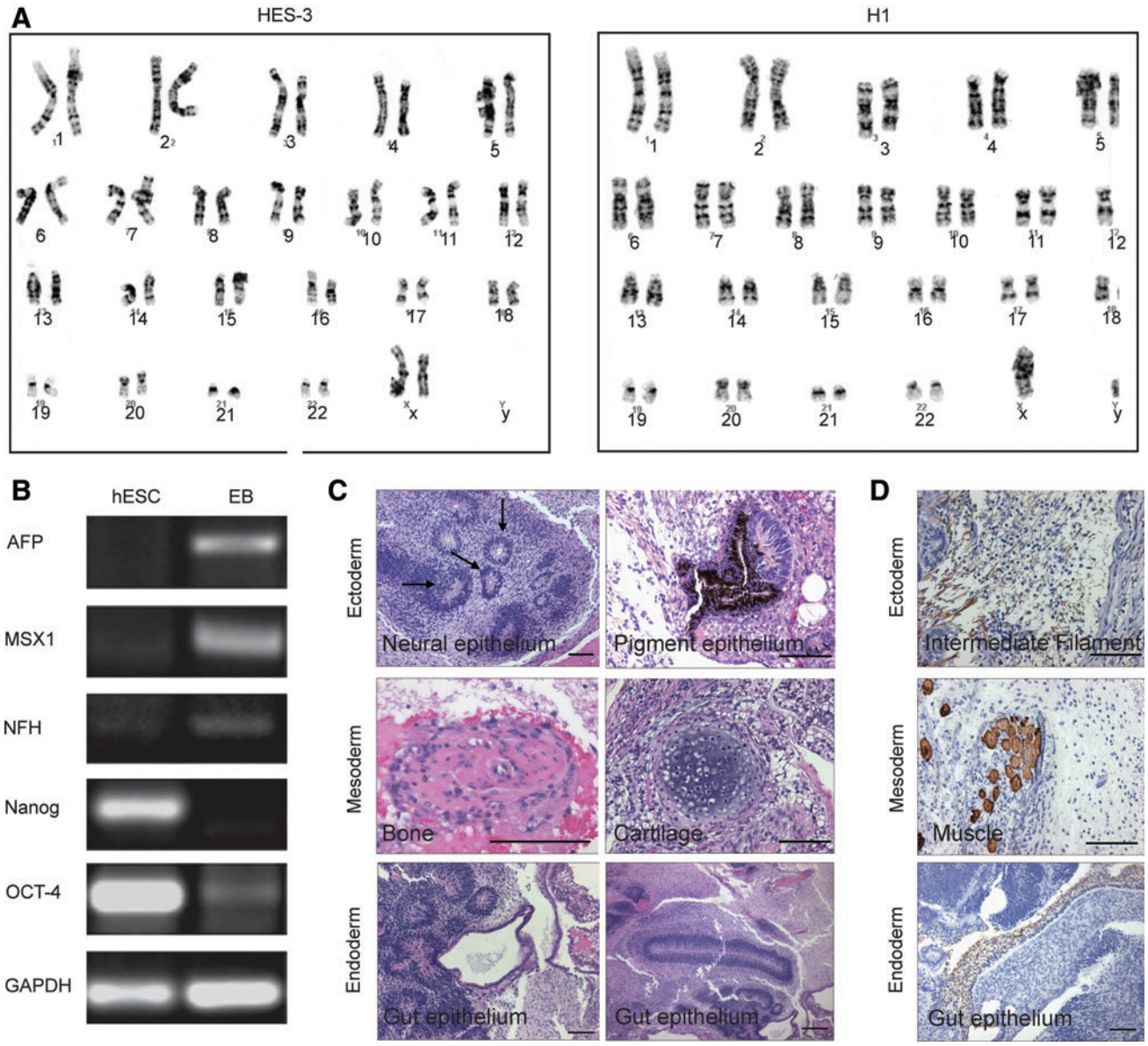

FIG. 2. HES-3 and H1 cells cultured on VN5 with mTeSR1 media were analyzed by karyotyping, embryoid body (EB) differentiation, and teratoma assay. **(A)** No chromosomal abnormality was observed in passage 9 and 5 of HES-3 and H1 cells, respectively, and they retained the normal diploid, 46, XY and 46, XX karyotype. **(B)** Reverse transcribed polymerase chain reaction analysis of EB-differentiated passage 25 HES-3 cells showed expression of alpha-feto protein (*AFP*) (endoderm), *MSX1* (mesoderm), and neurofilament heavy chain (*NFH*) (ectoderm) genes from the three germ layers that were previously absent in the undifferentiated cells. *OCT-4* marker diminished after 21 days of differentiation and *GAPDH* as house keeping gene. **(C)** Passage 18 HES-3 cells were injected intramuscularly into the rear limbs of SCID mice. Tissues representing the three germ layers were observed with hematoxylin and eosin staining. Neural epithelium (marked with arrows) and pigmented epithelium representing ectoderm lineage; bone and cartilage representing mesoderm lineage and gut epithelium representing endoderm lineage. **(D)** Teratoma was also stained with antibody for *GFAP* (ectoderm), desmin (mesoderm), and cytokeratin (endoderm). Scale bar = 100 μm. Color images available online at www.liebertonline.com/ten.

Short-term biological response to different VN surface density

Having established a defined condition for hESC culture, we sought to assess the variation in bioresponse arising from changes in the VN surface density. Several VN solution concentrations were used to coat TCPS by overnight incubation at 4°C. Cell attachment on these surfaces was compared across a range of VN densities in CM and mTeSR1 media (Fig. 3A). For all VN surface densities, cells attach in a VN density-dependent manner, with the highest number of attached cells resulting from the highest VN density. Notably, in CM, the cell density plateaus at concentrations above 1.25 μg/mL, with approximately two- to four-fold more cells attached in the presence of mTeSR1 as compared to CM.

As significant differences in cell attachment to VN-coated TCPS were observed over a 45 min period, we next chose to examine hESC attachment and proliferation at 1 and 7 days

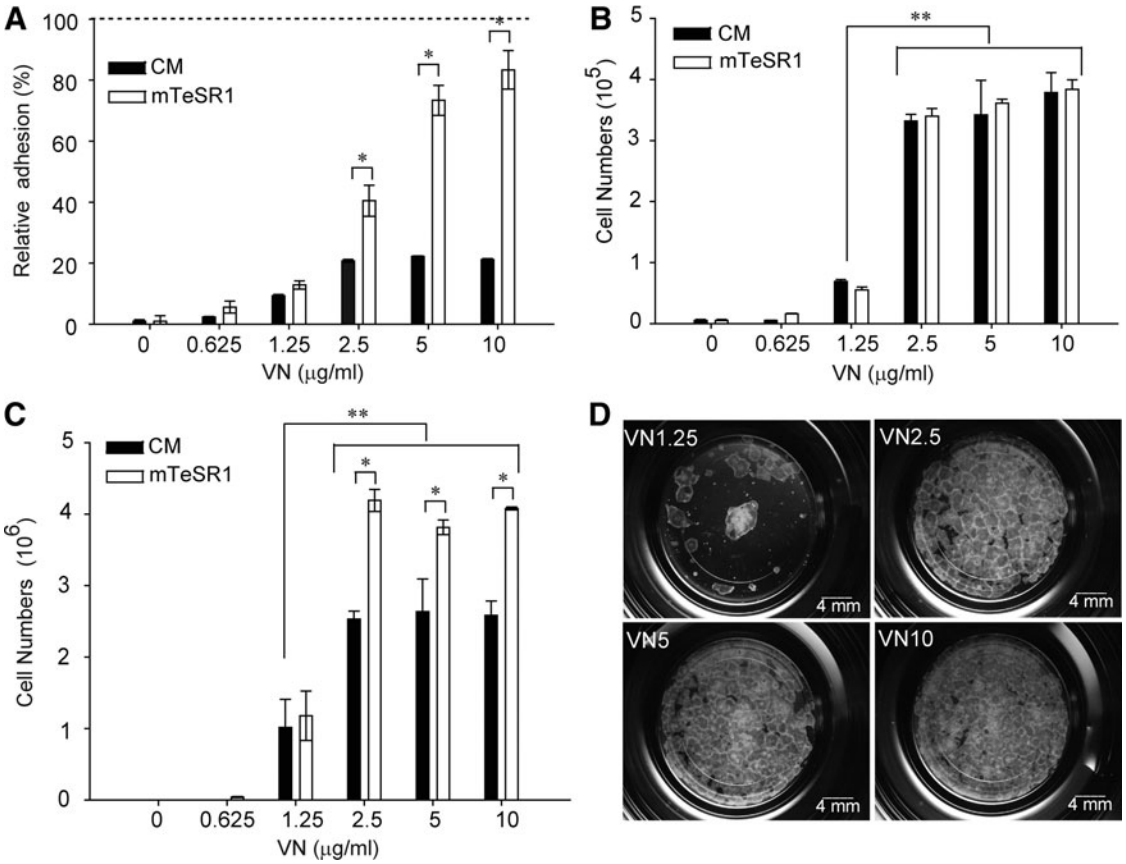

FIG. 3. Short-term adhesion assay on different VN-coated TCPS with HES-3 cells. **(A)** Forty-five minutes of adhesion assay were done with HES-3 either with CM or mTeSR1. Cell numbers were normalized to cell adhering to Matrigel surface (taken as 100%), as represented by the dashed line. $*p < 0.05$. **(B)** About 3×10^5 cells were seeded and a cell count was performed at day 1 after seeding; number of cells attached to <VN1.25 was insignificant as compared to the rest of the conditions. **(C)** After 1 week of culture, cell number was similar in VN2.5, VN5, and VN10, but the number of cells from VN1.25 was significantly lower than the rest. Cultures from VN1.25 did not reach confluence at day 7. $*p < 0.05$, cells cultured on CM and mTeSR1 media have significant differences. $**p < 0.001$, significant differences between cultures from VN1.25 and ≥VN2.5. Data are expressed as mean ± standard deviation ($n = 3$). **(D)** Day 7 representative pictures of HES-3 cells on TCPS coated with different VN concentration. VN1.25 did not support robust cell expansion as well as the rest; culture did not reach confluence at day 7.

(Fig. 3B, C). In contrast to the 45 min assay, at day 1 no differences in cell number were observed for both media treatments. There was, however, a similar VN density-effect between 45 min and 1 day with approximately threefold more cells in the ≥VN2.5 condition, when compared to VN1.25. Notably, when hESCs were cultured for 7 days at various VN densities, ≥VN2.5 was required for maximum proliferation; however, significant growth differences were observed between CM and mTeSR1 media, with mTeSR1 significantly outperforming CM (~30%).

The VN density threshold of 2.5 μg/mL, capable of supporting hESC attachment and expansion, was also evident from photomicrographs taken after 1 week in culture (Fig. 3D). Cells cultured on ≥VN2.5 had the typical mosaic/cobblestone appearance of confluent hESC, as compared to cells cultured <VN2.5 that were sparsely attached and failed to grow.

Long-term biological response to different VN surface densities

To fully evaluate the threshold VN surface density suitable for the long-term maintenance of pluripotent hESC, HES-3 cells were cultured for greater than five passages in mTeSR1 media. Pluripotency was then assessed by FACS, EB differentiation, and teratoma formation. Initially, cells cultured on VN1.25, VN2.5, and VN5 underwent a period of adaptation,[27,28] which was reflected by decreased expression of pluripotent markers at passage 1 (Table 3). After subsequent passaging, cultures at passage 2–6 were >90% positive for *Tra1-60* and *OCT-4* (Fig. 4A and Table 2). These levels were similar to those observed for cells maintained on Matrigel.

Differentiation was then assessed by RT-PCR for germline markers in EBs. Cells cultured on VN1.25 failed to expand sufficiently for differentiation assays and were not analyzed further by either EB or teratoma formation. However, cells readily expanded on VN2.5, with differentiation assays showing the presence of mRNA transcripts for *AFP* (endoderm), *Hand1* (mesoderm), and *NFH* (ectoderm) and the absence of *Nanog* and *OCT-4* genes (Fig. 4B). Importantly, despite their *in vitro* differentiation potential, cells cultured on VN2.5 failed to form a teratoma when transplanted into the muscle pouch of a SCID mouse (data not shown). As previously shown in Figures 1 and 2, cells cultured on VN5

Table 3. Tra1-60 and OCT-4 Marker Expression for HES-3 Cells Cultured on VN1.25, VN2.5, or VN5

	Tra1-60			*OCT-4*		
VN (μg/mL)	*1.25*	*2.5*	*5*	*1.25*	*2.5*	*5*
P1	85.0	83.2	89.3	90.0	76.6	89.0
P2	95.0	95.7	93.4	96.0	91.6	86.2
P3	94.7	99.6	99.7	90.0	92.9	95.7
P4	96.0	98.0	99.3	93.0	92.0	96.0
P5	99.4	99.5	99.8	96.4	96.0	93.1
P6	99.4	99.6	97.3	91.2	95.1	89.0

Cells maintained high levels of expression for 6 weeks.

maintained all the hESC characteristics of growth, differentiation, and teratoma formation. Further, hESC culture on VN1.25 and VN2.5 maintained normal karyotypes over five passages (Fig. 4C, D).

Surface characterization

Results from both the Bradford protein assay and Ponceau S staining (Fig. 5A and Fig. 5B, respectively) show similar trends for the adsorbed VN surface density versus the depositing solution concentration: a steady increase in surface-adsorbed VN with increasing solution concentration that reaches a plateau for >VN10. Adsorption and desorption kinetics (Fig. 5C, D) were modeled using an exponential time dependence. Modeling the data with an exponential in the square root of time, as proposed by Granick,[30–32] does not improve the fit. The associated fitting parameters (Table 4) indicate an adsorption time constant of $\sim$1 h and a desorption time constant of $\sim$4 h. The latter may not accurately represent surface depletion in actual cell culture conditions, where VN desorption is influenced by competing adsorption from other proteins. The y_0 parameter physically represents the VN protein that remains bound to TCPS after a desorption time of 2 days, and Figure 5D shows that only about 25% of the adsorbed VN is desorbed from the TCPS substrate after 48 h exposure to PBS. While 75% of VN adsorbed to TCPS after 2 days may arise from VN re-adsorbed from the PBS solution, this is mostly attributed to VN remaining durably bound to the TCPS substrate.

XPS detects the surface chemical composition of VN-coated TCPS, with data showing the presence of nitrogen, C-NH_2, C-O, and C=O bonds (Fig. 6A). The increasing signal from N and O atoms with depositing solution concentration indicates a monotonic increase in VN surface density, which reaches saturation for depositing solution concentrations >VN10, reproduces the same trend as observed with Ponceau S surface staining and Bradford quantification of the surface-adsorbed protein (Fig. 5A, B) and independently confirming the dependence of surface-adsorbed VN on depositing solution concentration.

AFM height images depict surface profilometry of the cell culture substrate. Bare TCPS shows an intrinsic, structured surface roughness, consisting of random line features that are presumably introduced by the tissue culture plates' manufacturing process. These substrate features are observed across all samples, from bare to TCPS coated from 0, 2.5, 5, 10, and 20 μg/mL VN (Fig. 6B–G), The TCPS morphology remains unchanged after exposure to PBS solution alone, implying that the features associated with VN aggregates, as observed on VN2.5, VN5, or VN10, are not an artefact generated by the exposure of TCPS to PBS solution (Fig. 6C). The surface roughness, Ra, of the bare TCPS substrates was found to range from 2.7 to 3.2 nm. Deposited VN aggregates, in the form of spot-like features, are visible on VN2.5 to VN10 (Fig. 6D–F). AFM phase images offer an enhanced contrast, improving the visibility of adsorbed VN aggregates, as seen on VN2.5 (Fig. 6I). A higher magnification of a selected area in Figure 6I (VN2.5) is shown in Figure 6J. The absence of spot-like features, associated with VN aggregates, on the AFM phase image of bare TCPS (Fig. 6H) confirms that these arise from adsorbed VN. Adsorbed VN aggregates did not significantly increase the Ra value for coated samples beyond the range quoted above. Finally, the AFM profilometry of VN20 shows a loss in resolution, whose physical origin remains unexplained.

Colloidal gold staining confirms that the surface density of adsorbed VN increases with concentration of the depositing solution (Fig. 6K–P). The sample shown in Figure 6K is indistinguishable from the bare TCPS. This demonstrates the absence of colloidal gold staining on a substrate uncoated with VN. As the depositing VN solution concentration is increased, the samples shown in Figure 6L do not show any stain, whereas Figure 6M, which shows samples coated with 5 μg/mL VN solution, shows a barely discernible stain. Figure 6N–P, which shows samples from VN10, VN15, and VN20, respectively, shows a discernible and increasing colloidal gold stain, whose uniformity indicates that VN adsorbed to the surface of TCPS is homogeneous, when averaged over length scales ranging from hundreds of microns to millimeters.

Bearing analysis integrates the height measured by AFM profilometry over a two-dimensional map of the sample surface. This may be used to calculate the volume under the sample surface and thus derive an estimate of the protein volume required to coat 95% of the surface features.[33,34] The volume required to fill in the TCPS surface roughness, leaving only 5%, by area, of its highest features exposed was calculated to be 0.22 μm^3 from a typical region of bare TCPS. Projecting this volume into a film over a two-dimensional area of 16 μm^2, this corresponds to an average coating thickness of 14 nm or a VN surface density of 1.7 $\mu g/cm^2$ (assuming VN protein density as 1.2 g/cm^3).[35]

Quantification of surface-adsorbed VN

Surface-adsorbed VN is quantified by measuring the depletion of the depositing solution concentration. Completing Bradford assay measurement of protein solution concentration within 10–20 min, which is an order of magnitude smaller than the several hours required to saturate nonspecific adsorption of VN on TCPS (Fig. 5C), effectively minimized losses of VN by nonspecific adsorption. This measurement estimates the surface density of VN deposited solutions of VN ranging from 5 to 20 μg/mL. These solution concentrations resulted in surface-adsorbed VN of 250 ng/cm^2 (VN5) to 500 ng/cm^2 (VN20), respectively (Fig. 5A). Analysis of the bioresponse indicates that hESCs do not attach on <VN2.5 and (Fig. 3C, D) and long-term proliferation is not supported on <VN5. Thus, the minimum threshold

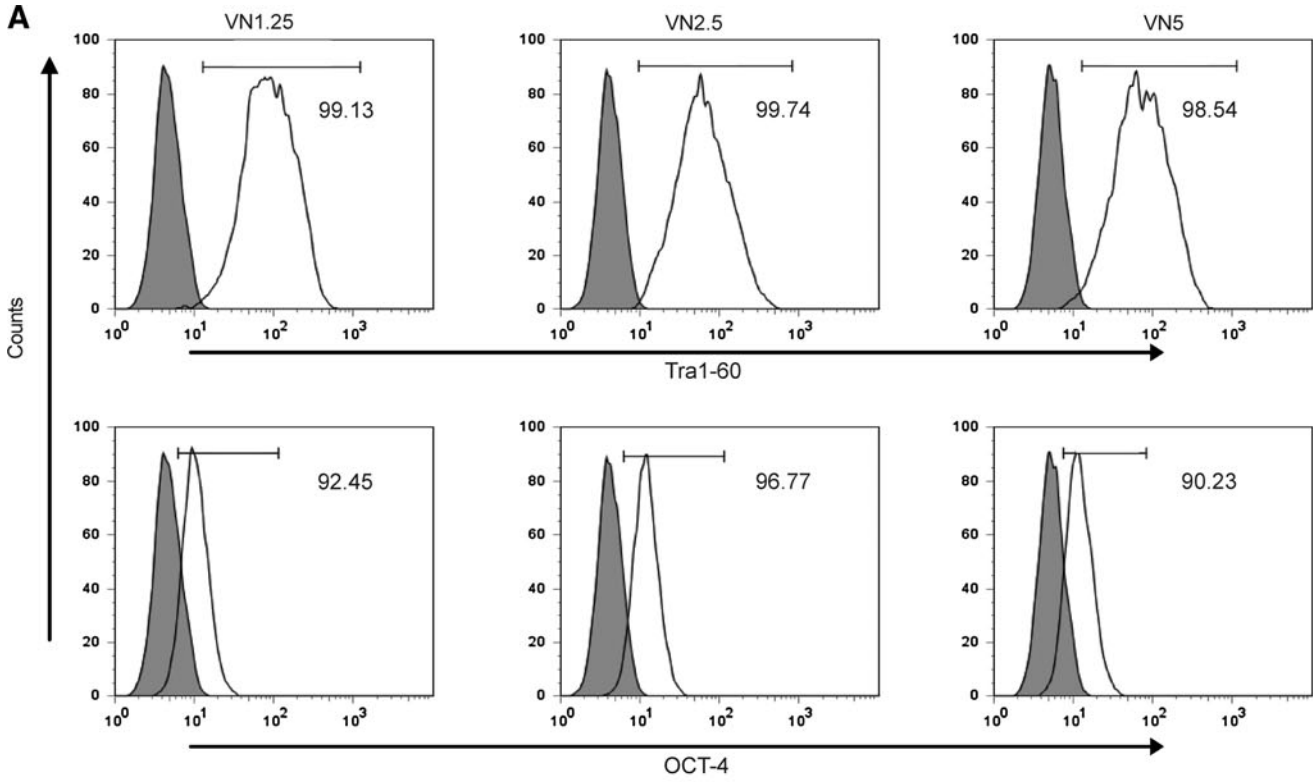
A
VN1.25
VN2.5
VN5
99.13
99.74
98.54
92.45
96.77
90.23
Counts
Tra1-60
OCT-4

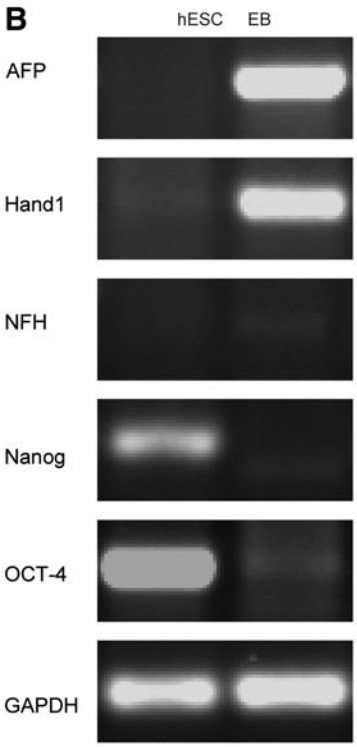
B
hESC
EB
AFP
Hand1
NFH
Nanog
OCT-4
GAPDH

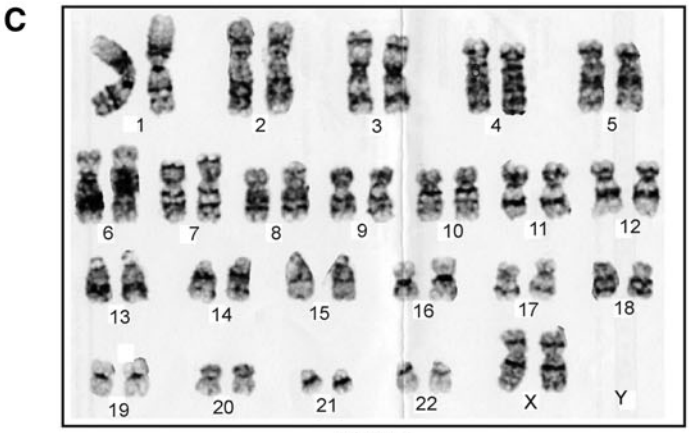
C
VN1.25

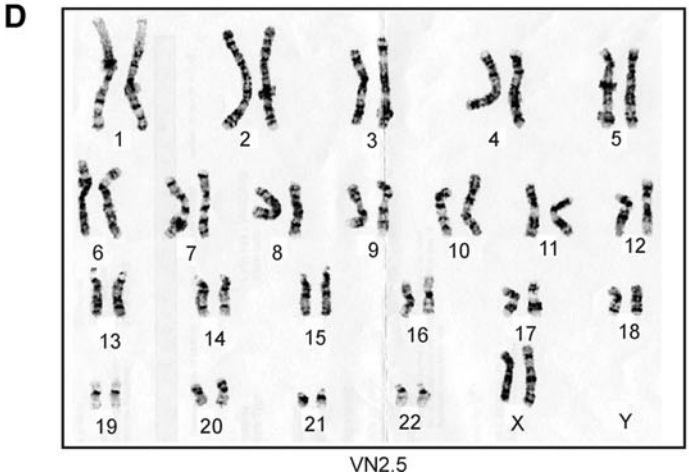
D
VN2.5

VN surface density, which is required for the long-term propagation of hESCs, is estimated at 250 ng/cm^2 (VN5).

Experimental data in Figure 5A allow a simple calculation of VN depletion from the depositing solution. From the surface density of VN adsorbed to TCPS, the reduction in solution concentration may be deduced. Given that 300 μL of 5 μg/mL solution contains 1.5 μg of VN and that 250 ng/cm^2 of surface-adsorbed VN on 3.5 cm^2 of TCPS is 0.88 μg, ~50% of VN in the solution is deposited onto TCPS. This is the case for VN solution concentrations up to 10 μg/mL. For higher VN concentrations, the lack of an increase in surface-adsorbed VN reduces its depletion in solution. For an initial solution concentration of 20 μg/mL, the final solution concentration after VN is deposited on TCPS is ~15 μg/mL, or 75% of the initial solution concentration. The staining uniformity of surface-adsorbed VN and AFM data indicate that this may be effectively considered as an average surface density, over length scales larger than tens of microns.

Discussion

Recent studies have demonstrated the ability of VN to support hESCs propagation, but they lack details concerning the characterization and quantification of VN on the culture surfaces.[15,17] In this study, we varied the concentration of VN in solution and determined the amount that adsorbed to TCPS with a view to developing a quantifiable platform on which to expand pluripotent hESC over multiple passages, and in a stable manner.

We showed that a threshold VN surface density of at least 250 ng/cm^2 (VN5) is required for the long-term expansion (>30 passages) of pluripotent hESCs in a serum-free defined medium (mTeSR1). Cells cultured at this VN threshold had sustained expression of *Tra1-60* and *OCT-4* at levels above 90%. The population doubling time for HES-3 cultured on VN5 is 32 h. For the same cells cultured on Matrigel, the doubling time is 25 h. These differences in cell growth rates are not associated with a loss in pluripotency for hESCs cultured on VN surfaces. They also retained the potential to differentiate to the three germ layers through EBs and readily formed teratomas when transplanted into the muscle pouch of SCID mice. Importantly, the cells had a normal diploid karyotype and they maintained a compact morphology. At VN surface densities below 250 ng/cm^2 cell attachment and proliferation were compromised and the cells failed to differentiate in EBs and were unable to develop teratomas *in vivo*.

Noteworthy is the finding that only 50% of the VN dissolved in PBS was able to adsorb to TCPS from VN solution concentrations ≤10 μg/mL. As the VN surface saturates, this waste increases, reaching ~75% from the higher initial solution concentration of 20 μg/mL. These findings may serve as process parameters, forming the basis of a scale-up system for hESCs, with a fully quantifiable, chemically defined culture conditions.

We also observed that hESCs cultured in mTeSR™ media achieved higher cell numbers after 1 week in culture than cells grown in CM. This observation was supported by Chin *et al.*, who reported that a defined medium such as mTeSR1 reduces the doubling time of hESCs to ~21 h, as compared to cells cultured in CM that require 28 h.[36] Another interesting observation was the absence of *in vivo* teratoma from the transplanted cells when cultured on VN2.5 with mTeSR1 media.

Previous studies by Braam *et al.* reported that VN adsorbed to TCPS from a solution containing 5 μg/mL is able to support hESC cultures and in another study, Rowland *et al.* coated TCPS with 10 μg/mL of human-plasma-purified VN for the culture of iPSCs (IMR90).[15,17] In both cases no surface characterization was performed to quantify the amount of VN bound to the surface. By comparison, in the present study we show that a VN threshold surface density of 250 ng/cm^2 (VN5) can be used as a xeno-free substrate for hESC culture. Although VN used in this study was purified from human plasma, this would serve as a bench mark for studies done with human recombinant VN in the future. More recently, Manton *et al.* demonstrated that a chimeric VN:insulin-like growth factor 1 complex when added into serum-free media could maintain pluripotent hESCs; however, in this study hESCs were cultured on a substrate of murine laminin that does not fulfill the requirements for a xeno-free culture platform.[37]

VN is known to synergize with numerous growth factors to maintain both embryonic and adult stem cells in an undifferentiated state.[38,39] Indeed, notable differences in the mitotic rate between embryonic and adult stem cells have been reported.[40] As such, there is a clear need to better understand the cellular context underlying hESC culture. An interesting aspect that merits further exploration is how ECM and growth factor signaling pathways interact in maintaining stem cell pluripotency.

Our characterization studies demonstrate that the long-term, stable propagation of hESCs is possible with VN5 and that this defined surface is a viable alternative to Matrigel. The threshold surface density is estimated at 250 ng/cm^2 of protein by assuming a linear dependence of adsorbed VN with solution concentration, as predicted by the Langmuir adsorption isotherm and corroborated by Ponceau S staining and the Bradford protein assay (Fig. 5A, B). Thus, VN is effective for promoting cell adhesion and supporting the expansion of pluripotent stem cells at surface densities well below its saturation, which is estimated at 500 ng/cm^2.

AFM image resolution was limited by the radius of the AFM probe tip, which is nominally 20 nm. This prevents the

FIG. 4. Long-term analysis of HES-3 cells cultured on TCPS coated from different VN concentration. **(A)** Representative Tra1-60 and OCT-4 marker expression by fluorescence-activated cell sorting at passage 5. HES-3 cells on VN1.25, VN2.5, and VN5 with mTeSR. Shaded bar represents isotype control expression and unshaded bar represents *Tra1-60* and *OCT-4* marker expression. Cells expressed >90% positive for these markers. **(B)** EB *in vitro* differentiation assay was done for passage 5 HES-3 cells cultured on VN2.5 with mTeSR1 medium. HES-3 cells were able to differentiate into the three germ layers with expression of *AFP* (endoderm), *Hand1* (mesoderm), and *NFH* (ectoderm) genes, downregulation of *Nanog* and *OCT-4* pluripotent markers, and *GAPDH* as house keeping gene. **(C)** Karyogram of HES-3 cells cultured on VN1.25 and **(D)** VN2.5 with mTeSR1 after five passages. No chromosomal abnormalities were observed in both conditions.

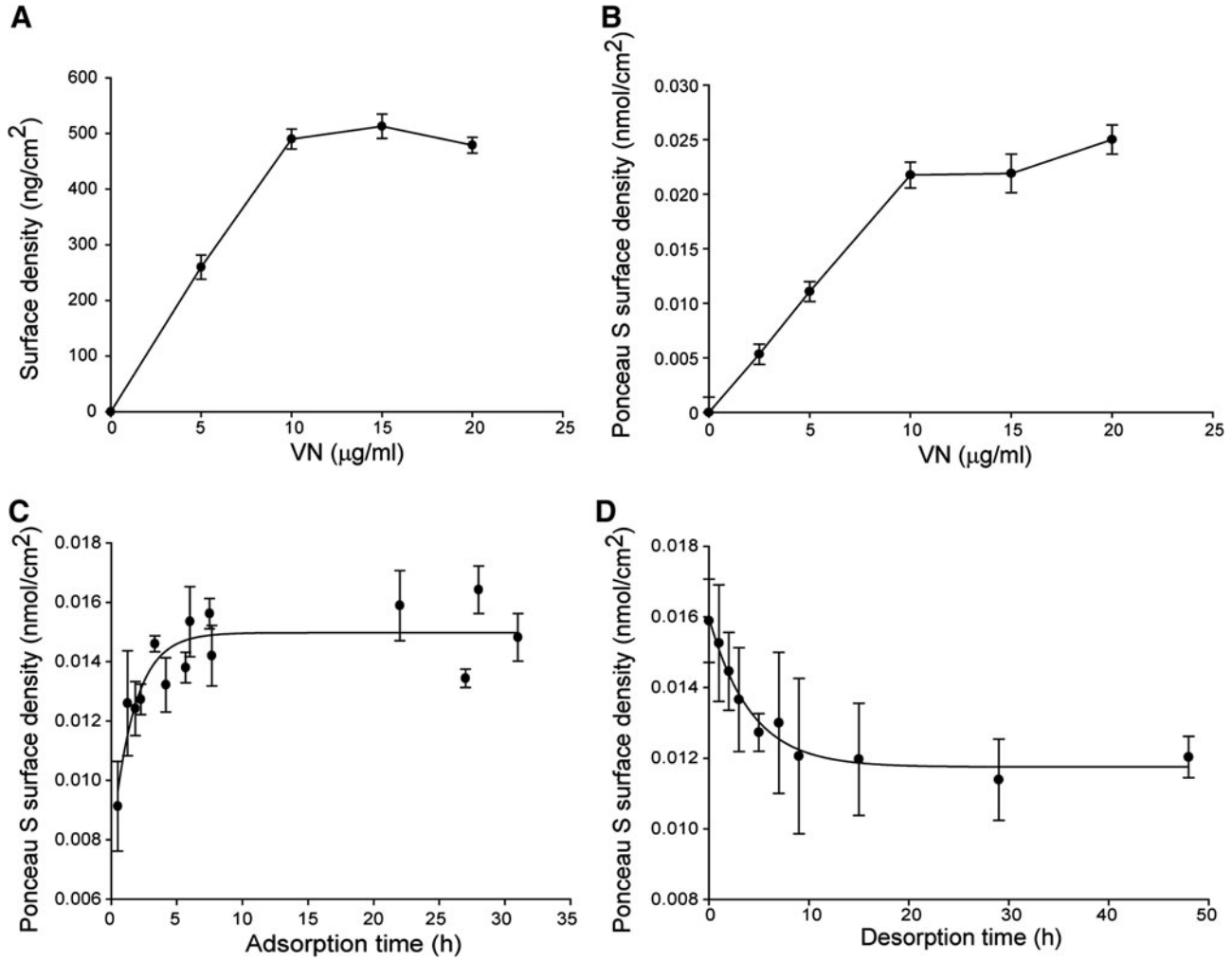

FIG. 5. **(A)** Quantification of VN adsorbed to TCPS, deduced from VN depletion in the depositing phosphate-buffered saline (PBS) as measured by Bradford assay. **(B)** Surface density of VN adsorbed to TCPS versus concentration of the depositing solution Ponceau S was used to stain VN on the coated surface. Both Bradford assay and Ponceau S staining showed that density plateau at VN10. **(C)** Ponceau S staining of VN adsorption kinetics onto VN5. **(D)** Ponceau S staining of VN5 desorption from TCPS. $n = 3, \pm$ standard error of the mean.

detection of individual VN molecules, which may be approximated by a cylinder of radius 3 nm and length 11 nm.[19] Larger VN aggregates appear as point-like asperities on the randomized line-feature background of the TCPS substrate. Only the height of VN aggregates is cited, since dimensions in the plane of the surface are convoluted with the tip diameter. Their size is comparable to that reported by Zhang *et al.*, for VN molecule aggregates adsorbed onto smooth mica surfaces.[23] Lynn *et al.* describe the formation of VN aggregates in solution and Izumi *et al.* report the presence of VN aggregates with a Stokes radius of 6.5 nm in human plasma.[19,41] Thus, the observed VN aggregates may have be adsorbed from solution or may be formed as VN adsorbs to TCPS. Higher VN solution concentrations may lead to its adsorption in a different configuration, potentially giving rise to the observed decrease in resolution when imaging VN20. This observation correlates with colloidal gold staining images (Fig. 6K–P). Colloidal gold staining, although not

Table 4. Equations, with x Representing the Ordinate and y, the Abscissa, with Fitting Parameters for Adsorption and Desorption Kinetics of Vitronectin on Tissue Culture Polystyrene

Data	*Equation*	A	y_0	T
Adsorption	$y = A(1 - \exp(-x/T))$	0.0146 ± 0.0003		1.2 ± 0.2
Desorption	$y = A \times \exp(-x/T) + y_0$	0.0042 ± 0.0003	0.0118 ± 0.0002	4.2 ± 0.7

Data and fitted curves shown in Figure 6. For adsorption, A reflects the maximum surface density of VN and T is the time constant. For desorption, A reflects the initial surface density of VN, T is the time constant, and y_0 reflects staining of nondesorbed VN.

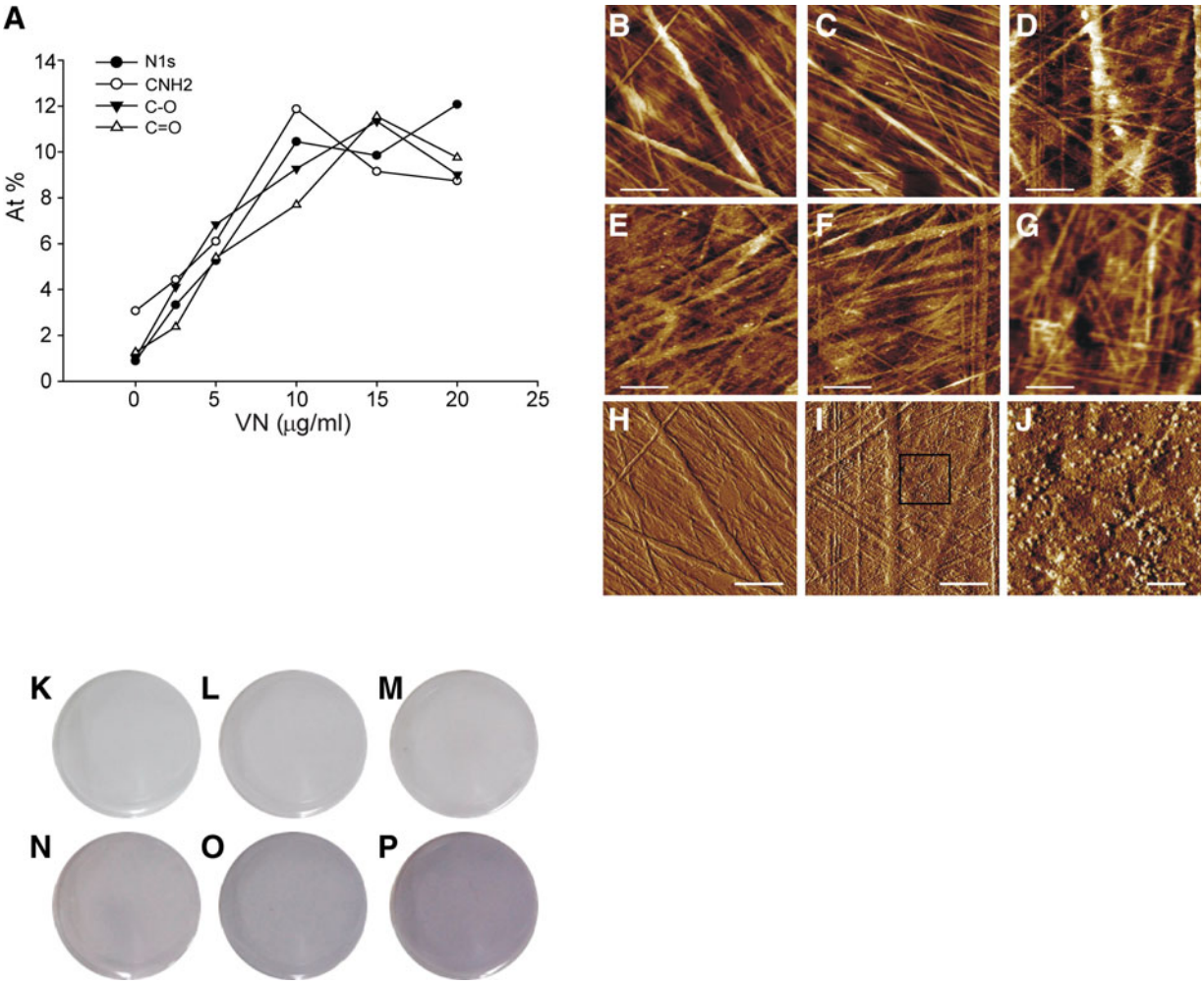

FIG. 6. **(A)** X-ray photoemission spectroscopy quantification of surface composition for TCPS coated with VN versus depositing solution concentration. Atomic force microscopy profilometry images, representing sample height, of **(B)** bare TCPS, **(C)** VNo, **(D)** VN2.5, **(E)** VN5, **(F)** VN10, and **(G)** VN20. **(H)** and **(I)** are images of phase data from same samples: **(B)** bare TCPS and **(D)** 2.5 μg/mL. Image **(J)** shows a closeup of the marked area on image **(I)**. The height range is 0–25 nm; the phase range is 0°–15°. The scale bar is 1 μm on all images except image **(J)**, where it is 200 nm. Colloidal gold staining of **(K)** VN0, **(L)** VN2.5, **(M)** VN5, **(N)** VN10, **(O)** VN15, and **(P)** VN20. The diameter of each disk is 15 mm. Color images available online at www.liebertonline.com/ten.

quantitative, may be used to discern increases in the adsorbed protein surface density. However, the increase in VN surface density deposited from solutions $\geq$10 μg/mL contrasts with Ponceau S staining, the Bradford assay, and XPS data.

An estimate of the minimum protein volume required for masking the roughness of the underlying substrate is obtained from bearing analysis of the AFM profile generated by bare TCPS. This yields a VN surface density of 1.7 μg/cm^2, which exceeds the highest quantified VN surface density, of $\sim$0.5 μg/cm^2 by a factor of three. Given that the adsorbed VN is not sufficient to fill in the roughness of the TCPS substrate surface, it is expected that only spot-like features associated with adsorbed VN aggregates are discernible.

We note that mTeSR1 is not a completely defined media, due to the presence of BSA. However, this is not expected to significantly alter our conclusion of a minimum threshold concentration of 5 μg/mL of VN to achieve a viable platform for long-term hESCs culture. A further examination of this threshold may be performed in a completely chemical defined xeno-free medium such as X-VIVO10. Although the field is moving toward the use of recombinant proteins, these proteins are cloned and expressed in animal cells that are a source of foreign antigen (Neu5Gc). Further, animal cells may provide an inappropriate glycosylation pattern to the protein of interest and thus render it inactive. Serum-derived proteins, despite being subject to lot-to-lot variability and the possibility of contamination from plasma, retain the biological activity of the protein. Future biotechnological innovations may provide the means to overcome these contradicting drawbacks in protein synthesis.[42]

The observation of a minimum VN surface density raises the issue of its efficiency and cost effectiveness within the context of large-scale industrial manufacturing processes. Characterization and quantification of defined substrates suitable for hESCs expansion will render the translation of this technology into a scaled-up process for generating clinical-grade stem cells more feasible and reliable.[20–22] As

described above, the nonspecific adsorption of VN on TCPS results in ~50% of VN in solution being deposited on the surface. Therefore, the production of large quantities of stem cells may benefit from an optimization of VN binding and VN bioactivity on these cell culture substrates.

Acknowledgments

This work was supported by the Joint Council Office, the Biomedical Research Council, the Science and Engineering Research Council, the Institute of Medical Biology, the Institute of Materials Research and Engineering, and the Bioprocessing Technology Institute of the Agency for Science, Technology and Research (A*STAR), Singapore.

Disclosure Statement

No competing financial interests exist.

References

1. Thomson, J.A., Itskovitz-Eldor, J., Shapiro, S.S., Waknitz, M.A., Swiergiel, J.J., Marshall, V.S., *et al.* Embryonic stem cell lines derived from human blastocysts. Science **282,** 1145, 1998.
2. Genbacev, O., Krtolica, A., Zdravkovic, P., Zdravkovic, T., Brunette, E., Powell, S., *et al.* Serum-free derivation of human embryonic stem cell lines on human placental fibroblast feeders. Fertil Steril **83,** 1517, 2005.
3. Choo, A.B.H., Padmanabhan, J., Chin, A.C.P., and Oh, S.K.W. Expansion of pluripotent human embryonic stem cells on human feeders. Biotechnol Bioeng **88,** 321, 2004.
4. Xu, C., Inokuma, M.S., Denham, J., Golds, K., Kundu, P., Gold, J.D., *et al.* Feeder-free growth of undifferentiated human embryonic stem cells. Nat Biotechnol **19,** 971, 2001.
5. Hakala, H., Rajala, K., Ojala, M., Panula, S., Areva, S., Kellomaki, M., *et al.* Comparison of biomaterials and extracellular matrices as a culture platform for multiple, independently derived human embryonic stem cell lines. Tissue Eng Part A **15,** 1775, 2009.
6. Nasonkin, I.O., and Koliatsos, V.E. Nonhuman sialic acid Neu5Gc is very low in human embryonic stem cell-derived neural precursors differentiated with B27/N2 and noggin: implications for transplantation. Exp Neurol **201,** 525, 2006.
7. Orner, B.P., Derda, R., Lewis, R.L., Thomson, J.A., and Kiessling, L.L. Arrays for the combinatorial exploration of cell adhesion. J Am Chem Soc **126,** 10808, 2004.
8. Derda, R., Li, L.Y., Orner, B.P., Lewis, R.L., Thomson, J.A., and Kiessling, L.L. Defined substrates for human embryonic stem cell growth identified from surface arrays. ACS Chem Biol **2,** 347, 2007.
9. Kolhar, P., Kotamraju, V.R., Hikita, S.T., Clegg, D.O., and Ruoslahti, E. Synthetic surfaces for human embryonic stem cell culture. J Biotechnol **146,** 143, 2010.
10. Melkoumian, Z., Weber, J.L., Weber, D.M., Fadeev, A.G., Zhou, Y.E., Dolley-Sonneville, P., *et al.* Synthetic peptide-acrylate surfaces for long-term self-renewal and cardiomyocyte differentiation of human embryonic stem cells. Nat Biotechnol **28,** 606, 2010.
11. Villa-Diaz, L.G., Nandivada, H., Ding, J., Nogueira-De-Souza, N.C., Krebsbach, P.H., O'Shea, K.S., *et al.* Synthetic polymer coatings for long-term growth of human embryonic stem cells. Nat Biotechnol **28,** 581, 2010.
12. Ludwig, T.E., Levenstein, M.E., Jones, J.M., Berggren, W.T., Mitchen, E.R., Frane, J.L., *et al.* Derivation of human embryonic stem cells in defined conditions. Nat Biotechnol **24,** 185, 2006.
13. Amit, M., and Itskovitz-Eldor, J. Maintenance of human embryonic stem cells in animal serum- and feeder layer-free culture conditions. Hum Embryonic Stem Cell Protoc **331,** 105, 2006.
14. Miyazaki, T., Futaki, S., Hasegawa, K., Kawasaki, M., Sanzen, N., Hayashi, M., *et al.* Recombinant human laminin isoforms can support the undifferentiated growth of human embryonic stem cells. Biochem Biophys Res Commun **375,** 27, 2008.
15. Braam, S.R., Zeinstra, L., Litjens, S., Ward-van Oostwaard, D., van den Brink, S., van laake, L., Lebrin, F., Kats, P., Hochstenbach, R., Passier, R., Sonnenberg, A., and Mummery, C.L. Recombinant vitronectin is a functionally defined substrate that supports human embryonic stem cell self-renewal via alphavbeta5 integrin. Stem Cells **26,** 2257, 2008.
16. Rodin, S., Domogatskaya, A., Strom, S., Hansson, E.M., Chien, K.R., Inzunza, J., *et al.* Long-term self-renewal of human pluripotent stem cells on human recombinant laminin-511. Nat Biotechnol **28,** 611, 2010.
17. Rowland, T.J., Miller, L.M., Blaschke, A.J., Doss, E.L., Bonham, A.J., Hikita, S.T., Johnson, L.V., and Clegg, D.O. Roles of integrins in human induced pluripotent stem cell growth on Matrigel and vitronectin. Stem Cells Dev **19,** 1231, 2010.
18. Schvartz, I., Seger, D., and Shaltiel, S. Vitronectin. Int J Biochem Cell Biol **31,** 539, 1999.
19. Lynn, G.W., Heller, W.T., Mayasundari, A., Minor, K.H., and Peterson, C.B. A model for the three-dimensional structure of human plasma vitronectin from small-angle scattering measurements. Biochemistry **44,** 565, 2005.
20. Unger, C., Skottman, H., Blomberg, P., Dilber, M.S., and Hovatta, O. Good manufacturing practice and clinical-grade human embryonic stem cell lines. Hum Mol Genet **17,** R48, 2008.
21. Skottman, H., Dilber, M.S., and Hovatta, O. The derivation of clinical-grade human embryonic stem cell lines. FEBS Lett **580,** 2875, 2006.
22. Oh, S.K.W., and Choo, A.B.H. Advances and perspectives in human and mouse embryonic stem cell bioprocessing. Drug Discov Today Technol **5,** 25, 2008.
23. Zhang, H.L., Bremmell, K., Kumar, S., and Smart, R.S.C. Vitronectin adsorption on surfaces visualized by tapping mode atomic force microscopy. J Biomed Mater Res Part A **68A,** 479, 2004.
24. Choo, A., Padmanabhan, J., Chin, A., Fong, W.J., and Oh, S.K. Immortalized feeders for the scale-up of human embryonic stem cells in feeder and feeder-free conditions. J Biotechnol **122,** 130, 2006.
25. Oh, S.K.W., Chen, A.K., Mok, Y.L., Chen, X.L., Lim, U.M., Chin, A., Choo, A.B.H., and Reuveny, S. Long term microcarrier suspension cultures of human embryonic stem cells. Stem Cell Res **2,** 219, 2009.
26. Salinovich, O., and Montelaro, R.C. Reversible staining and peptide mapping of proteins transferred to nitrocellulose after separation by sodium dodecylsulfate-polyacrylamide gel electrophoresis. Anal Biochem **156,** 341, 1986.
27. Borcherding, H., Hicke, H.G., Jorcke, D., and Ulbricht, M. Affinity membranes as a tool for life science applications. Ann N Y Acad Sci **984,** 470, 2003.
28. Bradford, M.M. A rapid and sensitive method for the quantitation of microgram quantities of protein utilizing the principle of protein-dye binding. Anal Biochem **72,** 248, 1976.
29. Zor, T., and Seliger, Z. Linearization of the Bradford protein assay increases its sensitivity: theoretical and experimental studies. Anal Biochem **236,** 302, 1996.

30. Douglas, J.F., Johnson, H.E., and Granick, S. A simple kinetic model of polymer adsorption and desorption. Science **262,** 2010, 1993.
31. Sukhishvili, S.A., and Granick, S. Kinetic regimes of polyelectrolyte exchange between the adsorbed state and free solution. J Chem Phys **109,** 6869, 1998.
32. Sukhishvili, S.A., and Granick, S. Adsorption of human serum albumin: dependence on molecular architecture of the oppositely charged surface. J Chem Phys **110,** 10153, 1999.
33. Gettens, R.T.T., Bai, Z.J., and Gilbert, J.L. Quantification of the kinetics and thermodynamics of protein adsorption using atomic force microscopy. J Biomed Mater Res Part A **72A,** 246, 2005.
34. Gettens, R.T.T., and Gilbert, J.L. Quantification of fibrinogen adsorption onto 316L stainless steel. J Biomed Mater Res Part A **81A,** 465, 2007.
35. Quillin, M.L., and Matthews, B.W. Accurate calculation of the density of proteins. Acta Crystallogr D Biol Crystallogr **56,** 791, 2000.
36. Chin, A., Padmanabhan, J., Oh, S.K., and Choo, A. Defined and serum-free media support undifferentiated human embryonic stem cell growth. Stem Cells Dev **19,** 753, 2010.
37. Manton, K.J., Richards, S., Lonkhuyzen, D., Leavesley, D., and Upton, Z. A chimeric vitronectin: IGF-1 protein supports feeder-cell free and serum-free culture of human embryonic stem cells. Stem Cells Dev 2010 Feb 3 [Epub ahead of print].
38. Yamada, K.M., and Even-Ram, S. Integrin regulation of growth factor receptors. Nat Cell Biol **4,** E75, 2002.
39. Ng, K.W., Speicher, T., Dombrowski, C., Helledie, T., Haupt, L.M., Nurcombe, V., *et al.* Osteogenic differentiation of murine embryonic stem cells is mediated by fibroblast growth factor receptors. Stem Cells Dev **16,** 305, 2007.
40. Ghule, P.N., Dominski, Z., Yang, X.C., Marzluff, W.F., Becker, K.A., Harper, J.W., *et al.* Staged assembly of histone gene expression machinery at subnuclear foci in the abbreviated cell cycle of human embryonic stem cells. Proc Natl Acad Sci U S A **105,** 16964, 2008.
41. Izumi, M., Yamada, K.M., and Hayashi, M. Vitronectin exists in two structurally and functionally distinct forms in human plasma. Biochim Biophys Acta **990,** 101, 1989.
42. Hamilton, S.R., Davidson, R.C., Sethuraman, N., Nett, J.H., Jiang, Y., Rios, S., *et al.* Humanization of yeast to produce complex terminally sialylated glycoproteins. Science **313,** 1441, 2006.

Address correspondence to:
William R. Birch, Ph.D.
Institute of Materials Research and Engineering
*Agency for Science, Technology and Research (A*STAR)*
3 Research Link
Singapore 117602
Singapore

E-mail: w-birch@imre.a-star.edu.sg

Received: June 4, 2010
Accepted: August 18, 2010
Online Publication Date: September 27, 2010

Impact of vitronectin concentration and surface properties on the stable propagation of human embryonic stem cells[a)]

Jian Li[b)]
*Institute of Materials Research and Engineering, Agency for Science, Technology and Research (A*STAR), Singapore 117602*
Jo'an Bardy[b)]
*Stem Cell Group, Bioprocessing Technology Institute, Agency for Science, Technology and Research (A*STAR), Singapore 138668*
Lynn Y. W. Yap
*Stem Cells and Tissue Repair Group, Institute of Medical Biology, Agency for Science, Technology and Research (A*STAR), Singapore 138648, Singapore and Graduate School for Integrative Sciences and Engineering, National University of Singapore, Singapore 117597*
Allen Chen
*Stem Cell Group, Bioprocessing Technology Institute, Agency for Science, Technology and Research (A*STAR), Singapore 138668*
Victor Nurcombe and Simon M. Cool
*Stem Cells and Tissue Repair Group, Institute of Medical Biology, Agency for Science, Technology and Research (A*STAR), Singapore 138648, Singapore and Department of Orthopedic Surgery, Yong Loo Lin School of Medicine, National University of Singapore, Singapore 119074*
Steve K. W. Oh[c),d)]
*Stem Cell Group, Bioprocessing Technology Institute, Agency for Science, Technology and Research (A*STAR), Singapore 138668*
William R. Birch[c),e)]
*Institute of Materials Research and Engineering, Agency for Science, Technology and Research (A*STAR), Singapore 117602*

(Received 1 October 2010; accepted 17 November 2010; published 14 December 2010)

The standard method for culturing human embryonic stem cells (hESC) uses supporting feeder layers of cells or an undefined substrate, Matrigel™, which is a basement membrane extracted from murine sarcoma. For stem cell therapeutic applications, a superior alternative would be a defined, artificial surface that is based on immobilized human plasma vitronectin (VN), which is an adhesion-mediating protein. Therefore, VN adsorbed to diverse polymer surfaces was explored for the continuous propagation of hESC. Cells propagated on VN-coated tissue culture polystyrene (TCPS) are karyotypically normal after >10 passages of continuous culture, and are able to differentiate into embryoid bodies containing all three germ layers. Expansion rates and pluripotent marker expression verified that a minimal VN surface density threshold is required on TCPS. Further exploration of adsorbed VN was conducted on polymer substrates with different properties, ranging from hydrophilic to hydrophobic and including cationic and anionic polyelectrolyte coatings. Despite differing surface properties, these substrates adsorbed VN above the required surface density threshold and were capable of supporting hESC expansion for >10 passages. Correlating wettability of the VN-coated surfaces with the response of cultured hESC, higher cell expansion rates and OCT-4 expression levels were found for VN-coated TCPS, which exhibits a water contact angle close to 65°. Importantly, this simple, defined surface matches the performance of the benchmark Matrigel, which is a hydrogel with highly complex composition. [DOI: 10.1116/1.3525804]

I. INTRODUCTION

Human embryonic stem cells (hESC) are isolated from the inner cell mass of blastocysts and thus retain the ability to differentiate into the three primary germ layers (endoderm, ectoderm, and mesoderm). They offer the potential for applications in tissue repair and drug discovery.[1] Obtaining significant numbers of hESC is a prerequisite for their use in both research and industrial scale applications. This drives efforts to explore cell culture environments that are capable of hESC propagation, which is defined as the expansion of hESC over multiple passages while preserving their karyotypic stability and pluripotency.[2] The current standard method for hESC culture employs a Matrigel™ (MG) cell culture substrate,[3] which is a commercial product distributed

[a)]This paper is part of an In Focus section on Biointerphase Science in Singapore, sponsored by Bruker Optik Southeast Asia, IMRE, the Provost's Office and School of Materials Science and Engineering of Nanyang Technological University, and Analytical Technologies Pte. Ltd.
[b)]These authors contributed equally to the work described in this article.
[c)]Authors to whom correspondence should be addressed.
[d)]Electronic mail: steve_oh@bti.a-star.edu.sg
[e)]Electronic mail: w_birch@imre.a-star.edu.sg

by Becton Dickinson. It consists of a gelatinous membrane extracted from a mouse sarcoma, rich in laminin-111, and contains collagen, entactin, heparan sulfate proteoglycans, and several growth factors.[3] Several methods also employ a cell culture medium that is conditioned by exposure to inactivated mouse or human feeder cells.[1,4–6] This conditioning, when supplemented by basic fibroblast growth factor, maintains pluripotency of hESC. However, these poorly defined cell culture environments may be a source of xenogenic risk and are not suitable for generating clinical-grade cells for medical applications. Recent efforts have focused on developing a defined cell culture environment that is capable of the stable and prolonged expansion of hESC. Hakala *et al.* recently showed the performance of MG to be superior to other cell culture substrates when used to expand hESC in defined cell culture media.[7] As a natural product, MG suffers from batch-to-batch variability and introduces a complex protein mixture. It may also expose cultured hESC to non-human sialic acid, an immunogenic molecule that can limit its industrial scale-up for clinical applications.

With the aim of defining surface properties that are suitable for hESC culture, a study by Derda *et al.* screened an array of surface-immobilized short peptide sequences.[8] Specific surface properties showed promise and the study identified a surface density threshold. However, the surface density threshold was not quantified and hESC pluripotency was inferred from expression of the OCT-4 genetic marker, which is necessary but not sufficient criterion for establishing hESC pluipotency. A later study demonstrated the stable propagation of hESC in a defined culture medium on a synthetic surface consisting of selected peptide sequences covalently bound to an acrylate polymer matrix.[9] Karyotypic stability of the expanded hESC was verified and their ability to differentiate into the three germ layers was established *in vitro*. Kolhar *et al.* showed that a cyclic arginine-glycine-aspartic acid (RGD) peptide sequence conjugated to amine moieties presented on tissue culture plastic is capable of supporting the long-term propagation of hESC and the peptide surface density was estimated at 10–30 fmol/cm^2 from fluorescence measurements.[10] A full synthetic polymer surface with tunable wettability and rigidity has been shown to support hESC expansion in conditioned cell culture medium.[11] However, this surface could not support the long-term propagation of multiple hESC lines in defined, serum-free medium. Indeed a recent comprehensive study reports that wettability may be optimally tuned to enhance hESC proliferation but integrin engagement with surface-presented vitronectin is required to promote hESC colony formation and ensure a viable platform.[12]

To develop a cell culture platform based on defined extracellular matrix (ECM) proteins, Ludwig *et al.* used human collagen IV, laminin, fibronectin, and vitronectin to expand hESC in a defined cell culture medium.[13] Although the propagated hESC expressed pluripotency markers and were able to differentiate *in vivo*, prolonged expansion resulted in karyotypic instability, which may result from adaptation to the new platform. Similar studies have found that single-component matrices provide viable substrates for the stable propagation of hESC: laminin, fibronectin, laminin-511, and vitronectin.[14–17]

With the emergence of a defined substrate as a realistic possibility, Braam *et al.* identified that surface-presented vitronectin (VN) enables the adhesion of hESC and activates a key integrin, which is believed to play a role in supporting the long-term propagation of hESC.[16] This study was extended to the propagation of human induced pluripotent stem cells cultured on VN by Rowland *et al.*[18] They identified the same integrin as mediating cell attachment but added that its subsequent inhibition enhanced cell proliferation.[18] VN is an ECM protein that promotes cell adhesion and spreading.[19] A recent study by Yap *et al.* demonstrated the long-term propagation of multiple hESC lines on VN immobilized by adsorption on tissue culture polystyrene (TCPS).[20] A novel aspect of this work was the quantification of the adsorbed VN surface density. Correlation of this data with the response from cultured hESC established that a threshold VN surface density of 250 ng/cm^2 is required to successfully expand these cells while preserving their pluripotency.[20] Moreover, VN surface density on TCPS equal to or greater than this threshold provides a cell culture surface that matches the performance of MG in both defined and conditioned cell culture media and provides the opportunity to adapt this platform to the culture of hESC at scale.

Having established that VN adsorbed to TCPS is a viable substrate capable of supporting the long-term propagation of multiple hESC lines,[20] the present study examines VN presented by polymer substrates with a variety of surface properties, namely: bare, coated with cationic and anionic polyelectrolyte, and rendered hydrophilic from plasma treatment. Heparin, which presents affinity-binding sites for VN,[19] was also introduced as an anionic polyelectrolyte. Following an initial screening of these surfaces, with and without VN coating, the long-term propagation of a single hESC line is tested on four promising candidates, whose performance is correlated with quantification of the adsorbed VN surface density. The relationship between the surface wettability and the propagation of hESC was also assessed. The scale-up potential of these surfaces was probed by measuring the hESC proliferation rate and estimating the population doubling time using optical detection followed by a final cell count.

II. EXPERIMENT

A. Preparing the cell culture substrates

1. Coating tissue culture polystyrene with varying vitronectin surface density

TCPS surfaces were coated with human plasma-purified VN at different surface densities, as described by Yap *et al.*[20] Briefly, VN solutions of varying concentration were prepared by diluting 1 mg/ml stock VN solution (Millipore CC080) with sterile 1× phosphate buffered saline (PBS), diluted from 10× PBS (Sigma P5493) using pure water (PURELAB® Option Q, Elga) to 1.25, 2.5, 5, and 10 μg/ml (VN1.25, VN2.5, VN5, and VN10, respectively). These so-

lutions were used to coat 60 mm center-well TCPS organ culture dishes, OCD, (Becton Dickinson Biosciences) by incubating the OCD with 300 μl of the solution at 4 °C for 15 h. The VN-coated OCDs were rinsed briefly with PBS before using them as substrates for cell culture.

2. Preparation of VN-coated polymer substrates with different surface properties

Biaxially oriented polyethylene terephthalate (PET) and polystyrene (PS) films, 100 and 125 μm thick, respectively, were sourced from Goodfellow (Cambridge, UK). Circular disks, 16 mm in diameter, were cut from the films and were cleaned by soaking in isopropanol. These were rinsed in pure water and blow-dried with nitrogen before use. An *in situ* polymerized, grafted poly(acrylic acid) (PAA) brush was developed on PET using the method described by Racine *et al.*,[21] with a UV activation time of 15 min and a UV polymerization time of 5 min. The surface density of the carboxylic acid groups on PET-PAA was quantified by Toluidine Blue O (Sigma-Aldrich T3260) staining and titration, as described by Racine *et al.*[21]

Bare PET films and PET-PAA films were briefly rinsed with water and dried under nitrogen airflow before sterilizing them for 15 min within 70% ethanol, followed by twice rinsing in sterile PBS, in the sterile environment of a biological safety cabinet (NuAire Nu-425-400E). The PET-PAA surfaces were activated by a 15 min exposure to a *p*H 10 buffer solution, consisting of 0.0214*M* NaOH (Goodrich Chemical Enterprise, Singapore) and 0.05*M* sodium hydrogen carbonate (Merck), which ensured charging of the PAA brush. This was followed by two rapid rinses in PBS before the surfaces were coated with poly-L-lysine (PLL). The PET and PET-PAA disks were coated with PLL in an OCD, which was filled with 400 μl of 50 μg/ml PLL (Sigma-Aldrich P6282) in PBS solution. The samples were incubated for 20 min followed by three rinses in PBS. The PLL surface density on PET was measured by Ponceau S staining, using the method described by Yap *et al.*[20] Similarly, surfaces were coated with heparin in an OCD by incubating with 400 μl of a 100 μg/ml heparin (Sigma H3149) solution in PBS for 30 min, followed by three rinses with PBS. Autoclaving was used to sterilize PBS and the *p*H 10 buffer solution. PLL and heparin solutions were sterilized by filtration through sterile NALGENE® syringe filter membranes with a pore size of 0.2 μm (Nalge Nunc International Corporation) using a 10 ml sterile Injekt® syringe (B. Braun Melsungen AG).

Oxygen-plasma-treated PET and PS films (PET-plasma and PS-plasma, respectively) were activated in a plasma chamber (Triple P, Duratek, Inc.) using a 100 W, 2.45 GHz radio frequency discharge applied to an oxygen gas pressure of 3.5×10^{-1} Torr for 1 min. These films were subsequently sterilized by a 15 min exposure to the UV light in the biological safety cabinet.

Coating of PET-plasma, PS-plasma, bare PET, PET+PLL, PET+PLL+heparin, PET-PAA, PET-PAA+PLL, and PET-PAA+PLL+heparin disks with VN was achieved by placing them in sterile (as-received) OCDs, where they were weighed down by cylindrical glass rings (borosilicate glass, outer diameter of 17 mm, wall thickness of 1.5 mm, and height of 10 mm). The surfaces were coated from a 400 μl volume of 5 μg/ml vitronectin in PBS by incubating them for 15 h at 4 °C, followed by a brief rinse with PBS immediately prior to cell seeding.

3. Control cell culture substrates coated with Matrigel™

Control cell culture plates consisted of OCDs coated with Matrigel™ (Becton Dickinson and Company, Franklin Lakes, NJ). Cold KnockOut (KO) medium, consisting of 85% KO-Dulbecco's modified eagle medium (Invitrogen 10829-018), 15% KO serum replacement (Invitrogen 10828-028), 1 mM *L*-glutamine (Invitrogen 25030-032), 1% nonessential amino acids (Invitrogen 11140-050), 10 ng/ml FGF-2 (Invitrogen PHG0021), 0.1 mM 2-mercaptoethanol (Invitrogen 21985-023), 25 u/ml penicillin, and 25 μg/ml streptomycin (Invitrogen 15140-122), was used to dilute MG in a 1:30 ratio. Each OCD was coated with 1 ml of this coating solution for 15 h at 4 °C, followed by a brief rinse in KO medium before cell passaging.

B. Biological responses of hESC on vitronectin surfaces

1. Culture of hESC on TCPS coated with different VN surface densities

HES-3 (46, XX) cells (ES Cell International) were cultured in conditioned medium (CM), prepared as described by Yap *et al.*[20] The received cells were first cultured at 37 °C/5% CO_2 on TCPS dishes coated with MG. They were then adapted to TCPS dishes coated with VN5 for over ten passages. Cells from VN5 were then tested on TCPS dishes coated with VN1.25, VN2.5, VN5, and VN10. In these experiments, the cell culture medium was changed daily and the cells were passaged weekly, as described by Yap *et al.*[20]

The passaging process for HES-3 cells grown on MG coated TCPS involved the removal of differentiated cells by pipetting and treatment with collagenase IV (200 u/ml) for 3 min at 37 °C. They were dissociated by scraping and repeated pipetting into small clumps and seeded into freshly coated OCD at a 1:5 split ratio. The passaging process for HES-3 cells cultured on all VN-coated surfaces followed the one used for MG. The hESC passage is abbreviated as P*n*, where *n* denotes the passage number (e.g., passage 2, P2).

2. Growth tracking of hESC on different matrices

In the first set of experiments, 1×10^5 HES-3 cells/cm^2 were seeded into TCPS coated with VN1.25, VN2.5, VN5, and VN10, as well as a MG control. These experiments were performed over 6 weeks and growth curves over 7 days were measured at P2, P6, and P7. Samples were run in triplicate at each passage and for each condition.

Freshly-seeded cells were cultured in an incubator (Galaxy R, RS Biotech Laboratory Equipment Ltd.) for 48 h, after which the media in the dish was refreshed and the cells were imaged with the stem cell imaging system (SCIS), de-

veloped by Oh *et al.*[22] The cell culture medium was subsequently refreshed daily and the cells were also imaged daily from day 2 to day 7. SCIS image analysis measured the surface area covered by cells. A threshold value was set on the system such that it detected cell colonies observed on the OCD, without the opaqueness of the different cell culture substrates impinging on the calculation of the total area covered by the cells. From the zone of linear cell area expansion, the expansion rate was calculated as the time-rate increase in area. Cells harvested on day 7 were resuspended in 1 ml and counted with a NucleoCounter® NC-100™ (ChemoMetec A/S, Denmark). Cell coverage of the surface and cell expansion rates on the OCD or polymer disks were normalized to the surface area available for cell attachment within the image or to the inner diameter of the glass ring. These surface areas in the OCD and on the disk are approximately 2.4 and 2 cm^2, respectively.

The second set of experiments used the same procedure as described above with HES-3 cells that were previously cultured for over ten passages on TCPS coated with VN5. HES-3 cells were mechanically passaged weekly and seeded onto PET, PET+PLL, PET-PAA, PET-plasma, or PS-plasma disks at a split ratio of 1:5. TCPS+VN5 and TCPS+MG were included as the positive controls in this experiment. At P13, 2.5×10^4 HES-3 cells/cm^2 were seeded onto these freshly coated surfaces, and their growth rates, maximum cell numbers, and pluripotent marker expression were monitored in triplicate.

3. Flow cytometry analysis

Flow cytometry, also known as fluorescence activated cell sorting (FACS), was performed by targeting the cell surface marker mAb 84[23] and transcription factor OCT-4, with an isotype control. After dissociating into a single cell suspension with TrypLE™ Express (Invitrogen), cells are fixed and permeabilized with reagent *A* and *B* (Caltag Laboratories, Invitrogen). During the cell permeabilization step, mAb 84 (1:20),[23] a cytotoxic antibody to hESC and OCT-4 (1:20, Santa Cruz) mouse monoclonal antibodies were added to reagent *B*. Cells were then washed with 1% bovine serum albumin in PBS, followed by incubation with fluorescein isothiocyanate conjugated goat antimouse antibody (1:500, DAKO) in the dark. They were then washed and resuspended with 1% bovine serum albumin in PBS and analyzed on a FACSCalibur (Becton Dickinson) as described by Yap *et al.* Briefly, data were collected from 10 000 cells, and the percentage of cells positive for the marker was gated at the intersection of the control and marker histograms.

4. Spontaneous differentiation and quantitative real time polymerase chain reaction analysis

Embryoid bodies were generated with HES-3 cells from P6, which were cultured on VN5 OCD for 1 week, after which they were scraped off and cultured in an ultralow attachment six-well plate (Corning, Inc.) in a differentiation medium, prepared as described in Chin *et al.*[24] Following their growth in suspension for 1 week, the cell aggregates were dissociated by repeated pipetting into small clumps and replated onto an OCD coated with 0.1% gelatin, then cultured for 2 weeks, with differentiation medium replaced every 2 days. On day 21 of differentiation, total ribonucleic acid (RNA) was harvested from these cells following the protocol of the RNeasy mini kit (Qiagen GmbH, Germany).

For each well of the MicroAmp® optical 96-well reaction plate (Applied Biosystems BV 4306737), 26 ng of total RNA was converted to complementary DNA using Superscript II (Invitrogen 18064-022). Quantitative real time polymerase chain reaction (qRT-PCR) was performed with a SYBR® green PCR master mix (Applied Biosystems BV) kit, used in an ABI PRISM® 7500 (Applied Biosystems BV), whose software analyzed the optical absorption data. The primers used for qRT-PCR are listed in the supplementary Table S1.[25]

5. Karyotype analysis

HES-3 cells expanded on TCPS coated with VN1.25, VN2.5, VN5, and VN10 were harvested following P10 and grown on an OCD coated with VN5 for 4 days. Karyotype analysis of these cells was carried out on 20 *G*-banded metaphases by the Cytogenetics Laboratories of the KK Women's and Children's Hospital.

6. Screening assay for HES-3 cells cultured on polymer substrates with and without VN5 coating

The short-term adhesion assay was designed to screen surfaces for HES-3 cell adhesion and subsequent expansion. If no significant numbers of cell colonies attached within 1 day, the surface was designated as nonviable. This designation is also applied when cultured cells did not attain sufficient numbers for passaging after 7 days. Continuous passaging of the cells relied on the number of colonies attached to the surface generating sufficient cells for the next passage. HES-3 cells were prepared as described above and seeded onto PET, PET+PLL, PET+PLL+Heparin, PET-PAA, PET-PAA+PLL, PET-PAA+PLL+Heparin, PET-plasma, and PS-plasma disks with and without VN5 coating. Surviving colonies from different surfaces were passaged for up to 8 weeks.

C. Surface characterization

1. Determination of VN surface density on surfaces by Ponceau S staining

Protein surface density was determined by Ponceau S staining.[20] For this experiment, 400 μl VN solutions of 0, 2.5, 5, 10, and 20 μg/ml were used to coat PET, PET-PAA, PET-plasma, and PS-plasma surfaces for 15 h at 4 °C, as described above for cell culture substrates. The top surface of the coated polymer films was exposed to Ponceau S staining solution (Sigma-Aldrich) for 15 h at room temperature. After three rinses in water and blow-drying, each sample was placed into a new OCD and 400 μl of 0.1*M* NaOH was added to each sample. The samples were then shaken gently for 20 min, allowing desorption of Ponceau S stain from the sample surface. Samples were run in duplicates, yielding four 200 μl aliquots per VN concentration. Each aliquot was

placed in a flat-bottom 96-well plate and neutralized with 15 μl of 50% acetic acid (J. T. Baker). Colorimetric absorption was measured at 515 nm on an Infinite® 200 multimode microplate reader (Tecan, Switzerland). This was compared to a standard curve, which was generated using Ponceau S concentrations ranging from 0 to 10 μg/ml in 5% (w/v) acetic acid. The Ponceau S surface density was converted into a VN surface density by establishing a relationship between the adsorbed Ponceau S stain and the quantification of VN adsorbed to TCPS, using data reported by Yap *et al.*[20] Assuming similar accessibility to Ponceau S stain of VN adsorbed to PET, PET-PAA, PET-plasma, and PS-plasma surfaces, the VN surface density was thus inferred from the Ponceau S stain surface density. The same Ponceau S staining and its subsequent quantification were used to estimate the PLL surface density on the PET+PLL substrate.

2. Contact angle measurements

The water contact angles (θ_w) of TCPS, PET, PET+PLL, PET-PAA, PET-plasma, and PS-plasma surfaces with and without different VN coating concentrations were measured at ambient temperature on a manual contact angle goniometer (model 100, Ramé-Hart, Inc.). Five 1 μl sessile pure water drops were measured on each sample. The average contact angle and its standard deviation were determined from contact angles measured on duplicates of each polymer surface.

D. Statistical analysis

Data values are reported as mean and standard deviation. Graphs were plotted and data were transformed with Microsoft Office Excel 2007 software. Student *t*-tests were performed between experimental and control conditions. *P* values < 0.05 were considered to represent statistically significant differences.

III. RESULTS AND DISCUSSION

A. Growth of HES-3 cells on TCPS coated with different concentrations of VN

Figure 1 shows representative images from triplicate cultures on different VN surface densities at P6. Growth of HES-3 cells on TCPS coated with VN1.25 and VN2.5 appears patchier than TCPS coated with VN5, VN10, and the MG control. Bare patches, devoid of hESC, appear on the VN1.25 and the VN2.5 samples at day 2 and growth over 7 days appears to be more clustered. In comparison, cells spread more evenly in the other three conditions. After 7 days' culture, cells have not fully occupied the surface of VN1.25. The SCIS quantifies this growth trend by plotting the total area of the OCD occupied by HES-3 colonies, showing the most rapid hESC expansion rates on VN5, VN10, and MG, while VN2.5 and VN1.25 substrates show progressively lower expansion rates [Fig. 1(b)]. Cell culture images at days 2 and 3 [Fig. 1(a)] indicate poorer cell attachment and lower numbers of spreading HES-3 colonies on VN1.25 and VN2.5. The area expansion rates in Fig. 2(a)

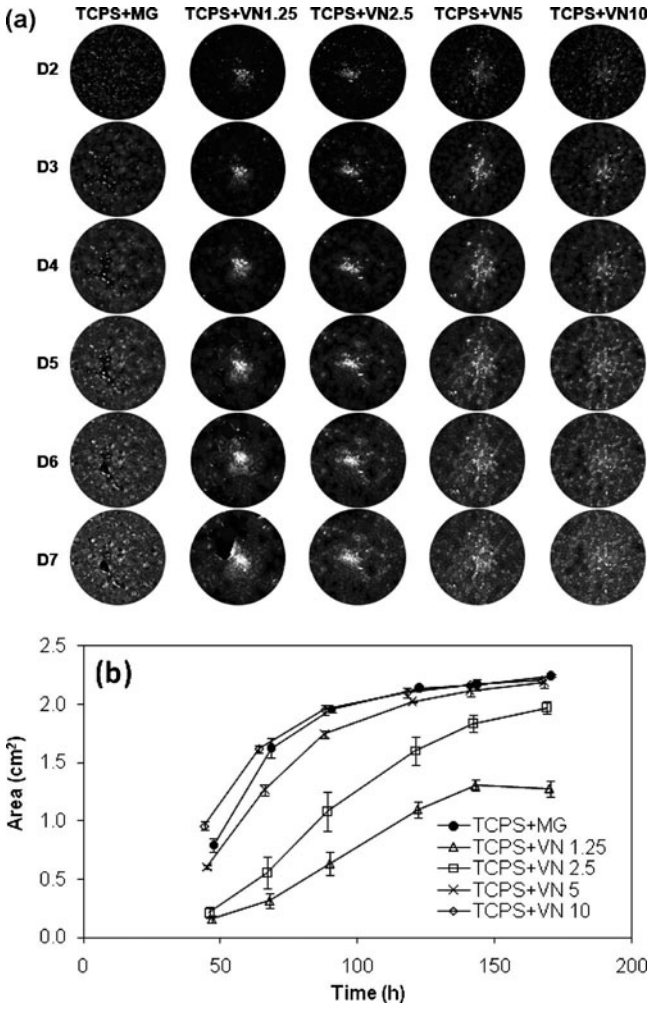

FIG. 1. (a) Images of HES-3 colonies cultured on TCPS coated with MG, VN1.25, VN2.5, VN5, and VN10, respectively, from day 2 to day 7 of P6. The diameter of each image circle is 14.5 mm. (b) Area data representing the surface covered by HES-3 cells from day 2 to day 7 on the same TCPS surfaces. These are calculated by SICS from triplicate runs of images similar to those shown in (a).

were derived from the linear growth portion of this data and similar data at P2 and P7. Although growth rates of HES-3 at P2 appear similar at all VN concentrations, the images taken from P6, shown in Fig. 1, indicate that hESC adapted to lower VN concentrations lose viability, resulting in a sharp decrease in growth rates of HES-3 cells cultured on TCPS coated with VN1.25 at P7 [Fig. 2(a)]. Indeed, despite the early signs of viable hESC culture on VN1.25, cells passaged on this surface all but lose their ability to adhere and expand by P7, highlighting the importance of testing the robustness of new culture platforms beyond five passages. Figure 2(b) shows the final cell numbers, measured with a cell counter, which differ slightly from the estimates generated by the SCIS area measurement. Moreover, the folded layer seen on day 7 [Fig. 1(a)], which is a consequence of the poor adherence of cells cultured on VN1.25, leads to larger discrepancies between the calculated areas on the TCPS surface and the final cell numbers, as observed for P7 in Figs. 2(a) and 2(b). Despite these differences, final cell numbers follow the

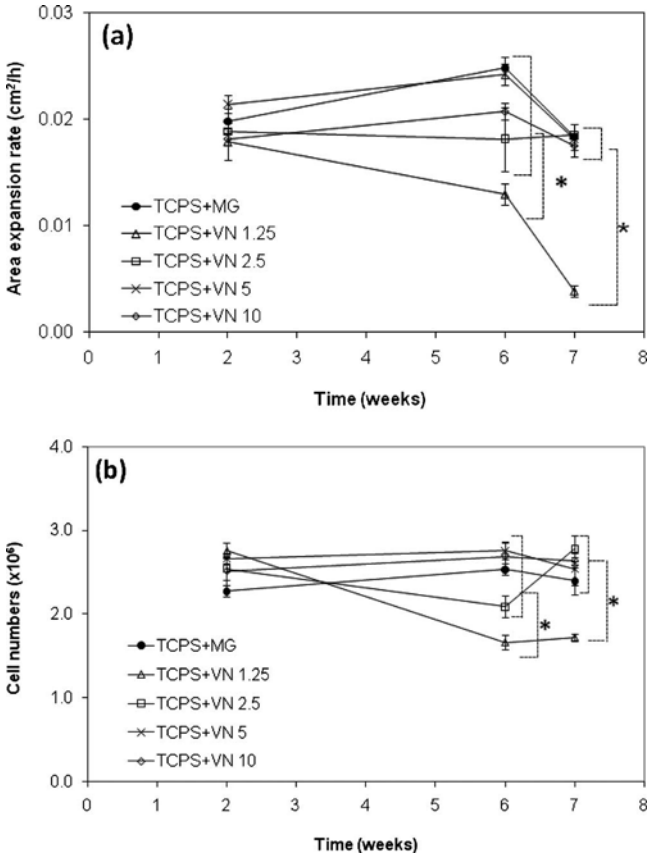

FIG. 2. (a) Area expansion rate during linear expansion phase and (b) cell numbers at day 7 for HES-3 cells at P2, P6, and P7 on TCPS surfaces coated with MG, VN1.25, VN2.5, VN5, and VN10, respectively. At P6 and P7, TCPS coated with VN1.25 shows a significant decrease in growth rate as compared to the other surfaces. $*=P<0.05$.

trends established from area expansion rates: both parameters are significantly lower on VN1.25 at P6 and P7 than on higher VN surface densities and the MG benchmark. Moreover, the VN1.25 OCD surface covered by hESC at day 7 of P6 is approximately half that of the other TCPS surfaces and the MG control. These results confirm that TCPS coated with VN1.25 is insufficient for optimal hESC expansion and that VN5 provides the required surface density to support hESC culture without compromise. The latter propagates hESC with an efficiency equal to VN10 and the MG positive control.

B. Pluripotency of HES-3 cells on TCPS coated with different concentration VN solutions

Flow cytometry analysis of OCT-4 and mAb 84 pluripotency markers at P10 are shown in Fig. 3. HES-3 cells cultured on TCPS coated with VN2.5, VN5, VN10, and the MG control surface express an equally high percentage of these pluripotent markers. Distinctly lower expression levels are exhibited by HES-3 cultured on TCPS coated with VN1.25, for which the downregulation of mAb 84 implies a probable loss of pluripotency. Moreover, visual examination of HES-3 cells cultured on VN1.25 at P10 reveals a more fibroblastic morphology and loss of the hESC phenotype (data not shown).

HES-3 cells cultured on TCPS coated with VN1.25, VN2.5, VN5, and VN10 were tested at P6 for their *in vitro* differentiation capability. As shown in Fig. 4(a), differentiated cells show downregulation of the NANOG and OCT-4 pluripotency markers and upregulation of GATA6, Hand1, and PAX6, which are representative of the endoderm, mesoderm, and ectoderm lineages, respectively. This verifies the ability of cultured HES-3 cells at P6 to differentiate into the three primary germ layers. Moreover, chromosome analysis of HES-3 at P10 indicates that the cells retain their normal

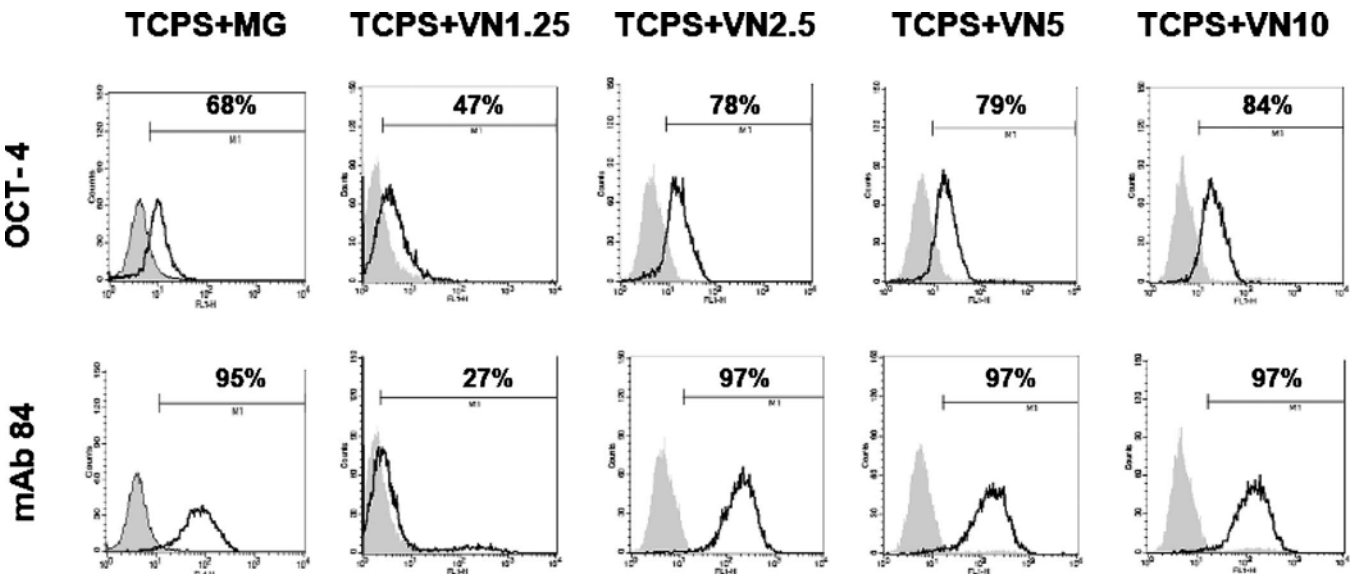

FIG. 3. FACS analysis of OCT-4 and mAb 84 pluripotent markers for P10 HES-3 cells cultured on surfaces of TCPS+MG, TCPS+VN1.25, TCPS+VN2.5, TCPS+VN5, and TCPS+VN10. Cells grown on MG were used as a positive control.

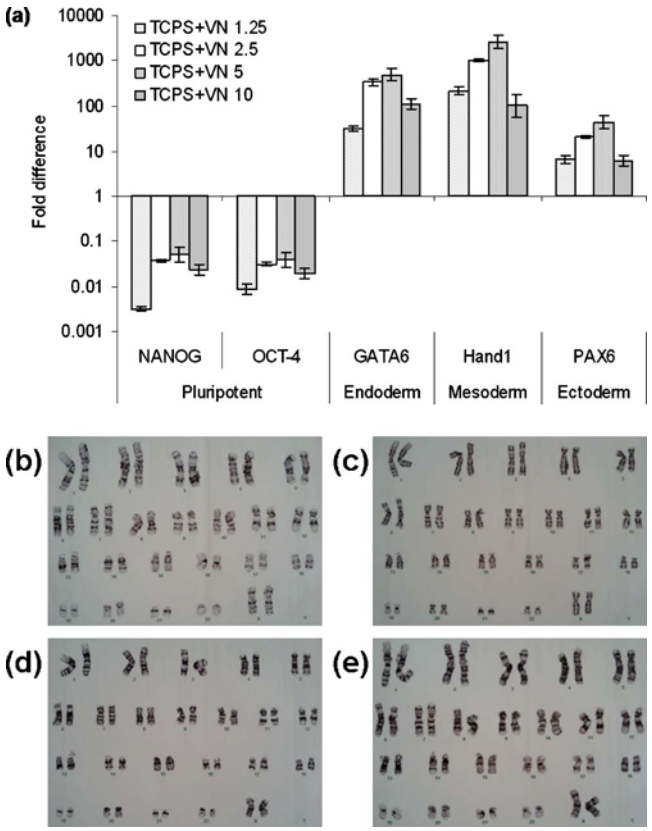

FIG. 4. (Color online) (a) Expression of genetic markers following the *in vitro* 21 days' spontaneous differentiation of P6 HES-3 cells cultured on TCPS coated with VN1.25, VN2.5, VN5, and VN10. Karyotype maps of P10 HES-3 cells cultured on TCPS coated with (b) VN1.25, (c) VN2.5, (d) VN5, and (e) VN10.

diploid karyotype, as depicted in Figs. 4(b)–4(e). Thus, cells cultured on TCPS coated with VN, irrespective of the surface density, retain their ability to differentiate (at least up to P6 on VN1.25) and maintain stable karyotype.

C. Growth of HES-3 cells on different polymer substrates coated with VN5

Preliminary cell adhesion and proliferation were used to screen the polymer substrate surface properties, bare and coated with VN5. As reported in Table I, surfaces without VN coating do not promote HES-3 attachment and cannot support the formation of viable HES-3 cell colonies, thus indicating that exogenous VN is required to promote the adhesion and support the expansion of hESC. Moreover, for surfaces with polyelectrolyte multilayer coatings comprising ≥ 4 layers (PET-PAA+PLL+heparin+VN5), the substrate cannot support HES-3 expansion, despite it being coated from VN5 solution. With a smaller number of multilayers, the surface is capable of supporting HES-3 propagation to at least P13 (TCPS+VN5, PET+VN5, PET+PLL+VN5, PET-PAA+VN5, PET-plasma+VN5, PS-plasma+VN5, PET+PLL+heparin+VN5, and PET-PAA+PLL+VN5).

SICS was used to track HES-3 proliferation on model polymer surfaces coated with VN5. Figure 5(a) shows images of P13 cells from day 2 to day 7, indicating that all the VN-coated surfaces promote cell adhesion and support their expansion. The increase in area covered by expanding cells, shown in Fig. 5(b), depicts a similar trend across all the surfaces tested, including the TCPS+VN5 and MG positive controls. The area expansion rates for the two positive control surfaces are moderately but distinguishably higher than those for other surfaces [Fig. 5(c)]. The PET+PLL+VN5 surface differs by having an initial high area expansion rate, followed by a lower area expansion rate after day 4. Figure 5(c) reports the final cell numbers, which are measured independently of the SICS data. Again, hESCs cultured on MG and VN5 show the highest cell densities compared to the other polymer surfaces at P10 ($P<0.05$). Looking more closely at the day 7 images [Fig. 5(a)], PET+VN5 and PET+PLL+VN5 appear to grow a thinner layer of HES-3 cells. This observation arises from the absence of brighter white areas, which are seen on other substrates. It is reflected in the final cell numbers, which indicate that these two surfaces yield the lowest cell numbers at day 7.

TABLE I. Screening results for short-term adhesion assay of HES-3 cells on different surfaces.

Surfaces	Attachment at P0	
	Without VN	With VN
TCPS+MG	√	···
TCPS	×	√
PS-plasma	×	√
PET-plasma	×	√
PET	×	√
PET+PLL	×	√
PET+PLL+Heparin	×	√
PET-PAA	×	√
PET-PAA+PLL	×	√
PET-PAA+PLL+Heparin	×	×

D. Undifferentiated state of HES-3 cells on different plastics coated with VN5

Flow cytometry measurements of mAb 84 and OCT-4 expression levels serve to indicate whether P13 HES-3 cells are differentiating. Figure 6 shows that greater than 50% and 90% of the cells are positive for OCT-4 and mAb 84, respectively, across the different plastic surfaces. Lower OCT-4 levels of expression occur for HES-3 cells cultured on VN-coated PET and PS-plasma. However, this decrease is not reflected by the levels of mAb 84 expression for these two surfaces. In general, hESC appear to express pluripotent markers across all polymer surfaces over several passages, implying that these substrates may be suitable for long-term culture.

E. Surface characterization

1. Quantification of surface-adsorbed VN

Ponceau S stain adsorbed to VN-coated polymer surfaces was quantified following its desorption. Assuming a linear

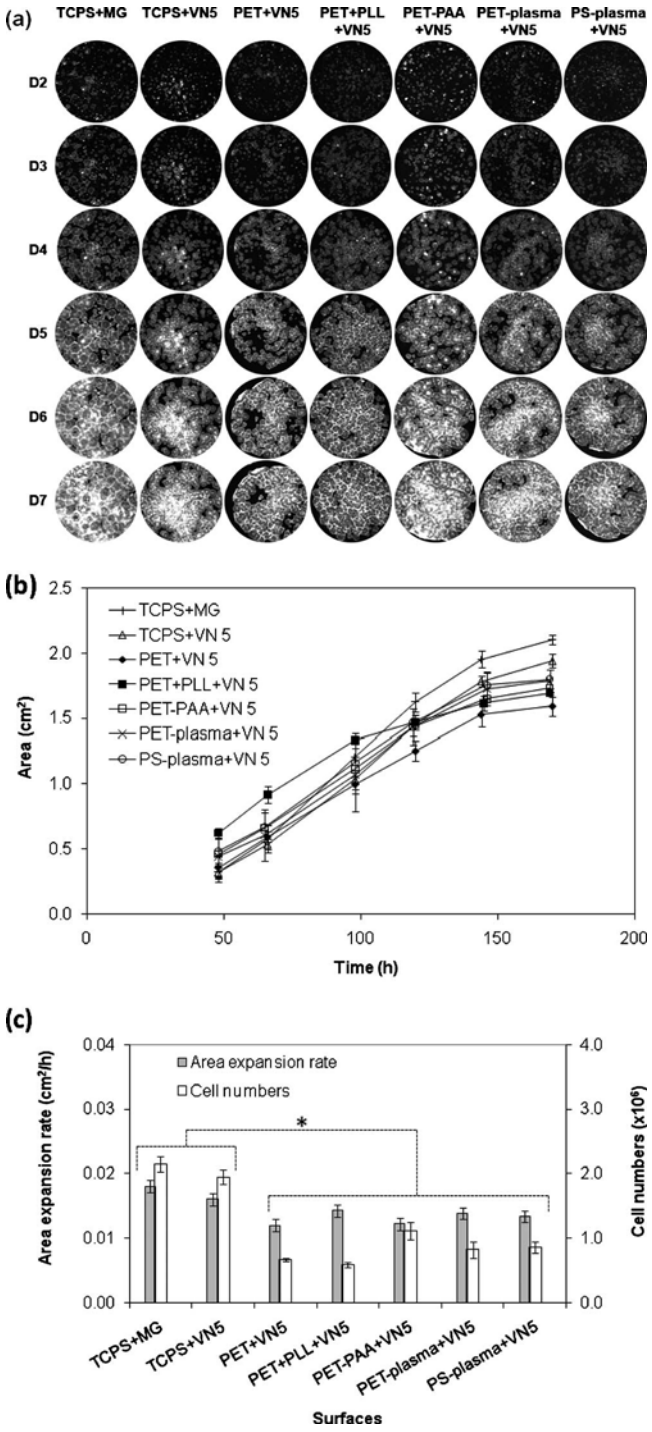

FIG. 5. (a) Representative images of HES-3 from day 2 to day 7 of P13 on the following surfaces: TCPS+MG, TCPS+VN5, PET+VN5, PET+PLL +VN5, PET−PAA+VN5, PET-plasma+VN5, and PS-plasma+VN5, respectively. Diameter of the image circles is 14.5 mm. (b) Area covered by HES-3 cells on these surfaces from day 2 to day 7 at P13. (c) Area expansion rate of HES-3 cells at P13 and total cell numbers on day 7 at P13. The data on the area expansion rate and HES-3 cell numbers are calculated by SICS from triplicate runs of images similar to those shown in (a). $*=P<0.05$, which applies only to the area expansion rate data.

increase in adsorbed VN surface density for solution concentrations below 10 μg/ml, the constant relating VN surface density to Ponceau S was determined to be $S_{VN}=22\,752^{*}S_P$, where S_P is the Ponceau S surface density in nmol/cm^2 and S_{VN} is the VN surface density in ng/cm^2. Figure 7 shows the adsorbed VN surface density, calculated from Ponceau S staining data using this relationship.

From Fig. 7, both PET and PET-PAA surfaces adsorb higher VN surface densities than PET-plasma and PS-plasma. Quantification of VN adsorbed to PET+PLL was not feasible due to Ponceau S staining of both PLL and VN. For these polymer substrates, the surface density adsorbed from VN5 is $\geq$250 ng/cm^2, which is the threshold established by Yap *et al.*[20] for culturing hESC on TCPS. This threshold is corroborated by HES-3 cell expansion rates on TCPS coated from $\geq$VN5 (Fig. 1). Thus, these polymer substrates immobilize a VN surface density that is expected to be sufficient for supporting the expansion of HES-3 cells.

2. Effects of surface wettability on the propagation and pluripotency of HES-3 cells

Substrate wettability can influence the bioresponse of cultured cells.[12,26–28] Figure 8(a) shows the sessile water drop wettability of polymer surfaces coated with increasing VN surface density. Adsorbed VN reduces the wettability of hydrophobic PET and increases the wettability of hydrophilic PS-plasma. As the VN surface density reaches saturation, the wettability of these two substrates converges to 47°–48°. For TCPS and PET-plasma, adsorbed VN gives rise to a modest rise in contact angle, from 58° to 66° and from 49° to 58°, respectively. Similarly, for PET-PAA and PET+PLL, the water contact angle increases from 52° to 67° and from 60° to 68°, respectively. With saturating VN adsorption, we may consider that the polymer substrate is fully coated with adsorbed protein molecules. Atomic force microscopy measurements reported by Yap *et al.*[20] discern aggregates of adsorbed VN molecules but are unable to resolve individual molecules, which are presumed to coat the intervening regions of the polymer substrate.

TCPS consists of plasma-treated PS, which has been stored and shipped, probably over several weeks or months. Given that bare PS exhibits a water contact angle approaching 90° and that freshly plasma-treated PS is fully wettable, the 58° measured contact angle of as-received TCPS reflects the evolution of this surface since its fabrication. The wettability increase following plasma treatment is due to the free-radicals and polar groups that were generated by polymer chain scission. During storage, these groups partially resorb into the bulk polymer, giving rise to a progressive decrease in wettability.[29] Even after their long-term storage, TCPS surfaces present polar groups within a surface layer of 3–5 nm.[29] Freshly plasma-treated PET and PS expose randomly charged hydrophilic polar moieties, such as C—O, C=O, O—C=O, and O—(C=O)—O components.[29,30] In contrast, PET+PLL exposes a cationic polymer with —NH— and —NH$_2$ moieties, and PET-PAA presents an anionic grafted polymer brush, with a carboxyl acid group (—COOH) surface density of 11.5 ± 1.4 nmol/cm^2. PET+PLL exhibits a Ponceau S density of 0.23 ± 0.4 nmol/cm^2, which is comparable to that of a saturated VN coating on

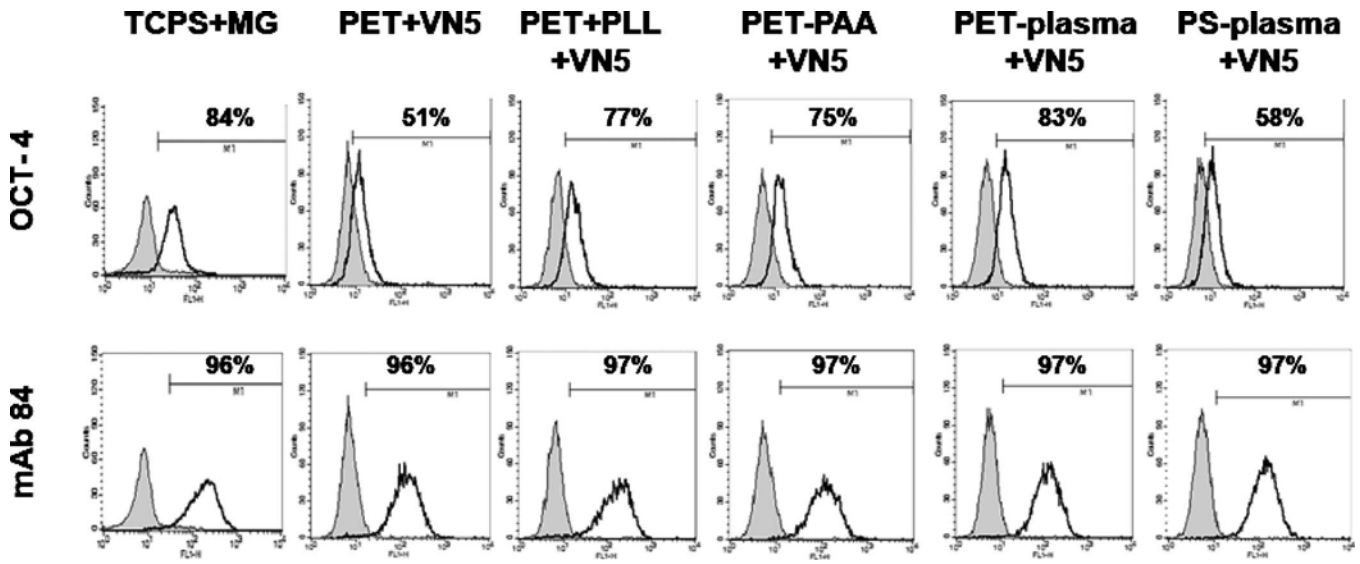

FIG. 6. FACS analysis of OCT-4 and mAb 84 surface marker for HES-3 cells at P13 cultured on the following surfaces: TCPS+MG, PET+VN5, PET +PLL+VN5, PET-PAA+VN5, PET-plasma+VN5, and PS-plasma+VN5, with MG used as a positive control.

TCPS.[20] Thus, polymer substrates without an overriding net surface charge are hydrophobic bare PET, hydrophilic PET-plasma and PS-plasma, and TCPS and PET-plasma, both of which have intermediate wettability. VN adsorbed by hydrophobic interactions is expected to expose hydrophilic groups. Conversely, VN coated on a hydrophilic surface may expose hydrophobic segments of the protein, thus decreasing the surface wettability.[31] While this may explain the convergence in wettability when VN adsorbs to bare PET and to PS-plasma substrates, the mere presence of a saturated VN coating may account for the observed wettability change. Similarly, VN adsorption to PET+PLL and PET-PAA is dominated by charge interactions and the adsorbed VN molecules contribute to the final surface wettability.

Given the surface charge presented by PET+PLL and PET-PAA, the HES-3 response to these VN-coated surfaces may also be influenced by the protein's configuration. VN

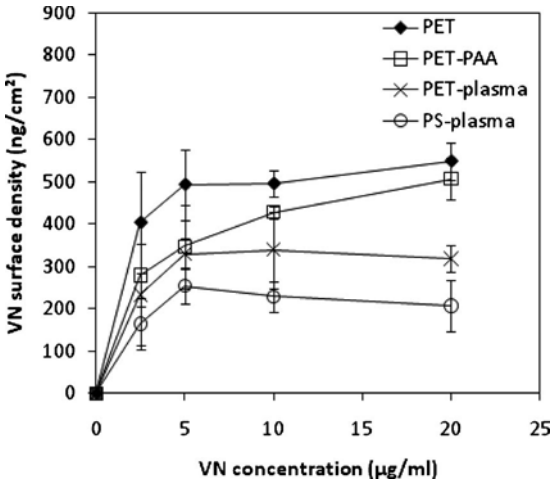

FIG. 7. Adsorbed VN surface density vs the concentration of the depositing solution for PET, PET-PAA, PET-plasma, and PS-plasma surfaces.

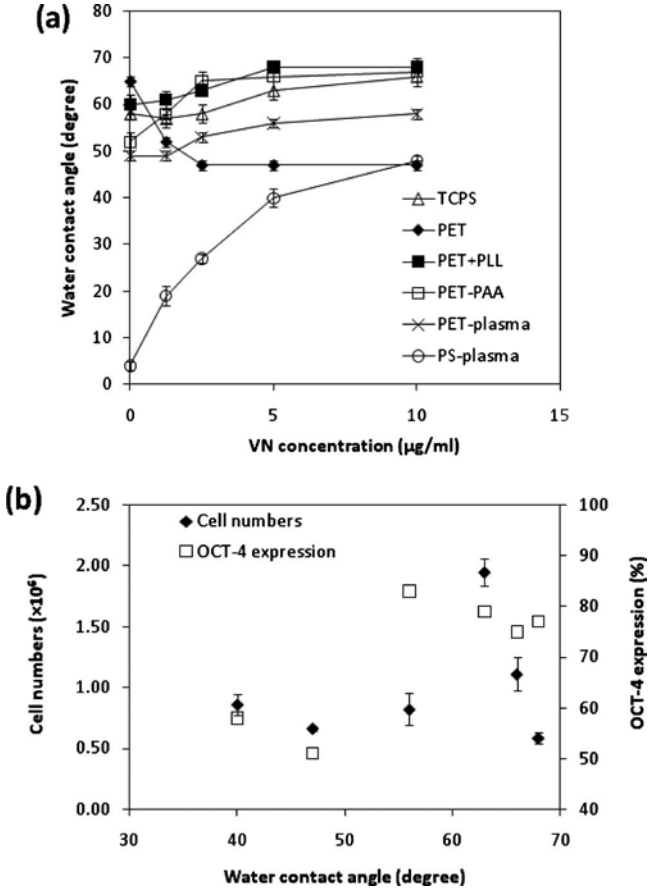

FIG. 8. (a) Water contact angles of VN-coated surfaces as a function of the depositing VN solution concentration. These surfaces include the following: TCPS, PET, PET+PLL, PET-PAA, PET-plasma, and PS-plasma. (b) Total cell numbers and expression of the OCT-4 pluripotency marker for HES-3 cells at P13. These are plotted vs the water contact angle of the following surfaces: TCPS+VN5, PET+VN5, PET+PLL+VN5, PET-PAA+VN5, PET-plasma+VN5, and PS-plasma+VN5.

contains a similar number of negatively (66) and positively (56) charged residues (ExPASy, human VN: P04004), which allow it to adsorb to both cationic and anionic surfaces, with similar efficiency but *via* different domains. The bare PET and PS-plasma surfaces represent the hydrophobic and hydrophilic extremes, respectively, of underlying substrate properties and are not expected to carry a strong net charge. When coated with VN5, these surfaces adsorb the highest and lowest levels of VN, which differ by almost a factor of 2 (Fig. 7). From Schvartz *et al.*,[19] the integrin-binding domain lies at the opposite end of the VN molecule, with respect to the heparin-binding domain. The latter is presumed to be cationic, adsorbing more favorably to PET-PAA. The collagen-binding domain, adjacent to the integrin-binding segment, may be expected to bind more favorably to PET+PLL. Thus, it is surprising that VN adsorbed to different surfaces is capable of promoting the adhesion and supporting the expansion of hESC. This is likely due to the protein's flexibility and the presence of several redundant RGD-binding sequences,[32] which facilitates their accessibility.

Long-term culture on these polymer substrates gives rise to different HES-3 proliferation rates and levels of pluripotency. Given that these surfaces are coated with a VN surface density ≥ 250 ng/cm^2, above the threshold for the HES-3 bioresponse, this leads to an examination of how their wettability may influence the expansion of HES-3 cells. Data from Figs. 5(c) and 6 are plotted versus surface wettability [Fig. 8(a)] to yield Fig. 8(b). VN-coated PS-plasma and PET exhibit the highest wettability and give rise to the lowest levels of OCT-4 expression for cultured HES-3 cells [Fig. 8(b)]. These surfaces, with underlying substrates that represent the uncharged extremes of the wettability spectrum, also generate lower final cell numbers. The highest efficiency for HES-3 culture, as measured by final cell number and OCT-4 expression level, is obtained on VN-coated TCPS with a contact angle of 63°. Lim *et al.* found that the adhesion efficiency of human fetal osteoblastic cells correlates strongly with substrate wettability, obtaining high rates of cell attachment on relatively hydrophilic surfaces and low rates on hydrophobic surfaces, with $\theta_w = 65°$ as the defined boundary.[12,28] For the cationic and anionic surfaces: PET+PLL+VN5 and PET-PAA+VN5, OCT-4 expression remains high but total cell numbers fall with respect to VN-coated TCPS. These data indicate that, the VN-coated polymer substrate properties, including surface wettability, influence the rate of HES-3 cell proliferation and their pluripotency.

The data reported in the present study and by Yap *et al.*[20] provide a clear indication that the TCPS substrate coated from VN5 provides an performance equivalent to MG, which is the current industry standard and benchmark.[7] Given that Matrigel is a water-swellable coating and contains a number of ECM proteins and polysaccharides,[33] it is interesting to note that VN-coated TCPS, which is a comparatively rigid substrate coated with only one ECM protein, is equally capable of supporting the expansion of multiple hESC lines. This efficiency has been measured by cell pluripotency, karyotype stability, and cell proliferation rates.

IV. CONCLUSIONS

The perspective of hESC manufacturing in respect of clinical-grade requirements for therapeutic applications drives the replacement of MG with a defined substrate that supports the stable propagation of hESC. VN-coated polymer surfaces were used for the long-term expansion of HES-3 cells in CM. TCPS coated with solution concentrations $\geq$VN5 provides a viable substrate, capable of expanding these cells for over ten passages. Cells maintain karyotypic stability and are able to spontaneously differentiate *in vitro*, where embryoid bodies show evidence of the three primary germ lineages. HES-3 cells cultured on TCPS coated with VN2.5 show a slight decrease in their cell expansion rate, as measured by SICS at P6. When cultured on VN1.25, the cells initially appear viable, but show a marked decrease in their adherence to the cell culture substrate at P6, terminating in a sharp reduction in the number of viable cell colonies at P7. This adaptation of the cells is also reflected in a decrease in their expression of the OCT-4 and mAb 84 pluripotency markers, which are expressed normally in HES-3 cultured on higher VN surface densities.

Other forms of VN surface presentation were pursued using diverse polymer surfaces, ranging from hydrophobic to hydrophilic, with the inclusion of anionic and cationic polyelectrolyte coatings. An initial screening confirmed that all these polymer substrates require a VN coating to promote the adhesion and support the expansion of HES-3 cell colonies. The only exception was a four multilayer coating (PET-PAA+PLL+heparin+VN5), which did not support the growth of HES-3 colonies. Coatings of $\leq$3 multilayers were able to support HES-3 expansion over at least 13 passages, indicating that VN adsorbed to these surfaces with different properties is capable of the long-term expansion of hESC. The performance of simple model surfaces (TCPS, PET, PET+PLL, PET-PAA, PET-plasma, and PS-plasma) coated with VN5 was correlated with their wettability to sessile water drops. From the expression of OCT-4 and mAb 84 markers at P13, VN-coated PET and PS-plasma exhibit a higher wettability and generate a potential loss in HES-3 pluripotency. Cationic and anionic PET+PLL and PET-PAA, respectively, give rise to slower expansion rates at P13. The highest expansion rates and pluripotency marker expression levels are observed with VN-coated TCPS, which exhibits a contact angle of 65°, a result that compares favourably with data generated by Mei *et al.*[12]

TCPS+VN5 and the benchmark MG matrix show equal performance, both for the proliferation rate and the expression of pluripotency markers in HES-3 cells. These surfaces are capable of the long-term expansion of multiple hESC lines,[20] while preserving karyotypic stability and pluripotency. This similarity in performance between VN-coated TCPS and Matrigel is remarkable, given that the former is an adsorbed ECM protein, while the latter is a hydrogel coating of complex composition.

ACKNOWLEDGMENTS

This work was supported by the Joint Council Office, the Biomedical Research Council, the Science and Engineering Research Council, the Institute of Medical Biology, the Institute of Materials Research and Engineering, and the Bioprocessing Technology Institute of Agency for Science, Technology and Research (A*STAR), Singapore.

[1]J. A. Thomson, Science **282**, 1145 (1998).
[2]M. Amit, M. K. Carpenter, M. S. Inokuma, C. P. Chiu, C. P. Harris, M. A. Waknitz, J. Itskovitz-Eldor, and J. A. Thomson, Dev. Biol. **227**, 271 (2000).
[3]C. H. Xu, M. S. Inokuma, J. Denham, K. Golds, P. Kundu, J. D. Gold, and M. K. Carpenter, Nat. Biotechnol. **19**, 971 (2001).
[4]O. Genbacev *et al.*, Fertil. Steril. **83**, 1517 (2005).
[5]A. B. H. Choo, J. Padmanabhan, A. C. P. Chin, and S. K. W. Oh, Biotechnol. Bioeng. **88**, 321 (2004).
[6]A. Choo, J. Padmanabhan, A. Chin, W. J. Fong, and S. K. W. Oh, J. Biotechnol. **122**, 130 (2006).
[7]H. Hakala, K. Rajala, M. Ojala, S. Panula, S. Areva, M. Kellomäki, R. Suuronen, and H. Skottman, Tissue Eng. A **15**, 1775 (2009).
[8]R. Derda, L. Li, B. Orner, R. Lewis, J. Thomson, and L. Kiessling, ACS Chem. Biol. **2**, 347 (2007).
[9]Z. Melkoumian *et al.*, Nat. Biotechnol. **28**, 606 (2010).
[10]P. Kolhar, V. R. Kotamraju, S. T. Hikita, D. O. Clegg, and E. Ruoslahti, J. Biotechnol. **146**, 143 (2010).
[11]L. G. Villa-Diaz, H. Nandivada, J. Ding, N. C. Nogueira-de-Souza, P. H. Krebsbach, K. S. O'Shea, J. Lahann, and G. D. Smith, Nat. Biotechnol. **28**, 581 (2010).
[12]Y. Mei *et al.*, Nature Mater. **9**, 768 (2010).
[13]T. E. Ludwig *et al.*, Nat. Biotechnol. **24**, 185 (2006).
[14]M. Amit and J. Itskovitz-Eldor, Methods Mol. Biol. **331**, 105 (2006).
[15]T. Miyazaki *et al.*, Biochem. Biophys. Res. Commun. **375**, 27 (2008).
[16]S. R. Braam *et al.*, Stem Cells **26**, 2257 (2008).
[17]S. Rodin, A. Domogatskaya, S. Strom, E. M. Hansson, K. R. Chien, J. Inzunza, O. Hovatta, and K. Tryggvason, Nat. Biotechnol. **28**, 611 (2010).
[18]T. J. Rowland, L. M. Miller, A. J. Blaschke, E. L. Doss, A. J. Bonham, S. T. Hikita, L. V. Johnson, and D. O. Clegg, Stem Cells. Dev. **19**, 1231 (2010).
[19]I. Schvartz, D. Seger, and S. Shaltiel, Int. J. Biochem. Cell Biol. **31**, 539 (1999).
[20]L. Y. W. Yap *et al.*, Tissue Eng. C: Methods (in press, doi:10.1089/ten.tec.2010.0328).
[21]J. Racine, E. Luong-Van, Y. Sadikin, R. K. C. Kang, Y. S. Chu, V. Racine, J. P. Thiery, and W. R. Birch, J. Adhes. Sci. Technol. **24**, 975 (2010).
[22]S. K. W. Oh, A. K. Chen, A. B. H. Choo, and I. Reading, "Quantitative 2D Imaging of Human Embryonic Stem Cells, in *Emerging Technology Platforms for Stem Cells*, edited by U. Lakshmipathy, J. D. Chestnut, and B. Thyagarajan (Wiley, Hoboken, NJ, 2009), pp. 283–290.
[23]H. L. Tan, W. J. Fong, E. H. Lee, M. Yap, and A. Choo, Stem Cells **27**, 1792 (2009).
[24]A. C. Chin, W. J. Fong, L. T. Goh, R. Philp, S. K. Oh, and A. B. Choo, J. Biotechnol. **130**, 320 (2007).
[25]See supplementary material for the primers used in qRT-PCR.
[26]E. A. Vogler, J. Biomater. Sci., Polym. Ed. **10**, 1015 (1999).
[27]C. C. Barrias, M. C. L. Martins, G. Almeida-Porada, M. A. Barbosa, and P. L. Granja, Biomaterials **30**, 307 (2009).
[28]J. Y. Lim, X. M. Liu, E. A. Vogler, and H. J. Donahue, J. Biomed. Mater. Res. **68A**, 504 (2004).
[29]E. Occhiello, M. Morra, P. Cinquina, and F. Garbassi, Polymer **33**, 3007 (1992).
[30]S. Guruvenket, G. M. Rao, M. Komath, and A. M. Raichur, Appl. Surf. Sci. **236**, 278 (2004).
[31]L. Feng, Y. L. Song, J. Zhai, B. Q. Liu, J. Xu, L. Jiang, and D. B. Zhu, Angew. Chem., Int. Ed. **42**, 800 (2003).
[32]M. R. Doran, J. E. Frith, A. B. J. Prowse, J. Fitzpatrick, E. J. Wolvetang, T. P. Munro, P. P. Gray, and J. J. Cooper-White, Biomaterials **31**, 5137 (2010).
[33]N. T. Kohen, L. E. Little, and K. E. Healy, BioInterphases **4**, 69 (2009).